

การวิเคราะห์เชิงสมรรถนะของระบบเซลล์เชื้อเพลิงชนิดออกไซด์แข็งที่ป้อนด้วยแก๊สชีวภาพ

นาย ปกรณ์ พิรุณฤกษ์กุล

ศูนย์วิทยุทรัพยากร

วิทยานิพนธ์นี้เป็นส่วนหนึ่งของการศึกษาตามหลักสูตรปริญญาวิศวกรรมศาสตรดุษฎีบัณฑิต

สาขาวิชาวิศวกรรมเคมี ภาควิชาวิศวกรรมเคมี

คณะวิศวกรรมศาสตร์ จุฬาลงกรณ์มหาวิทยาลัย

ปีการศึกษา 2551

ลิขสิทธิ์ของจุฬาลงกรณ์มหาวิทยาลัย

PERFORMANCE ANALYSIS OF SOLID OXIDE FUEL CELL SYSTEMS
FED BY BIOGAS



Mr. Pakorn Piroonlerkgul

A Dissertation Submitted in Partial Fulfillment of the Requirements
for the Degree of Doctor of Engineering Program in Chemical Engineering

Department of Chemical Engineering

Faculty of Engineering

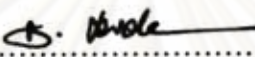
Chulalongkorn University

Academic Year 2008

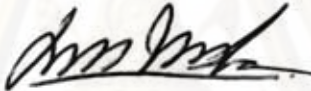
Copyright of Chulalongkorn University

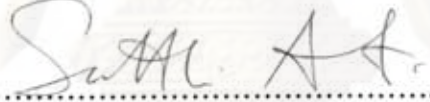
Thesis Title PERFORMANCE ANALYSIS OF SOLID OXIDE FUEL
CELL SYSTEMS FED BY BIOGAS
By Mr. Pakorn Piroonlerkgul
Field of Study Chemical Engineering
Advisor Professor Suttichai Assabumrungrat, Ph.D.
Co-Advisor Assistant Professor Navadol Laosiripojana, Ph.D.

Accepted by the Faculty of Engineering, Chulalongkorn University in Partial
Fulfillment of the Requirements for the Doctoral Degree

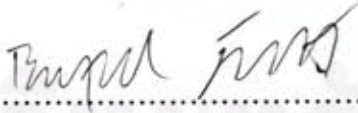

..... Dean of the Faculty of Engineering
(Associate Professor Boonsom Lerdhirunwong, Dr.Eng.)

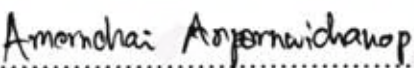
THESIS COMMITTEE



..... Chairman
(Associate Professor ML Supakanok Thongyai, Ph.D.)


..... Advisor
(Professor Suttichai Assabumrungrat, Ph.D.)


..... Co-Advisor
(Assistant Professor Navadol Laosiripojana, Ph.D.)


..... Examiner
(Assistant Professor Bunjerd Jongsomjit, Ph.D.)


..... Examiner
(Assistant Professor Amornchai Arpornwichanop, D.Eng.)


..... External Examiner
(Assistant Professor Worapon Kiatkittipong, D.Eng.)

ปรกรณ์ พิรุณฤกษ์กุล : การวิเคราะห์เชิงสมรรถนะของระบบเซลล์เชื้อเพลิงชนิดออกไซด์แข็งที่ป้อนด้วยแก๊สชีวภาพ (PERFORMANCE ANALYSIS OF SOLID OXIDE FUEL CELL SYSTEMS FED BY BIOGAS) อ. ที่ปรึกษาวิทยานิพนธ์หลัก: ศ. ดร. สุทธิชัย อัสสะบำรุงรัตน์, อ. ที่ปรึกษาวิทยานิพนธ์ร่วม: ผศ. ดร. นวพล เหล่าศิริพจน์, 167 หน้า.

การวิเคราะห์เชิงสมรรถนะของระบบเซลล์เชื้อเพลิงออกไซด์แข็งที่ป้อนด้วยแก๊สชีวภาพ แบ่งได้เป็น 4 ส่วนหลักคือ การวิเคราะห์การเกิดคาร์บอนภายในเซลล์เชื้อเพลิง การพิจารณาเลือกตัวทำปฏิกิริยารีฟอร์มมิ่งที่เหมาะสมกับระบบเซลล์เชื้อเพลิง การประเมินสมรรถนะของระบบเซลล์เชื้อเพลิงที่มีการจัดเรียงระบบที่แตกต่างกัน และการวิเคราะห์ความเป็นไปได้ในการดำเนินการของเซลล์เชื้อเพลิงที่ป้อนด้วยเชื้อเพลิงต่างชนิดกัน ผลของการศึกษากาการเกิดคาร์บอนในเซลล์เชื้อเพลิงบ่งชี้ว่าการป้อนตัวทำปฏิกิริยารีฟอร์มมิ่งเพิ่มเติมเป็นสิ่งจำเป็นในการป้องกันการเกิดคาร์บอนในเซลล์เชื้อเพลิงที่ใช้แก๊สชีวภาพเป็นเชื้อเพลิง ในการพิจารณาเลือกตัวทำปฏิกิริยารีฟอร์มมิ่งที่เหมาะสมกับระบบเซลล์เชื้อเพลิงพบว่า ไอน้ำเป็นตัวทำปฏิกิริยารีฟอร์มมิ่งที่เหมาะสมที่สุดสำหรับระบบเซลล์เชื้อเพลิงเมื่อเทียบกับอากาศ หรือ การใช้ไอน้ำร่วมกับอากาศ ทั้งนี้เนื่องจากระบบเซลล์เชื้อเพลิงที่ป้อนด้วยไอน้ำมีความหนาแน่นของไฟฟ้าสูงกว่าระบบเซลล์เชื้อเพลิงที่ป้อนด้วยตัวทำปฏิกิริยารีฟอร์มมิ่งชนิดอื่น ในการพิจารณาระบบเซลล์เชื้อเพลิงออกไซด์ที่มีการจัดเรียงระบบที่แตกต่างกันนั้น ได้แบ่งการจัดเรียงระบบออกเป็น 3 ลักษณะได้แก่ ระบบเซลล์เชื้อเพลิงที่ทำงานร่วมกับเครื่องปฏิกรณ์ชนิดเชื้อเพลิงผ่าน ระบบเซลล์เชื้อเพลิงที่ทำงานร่วมกับเครื่องดักจับแก๊สคาร์บอนไดออกไซด์ และระบบเซลล์เชื้อเพลิงที่ทำงานร่วมกับทั้งเครื่องปฏิกรณ์เชื้อเพลิงผ่านและระบบดักจับแก๊สคาร์บอนไดออกไซด์ ผลการศึกษาพบว่าเครื่องปฏิกรณ์ชนิดเชื้อเพลิงผ่านในระบบเซลล์เชื้อเพลิงสามารถเพิ่มสมรรถนะของระบบเซลล์เชื้อเพลิงได้ อย่างไรก็ตามระบบเซลล์เชื้อเพลิงนี้ยังไม่คุ้มค่าที่จะลงทุนเมื่อพิจารณาในเชิงเศรษฐศาสตร์ ขณะที่ระบบเซลล์เชื้อเพลิงที่ทำงานร่วมกับระบบดักจับแก๊สคาร์บอนไดออกไซด์จะให้ผลดีทั้งในทางเทคนิคและในทางเศรษฐศาสตร์ก็ต่อเมื่อใช้ระบบตัวดูดซับแคลเซียมออกไซด์เป็นระบบดักจับแก๊สคาร์บอนไดออกไซด์ อย่างไรก็ตามระบบเซลล์เชื้อเพลิงนี้ไม่สามารถดักจับแก๊สคาร์บอนไดออกไซด์ทั้งหมดที่ผลิตในระบบได้ การทำงานร่วมกันของเครื่องปฏิกรณ์ชนิดเชื้อเพลิงผ่านและเครื่องดักจับแก๊สคาร์บอนไดออกไซด์สามารถเพิ่มสมรรถนะของระบบเซลล์เชื้อเพลิงเมื่อเทียบกับสองระบบแรก อย่างไรก็ตามระบบเซลล์เชื้อเพลิงนี้ยังไม่คุ้มค่าในการลงทุนทางเศรษฐศาสตร์ ข้อดีของระบบเซลล์เชื้อเพลิงชนิดนี้คือสามารถดักจับแก๊สคาร์บอนไดออกไซด์ที่เกิดขึ้นในระบบได้เกือบทั้งหมด ขณะที่ผลของการพิจารณาความเป็นไปได้ในการดำเนินการของเซลล์เชื้อเพลิงออกไซด์แข็งที่ป้อนด้วยเชื้อเพลิงต่างชนิดกันพบว่า แก๊สไฮโดรเจนบริสุทธิ์เป็นเชื้อเพลิงที่ให้ค่าสมรรถนะของเซลล์เชื้อเพลิงสูงที่สุดเมื่อเทียบกับเชื้อเพลิงชนิดอื่น การใช้แก๊สชีวภาพเป็นเชื้อเพลิงของเซลล์เชื้อเพลิงโดยตรงจำเป็นต้องป้อนอากาศเข้าไปในเซลล์เชื้อเพลิงเป็นจำนวนมาก เพื่อให้เซลล์เชื้อเพลิงสามารถดำเนินการได้อีกทั้งค่าสมรรถนะของระบบเซลล์เชื้อเพลิงยังมีค่าต่ำมาก ขณะที่เซลล์เชื้อเพลิงที่ใช้แก๊สมีเทนที่ผ่านปฏิกิริยารีฟอร์มมิ่งเป็นเชื้อเพลิงจะมีสมรรถนะสูงกว่าเซลล์เชื้อเพลิงที่ใช้แก๊สชีวภาพที่ผ่านปฏิกิริยารีฟอร์มมิ่งเป็นเชื้อเพลิง

ภาควิชา.....วิศวกรรมเคมี
สาขาวิชา.....วิศวกรรมเคมี
ปีการศึกษา..... 2551

ลายมือชื่อนิติคุณ ปกรณ์ พิรุณฤกษ์กุล
ลายมือชื่อ อ. ที่ปรึกษาวิทยานิพนธ์หลัก.....
ลายมือชื่อ อ. ที่ปรึกษาวิทยานิพนธ์ร่วม.....

4871866721 : MAJOR CHEMICAL ENGINEERING

KEYWORDS : SOLID OXIDE FUEL CELL (SOFC)/BIOGAS/SIMULATION

PAKORN PIROONLERKGUL: PERFORMANCE ANALYSIS OF SOLID OXIDE FUEL CELL SYSTEMS FED BY BIOGAS. ADVISOR: PROF.

SUTTICHA ASSABUMRUNGRAT, Ph.D., CO-ADVISOR: ASST. PROF.

NAVADOL LAOSIRIPOJANA, Ph. D., 167 pp.

The research focuses on the simulation of solid oxide fuel cell (SOFC) systems fuelled by biogas. The study is divided into four parts: the investigation of carbon formation in SOFC system, the selection of suitable reforming agent for SOFC system, the technical and economic analyses of different configurations of SOFC systems, and the study on the operation viability of SOFC stack fed by different feedstocks. The study on carbon formation in SOFC system indicates that the addition of supplementary reforming agent such as steam and air simultaneously with biogas to SOFC system is required to alleviate the carbon formation. The use of oxygen-ion conducting electrolyte in SOFC stack is preferred since steam produced in anode section can inhibit the carbon formation. For the topic of reforming agent selection, steam is found to be the most suitable reforming agent for SOFC system relative to air, and combined steam and air. SOFC system fed by steam offers extremely higher power density compared to that fed by the other reforming agents. Three major configurations of SOFC system are proposed in this research; i.e., SOFC equipped with palladium membrane reactor (PMR-SOFC), SOFC equipped with CO₂ separator (M-SOFC/A-SOFC) and SOFC equipped with both palladium membrane reactor and CO₂ separator (SE-PMR-SOFC/SER-PMR-SOFC). For PMR-SOFC, it can offer higher power density compared with conventional SOFC system (CON-SOFC); however, it is not a good choice in the economic viewpoint. SOFC equipped with CO₂ separator is divided into two configurations; SOFC equipped with CO₂-selective membrane (M-SOFC) and SOFC equipped with CaO-CO₂ acceptor (A-SOFC). M-SOFC is not the interesting configuration due to the loss of CH₄ in permeation section of membrane module. A-SOFC can become attractive candidate for SOFC system since it offers higher performance and potential benefit compared to CON-SOFC. SE-PMR-SOFC can offer superior power density to CON-SOFC. The recycle of retentate gas of PMR (SER-PMR-SOFC) can improve the performance of SE-PMR-SOFC; however, both SE-PMR-SOFC and SER-PMR-SOFC are not the interesting alternative in economic viewpoint. Nevertheless, with this configuration, all CO₂ generated in this system can be captured. Operating viability of SOFC stack fuelled by different feedstocks is finally investigated employing 1-D analysis. Pure-H₂ feed offers the highest performance for SOFC among the other feeds. Extremely high excess air is required for SOFC fed by biogas to become operation viable. Moreover, its power density is much lower than those of SOFCs fed by the other feeds. Methane-reformed feed offers higher power density than biogas-reformed feed since H₂ concentration of the former one is higher.

Department : Chemical Engineering Student's Signature

Field of Study : Chemical Engineering Advisor's Signature

Academic Year : 2008 Co-Advisor's Signature

ACKNOWLEDGEMENTS

The author would like to show highly appreciation to Professor Suttichai Assabumrungrat for his great guidance in both research study and life attitude throughout the author's research study and Professor Adesoji A. Adesina for his good advice and kind assistance, especially during the author's stay in Australia. In addition, the author wishes to thank Assistant Professor Navadol Laosiripojana, Assistant Professor Amornchai Arpornwichanop, Assistant Professor Worapon Kiatkittipong, Dr. Apinan Soottitantawat and Dr. Wisitsree Wiyaratn for their collaboration in accomplished papers. Special thank to Associate Professor ML Supakanok Thongyai as the chairman, Assistant Professor Bunjerd Jongsomjit, Assistant Professor Amornchai Arpornwichanop and Assistant Professor Worapon Kiatkittipong as the members of the thesis committee.

Many thanks Thailand Research Fund (TRF) for providing his financial supports and great opportunity of working aboard during his Doctoral degree.

Finally, the author would like to express great gratitude to his parents and sisters. The author cannot completely achieve a success in his study without the support from his family.

ศูนย์วิทยทรัพยากร
จุฬาลงกรณ์มหาวิทยาลัย

CONTENTS

	page
ABSTRACT (THAI).....	iv
ABSTRACT (ENGLISH).....	v
ACKNOWLEDGEMENTS.....	vi
CONTENTS.....	vii
LIST OF TABLES.....	xi
LIST OF FIGURES.....	xiii
NOMENCLATURE.....	xix
CHAPTERS	
I INTRODUCTION.....	1
II THEORY.....	5
2.1 Fuel cell description.....	5
2.1.1 Fundamental principle.....	5
2.1.2 Type of fuel cell.....	7
2.2 Solid oxide fuel cell (SOFC).....	8
2.2.1 Characteristics of SOFC.....	8
2.2.2 SOFC system components.....	10
III LITERATURE REVIEW.....	12
3.1 Biogas source and its application as SOFC fuel.....	12
3.2 H ₂ generation reaction.....	13
3.2.1 Steam reforming.....	13
3.2.2 Dry reforming.....	14
3.2.3 Partial oxidation and autothermal reforming.....	14
3.3 SOFC modelling.....	15
3.3.1 Electrochemical model.....	15
3.3.2 Macro-modelling.....	16
3.3.2.1 Zero-dimensional analysis.....	16
3.3.2.2 One-dimensional (1-D) analysis.....	17
3.4 Palladium membrane reactor and its application in SOFC system....	18
3.5 CO ₂ separation technology.....	20

CHAPTERS	page
IV MODELLING.....	23
4.1 SOFC modelling.....	23
4.1.1 Electrochemical model.....	23
4.1.1.1 Open circuit voltage.....	24
4.1.1.2 Overpotentials.....	24
4.1.2 Zero-dimensional analysis.....	28
4.1.2.1 Mass balance equations.....	28
4.1.2.2 Energy balance equation.....	31
4.1.2.3 Calculation procedure.....	31
4.1.3 One-dimensional analysis (1-D analysis).....	36
4.2 Fuel processing modelling.....	38
4.2.1 Conventional fuel processor.....	38
4.2.2 Palladium membrane reactor (PMR).....	40
4.3 Vacuum pump and compressor.....	44
4.4 Afterburner and heat exchanger.....	44
4.5 Membrane module.....	44
4.6 CaO-CO ₂ acceptor system.....	47
4.7 Boundary of carbon formation.....	50
4.7.1 Direct internal reforming SOFC (DIR-SOFC).....	50
4.7.2 Conventional fuel processor.....	52
4.8 Economic consideration.....	53
V DETERMINATION OF BOUNDARY OF CARBON FORMATION FOR DRY REFORMING OF METHANE IN SOLID OXIDE FUEL CELL.....	55
5.1 Introduction.....	55
5.2 Results and discussion.....	57
5.3 Conclusions.....	70
VI SELECTION OF APPROPRIATE FUEL PROCESSOR FOR BIOGAS-FUELLED SOFC SYSTEM.....	71
6.1 Introduction.....	71

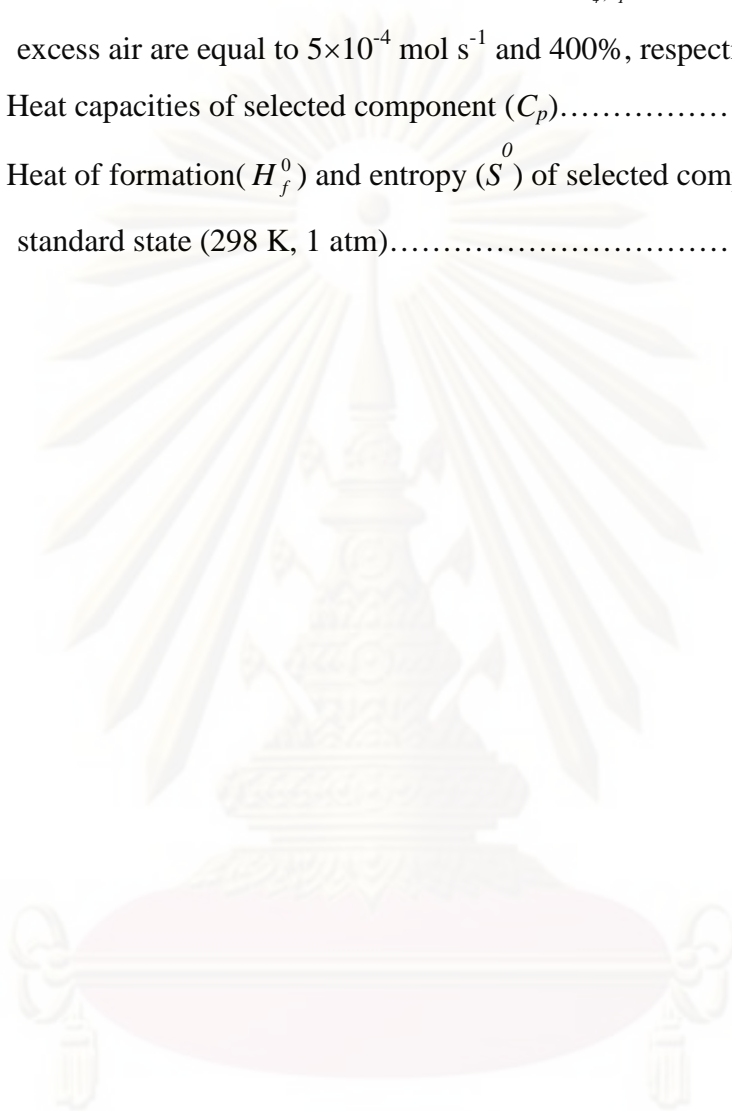
CHAPTERS	page
6.2 SOFC system configurations.....	72
6.3 Results and discussion.....	75
6.4 Conclusions.....	86
VII PERFORMANCE OF BIOGAS-FED SOLID OXIDE FUEL CELL SYSTEM INTEGRATED WITH CO₂ CAPTURE TECHNOLOGY.....	87
7.1 Introduction.....	87
7.2 SOFC system configurations.....	88
7.3 Results and discussion.....	90
7.4 Conclusions.....	99
VIII INTEGRATION OF SOLID OXIDE FUEL CELL AND PALLADIUM MEMBRANE REACTOR: TECHNICAL AND ECONOMIC ANALYSIS.....	101
8.1 Introduction.....	101
8.2 SOFC system configurations.....	102
8.3 Results and discussion.....	103
8.4 Conclusions.....	112
IX THE TECHNICAL AND ECONOMIC STUDY OF THE INTEGRATED SYSTEM OF SOLID OXIDE FUEL CELL, CaO-CO₂ ACCEPTOR AND PALLADIUM MEMBRANE REACTOR.....	114
9.1 Introduction.....	114
9.2 SOFC system configurations.....	115
9.3 Results and discussion.....	117
9.4 Conclusions.....	131
X OPERATION VIABILITY AND PERFORMANCE OF SOLID OXIDE FUEL CELL FUELLED BY DIFFERENT FEEDS.....	132
10.1 Introduction.....	132
10.2 Type of feed in consideration	133
10.3 Results and discussion.....	134
10.4 Conclusions.....	146

CHAPTERS	page
XI CONCLUSIONS AND RECOMMENDATION.....	148
11.1 Introduction.....	148
11.1.1 The investigation of carbon formation in SOFC system....	148
11.1.2 The selection of suitable reforming agent for SOFC system.....	148
11.1.3 The technical and economical analyses of different configurations of SOFC system.....	149
11.1.4 The study on the operation viability of SOFC stack fed by different feedstocks.....	150
11.2 Recommendation for future works.....	151
REFERENCES.....	152
APPENDICES.....	163
APPENDIX A. THERMODYNAMIC DATA OF SELECTED COMPONENT.....	164
APPENDIX B. DETERMINING GIBB ENERGY AND EQUILIBRIUM CONSTANT.....	165
APPENDIX C. LIST OF PUBLICATIONS.....	166
VITAE.....	167

LIST OF TABLES

	page
Table 2.1 Descriptions for each type of fuel cell.....	7
Table 4.1 Summary of model parameters.....	24
Table 4.2 Summary of activation polarization parameters.....	26
Table 4.3 The parameters used in collision integral computation.....	28
Table 4.4 Feed compositions and SOFC stack dimensions used in model validation.....	34
Table 4.5 Feed compositions and SOFC stack dimensions used in model validation.....	35
Table 4.6 Model validation of the SOFC model.....	35
Table 4.7 Summary of model parameters used in 1-D analysis.....	38
Table 4.8 Kinetic parameters for methane steam reforming.....	41
Table 4.9 Summary of model parameters of palladium membrane reactor.....	42
Table 4.10 Membrane thickness and permeability of each gas component.....	45
Table 4.11 Summary of feed characteristics and parameters used in the model verification of membrane separation.....	46
Table 4.12 Value of model parameters used in the calculation of CaO-CO ₂ acceptor.....	50
Table 4.13 Costing models and parameters used in the economic analysis.....	54
Table 7.1 The summary of electrical efficiency, power density and stack size of each SOFC system. ($Q_E = 416.8$ kW).....	98
Table 8.1 The technical and economical comparison of four scenarios.....	112
Table 9.1 The technical and economical comparison among different configurations of SOFC system.....	130
Table 10.1 Base case in consideration for different feed ($U_f = 0.8$).....	135
Table 10.2 Summary of SOFC fed by different feed operating at the optimum operating condition in case that $F_{CH_4,eq}$ and %excess air are equal to 3×10^{-4} mol/s and 400%, respectively.....	145

Table 10.3 Summary of SOFC fed by different feed operating at the optimum operating condition in case that $F_{CH_4,eq}$ and Percent excess air are equal to $5 \times 10^{-4} \text{ mol s}^{-1}$ and 400%, respectively.....	146
Table A1 Heat capacities of selected component (C_p).....	164
Table A2 Heat of formation(H_f^0) and entropy (S^0) of selected component at standard state (298 K, 1 atm).....	164



ศูนย์วิทยทรัพยากร
จุฬาลงกรณ์มหาวิทยาลัย

LIST OF FIGURES

	page
Figure 2.1 Components of a fuel cell and its operation.....	5
Figure 4.1 The scheme showing the zero-dimensional analysis of SOFC.....	29
Figure 4.2 The flowchart of the program used in zero-dimensional analysis of SOFC.....	32
Figure 4.3 Verification of SOFC model for pure hydrogen fuel.....	33
Figure 4.4 Verification of SOFC model for the feed with CH ₄ , CO and H ₂ mixtures.....	34
Figure 4.5 A small element divided for the calculation in SOFC cell.....	36
Figure 4.6 The scheme showing the basic working of the membrane reactor..	43
Figure 4.7 The comparison of the methane conversion in the fuel processor between the modeling results and the experimental results. (sweep gas flow rate = 3.62×10^{-5} mol/s, $P_R = 1.22$ bar, $P_P = 1.1$ bar, H ₂ O/CH ₄ = 3).....	43
Figure 4.8 The configuration of membrane module.....	45
Figure 4.9 Verification of the membrane separation model.....	47
Figure 4.10 The scheme showing the basic working of the CaO-CO ₂ acceptor.....	48
Figure 4.11 Values of equilibrium constants.....	51
Figure 5.1 Effect of inlet CO ₂ /CH ₄ ratio on mole of each component in a conventional reformer ($n_{CH_4, in}^a = 1$ mol, $P = 101.3$ kPa and $T =$ 900 K).....	58
Figure 5.2 Effect of inlet CO ₂ /CH ₄ ratio on mole of each component mole: a) SOFC-O ²⁻ , and b) SOFC-H ⁺ ($n_{CH_4, in}^a = 1$ mol, $e = 1.6$ mol, $P =$ 101.3 kPa and $T = 900$ K).....	59
Figure 5.3 Effect of inlet CO ₂ /CH ₄ ratio on carbon activity (conventional reactor, $n_{CH_4, in}^a = 1$ mol, and $P = 101.3$ kPa).....	60

Figure 5.4 Influence of the extent of electrochemical reaction of H ₂ on the requirement of inlet CO ₂ /CH ₄ ratio at different operating temperature (SOFC-O ²⁻ , $n_{CH_4,in}^a = 1$ mol and $P = 101.3$ kPa).....	61
Figure 5.5 Influence of the extent of electrochemical reaction of H ₂ on the requirement of inlet CO ₂ /CH ₄ ratio at different operating temperature: a) $T = 800-950$ K, and b) $950-1100$ K (SOFC-H ⁺ , $n_{CH_4,in}^a = 1$ mol and $P = 101.3$ kPa).....	62
Figure 5.6 Required inlet H ₂ O/CH ₄ ratio at different inlet CO ₂ /CH ₄ ratio: a) $T = 900$ K, b) $T = 1050$ K and c) $T = 1200$ K (SOFC-O ²⁻ , $n_{CH_4,in}^a = 1$ mol and $P = 101.3$ kPa).....	65
Figure 5.7 Required inlet H ₂ O/CH ₄ ratio at different inlet CO ₂ /CH ₄ ratio: a) $T = 900$ K, b) $T = 1050$ K and c) $T = 1200$ K (SOFC-H ⁺ , $n_{CH_4,in}^a = 1$ mol and $P = 101.3$ kPa).....	66
Figure 5.8 Required inlet air/CH ₄ ratio at different inlet CO ₂ /CH ₄ ratio: a) $T = 900$ K, b) $T = 1050$ K and c) $T = 1200$ K (SOFC-O ²⁻ , $n_{CH_4,in}^a = 1$ mol and $P = 101.3$ kPa).....	68
Figure 5.9 Required inlet air/CH ₄ ratio at different inlet CO ₂ /CH ₄ ratio: a) $T = 900$ K, b) $T = 1050$ K and c) $T = 1200$ K (SOFC-H ⁺ , $n_{CH_4,in}^a = 1$ mol and $P = 101.3$ kPa).....	69
Figure 6.1 The plant configurations for (a) the steam-fed SOFC, (b) the air-fed SOFC and (c) the co-fed SOFC.....	74
Figure 6.2 Boundary of carbon formation for the biogas-fed fuel processors with different reforming agents; a) steam and b) air.....	76
Figure 6.3 The effect of fuel utilization and steam contents on the power density and energy self-sufficient point of steam-fed SOFC. ($V = 0.64$ V and CH ₄ :CO ₂ = 60:40).....	77
Figure 6.4 The effect of steam contents on electrical efficiency of steam-fed SOFC.....	78

Figure 6.5 The effect of fuel utilization and CH ₄ :CO ₂ ratios in biogas on the power density and energy self-sufficient point of steam-fed SOFC. ($V = 0.64$ V and $H_2O/CH_4 = 2.5$).....	78
Figure 6.6 The effect of operating voltage and steam contents on the power density of steam-fed SOFC operating at energy self-sufficient point. CH ₄ :CO ₂ = 60:40).....	79
Figure 6.7 The effect of the fuel utilization on the power density and electrical efficiency at different (a) O ₂ /CH ₄ (CH ₄ :CO ₂ = 60:40) and (b) CH ₄ :CO ₂ ratios in biogas (O ₂ /CH ₄ = 0.6). ($V = 0.64$ V).....	80
Figure 6.8 Electrical efficiency and power density of air-fed SOFC at different operating voltage and air contents. (CH ₄ :CO ₂ = 60:40)...	81
Figure 6.9 Electrical efficiency and power density of co-fed SOFC operating at H ₂ O:CH ₄ ratios of (a) 1, (b) 1.5, (c) 2 and (d) 2.5 at different operating voltage and air contents. (CH ₄ :CO ₂ = 60:40).....	84
Figure 6.10 SOFC performance: a) overall electrical efficiency and b) power density (CH ₄ :CO ₂ = 60:40).....	85
Figure 7.1 The plant configurations for (a) the m-SOFC and (b) the a-SOFC.	90
Figure 7.2 The %CO ₂ removal and %CH ₄ loss at different operating pressure at permeate section (P_P) and retentate section (P_R).....	91
Figure 7.3 The electricity consumption in compressor and vacuum pump at different P_P and P_R	91
Figure 7.4 The effect of a) P_P ($P_R = 20$ bar) and b) P_R ($P_P = 0.5$ bar) on the energy self-sustainable point and the power density of m-SOFC ($V = 0.64$ volt).....	93
Figure 7.5 The effect of the operating voltage on the power density at different a) P_P ($P_R = 20$ bar) and b) P_R ($P_P = 1$ bar) in case that m-SOFC operates at energy self-sufficient point.....	94
Figure 7.6 The correlation between make-up CaO rate and CO ₂ removal rate for CaO-CO ₂ acceptor technology ($F_R/F_{CO_2} = 10$ and $W_S = 50$ kg).	95

Figure 7.7 The effect of the CO ₂ removal rate and fuel utilization on the energy self-sustainable point and the power density of m-SOFC. (V = 0.64 volt).....	96
Figure 7.8 The effect of the operating voltage on the power density at different CO ₂ removal rate in case that m-SOFC operates at energy self-sufficient point.....	97
Figure 7.9 Saving in SOFC stack cost, additional cost, net cost saving, benefit of carbon credit and total benefit of a-SOFC at different CO ₂ removal rate.....	99
Figure 8.1 The plant configuration of the PMR-SOFC.....	103
Figure 8.2 Q _{NET} at different operating voltage and fuel utilization for methane-fuelled CON-SOFC.....	104
Figure 8.3 Power density and fuel utilization at different operating voltage in case that Q _{NET} = 0.....	105
Figure 8.4 Electrical power consumed in HPC and vacuum pump at different retentate pressure (P _R) and permeate pressure (P _P) in case that ζ = 0.95 for (a) methane feed and (b) biogas feed.....	106
Figure 8.5 Q _{NET} and power density at different permeate pressure and fuel utilization (U _f) for PMR-SOFC in the case of methane feed.....	107
Figure 8.6 Power density and fuel utilization at different permeate pressure and operating voltage in case that Q _{NET} = 0 for (a) methane-fuelled PMR-SOFC and (b) biogas-fuelled PMR-SOFC.....	108
Figure 8.7 The effect of change in permeate pressure on power density and (b) SOFC area at optimum operating voltage in case that Q _{NET} = 0	109
Figure 8.8 Saving in SOFC stack cost/additional cost at different permeate pressure (optimum operating voltage and Q _{NET} = 0) for a) methane-fuelled PMR-SOFC and b) biogas-fuelled PMR-SOFC...	111
Figure 9.1 The plant configuration of the PMR-SOFC, SE-PMR-SOFC and SER-PMR-SOFC.....	116
Figure 9.2 Fuel processing systems of a) PMR-SOFC, b) SE-PMR-SOFC and c) SER-PMR-SOFC.....	117

Figure 9.3 The effect of the extent of CO ₂ removal and retentate pressure on a) H ₂ recovery and b) fresh CaO feed rate in case of SE-PMR-SOFC system.....	118
Figure 9.4 The effect of the recycle ratio and retentate pressure on a) H ₂ recovery, CO ₂ removal rate and b) fresh CaO feed rate, CO ₂ removal rate in case of SER-PMR-SOFC system.....	120
Figure 9.5 The effect of fuel utilization and CO ₂ removal rate on the power density and energy self-sufficient point for SE-PMR-SOFC system (retentate pressure = 25 bar, $V = 0.65$ V).....	121
Figure 9.6 The power density of SE-PMR-SOFC system with equilibrium CO ₂ removal rate operating at energy self-sufficient point at each operating voltage and retentate pressure.....	122
Figure 9.7 The effect of fuel utilization and recycle ratio on the power density and energy self-sufficient point for SER-PMR-SOFC system (retentate pressure = 17.5 bar, $V = 0.65$ V).....	123
Figure 9.8 The effect of permeate pressure and operating pressure on a) the power density and b) fuel utilization for SER-PMR-SOFC system operating at energy self-sufficient point and recycle ratio of 0.5...	124
Figure 9.9 The effect of permeate pressure and operating pressure on a) the power density and b) fuel utilization for SER-PMR-SOFC system operating at energy self-sufficient point and recycle ratio of 0.9...	125
Figure 9.10 The maximum power density SER-PMR-SOFC can achieve, SOFC stack size and the fresh CaO supplying rate at each recycle ratio in case that $Q_{NET} = 0$	126
Figure 9.11 Saving in SOFC stack cost, additional cost and net cost saving of PMR-SOFC, SE-PMR-SOFC with equilibrium CO ₂ capture and SER-PMR-SOFC operating at different recycle ratios.....	128
Figure 9.12 % Total CO ₂ capture and cost of CO ₂ capture of SE-PMR-SOFC with equilibrium CO ₂ capture and SER-PMR-SOFC operating at different recycle ratio.....	129

- Figure 10.1** The variation of a) cell temperature and b) power density with cell distance in SOFC cell fed by different types of feed. ($F_{CH_4,eq} = 3 \times 10^{-4} \text{ mol s}^{-1}$, Percent excess air = 400%, $U_f = 0.8$)..... 136
- Figure 10.2** The effect of the change in percent excess air on the maximum temperature gradient, maximum cell temperature, b) power density, fuel utilization and c) electrical efficiency for SOFC fed by different types of feed. ($F_{CH_4,eq}$ and operating voltage are equal to base case values.)..... 138
- Figure 10.3** The effect of the change in $F_{CH_4,eq}$ on a) the maximum temperature gradient, maximum cell temperature, b) power density, fuel utilization and c) electrical efficiency for SOFC fed by different types of feed. (percent excess air and operating voltage are equal to base case values.)..... 140
- Figure 10.4** The effect of the change in operating voltage on a) the maximum temperature gradient, maximum cell temperature, b) power density, fuel utilization and c) electrical efficiency for SOFC fed by different types of feed in case that $F_{CH_4,eq}$ is equal to $3 \times 10^{-4} \text{ mol s}^{-1}$ (percent excess air is equal to base case values.)..... 143
- Figure 10.5** The effect of the change in operating voltage on a) the maximum temperature gradient, maximum cell temperature, b) power density, fuel utilization and c) electrical efficiency for SOFC fed by different types of feed in case that $F_{CH_4,eq}$ is equal to $5 \times 10^{-4} \text{ mol s}^{-1}$. (Percent excess air is equal to base case values.)... 144

NOMENCLATURE

A_f	active area of f -th fuel utilization region	[m ²]
A_k	pre-exponential factor for reaction k	[various units]
$A_{\text{single cell}}$	active area of SOFC single cell	[m ²]
A_{total}	total active area of SOFC	[m ²]
A^j	active area of j -th control volume	[m ²]
B_i	pre-exponential factor for component I	[various units]
C_{cell}	capital cost of SOFC single cell	[\$]
$C_{\text{compressor}}$	capital cost of compressor	[\$]
$C_{\text{vacuum pump}}$	capital cost of vacuum pump	[\$]
C_p	heat capacity	[J mol ⁻¹ K ⁻¹]
C_{stack}	capital cost of SOFC stack	[\$]
d	diameter of inner tube of membrane reactor	[mm]
d_p	CaO sorbent particle size	[μm]
D	carbonator bed diameter	[m]
$D_{i,K}$	Knudsen diffusivity of component i	[cm ² s ⁻¹]
D_{A-B}	ordinary diffusivity of gas A versus gas B	[cm ² s ⁻¹]
$D_{m(\text{eff})}$	effective diffusion coefficient of electrode m	[cm ² s ⁻¹]
$D_{i,K(\text{eff})}$	effective Knudsen diffusivity of component i	[cm ² s ⁻¹]
$D_{A-B(\text{eff})}$	effective ordinary diffusivity of gas A versus gas B	[cm ² s ⁻¹]
D_p	catalyst pore diameter	[μm]
DEN	term given for the reforming kinetics	[-]
e	extent of electrochemical reaction	[mol s ⁻¹]
e_{max}	maximum thickness of the layer of CaCO ₃ on the pore wall	[nm]
E	theoretical open-circuit voltage of the cell	[V]
E^0	theoretical open-circuit voltage of the cell at standard pressure	[V]

E_{act}	activation energy	[kJ mol ⁻¹]
E_{carb}	CO ₂ capture efficiency	[-]
E_p	activation energy for hydrogen permeation	[J mol ⁻¹]
f_0	inlet molar fraction of CO ₂	[-]
f_a	volumetric fraction of CaO that reacts in the carbonator	[-]
f_e	molar fraction of CO ₂ at equilibrium of carbonation reaction	[-]
f_f	gas friction factor	[-]
f_P	solid friction factor	[-]
F	Faraday constant (9.6495x10 ⁴)	[C mol ⁻¹]
$F_{CH_4,eq}$	methane equivalent flow	[mol s ⁻¹]
F_0	Fresh CaO supplying rate	[mol s ⁻¹]
F_R	CaO-circulating rate	[mol s ⁻¹]
F_{CO_2}	CO ₂ flow rate in gas mixture	[mol s ⁻¹]
g	gravity acceleration (9.81)	[m s ⁻²]
ΔG_k	Gibb's free energy of reaction k	[kJ mol ⁻¹]
h	heat transfer coefficient	[W m ⁻² K ⁻¹]
H	energy flow of gas stream	[kW]
HP	power consumption in compressor	[HP]
ΔH_k	heat of reaction k	[kJ mol ⁻¹]
ΔH_i	heat of adsorption for component i	[J mol ⁻¹]
i	current density	[A cm ⁻²]
i_o	exchange current density	[A cm ⁻²]
k_k	reaction rate constant for reaction k	[various units]
k_S	kinetic constant of carbonation reaction	[mol m ⁴ s ⁻¹]
K_i	adsorption constant for component i	[various units]
K_k	equilibrium constant of reaction k	[various units]
l_a	thickness of anode electrode	[μm]
l_c	thickness of cathode electrode	[μm]
L	thickness of electrolyte	[μm]

L_b	carbonator bed height	[m]
M_i	molecular weight of gas i	[g]
M_{CaO}	molecular weight of CaO	[g mol ⁻¹]
n	electrode porosity	[-]
n_i	molar flow rate of component i	[mol s ⁻¹]
n_{total}	total molar flow rate	[mol s ⁻¹]
N	number of carbonation-calcination cycle	[-]
N_k	permeation flux of component k	[mol m ⁻² s ⁻¹]
N_{cell}	number of SOFC single cell	[-]
N_{stack}	number of SOFC stack	[-]
p_{ave}	average power density	[W cm ⁻²]
p_i	partial pressure of component i	[Pa]
p_i^I	inlet pressure of component i	[Pa]
$p_{H_2,P}$	partial pressure of hydrogen in permeate side of membrane reactor	[Pa]
$p_{H_2,R}$	partial pressure of hydrogen in retentate side of membrane reactor	[Pa]
pe_i	permeability of component i	[barrer]
P	pressure	[Pa]
P_{ref}	reference pressure (10 ⁵)	[Pa]
ΔP	pressure drop	[Pa]
PE_i	molar flow rate of component i at permeate side of membrane	[mol s ⁻¹]
Q_0	pre-exponential factor for hydrogen permeation	[mol m ⁻¹ Pa ^{-0.5} s ⁻¹]
Q_{NET}	difference between heat demand and heat generated in SOFC system	[kW]
r	catalyst pore radius	[μ m]
r_k	rate of reaction k	[mol s ⁻¹]
r_N	mass fraction of solid that have circulated N times	[-]
R	gas constant (8.3145)	[J mol ⁻¹ K ⁻¹]

R_i	molar flow rate of component i at retentate side of membrane	[mol s ⁻¹]
S_{ave}	maximum average reaction surface	[m ⁻¹]
T	temperature	[K]
u_f	gas velocity	[m s ⁻¹]
u_p	particle velocity	[m s ⁻¹]
U_f	fuel utilization	[-]
v_t	gas terminal velocity	[m s ⁻¹]
V	cell voltage	[V]
$V_{M,CaCO_3}$	molar volume of CaCO ₃	[m ³ mol ⁻¹]
\dot{W}_{comp}	electricity consumed in the compressor	[kW]
W_e	electricity produced in SOFC	[kW]
W_S	CaO inventory in carbonator	[kg]
x_i	mole fraction of component i at retentate side of membrane	[-]
x_k	extent of reaction k	[mol s ⁻¹]
Δx	length of control volume in membrane Reactor	[m]
X_{ave}	average maximum carbonation conversion	[-]
X_N	carbonation conversion after N cycle of carbonation-calcination	[-]
y_i	mole fraction of component i at permeate side of membrane	[-]
z	number of electron participating in the electrochemical reaction	[-]
Greek letters		
α	charge transfer coefficient	[-]
$\alpha_{c,k}$	carbon activity of reaction k	[-]
ε	bed void fraction	[-]
ξ	electrode tortuosity	[-]
δ	membrane thickness	[μ m]

δ_{O_2}	coefficient used in concentration	
	overpotential	[-]
ζ	hydrogen recovery	[-]
η_{act}	activation loss	[V]
η_{Conc}	concentration loss	[V]
η_{com}	compressor or pump efficiency	[-]
η_{ohm}	ohmic loss	[V]
σ_{AB}	collision diameter	[Å]
Ω_D	collision integral	[-]
ε_{AB}	Lennard-Jones energy interaction parameter scaled with respect to the Boltzman constant	[-]
ρ_c	catalyst density	[kg m ⁻³]
ρ_f	gas density	[kg m ⁻³]
ρ_{CaO}	CaO density	[kg m ⁻³]
$\rho_{M,g}$	molar density of gas	[mol m ⁻³]
μ	gas viscosity	[kg m ⁻¹ s ⁻²]
$\nu_{i,k}$	stoichiometric coefficient of component i in chemical reaction k	[-]
γ_a	pre-exponential factor for anode exchange current density	[A m ⁻²]
γ_c	pre-exponential factor for anode exchange current density	[A m ⁻²]
Superscripts		
a	anode	
c	cathode	
j	j -th control volume	

Subscripts

<i>ave</i>	average
dry	dry reforming reaction
<i>f</i>	<i>f</i> -th fuel utilization region
<i>i</i>	component
<i>in</i>	input
<i>k</i>	chemical reaction
<i>m</i>	electrode
<i>out</i>	output
<i>p</i>	particle
<i>P</i>	Permeate section
<i>R</i>	Retentate section
<i>RWGS</i>	reverse water gas shift reaction
<i>s</i>	solid trilayer
steam	steam reforming reaction
WGS	water gas shift reaction



ศูนย์วิทยทรัพยากร
จุฬาลงกรณ์มหาวิทยาลัย

CHAPTER I

INTRODUCTION

With the increasing concern on environmental problems, many countries are pursuing efforts to develop more sustainable energy systems to replace conventional combustion heat engines. Solid oxide fuel cell (SOFC) power generation shows great promise to serve as an alternative in the near future. For SOFC, the chemical energy can be transformed directly into the electrical energy. Therefore, the energy loss in an SOFC is lower than that in the conventional heat engines. Furthermore, additional efficiency can be gained by incorporating with a steam/gas turbine cycle to recover heat from the hot gas exhausted from the SOFC which is typically operated at high temperatures between 1073 and 1273 K. By the same reason, various types of fuel, e.g. methane, methanol, ethanol, natural gas, and oil derivatives, can be directly used as fuel in SOFC. Biogas is also one of the interesting alternatives. It can be derived from an anaerobic digestion of plant. The major components in biogas are methane (40-65%) and carbon dioxide (30-40%) (Dayton, 2001). By using biogas in power generation, zero greenhouse gas emission can be achieved since CO₂ released from the process could be consumed in the photo-synthesis of plant.

An SOFC system can be divided into three main parts: 1) a fuel processor to reform the raw fuel into hydrogen gas, 2) SOFC stacks which subsequently generate electricity and useful heat from the reformed gas and 3) an afterburner where the residual fuel is combusted in order to supply heat to preheaters and the fuel processor. When biogas is considered as a feedstock for the SOFC system, three main chemical reactions, namely; steam reforming, dry reforming and partial oxidation can take place in the fuel processor (Ferreira-Aparicio et al., 2005). Dry reforming is perhaps the most interesting option for the conversion of biogas since the major constituents of the biogas are carbon dioxide and methane. However, the quantity of carbon dioxide available is not sufficient to convert all methane in biogas into hydrogen. Air and steam are the common reforming agents to combine with CO₂ in the fuel processor. The determination of a suitable reforming agent when the fuel processor is integrated with an SOFC system is still a matter for further investigation. Moreover,

boundary of carbon formation should also be determined to investigate the degree of carbon deposition in SOFC system fed by different reforming agents.

Due to the presence of CO_2 in biogas, the H_2 yield of the fuel processor reduces due to the reaction between CO_2 and H_2 via reverse water gas shift reaction, RWGS. Furthermore, the presence of large amounts of CO_2 in the SOFC feed gas can decrease the cell potential. Suwanwarangkul et al. (2006) reported that when H_2 concentration decreases from 100 to 20%, the SOFC cell potential decreases by 20% due to the impact of the RWGS reaction. Hence, the separation of CO_2 from the biogas feed is the interesting way to increase the performance of biogas-fuelled SOFC system. Nowadays, there are several available CO_2 separation technologies, e.g. membrane and adsorption technology. Membrane technology is the interesting alternative since it could handle feed streams with variable flow rates and compositions. Polyimide membrane could be a promising CH_4/CO_2 separation membrane because it offers higher permselectivity and permeability compared to membranes derived from other polymers (Shekhawat et al., 2003). It should be noted that a common problem arising from the use of polymeric membranes is the instability of the membranes at high operating temperature (Amelio et al., 2007). For the adsorption technology, $\text{CaO}-\text{CO}_2$ acceptor (CaO carbonation) is one of attractive options. With this operation, CO_2 -rich gas reacts with CaO in the carbonator and CaCO_3 is generated. CaCO_3 is then fed to regenerate in the calcinator. Unlike membrane technology, 100% selectivity of CO_2 capture can be achieved for an $\text{CaO}-\text{CO}_2$ acceptor. Nevertheless, make-up CaO is required to be fed to $\text{CaO}-\text{CO}_2$ acceptor owing to sintering of CaO sorbent after several cycles of carbonation-calcination (Abanades, 2002; Grasa et al., 2008) and operating cost therefore increases.

The use of pure- H_2 as an SOFC feed is also an interesting alternative to improve SOFC performance; however, pure- H_2 is not available in natural resources. The use of a hydrogen-selective membrane reactor can offer pure hydrogen with high methane conversion. Palladium membrane is the attractive candidate due to its extremely high H_2 selectivity (Lu et al., 2007). The use of palladium membrane reactor for hydrogen-generating reactions has been widely investigated (Basile et al., 2003; Gallucci et al., 2004; Patel and Sunol, 2007). Under this operation, pure- H_2 could be obtained at the permeation side. Moreover, higher methane conversion can

be achieved when compared with the conventional fuel processor. A superior SOFC performance was reported as pure-H₂ is used as feedstock of SOFC system instead of reformed gas (Suwanwarangkul et al., 2006). To increase a driving force of H₂ permeation, The idea of membrane reactor operating with both high pressure compressor and vacuum pump was proposed (Vivanpatarakij et al., 2009). Even if the results indicate that this operation mode could offer higher performance compared with conventional SOFC system, this work did not take into account the thermal management within the integrated systems.

Although the use of pure-H₂ or CO₂-removed reformed gas as SOFC feed can offer fast electrochemical reaction and thus high power density, solid parts in an SOFC stack may be damaged due to extreme increase in the irreversibility. Steep temperature profile of the solid parts in SOFC cell could be found when severe electrochemical reaction takes place. The maximum allowable temperature gradient for YSZ which is widely employed as the electrolyte in SOFC is around 10 K cm⁻¹. To control the temperature gradient of YSZ at the reasonable value, SOFC feedstock should be carefully selected. Moreover the tuning of operating conditions; i.e., operating voltage, fuel feed rate and oxidizing agent feed rate which also affect the rate of electrochemical reaction is also interesting issue in thermal consideration. To investigate thermal behavior in SOFC cell, one dimensional analysis (1-D analysis) is an attractive approach. Sorrentino et al. (2008) have employed this simulation method for computing the temperature and current density profiles along the flow direction of SOFC. It was found that the simulation results can well predict the experimental results.

According to the reasons mentioned above, this research was, hence, focused on the biogas-fuelled SOFC system. The objectives of this research were:

1. To predict the boundary of carbon formation for DIR-SOFCs fueled by mixtures of methane and carbon dioxide and investigate the influences of electrolyte type, operating temperature, extent of electrochemical reaction, and steam/air addition on the carbon deposition.
2. To determine a suitable reforming agent when the fuel processor is integrated with a SOFC system fuelled by desulfurized biogas.

3. To find the best plant configuration of SOFC system fed by desulfurized biogas considering technical and economic indicators.

4. To investigate performance and thermal behavior of SOFC system fuelled by four types of feedstock; i.e. desulfurized biogas, desulfurized biogas-reformed feed, methane-reformed feed and pure-H₂ employing 1-D analysis.



ศูนย์วิจัยทรัพยากร
จุฬาลงกรณ์มหาวิทยาลัย

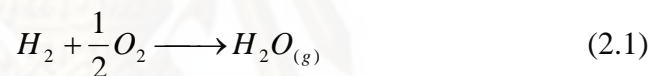
CHAPTER II

THEORY

2.1 Fuel Cell Description

2.1.1 Fundamental principle

Fuel cells are electrochemical devices that transform the chemical energy directly into electrical energy. Generally, the basic physical structure of a fuel cell consists of an electrolyte layer in contact with a porous anode on one side and a cathode on the other. Fuel cells and batteries are similar in the point of view that both of them can generate the electricity via the chemical reaction; however, the batteries must be recharged after being used up but fuel cells can be theoretically operated as long as raw fuel is continuously fed into them. Generally, most types of fuel cell are based on the following chemical reaction (Eq. 2.1).



As shown in Figure 2.1, fuel cell consists of four main components, i.e. electrolyte, anode, cathode and interconnector. The required properties for each component can be summarized as follows.

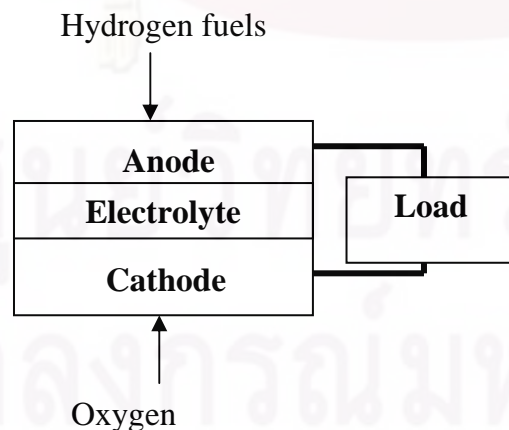


Figure 2.1 Components of a fuel cell and its operation

a) Cathode/anode

As shown in Figure 2.1, the cathode surrounded in the oxidizing atmosphere at high temperature provides pathway of electrons. Therefore, the properties that the cathode should have are presented as follows.

- High electronic conductivity
- Chemical and structural stability during operation and fabrication
- Suitable thermal expansion with other components (electrolyte and interconnector)
- Less reactivity in the vicinity of the electrolyte and interconnector
- Sufficient porosity for gas transport into the cathode

For the anode, the high electronic conductivity is also needed. Because the anode is operated in the reducing atmosphere as presented in the scheme, the required properties are different from that of the cathode. The anode should tolerate a reducing atmosphere. In some cases, the anode is used for catalytic reforming reaction in hydrocarbon-based fuelled system.

b) Electrolyte

The electrolyte provides the pathway of ion produced from electrochemical reaction at the electrodes. The required properties of electrolyte are:

- High ion conductivity
- Less electrical conductivity
- Thermal stability during operation
- Dense electrolyte for preventing gas mixing

c) Interconnector

The interconnector is the component which collects current from the SOFC cell; therefore, its required properties are:

- High electronic conductivity
- Chemical and structural stability during operation and fabrication
- Suitable thermal expansion with other components
- Less reactivity with vicinity electrolyte and interconnector

2.1.2 Type of fuel cell

Fuel cells can be categorized according to the types of electrolyte into the following five major types:

1. Proton exchange membrane fuel cell (PEMFC)
2. Alkaline Fuel Cell (AFC)
3. Phosphoric Acid Fuel Cell (PAFC)
4. Molten Carbonate Fuel Cell (MCFC)
5. Solid Oxide Fuel Cell (SOFC)

The descriptions for these types of fuel cell are summarized in Table 2.1.

Table 2.1 Descriptions for each type of fuel cell (Rayment and Sherwin, 2003):

	PEMFC	AFC	PAFC	MCFC	SOFC
Electrolyte	Ion Exchange membrane	Mobilized or Immobilized Potassium Hydroxide	Immobilized Liquid Phosphoric Acid	Immobilized Liquid Molten Carbonate	Ceramic
Operating Temperature	353 K	338-493 K	473 K	923 K	1073–1273 K
Catalyst	Pt	Pt	Pt	Ni	Perovskite
Fuels	H ₂	H ₂	H ₂	CO, H ₂	CO, H ₂ , CH ₄
Poisons	CO, S [*]	CO, CH ₄ , CO ₂ , H ₂ O, S [*]	CO, S [*]	S [*]	S [*]
Diluents	CO ₂ , H ₂ O, CH ₄	-	CO ₂ , H ₂ O, CH ₄	CO ₂ , H ₂ O	CO ₂ , H ₂ O

S^{*} = Sulfur compound for example H₂S and COS

Fuel cells have been used as electrical power generators for many stationary, mobile and portable applications. To indicate which type of fuel cell is suitable for each type of application, the operating temperature and the size of power generation can be utilized as the indices.

2.2 Solid oxide fuel cell (SOFC)

Solid oxide fuel cell is a high temperature fuel cell. Because it employed a ceramic as electrolyte, it can reduce corrosion problems which always occur in the liquid-phase electrolyte fuel cells. Due to its intermediate to high operating temperature (between 873 and 1273 K), it offers several advantages as summarized below:

- SOFC offers the highest electrical performance (electricity output to fuel input heating value ratio)
- The solid-phase electrolyte can be utilized as part of the structural members of the cells which make the SOFC stack more durable compared to liquid-phase electrolyte fuel cells.
- The internal reforming of fuel gas within the cell is possible. This promotes rapid reaction rate even with non-precious materials.
- The SOFC can generate high quality heat from the electrochemical reaction which can subsequently be utilized in other systems such as combined heat and power system and SOFC-Gas Turbine system for upgrading the plant performance.
- The SOFC can be applied in a small-scale stationary application.
- The SOFC is flexible to use various types of fuel, such as methane, methanol, ethanol, natural gas or gasoline.

The widely used electrolyte of SOFC is a solid, nonporous ceramic yttria (Y_2O_3)-stabilized zirconia (ZrO_2), which can be briefly called as YSZ. Nickel/ yttria-stabilized zirconia (Ni/YSZ) is chosen as the material in SOFC anode, hence, hydrocarbons can be reformed directly in SOFC anode. SOFC cathode is made of Sr-doped $LaMnO_3$.

2.2.1 Characteristics of SOFC

2.2.1.1 Open circuit voltage

Open circuit voltage (OCV) is the maximum possible voltage that can be achieved when operated at a specific condition. Due to different concentration of components between the anode and the cathode, this causes different potential at the

anode and cathode and results in OCV of the cell. OCV drives electrons from one electrode to another and generates current.

2.2.1.2 Overpotentials

Though the OCV is the theoretical maximum possible voltage, the actual voltage of SOFC is always less than the theoretical value due to presence of overpotentials. Overpotentials can be categorized into four types.

a) Activation overpotential

Activation overpotential is the overpotential which occurs from electrochemical reaction at the electrodes. Some energy is required as an activation energy for electrochemical reaction, e.g. adsorption of reactant on the electrode surface and desorption of product out of the surface. Normally, activation overpotential dominates at low current density and the characteristics curve also exhibits non-linear. However, at the high operating temperature like SOFC temperature, the rate of this step is very fast, resulting in small value of activation overpotentials. The linear characteristics curve can be observed.

b) Ohmic overpotential

Ohmic loss results from the resistance of flow of electrons through the electrodes and an interconnector and the resistance of flow of ion passing through an electrolyte.

c) Fuel crossover or internal current overpotential

Generally, an electrolyte should transport only ions through the cell and no fuel cross over the electrolyte. However, fuel crossing through an electrolyte or electrons leaking to an electrolyte is possible. Normally, fuel crossover loss is very small.

d) Concentration overpotential

Concentration overpotential is caused by the large reduction in concentration of fuel or oxidizing agent when operating SOFC at high current density or high fuel utilization. The difference between the concentration of gas in the bulk and the

concentration of gas on the electrode surface causes this type of overpotential. At lower fuel utilization and current density, concentration overpotential is very small.

2.2.2 SOFC system components

In the electricity generation of SOFC, some additional process equipments are required. The processes in addition to the SOFC, which is the most significant process for electric generation, are called 'balance of plant'. Normally, the SOFC system can be classified into four major sections: fuel processing section, electric generating section, heat recovery section and electric power conditioning section.

2.2.2.1 Fuel processing section

Prior to be fed to SOFC stack, hydrocarbon fuels should be pre-conditioned in the fuel processing section in order to avoid carbon formation in the SOFC stack. Considering biogas as fuel, the major equipments in fuel processor are listed below.

- A blower which is used for transporting reactants (fuels and oxidants) into equipments.
- A desulfurization process which is used in removing sulfur compounds which are prone to SOFC stack and other components.
- A vaporizer which is used in steam generation before feeding into a reformer.
- A reformer which is employed in converting hydrocarbon fuels into the hydrogen fuel for the SOFC unit.

2.2.2.2 Electric generation section

The main unit operation is an SOFC stack. The synthesis gas from the fuel processing section and the preheated air are fed to the anode and cathode, respectively. The SOFC produces DC power via electrochemical reaction.

2.2.2.3 Heat recovery section

The heat recovery system consists of heat exchangers and an afterburner used for burning unreacted fuel from the anode chamber with depleted air from the cathode chamber. The heat obtained from the afterburner is used to provide energy to other equipments. Moreover, the anode off-gas can also be used for preheating streams.

2.2.2.4 Electric power conditioning

The electric power conditioning consists of a direct current-alternating current (DC-AC) inverter which is used for converting DC into AC for actual utilization.



ศูนย์วิทยทรัพยากร
จุฬาลงกรณ์มหาวิทยาลัย

CHAPTER III

LITERATURE REVIEWS

3.1 Biogas source and its application as SOFC fuel

Up to now, fossil fuels (such as natural gas, oil, etc.) are mostly used in electricity generation due to its high heating value. The demand for fossil fuel in electrical power generation has significantly increased in the past decade due to the rapid changes in global economic activities. This upsurge in fossil fuel consumption poses serious fuel supply insecurity and increases the amount of greenhouse gases accumulating in the environment. To alleviate these problems, several environmental-friendly fuels have been proposed as alternatives to conventional fossil fuels. Biogas is an attractive fuel as it is derived renewably from the anaerobic digestion of biomass. This type of fuel is suitable for Thailand since it can be easily found as shown in Table 1.1. It mainly consists of methane (CH₄) and carbon-dioxide (CO₂), both of them are the greenhouse gas. Therefore, the usage of biogas in generating the electrical power does not only help relieve the fossil fuel shortage crisis but also diminishes the quantities of greenhouse gas released to the environment.

Table 3.1 Quantities of biomass from agricultural activities in Thailand (*Biomass Potential, Energy for Environmental Foundation, 2006*)

Agricultural product	Type of biomass	Quantities of biomass (tones per year)
Rice	Husk	100,000
Rice	Rice Straw	1,000,000
Sugar Cane	Bagasse	500,000
Rubber	Sawdust	500,000
Palm	Palm Chips	400,000
Cassava	Cassava Residue	800,000
Corn	Corn-cob	700,000

A common problem for biogas utilization is that most biogas is derived from small-scale sources, e.g. farm and municipal wastes. Hence, the use of biogas is applicable to a small-size power generation (5-100 kW) (Van Herle et al., 2004). Moreover, the biogas composition fluctuates markedly, depending on its source (Dayton, 2001). The major components of biogas derived from the anaerobic digestion process, on a dry basis, are: CH₄ (55-65%), CO₂ (30-40%), N₂ (1-10%), and less than 0.5% O₂. Trace anaerobic digester gases include up to 200 ppm H₂S, 4 ppm halogens, and other hydrocarbons.

A solid oxide fuel cell (SOFC) is an appropriate technology for generating electricity from biogas due to its high efficiency (30-40%) for small size power generations (< 20 kW) (Van Herle et al., 2004). Recently, a 100 kW class SOFC system fed by biogas has been proposed, and the electrical efficiency of almost 48.7% (Van herle et al., 2004) was reported compared to 41.5% of a conventional system (Layi Fagbenle et al., 2005). Additionally, its performance is still remarkable even at low methane contents in biogas. In laboratory test, the performance of SOFC drops only 5% when the biogas composition (CH₄:CO₂) is reduced from 70:30 to 30:70 (Jenne et al., 2002). The equimolar CO₂/CH₄ composition is the most favorite biogas composition for SOFC operation. With this feed composition, power densities up to 51.6 mW/cm² could be achieved (Goula et al., 2006). Carbon dioxide presenting in biogas could improve the direct internal reforming SOFC (DIR-SOFC) system efficiency since it aids the internal reforming in SOFC stack. However, the carbon formation is the major problem of this operation (Staniforth and Kendall, 1998).

3.2 H₂ generation reaction

3.2.1 Steam reforming

Steam reforming is the highest performance hydrogen generation reaction in term of the quantities of H₂ generated per mole of reactant. However, it is an endothermic reaction; therefore, external heat source is required. Generally, natural gas steam reforming and water gas shift reaction (WGS) can operate simultaneously at 773 K and are carried out over Ni-supported catalyst (Dicks, 1996). The major problem of steam reforming is the coke deposition on the catalyst surface. The coke generated is clogged up on the catalyst surface or in its pore which reduces its activity. There are many solutions to resolve this disadvantage. In real operation, steam to carbon ratio is set to be higher than 1.4 to maintain the catalytic activity. Air

addition can also improve the resistance to coke deposition and reduce the heat energy consumption (Dias and Assaf, 2004). In addition, adding some additives such as ceria into Ni-supported catalyst has been reported in suppressing the coke deposition (Laosiripojana et al., 2005). Alkaline earth oxides can also inhibit the coke formation when adding into Ni-supported catalyst (Takeguchi et al., 2002). For performance investigation of methane steam reforming, several works concentrated on the equilibrium calculations (Hufton et al., 1999; Ding and Alpay, 2000). The kinetic study of methane steam reforming was also carried out by Xu and Froment (Xu and Froment, 1989). The result obtained is the intrinsic rate equation of methane steam reforming which can be extensively used in the performance approximation and reformer design of reformer.

3.2.2 Dry reforming

Dry reforming or carbon dioxide reforming has been a popular method for syngas production. However, like methane steam reforming, its main problem is the coke deposition on catalyst surface. The carbon deposition in dry reforming is more severe than that in steam reforming (Edwards and Maitra, 1995). It was suggested the use of excess CO_2 for the dry reforming can reduce the prone to coke formation (Assabumrungrat et al., 2006). Nickel and cobalt are usually applied as the catalysts for this reaction. Modifications of the catalysts by adding additives such as alkaline-earth metal oxides and noble metals such as Pt, Ni and Ru showed a major improvement on the catalytic stability by reducing the metal oxidation and coke deposition (Bouarab et al., 2004; Nagaoka et al., 2004). Effect of promoters such as Cu, La and Mo in the Ni catalysts supported on Al_2O_3 for methane dry reforming was also investigated and the results showed that all these promoters can improve both the activity and stability of the catalyst (Xiao et al., 2003; Lee et al., 2004; Martinez et al., 2004). In the performance analysis, both equilibrium model and kinetic model can be utilized. For the kinetic study, all kinetic parameters of dry reforming are estimated and the rate determining step is also indicated (Cui et al., 2006). These kinetic models are the important tools for the reformer design.

3.2.3 Partial oxidation and autothermal reforming

Partial oxidation is the interesting syngas processing reaction because it can produce syngas without relying on heat from other sources. It can be carried out at

high temperature without the use of catalyst (Docter and Lamm, 1999). This feature of partial oxidation implies that it can handle much heavier petroleum fractions than other catalytic reactions and is therefore suitable in case that diesels or logistic fuels play a role as fuel. However, the quantities of H_2 generated from partial oxidation per mole of fuel are less than those produced from steam reforming reaction. In high temperature operation, some soot can normally generate but it can be removed in a separate scrubber (Joensen and Rostrup-Nielsen, 2002). Catalytic partial oxidation can also take place. Its residence times are very short, in order of milliseconds (Hickman and Schmidt, 1992). For natural gas conversion, the catalysts used in partial oxidation are Ni and Rh. The selectivities obtained are higher than 90% and the 90% conversion can be achieved (Bharadwaj and Schmidt, 1994; Tornaiainen et al., 1994). The other side reactions comprise of further oxidation of hydrogen and carbon-monoxide product.

Autothermal reforming is the combination of the exothermic partial oxidation and endothermic steam reforming. With the proper oxygen to carbon ratio and steam to carbon ratio, the partial combustion can supply the heat for the endothermic steam reforming. Dvorak et al. (1998) determined the relatives of the steam reforming and the partial oxidation and the results showed that the oxidation reaction became equilibrium faster than the steam reforming over Ni catalyst. However, over supported ruthenium catalysts, both oxidation reaction and partial oxidation occur in parallel.

3.3 SOFC modeling

3.3.1 Electrochemical model

The set of mathematical models which is called “electrochemical model” is a necessary tool for the SOFC system design and performance analysis. In the electrochemical model, the correlations used in the calculation of overpotentials in SOFC are given. The overpotentials could be divided into three major types; i.e., activation overpotential, ohmic overpotential and concentration overpotential. Several expressions are proposed to predict the activation overpotential; e.g. semi-correlation model (Achenbach, 1994), Butler-Volmer equation (Larminie and Dicks, 2003), Tafel equation, etc. The comparison of these correlations was investigated by Hernandez-Pacheco et al. (Hernández-Pacheco et al., 2005). It was found that Butler-Volmer was the best model which gives only 5% error related to the experimental result. The

semi-correlation model could well predict the activation loss at the temperature range of 1173-1273 K. The activation overpotential is found in both cathode and anode; however, the activation overpotential of cathode is higher than that of anode due to the lower exchange current density of the former. The activation overpotential significantly increases with current density at low current density and gradually increases at high current density (Chan and Xia, 2002). The activation overpotential vary with current density and anode thickness but inverse to hydrogen molar fraction (Costamagna et al., 2004). Moreover, the addition of H₂O in fuel stream diminished the activation overpotential since H₂O could enhance the dissociative adsorption/diffusion of H₂ on the electrode surface (Jiang and Badwal, 1997; Jiang and Badwal, 1999). For intermediate temperature direct internal reforming (IT DIR-SOFC); cathode activation overpotential represents the major sources of voltage loss for co-flow operated at steady state condition (Aguilar et al., 2004). Considering the ohmic overpotential, it was found that the electrical conductivities of the interconnection and electrodes are extremely higher compared with that of the electrolyte. Hence, their influences on the ohmic overpotential can be neglected (Ferguson et al., 1996; Ni et al., 2007). For concentration overpotential, several models; i.e., Dusty gas model, Stefan-Maxwell and Fick's law were proposed to explain it. The investigation of these concentration loss model was conducted (Suwanwarangkul et al., 2003). It was found that Dusty gas model can well predict the concentration loss due to the presence of Knudsen effect. Moreover, the dimension and size of the anode pore also affects the concentration loss.

3.3.2 Macro-modelling

In SOFC system investigation, the electrochemical model given in Section 3.3.1 is employed in macro-modelling. There are several macro-modelling approaches based on their complexities (Bove and Ubertini, 2006). In this study, two approaches are considered; i.e. zero-dimensional analysis and one-dimensional analysis.

3.3.2.1 Zero-dimensional analysis

Zero-dimensional analysis which could be so-called "black box model" was the simplest method for the performance evaluation of SOFC stack. This kind of approach could save computational time while maintaining an acceptable accuracy in the SOFC performances evaluation. With this approach, the variation of operating

condition, compositions of anode and cathode gases and power density with cell dimension were not taken into account. SOFC model was considered as one black box including the sets of mathematic equation. A zero-dimensional model could be developed to investigate the impact of inlet composition, fuel utilization, operating temperature and operating pressure on the performance of an SOFC in terms of efficiency and characteristic curve. This black box model was always employed in the investigation of SOFC based energy systems, e.g. SOFC-GT (combined SOFC and gas turbine) system, SOFC-CHP (combined heat and power system), etc. In these systems, several unit operations, i.e. SOFC, compressor, fuel processor, burner were simulated using independent box models and the results of each box is the input of the next box (Costamagna et al., 2001). Lunghi and Ubertini (2001) have used a zero-dimensional model in studying the performance of different SOFC-GT systems. The inputs of the calculations consist of operating temperature, operating pressure, inlet gas flow rate, gas composition and fuel utilization. Bove et al. (2005) have studied in the change of the characteristic curve with inlet and outlet gas compositions employing zero-dimensional approach.

3.3.2.2 One-dimensional (1-D) analysis

In 1-D analysis, only one geometry dimension of SOFC cell is considered. This indicates that the variations of all operating conditions and gas compositions in the other dimensions are neglected. This kind of approach can be employed in calculating the power density and temperature distribution along the cell length. Temperature distribution along the cell length should also receive closer attention since large amount of heat could generate in the electrochemical process. With inappropriate operating conditions, solid part in SOFC stack may be damaged due to extremely increase in its temperature. At the present state-of-the-art of SOFC, YSZ using as an electrolyte material, the maximum allowable temperature gradient is around 10 Kcm^{-1} (Lim et al., 2005). A selection of suitable feedstock for SOFC is also an interesting issue in thermal consideration. Although the use of pure- H_2 as SOFC feed can offer high power density, its rapid electrochemical reaction may cause high temperature gradient in solid part of SOFC. One dimensional analysis (1-D analysis) is an attractive technique to investigate the thermal behavior of SOFC stack. Sorrentino et al. (Sorrentino et al., 2008) have employed 1-D analysis in investigating temperature and current density profiles in the flow direction of planar SOFC fed by

reformed gas. The results obtained from the simulation shows the good level of accuracy compared with the experimental results. The investigation on the operation of indirect internal reforming SOFC (IIR-SOFC) fed by methane employing 1-D analysis is performed by Lim et al. (Lim et al., 2005). The results indicated that the temperature gradient of SOFC is extremely high at the exit of anode section (entrance of reforming section) due to high extent of endothermic steam reforming reaction. Several methods were also proposed in this literature to minimize the temperature gradient of SOFC, i.e. catalyst activity reduction, the use of nonuniform distributed catalyst and autothermal reforming.

Aguilar et al. (2002) have studied on the thermal behavior of IIR-SOFC towards the change in catalyst activity, fuel inlet temperature, current density and operating pressure utilizing 1-D analysis. It was concluded that the increase in operating pressure can diminish both temperature gradient and overall temperature of IIR-SOFC due to the inhibition in reforming reaction rate and the improvement of electrochemical reaction rate. The deeply details of the SOFC temperature gradient reduction by minimize the catalyst activity was also given by Aguilar et al. (Aguilar et al., 2004). With this idea, less active catalyst is used in the reforming chamber of IIR-SOFC, therefore, the local cooling effect caused from the reforming reaction is inhibited. However, the local cooling also generates, causing from the reforming reaction of unreacted methane at the entrance of the anode chamber. The results indicated that considerable decrease in temperature gradient can be achieved by reducing reforming activity of catalyst in both reforming chamber and anode chamber.

3.4 Palladium membrane reactor and its application in SOFC system

In general, the performance of SOFC depends on the composition of fuel gas fed to the anode chamber of SOFC. Baron et al. (2004) have reported that the presence of methane in the SOFC feed decreased the SOFC performance due to carbon deposition and partial blocking of anode pores. Likewise, the SOFC performance also decreases as the amount of carbon monoxide in anode feed gas increases due to increases in activation and concentration polarizations (Eguchi et al., 2002; Baron et al., 2004). The presence of carbon dioxide could also lower the SOFC performance via the reverse water gas shift reaction (RWGS) (Suwanwarangkul et al., 2006). From these reasons, pure hydrogen seems to be an ideal fuel for SOFC;

however, it is not available in natural resources. Various types of fuels such as alcohols, natural gas, coal and petroleum-based compounds may be used to produce hydrogen. Considering the conventional hydrogen generator fuelled by biogas, the presence of carbon dioxide (30-40 mol%) in biogas inhibits the production of H₂ due to the effect of the RWGS. Effendi et al. (Effendi et al., 2005) proposed the installation of high-temperature and low-temperature shift reactors with the biogas-fed reformer. They showed that hydrogen product with the purity of 68 mol% can be achieved. To remove carbon dioxide, an adsorption unit can be employed but requires high running costs.

The use of a hydrogen-selective membrane reactor can offer pure hydrogen with high methane conversion. A suitable membrane is chosen based on its ability to offer high hydrogen permeability and selectivity. Although some polymeric membranes can offer high hydrogen selectivity, they cannot be operated at high temperatures necessary for steam reforming reaction. An inorganic membrane particularly a palladium membrane is a preferred choice due to its high selectivity of hydrogen (Lu et al., 2007). The use of palladium membrane reactors (the combined palladium membrane and steam reforming reactor) for hydrogen-generating reactions has been widely investigated (Basile et al., 2003; Gallucci et al., 2004; Patel and Sunol, 2007). Under this operation, hydrogen gas produced in the reaction side permeates through the palladium membrane to the permeation side where pure hydrogen is collected. The simultaneous removal of hydrogen from the reaction side helps improve the reaction conversion. The increase in the operating pressure at permeation side can improve the methane conversion. Moreover, the methane conversion in palladium membrane reactor also varies with membrane thickness, reactor length and operating temperature (Gallucci et al., 2004). The palladium membrane reactor could offer higher methane conversion yield and could be operated under milder conditions than the conventional fixed bed reformer (Fernandes and Soares Jr, 2006).

When pure hydrogen instead of a conventional reformed gas is fed to an SOFC, a superior SOFC performance is reported (Suwanwarangkul et al., 2006). Sangtongkitcharoen et al. (2008) analyzed performance of methanol-fueled solid oxide fuel cell system incorporated with a palladium membrane reactor. It was demonstrated that when the membrane reactor (operated under high pressure compressor mode) is employed, the maximum power density was about 13% higher

than that from the system with the conventional reformer. Comparison between the two SOFC systems which provide the same net electrical efficiency indicates that the SOFC system with the membrane reactor requires a smaller SOFC stack than the conventional SOFC system. However, the former requires an extra cost on palladium membranes and extra electrical power for operating the compressor for the membrane reactor. Preliminary economic analysis reveals that the use of the membrane reactor to the SOFC system is not cost-effective due to high cost of palladium membranes. A further study was carried out for methane-fed SOFC systems considering three operation modes of membrane reactors; i.e., high pressure compressor, combined low pressure compressor and vacuum pump and combined high pressure compressor and vacuum pump (Vivanpatarakij et al., 2009). Their overall SOFC system characteristics are compared with those of the SOFC system with the conventional reformer. The economic analysis reveals that the total capital cost/net electrical power is dependent on hydrogen recovery, net electrical efficiency and operation mode. At high electrical efficiency, the replacement of the conventional reformer with the membrane reactor becomes attractive. It was also demonstrated that the combined high pressure compressor and vacuum pump is the best operation mode for integration with the SOFC system. However, this work did not take into account the thermal management within the integrated systems.

3.5 CO₂ separation technology

Currently, there are various available CO₂ separation technologies e.g. chemical absorption, adsorption and membrane technology (Gottlicher and Pruscsek, 1997). For the absorption technology, a chemical solvent such as monoethanolamine is used to absorb CO₂ in absorber and CO₂ is then released from the solvent at stripper. The energy demand in the absorber comprises of the compression and pumping of the solvent which consume about 0.03 kWh per kg CO₂ removed from the gas (Condorelli et al., 1991). When considering the energy consumption for the stripper (Regeneration process), it consumes about 0.34 kWh per kg CO₂ removed (Smelser et al., 1991).

Membrane technology has been widely tested and presently applied in the capture of CO₂ in natural gas (Granite and O'Brien, 2005). Compared with CO₂ absorption technology which is conventionally used, membrane technology offers the

advantages of operational flexibility in handling feed streams with variable flow rates and compositions. Polymeric membrane is one of the interesting choices due to its low capital investment costs compared with other types of membrane (Alexander Stern, 1994). Moreover, the process equipment for the polymeric membrane operation is also simple and easy to handle. Selection of polymeric membrane for gas separation is based on two parameters; permeability and permselectivity. Polyimide membrane is the more attractive gas separator because it offers higher permselectivity and permeability compared to membranes derived from other polymers (Shekhawat et al., 2003). The use of capillary module with polyimide membrane for the CH₄ enrichment in biogas mixtures (CH₄, CO₂ and H₂S) was also investigated and the results showed that CH₄ concentration in biogas increases from 55-85% up to 91-94.4% (Harasimowicz et al., 2007). Poly(dimethylsiloxane) (PDMS) and poly(1-trimethylsilyl-1-propyne) (PTMSP) can be utilized in the separation of acid gases (CO₂ and H₂S) from syngas at room temperature due to their high CO₂/H₂ selectivity. Nonetheless, H₂ permeance increases at elevated temperature (Merkel et al., 2001). It should be noted that a common problem arising from the use of these polymeric membranes is the instability of the membranes at high operating temperature (Amelio et al., 2007). For the energy consumption using membrane technology, it is in the range of 0.04-0.07 kWh/kg CO₂ in case of a shifted coal-derived fuel gas. CO shift reaction coupled with membrane reactor can diminish the energy losses owing to the lower steam demand in the syngas processing part (Bracht et al., 1996).

The other CO₂ separation technology which is under development is the removal of CO₂ by the carbonation of CaO to CaCO₃. The kinetic of carbonation reaction is studied by Lee et al (2004). The results indicate that the kinetic model for this reaction is distinguished into two regimes; chemical reaction control regime and diffusion control regime. The activation energy in the carbonation of the mesoporous CaO and CO₂ is 72 kJ/mol and 102.5 kJ/mol for chemical reaction control regime and diffusion control regime, respectively. The circulating fluidized bed is the interesting operation for the CaO-CO₂ carbonation reaction since the CO₂ capture process can take place continuously and CaO particle can be recycled (Grasa et al., 2008). However, make-up CaO is required to be fed to CaO-CO₂ acceptor due to sintering of CaO sorbent after several cycles of carbonation-calcination (Abanades, 2002; Grasa et al., 2008) and operating cost also increases. As this technology is installed in the fuel processing section, not only CO₂ is captured but also the partial pressure of H₂ in

reformato increases due to the forward shift of water gas shift reaction (Balasubramanian et al., 1999; Lee et al., 2006; Wang et al., 2006). The combined operation of the carbonation reaction, methane steam reforming reaction and H₂-selective membrane (palladium membrane) is also studied by Chen et al (Chen et al., 2008). This operation could provide very high hydrogen yields. Moreover, the heat supply is not required for the reformer since the heat released from the exothermic carbonation reaction could compensate the heat demand in endothermic steam reforming reacton. The overall heat required in this process would be supplied to a separate calciner performing as a sorbent regenerator. Vivanpatarakij et al. (2008) studied on the use of CaO-CO₂ acceptor in methane-fuelled SOFC system. It is found that the removal of CO₂ from syngas prior to be fed to SOFC stack can improve SOFC performance. Nevertheless, this configuration is not superior in environmental point of view since CO₂ generated in SOFC stack via WGS reaction cannot be captured and must be released to the environment. The use of the carbonation of CaO in the phosphoric acid fuel cell (PAFC) system have also been examined (Iordanidisa et al., 2006). The results imply that PAFC can operate at high-efficiency mode despite of the high carbon to hydrogen ratio of bio-fuel.

CHAPTER IV

MODELLING

This chapter presents all mathematical models and calculation procedures used in the performance evaluation of solid oxide fuel cell (SOFC) fuelled by biogas. Several unit operations; e.g., fuel processor, palladium membrane reactor, CO₂ separator, heater, cooler, afterburner, vaporizer, etc., are included in this consideration to calculate the actual performances of different SOFC systems. The correlations used in the calculation of the boundary of carbon formation of SOFC with different electrolytes are given in this chapter. Costing models, expressions and parameters used in the economic consideration is also presented in this chapter. It should be noted that all mathematical models used in this study are written in Visual Basic. The ideal gas is assumed in the thermodynamic calculation in this study.

4.1 SOFC modelling

In this section, the electrochemical model and the calculation procedures are given. The calculations are classified into two levels of consideration; i.e., zero-dimensional analysis and one-dimensional analysis. In zero-dimensional analysis, mass balance, energy balance and electrochemical performance evaluation of SOFC stack take place without the consideration of cell dimension. For one-dimensional analysis, temperature profiles and power density profiles in SOFC cell are computed in order to examine the operating viability and the performance of SOFC.

4.1.1 Electrochemical model

In this section, equations used for calculating SOFC performances (e.g. open circuit voltage, overpotentials, power density, power, electrical efficiency) are presented. It should be noted that, for the SOFC stack, Ni-YSZ, YSZ and LSM-YSZ are used as the materials in the anode, electrolyte and cathode, respectively. The parameters of SOFC stack and operating conditions used in the calculation is given in Table 4.1.

4.1.1.1 Open circuit voltage

The open circuit voltage (E) of the cell can be calculated from the Nernst equation which is expressed as:

$$E = E^0 + \frac{RT}{2F} \ln \left(\frac{P_{H_2} P_{O_2}^{\frac{1}{2}}}{P_{H_2O}} \right) \quad (4.1)$$

The actual cell potential (V) is always less than the open circuit voltage (E) owing to the existence of overpotentials as shown in Eq. (4.2). The overpotentials can be categorized into three main sources: ohmic overpotential (η_{ohm}), activation overpotential (η_{act}) and concentration overpotential (η_{conc}).

$$V = E - \eta_{act} - \eta_{ohm} - \eta_{conc} \quad (4.2)$$

Table 4.1 Summary of model parameters (Ni et al., 2007).

<i>Parameters</i>	<i>Value</i>
n	0.48
ξ	5.4
D_p	1 μm
d_a	750 μm
d_c	50 μm
L	50 μm
T_{SOFC}	1073 K
P_{SOFC}	1 bar

4.1.1.2 Overpotentials

In the calculation, overpotentials are categorized into three major types; i.e., ohmic overpotential, activation overpotential and concentration overpotential.

a) Ohmic overpotential (η_{Ohm})

This overpotential is the resistance to flow of electron through the electrodes and the interconnections as well as resistance to the flow of ions through electrolyte. This voltage drop is the vital one in all types of cells and is linearly proportional to

current density (i). Due to the higher electronic conductivity of the electrodes compared to the electrolyte, only ohmic overpotential in the electrolyte is concerned. Hence, the ohmic overpotential of SOFC can be expressed by (Ferguson et al., 1996):

$$\eta_{ohmic} = 2.99 \times 10^{-11} iL \exp\left(\frac{10300}{T}\right) \quad (4.3)$$

b) Activation overpotential (η_{Act})

Activation overpotential is controlled by the kinetics at the electrode surface. It is directly related to the activation barrier to be overcome by the reacting species in order to conduct the electrochemical reaction. The electrode reaction rate at high temperatures is fast, leading to low activation polarization as normally observed in SOFC.

These activation overpotentials in electrodes can be expressed by the Butler-Volmer equation,

$$i = i_0 \left[\exp\left(\frac{\alpha z F \eta_{act}}{RT}\right) - \exp\left(-\frac{(1-\alpha) z F \eta_{act}}{RT}\right) \right] \quad (4.4)$$

In case of SOFC, α and z are set to 0.5 and 2 (Chan et al., 2001). Therefore, the activation potential at the anode and cathode can be explicitly written as:

$$\eta_{act,m} = \frac{RT}{F} \sinh^{-1}\left(\frac{i}{2i_{0,m}}\right), \quad m = a, c \quad (4.5)$$

The exchange current density (i_0) for the anode side depends on partial pressure of both hydrogen and water as well as the operating temperature (Jiang and Badwal, 1997; Jiang and Badwal, 1999). For the cathode side, i_0 depends on oxygen partial pressure and operating temperature as expressed in Eqs. (4.6)-(4.7) (Fleig, 2003). The values of all parameters used in the calculation of i_0 are given in Table 4.2.

$$i_{0,a} = \gamma_a \left(\frac{P_{H_2}}{P_{ref}}\right) \left(\frac{P_{H_2O}}{P_{ref}}\right) \exp\left(-\frac{E_{act,a}}{RT}\right) \quad (4.6)$$

$$i_{0,c} = \gamma_c \left(\frac{p_{O_2}}{P_{ref}} \right)^{0.25} \exp \left(- \frac{E_{act,c}}{RT} \right) \quad (4.7)$$

Table 4.2 Summary of activation polarization parameters (Ni et al., 2007).

Parameter	Value
γ_a (A m ⁻²)	1.344×10^{10}
γ_c (A m ⁻²)	2.051×10^9
$E_{act,a}$ (J mol ⁻¹)	1.0×10^5
$E_{act,c}$ (J mol ⁻¹)	1.2×10^5

c) Concentration overpotential (η_{Conc})

The concentration overpotential is the electrical loss owing to the difference between the reactant concentration on the reaction site and that in the bulk of the gas stream. This is due to the effect of the diffusion of the reactant gas into the pore of the electrochemical catalyst. It can be calculated by Eqs. (4.8) and (4.9):

$$\eta_{Conc,a} = \frac{RT}{2F} \ln \left[\frac{\left(1 + \left(\frac{RT}{2F} \right) \left(\frac{l_a}{D_{a(eff)} p_{H_2O}^I} \right) i \right)}{\left(1 - \left(\frac{RT}{2F} \right) \left(\frac{l_a}{D_{a(eff)} p_{H_2}^I} \right) i \right)} \right] \quad (4.8)$$

$$\eta_{Conc,c} = \frac{RT}{4F} \ln \left[\frac{p_{O_2}^I}{(P_c - \delta_{O_2}) - ((P_c - \delta_{O_2}) - p_{O_2}^I) \exp \left[\left(\frac{RT}{4F} \right) \left(\frac{\delta_{O_2} l_c}{D_{c(eff)} P_c} \right) i \right]} \right] \quad (4.9)$$

where δ_{O_2} , $D_{a(eff)}$ and $D_{c(eff)}$ can be expressed by:

$$\delta_{O_2} = \frac{D_{O_2,k(eff)}}{D_{O_2,k(eff)} + D_{O_2-N_2(eff)}} \quad (4.10)$$

$$\frac{1}{D_{c(eff)}} = \frac{\xi}{n} \left(\frac{1}{D_{O_2,k}} + \frac{1}{D_{O_2-N_2}} \right) \quad (4.11)$$

$$D_{a(eff)} = \left(\frac{P_{H_2O}}{P_a} \right) D_{H_2(eff)} + \left(\frac{P_{H_2}}{P_a} \right) D_{H_2O(eff)} \quad (4.12)$$

$$\frac{1}{D_{H_2(eff)}} = \frac{\xi}{n} \left(\frac{1}{D_{H_2,k}} + \frac{1}{D_{H_2-H_2O}} \right) \quad (4.13)$$

$$\frac{1}{D_{H_2O(eff)}} = \frac{\xi}{n} \left(\frac{1}{D_{H_2O,k}} + \frac{1}{D_{H_2-H_2O}} \right) \quad (4.14)$$

The correlation between the effective parameter and the normal parameter can be expressed by Eq. (4.15)

$$D_{(eff)} = \frac{n}{\xi} D \quad (4.15)$$

Knudsen diffusivity can be computed by the correlation below:

$$D_{i,K} = 9700r \sqrt{\frac{T}{M_i}} \quad (4.16)$$

Ordinary diffusivity can be calculated by Chapman-Enskog equation (Eq. (4.17)) (Massman, 1998):

$$D_{A-B} = 1.8583 \times 10^{-3} \left(\frac{T^{\frac{3}{2}} \left(\frac{1}{M_A} + \frac{1}{M_B} \right)^{\frac{1}{2}}}{P \sigma_{AB}^2 \Omega_D} \right) \quad (4.17)$$

where σ_{AB} is the collision diameter (\AA) which is equal to $\frac{\sigma_A + \sigma_B}{2}$. Ω_D is computed from (Yakabe et al., 2000):

$$\Omega_D = \frac{A}{T_k^B} + \frac{C}{\exp(D \cdot T_k)} + \frac{E}{\exp(F \cdot T_k)} + \frac{G}{\exp(H \cdot T_k)} \quad (4.18)$$

where T_k is equal to $\frac{T}{\varepsilon_{AB}}$ and A, C, E and G are constants for each gas.

Table 4.3 The parameters used in collision integral computation (Yakabe et al., 2000).

Parameter	A	B	C	D	E	F	G	H
Value	1.06036	0.15610	0.19300	0.47635	1.03587	1.52996	1.76474	3.89411

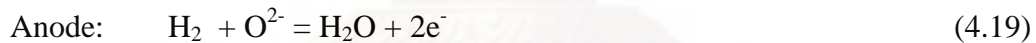
4.1.2 Zero-dimensional analysis

The details for the calculation of zero-dimensional analysis consist of mass balance, energy balance and calculation procedure.

4.1.2.1 Mass balance equations

Theoretically, two types of solid electrolytes can be employed in the SOFC; i.e., oxygen ion- and proton-conducting electrolytes. The reactions taking place in the anode and the cathode can be summarized as follows.

Oxygen ion-conducting electrolyte:



Proton-conducting electrolyte:



The difference of the SOFCs with two electrolyte types is the location of the water produced. For the SOFC with the oxygen ion-conducting electrolyte (SOFC-O²⁻), water is produced in the anode chamber whereas it appears in the cathode chamber for the SOFC with the proton-conducting electrolyte (SOFC-H⁺). In this study, only SOFC-O²⁻ is considered since it could offer superior actual voltage and power density compared with SOFC-H⁺ (Jamsak et al., 2007). The mass balance takes place for each small fuel utilization region.

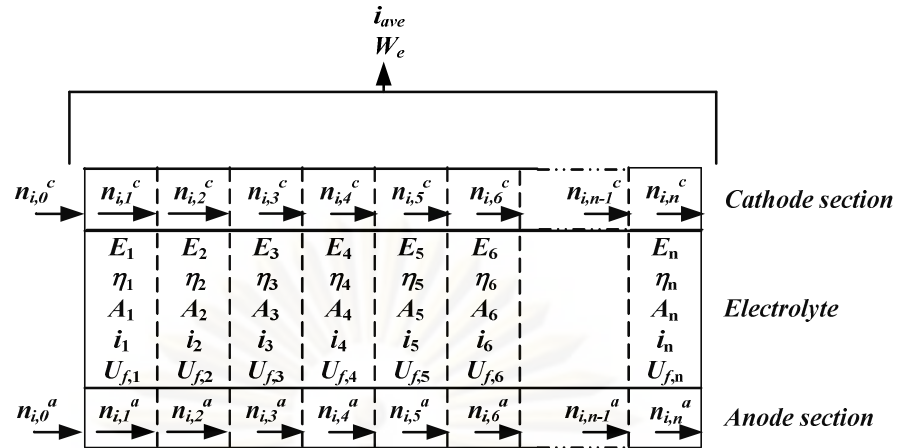


Figure 4.1 The scheme showing the zero-dimensional analysis of SOFC.

The number of moles of each component entering each fuel utilization region is given by the following expressions:

For anode's components

$$n_{CH_4,f+1}^a = n_{CH_4,f}^a - x_{steam,f}^a \quad (4.23)$$

$$n_{CO_2,f+1}^a = n_{CO_2,f}^a + x_{WGS,f}^a \quad (4.24)$$

$$n_{CO,f+1}^a = n_{CO,f}^a + x_{steam,f}^a - x_{WGS,f}^a \quad (4.25)$$

$$n_{H_2,f+1}^a = n_{H_2,f}^a + 3x_{steam,f}^a + x_{WGS,f}^a - e_f \quad (4.26)$$

$$n_{inert,f+1}^a = n_{inert,f}^a \quad (4.27)$$

$$n_{H_2O,f+1}^a = n_{H_2O,f}^a - x_{steam,f}^a - x_{WGS,f}^a + e_f \quad (4.28)$$

$$n_{total,f}^a = \sum_{i=1}^6 n_{i,f}^a \quad (4.29)$$

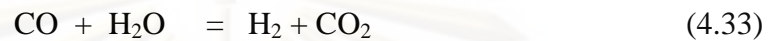
For cathode's components

$$n_{O_2,f+1}^c = n_{O_2,f}^c - 0.5e_f \quad (4.30)$$

$$n_{N_2,f+1}^c = n_{N_2,f}^c \quad (4.31)$$

where $n_{CH_4,f}^a$, $n_{H_2O,f}^a$, $n_{CO_2,f}^a$, $n_{H_2,f}^a$ and $n_{CO,f}^a$ represent moles of methane, steam, carbon dioxide, hydrogen and carbon monoxide, respectively, at fuel utilization

region f of anode section of SOFC, and $n_{O_2,f}^c$ and $n_{N_2,f}^c$ represent moles of oxygen and nitrogen, respectively, at fuel utilization region f of cathode section of SOFC. $x_{steam,f}^a$, $x_{WGS,f}^a$ and e_f stand for the converted moles associated to the steam reforming reaction (Eq. (4.32)), water gas shift reaction (WGS) (Eq. (4.33)) and electrochemical reaction (Eq. (4.19)), respectively.



Only hydrogen is assumed to react electrochemically with oxygen ions. It was observed that the H_2 electro-oxidation is much faster than the CO electro-oxidation (Khaleel et al., 2004) and in addition the rate of WGS reaction is fast at high temperatures (Blom et al., 1994; Swaan et al., 1994; Bradford and Vannice, 1996). It is also assumed that little amount of methane remaining from the fuel processor is consumed via the steam reforming and that the anode compositions always reach their equilibrium along the cell length due to the fast kinetics at high temperature. Therefore, $x_{ref,f}^a$ and $x_{WGS,f}^a$ are calculated employing the following equations:

$$p_{i,f} = \frac{n_{i,f}}{n_{tot,f}} P \quad (4.34)$$

$$K_{steam,f} = \frac{P_{H_2,f}^3 P_{CO,f}}{P_{CH_4,f} P_{H_2O,f}} \quad (4.35)$$

$$K_{WGS,f} = \frac{P_{CO_2,f} P_{H_2,f}}{P_{CO,f} P_{H_2O,f}} \quad (4.36)$$

where $p_{i,f}$, $K_{ref,f}$ and $K_{WGS,f}$ represent partial pressure of component i , equilibrium constant of reforming reaction and equilibrium constant of WGS reaction at fuel utilization region f .

4.1.2.2 Energy balance equation

For energy balance around SOFC stack, the heat loss to the environment is neglected. The energy equation takes place around the SOFC stack as presented in Eq. (4.37).

$$0 = H_{fuel,in} + H_{air,in} - H_{fuel,out} - H_{air,out} - W_e \quad (4.37)$$

The isothermal operation is assumed for the electrochemical reaction. To achieve a desired temperature of the SOFC stack, heat generated in the SOFC stack due to the irreversibility is utilized for air and H₂-rich gas preheating.

4.1.2.3 Calculation procedure

The flowchart of the program used in zero-dimensional analysis is shown in Figure 4.2. The mathematical models were programmed using Visual Basic. The desired values of anode and cathode inlet flow rate of each gas component ($n_{i,0}^a$ and $n_{i,0}^c$), operating voltage (V), final fuel utilization ($U_{f,final}$) and fuel utilization step size (ΔU_f) are initially input into the program. The calculation begins at the entrance of the anode chamber where U_f is equal to zero. The mass balance of each component is firstly calculated in the first fuel utilization region employing the sets of equation given in Section 4.1.2.1. It should be noted that the extent of electrochemical reaction ($x_{e,f}$) at each fuel utilization region is always equal to ΔU_f . Subsequently, the electrochemical calculation performs using the sets of equations shown in Section 4.1.1. Open circuit voltage (E) is initially computed. The trial and error of current density (i) takes place until the difference between E and total overpotentials is equal to the operating voltage (V). SOFC area of this fuel utilization region (A_f) is then calculated using the following equation:

$$A_f = \frac{2F(\Delta U_f)}{i_f} \quad (4.38)$$

The value of $U_{f,f}$ is checked whether it reaches the $U_{f,final}$ or not. If $U_{f,f}$ is still lower than $U_{f,final}$, the mass balance and electrochemical calculation are then re-calculated with a new $U_{f,f}$. The iteration runs until $U_{f,f}$ is equal to $U_{f,final}$ which means

that SOFC operate till it meets the desired value of $U_{f,final}$. The performances of SOFC are then achieved by electrochemical model. A_f derived from the calculation at each fuel utilization region are added up to achieve total SOFC area (A_{total}).

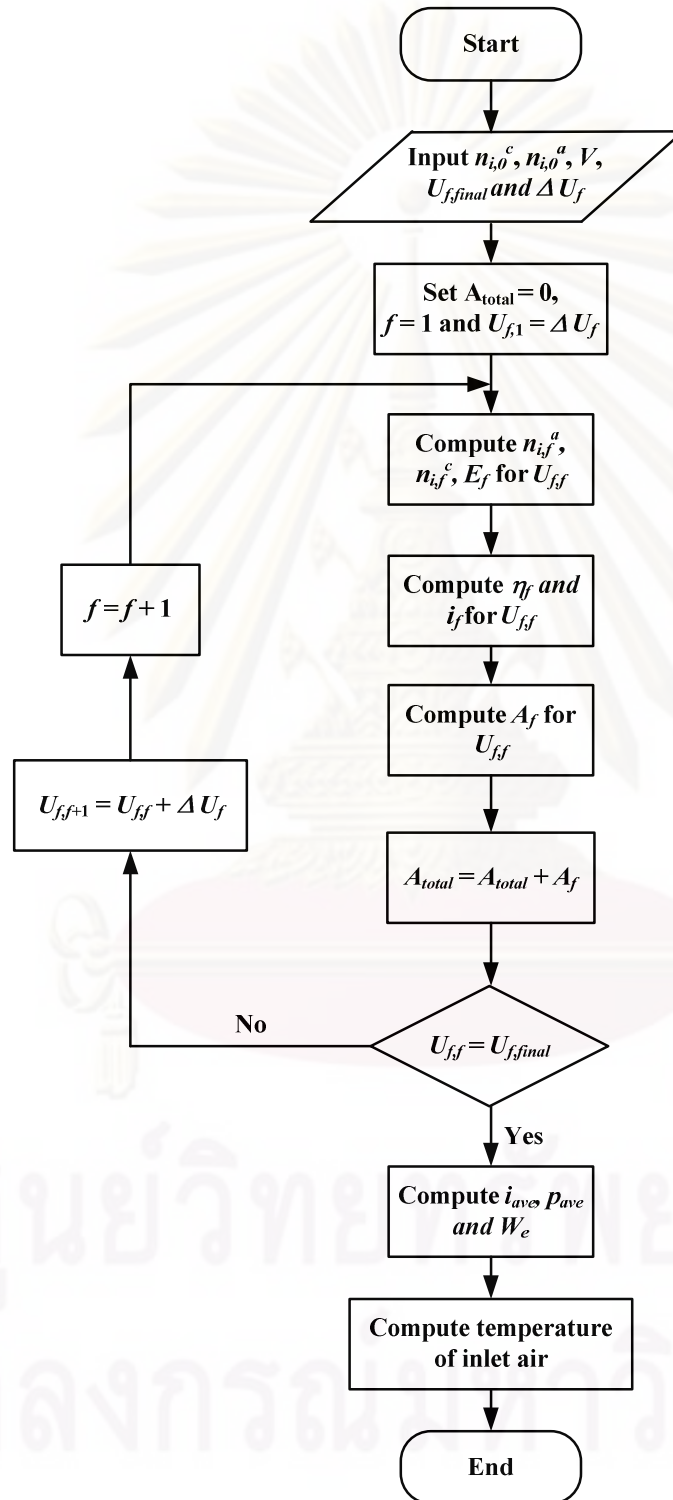


Figure 4.2 The flowchart of the program used in zero-dimensional analysis of SOFC.

Average current density (i_{ave}), average power density (p_{ave}) and total electricity (W_e) are also computed employing Eqs. (4.39), (4.40) and (4.41), respectively. Finally, energy balance around SOFC stack take place. Temperature of air inlet is tuned up until total energy input of SOFC is equal to total energy output of SOFC.

$$i_{ave} = \frac{2F(U_{f,final})}{A_{total}} \quad (4.39)$$

$$p_{ave} = i_{ave}V \quad (4.40)$$

$$W_e = \frac{P_{ave}}{A_{total}} \quad (4.41)$$

For model validation, the computed results are compared with the experimental results of Zhao et al. (2005) and Tao et al. (2005). The feed compositions and the SOFC stack dimensions used in model validation are summarized in Table 4.4. As shown in Figure 4.3, the simulation shows good agreement with the experimental data using pure hydrogen fuel (Zhao and Virkar, 2005) for all temperature levels particularly at the operating temperature of 1073 K which is used in the subsequent studies of this work. Moreover, with inlet gas containing various fuel types ($\text{CH}_4\text{-CO-H}_2$), the simulation could also predict the experimental data (Tao et al., 2005) well as illustrated in Figure 4.4.

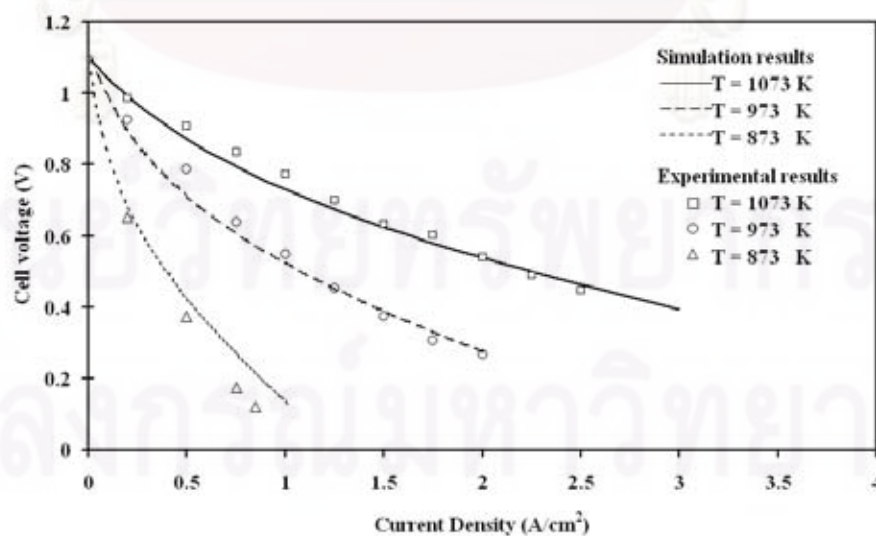
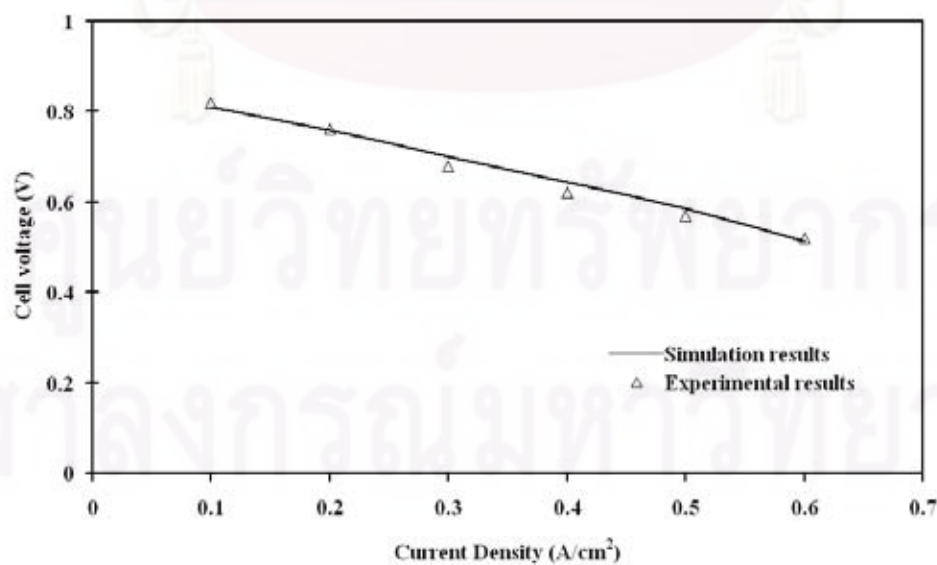


Figure 4.3 Verification of SOFC model for pure hydrogen fuel.

Table 4.4 Feed compositions and SOFC stack dimensions used in model validation.

Parameters	Zhao et al. (2005)	Tao et al. (2005)
Fuel compositions (Mole fraction):		
CH ₄	-	0.21
H ₂	0.97	0.4
CO	-	0.2
CO ₂	-	0.18
N ₂	-	0.01
H ₂ O	0.03	-
Stack dimensions:		
Type of cell	Button cell	Planar SOFC with 100 cm ² active surface area
n	0.48	0.48
ξ	5.4	5.4
D_p	1 μm	1 μm
d_a	750 μm	500 μm
d_c	50 μm	50 μm
L	50 μm	10 μm
Stack average temperature	873-1073 K	1073 K

**Figure 4.4** Verification of SOFC model for the feed with CH₄, CO and H₂ mixtures.

The model is further verified with the simulation results for the case with a lower concentration of hydrogen. Based on the condition listed in Table 4.5, the results shown in Table 4.6 indicate that the calculation results from our model are in good agreement with those from the literature (Petruzzi et al., 2003). This strengthens confidence in the reliability of the model for SOFC.

Table 4.5 Feed compositions and SOFC stack dimensions used in model validation.

<i>Parameters</i>	Values (Petruzzi et al., 2003)
Fuel compositions (Mole fraction):	
CH ₄	-
H ₂	0.26
CO	0.24
CO ₂	0.025
N ₂	0.46
H ₂ O	0.015
<i>Stack dimensions:</i>	
Type of cell	Planar SOFC with 225 cm ² active surface area
n	0.48
ξ	5.4
D_p	3 μm
l_a	40 μm
l_c	40 μm
L	70 μm
Stack average temperature	1073 K

Table 4.6 Model validation of the SOFC model.

T = 1073 K	Petruzzi et al., 2003			Petruzzi et al., 2003		
	Model	Error (%)		Model	Error (%)	
Cell Voltage (V)	0.8	0.8	0	0.75	0.77	2.67
Electrical Power (W)	62.9	63	0.16	70	71.6	2.29
Fuel Utilization (%)	70	70	-	80	80	-

4.1.3 One-dimensional analysis (1-D analysis)

Mass and energy balance computations take place for each control volume (1 mm distance) in the flow direction of the SOFC stack as illustrated in Figure 4.5. To simplify the problem, the following assumptions are made: (i) the pressure drop across the cell is neglected; (ii) heat radiation between solid components of the cell is negligible (Sorrentino et al., 2008); (iii) heat conduction in the solid electrolyte of the cell and in the bulk of fluid is neglected (Sorrentino et al., 2008).

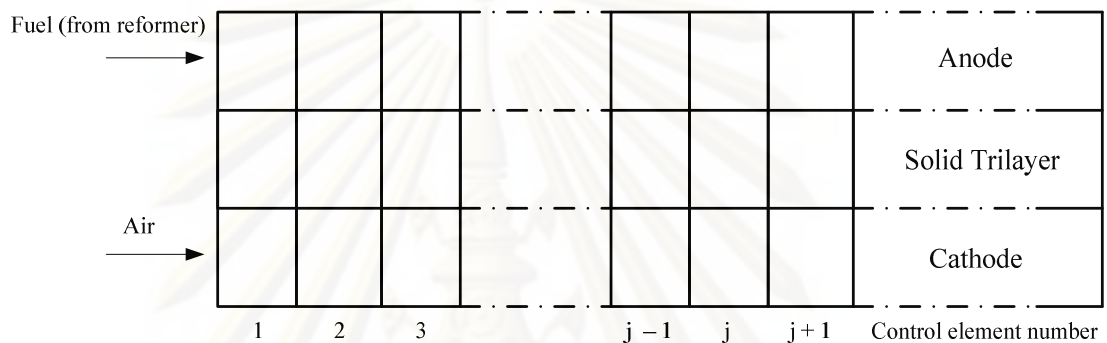


Figure 4.5 A small element divided for the calculation in SOFC cell.

For pure- H_2 feed, only the electrochemical reaction (Eqs. (19) and (20)) takes place in the cell anode side. However, for biogas, methane and reformed gas feed, steam reforming reaction (Eq. (4.32)) and WGS reaction (Eq. (4.33)) also occur in the anode side of the cell. Thermodynamic equilibrium is assumed for the WGS reaction in each region since its reaction rate is very fast at high temperature. The rate of the reforming reaction in the SOFC stack (Achenbach and Riensche, 1994) can be calculated employing Eq. (4.42) and the mass balance equations for each component in the anode and cathode sides are given in Eqs. (4.43) and (4.44), respectively.

$$r_{ref}^j = 4274 A^j e^{-\left(\frac{82000}{RT_s^j}\right)} p_{CH_4}^j \left(1 - \frac{p_{CO}^j (p_{H_2}^j)^3}{p_{CH_4}^j p_{H_2O}^j K_{ref}^j}\right) \quad (4.42)$$

$$n_{a,i}^{j+1} = n_{a,i}^j + \sum_k v_{i,k} r_k^j + \frac{v_{i,elec} i^j A^j}{2F} \quad (4.43)$$

$$n_{c,i}^{j+1} = n_{c,i}^j + \frac{v_{i,elec} i^j A^j}{2F} \quad (4.44)$$

For the energy calculation, excess heat produced in the solid trilayer caused from reactions (4.19), (4.20) and the irreversibility of the electrochemical reaction is transferred to the anode and cathode channels. Energy balance equations for each small element in anode, cathode and solid trilayer are given in Eqs. (45)-(47), respectively.

$$H_a^{j+1} = H_a^j + h_a A^j (T_s^j - T_a^j) \quad (4.45)$$

$$H_c^{j+1} = H_c^j + h_c A^j (T_s^j - T_c^j) \quad (4.46)$$

$$-h_a A^j (T_s^j - T_a^j) - h_c A^j (T_s^j - T_c^j) + \left[\frac{(-\Delta H)_{elec}^j}{2F} - V \right] i^j A^j + \sum_k r_k^j (-\Delta H)_k^j = 0 \quad (4.47)$$

A constant operating voltage along the cell length is assumed as the current collector usually has high electrical conductivity. A current density and temperature of each control volume is calculated employing mass balance equations (Eqs. (4.43) and (4.44)), energy balance equations (Eqs. (4.45)-(4.47)) and electrochemical models (Section 4.1.1) in order to study the performance and thermal behaviors in SOFC cell. The temperature and power density profiles are the outputs of the calculation. In the consideration, maximum temperature gradient and maximum temperature in the solid trilayer are determined and compared with maximum acceptable temperature gradient and maximum acceptable cell temperature. Also, the technical terms, i.e. average current density (i_{ave}), fuel utilization (U_f), electrical efficiency and %excess air, are defined as follows:

$$i_{ave} = \frac{\sum_j i^j A^j}{\sum_j A^j} \quad (4.48)$$

$$U_f = \frac{\left(\frac{\sum_j i^j A^j}{2F} \right)}{4F_{CH_4,eq}} \quad (4.49)$$

$$\% \text{Electrical efficiency} = \frac{\text{Electrical power}}{\text{LHV of SOFC anode feed} \times \text{anode feed rate}} \times 100 \quad (4.50)$$

$$\% \text{Excess air} = \frac{0.21 \times \text{Air feed rate}}{2 F_{CH_4,eq}} \times 100 \quad (4.51)$$

It should be noted that for different types of feed, the feed rates are based on the same “methane equivalent flow ($F_{CH_4,eq}$)” as defined in Chapter 10. The cell dimensions and the operating conditions employed in 1-D analysis are given in Table 4.7.

Table 4.7 Summary of model parameters used in 1-D analysis (Aguilar et al., 2004; Ni et al., 2007).

<i>Parameters</i>	<i>Value</i>
SOFC cell	
l_a	750 μm
l_c	50 μm
L	50 μm
Cell length	400 mm
Cell width	100 mm
Anode channel height	1 mm
Cathode channel height	1 mm
$h_a = h_c$	0.2 $\text{kJ m}^{-2} \text{s}^{-1} \text{K}^{-1}$
Operating pressure	1 bar
SOFC feed temperature	998 K
Reformer	
Operating temperature	998 K
Operating pressure	1 bar

4.2 Fuel processor modelling

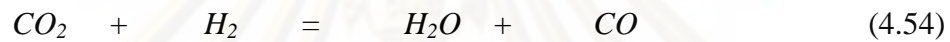
4.2.1 Conventional fuel processor

The main reaction in the fuel processor fed by biogas is the dry reforming reaction (Eq. (4.52)) due to the high content of carbon dioxide in biogas. When this is

supplemented with steam, Eq. (4.32) also takes place in the fuel processor. In a third option, air is fed along with biogas to the system so that the exothermic partial oxidation (Eq. (4.53)) occurs and provides the energy for the endothermic dry reforming and steam reforming.



It should be noted that the mildly endothermic reverse water gas shift reaction (RWGS) (Eq. (4.54)) always takes place in the fuel processor due to the presence of CO_2 in biogas feed. This reaction inhibits the generation of hydrogen.



The thermodynamic features of dry and steam reforming are similar (since both are highly endothermic) while the methane partial oxidation is exothermic. However, carbon formation during dry reforming is more severe compared with that of steam reforming due to its lower H/C ratio (Edwards and Maitra, 1995). In order to simplify the calculations, in this study the fuel processor is assumed to operate at isothermal condition and the exit gas reaches its equilibrium composition. In this study, operating temperature and pressure of the conventional fuel processor are always kept at 973 K and 1 bar, respectively. The relationships of the thermodynamic equilibrium for the dry reforming, steam reforming, partial oxidation and RWGS are shown in Eqs. (4.55), (4.56), (4.57) and (4.58), respectively.

$$K_{dry} = \frac{P_{H_2}^2 P_{CO}^2}{P_{CH_4} P_{CO_2}} \quad (4.55)$$

$$K_{steam} = \frac{P_{H_2}^3 P_{CO}}{P_{CH_4} P_{H_2O}} \quad (4.56)$$

$$K_{pox} = \frac{P_{H_2}^2 P_{CO}}{P_{CH_4} P_{O_2}^{\frac{1}{2}}} \quad (4.57)$$

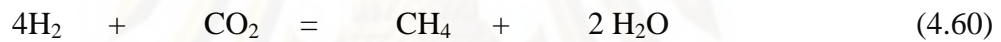
$$K_{RWGS} = \frac{p_{H_2O} p_{CO}}{p_{H_2} p_{CO_2}} \quad (4.58)$$

Where K_k , the equilibrium constant of reaction k , can be calculated from this expression:

$$K_k = e^{-\frac{\Delta G_k}{RT}} \quad (4.59)$$

4.2.2 Palladium membrane reactor (PMR)

The result in Chapter 6 indicated that steam is the most suitable reforming agent for the SOFC system. Given that methane (or biogas) is the feedstock, the major reactions taking place in the reactors are methane steam reforming (Eq. (4.32)), water gas shift reaction (Eq. (4.33)) and carbon dioxide methanation (Eq. (4.60)).



The kinetic rates derived from the experimental results on Ni/MgAl₂O₄ catalyst (Xu and Froment, 1989) were used in the calculation. The rate expressions for the reactions shown in Eqs. (4.32), (4.33) and (4.60) are given by;

$$r_1 = \frac{k_1}{p_{H_2}^{2.5}} \left(p_{CH_4} p_{H_2O} - \frac{p_{H_2}^3 p_{CO}}{K_1} \right) / (DEN)^2 \quad (4.61)$$

$$r_2 = \frac{k_2}{p_{H_2}} \left(p_{CO} p_{H_2O} - \frac{p_{H_2} p_{CO_2}}{K_2} \right) / (DEN)^2 \quad (4.62)$$

$$r_3 = \frac{k_3}{p_{H_2}^{3.5}} \left(p_{CH_4} p_{H_2O}^2 - \frac{p_{H_2}^4 p_{CO_2}}{K_3} \right) / (DEN)^2 \quad (4.63)$$

$$DEN = 1 + K_{CO} p_{CO} + K_{H_2} p_{H_2} + K_{CH_4} p_{CH_4} + \frac{K_{H_2O} p_{H_2O}}{p_{H_2}} \quad (4.64)$$

$$k_k = A_k \exp\left(\frac{-E_k}{RT}\right); k = 1, 2, 3 \quad (4.65)$$

$$K_i = B_i \exp\left(\frac{-\Delta H_i}{RT}\right); i = \text{CO}, \text{H}_2, \text{CH}_4, \text{H}_2\text{O} \quad (4.66)$$

The parameters used in the rate equations are summarized in Table 4.8.

Table 4.8 Kinetic parameters for methane steam reforming (Xu and Froment, 1989).

Parameter	Pre-exponential factor (<i>A</i> or <i>B</i>)	<i>E</i> or ΔH (kJ mol ⁻¹)
k_1	4.225×10^{15} (mol atm ^{0.5} (g h) ⁻¹)	240.10
k_2	1.955×10^6 (mol (g h) ⁻¹)	67.13
k_2	1.020×10^{15} (mol atm ^{0.5} (g h) ⁻¹)	243.9
K_{CH_4}	6.65×10^{-4} (atm ⁻¹)	-38.28
$K_{\text{H}_2\text{O}}$	1.77×10^5 (-)	88.68
K_{H_2}	6.12×10^{-9} (atm ⁻¹)	-82.90
K_{CO}	8.23×10^{-5} (atm ⁻¹)	-70.65

A palladium membrane reactor (PMR) can be divided into two main sections, i.e., a permeate side and a retentate side. Methane (or biogas) and reforming agent are compressed and fed into the retentate side of PMR where three major chemical reactions (Eqs. (4.32), (4.33) and (4.60)) take place to generate H₂. Due to the difference in partial pressure, H₂ in the retentate side can permeate through the palladium membrane to the permeate side. Therefore, pure H₂ can be derived from the permeate side of PMR. Generally, hydrogen flux is inversely proportional to the membrane thickness and also varies with the operating temperature. The expression used for the hydrogen flux calculation is given in Eq. (4.67).

$$N_{\text{H}_2} = \frac{Q_0}{\delta} \exp\left(\frac{-E_p}{RT}\right) (p_{\text{H}_2,R}^{0.5} - p_{\text{H}_2,P}^{0.5}) \quad (4.67)$$

The values of the pre-exponential factor (Q_0) and the activation energy (E_p) are 6.33×10^{-7} mol/(m Pa^{1/2} s) and 15,700 J/mol, respectively (Patel and Sunol, 2007). The membrane thickness (δ) is set to be 4.5 μm (Patel and Sunol, 2007).

For the calculations, the pressure drop in the reactor was assumed to be negligible and the reactor was divided into several small volumes (cf. Figure 4.6). The finite difference method was employed in the numerical algorithm. The mass balances for the retentate side and permeate side of the membrane reactor are given in Eqs. (4.58) and (4.59), respectively. All model parameters used in the calculation of PMR are given in Table 4.9.

$$R_i^{j+1} = R_i^j + \frac{\rho_c \pi d^2 \Delta x}{4} \sum_k v_{ik} r_k^j - N_i^j \pi d \Delta x \quad (4.68)$$

$$PE_i^{j+1} = PE_i^j + N_i^j \pi d \Delta x \quad (4.69)$$

Table 4.9 Summary of model parameters of palladium membrane reactor.

<i>Parameters</i>	<i>Value</i>
Palladium membrane reactor	
<i>T</i>	823 K
<i>P</i>	1 bar
ρ_c	2355 kg/m ³
ε	0.5
<i>d</i>	10 mm
Reactor tube length	0.15 m
Number of reactor tube	1000

Hydrogen recovery (ζ) is regarded as the performance indicator of PMR. It is defined as the mole of hydrogen extracted by the membrane divided by the mole of hydrogen theoretically produced based on the mole of methane feed (4 mol of H₂: 1 mol of CH₄).

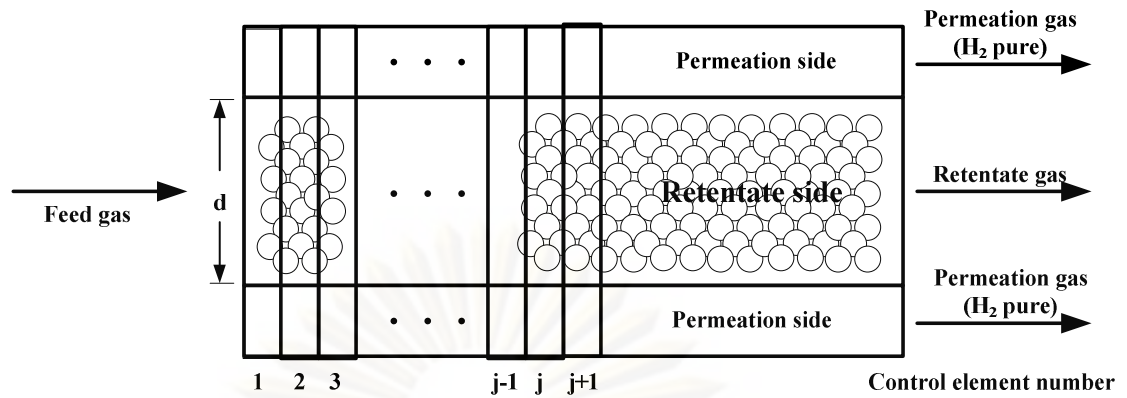


Figure 4.6 The scheme showing the basic working of the membrane reactor.

The kinetic model and H_2 permeation model for the membrane reactor were also verified. Again, our modeling results are in good agreement with the experimental results reported in the literature (Shu et al., 1995; Gallucci et al., 2004) as illustrated in Figure 4.7.

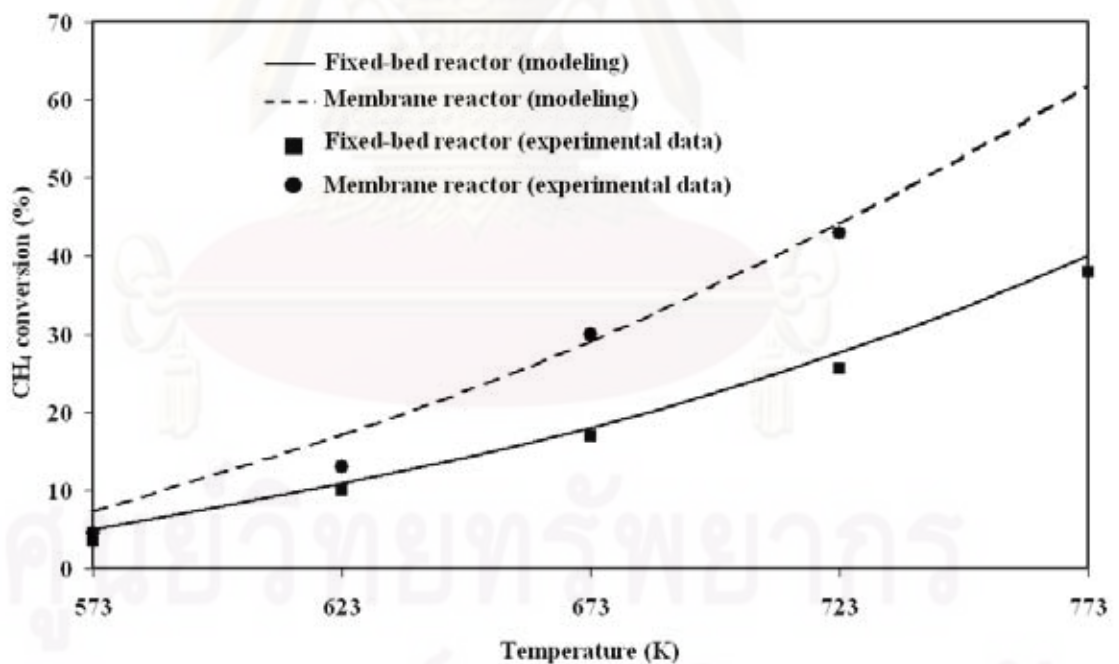


Figure 4.7 The comparison of the methane conversion in the fuel processor between the modeling results and the experimental results. (sweep gas flow rate = 3.62×10^{-5} mol/s, $P_R = 1.22$ bar, $P_P = 1.1$ bar, $H_2O/CH_4 = 3$)

4.3 Vacuum pump and compressor

For the calculation of vacuum pump and compressor, their outlet gas temperature and power consumption can be estimated by using Eqs. (4.70) and (4.71), respectively (Kaneko et al., 2006). In this study, the efficiency of both the vacuum pump and compressor was determined to be 75% (Kaneko et al., 2006).

$$T_{out} = T_{in} \left(1 + \frac{1}{\eta_{com}} \left(\left(\frac{P_{out}}{P_{in}} \right)^{\frac{\gamma-1}{\gamma}} - 1 \right) \right) \quad (4.70)$$

$$\dot{W}_{comp} = -n_{total} \int_{T_{in}}^{T_{out}} C_p dT \quad (4.71)$$

$$\text{where } \gamma = \frac{C_p}{C_p - R}. \quad (4.72)$$

4.4 Afterburner and heat exchanger

At the exit of the SOFC stack, the anode and cathode outlet gases are mixed for post combustion. Complete combustion was assumed in the afterburner; hence, the composition of methane, carbon monoxide and hydrogen in the flue gas were deemed to be zero. The heat exchanger was also assumed to operate adiabatically. Negligible axial pressure gradient is assumed in this study.

4.5 Membrane Module

Figure 4.8 shows the configuration of the membrane tube. Feed gas containing CO₂ is introduced to the inner side of the membrane, called “retentate side”. CO₂ permeates through CO₂-selective membrane to the shell side, called “permeate side”. To enhance the rate of CO₂ removal, the partial pressure of CO₂ in permeate side can be reduced by using a vacuum pump at the shell side of the membrane. The increase in operating pressure at the retentate side can also improve the rate of CO₂ removal. Steady-state mass balances in both tube and shell sides of the membrane provide:

$$\frac{dR_i}{dA} = -\frac{Pe_i}{\delta} (P_R x_i - P_P y_i) \quad (4.73)$$

$$\frac{dPE_i}{dA} = \frac{pe_i}{\delta} (P_R x_i - P_P y_i) \quad (4.74)$$

Where R_i and PE_i is flow rate of gas i in the retentate and permeate side, respectively. Finite difference method is used in the calculation. The permeation rate of CO_2 and CH_4 is calculated for each small membrane area. Negligible axial pressure gradient is assumed in this study.

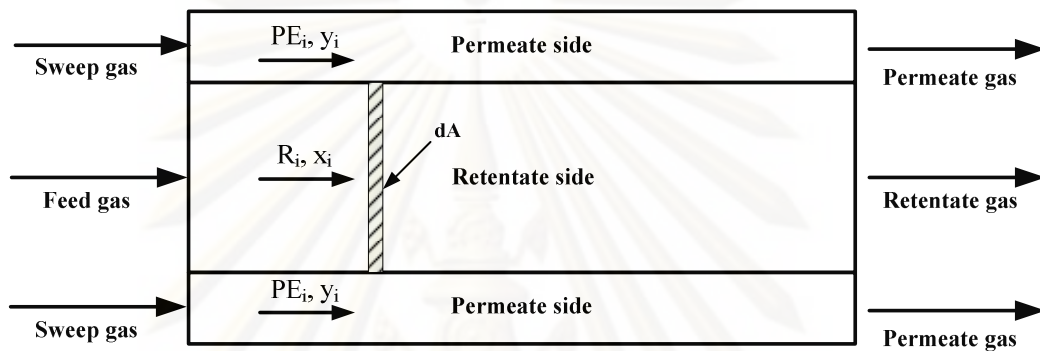


Figure 4.8 The configuration of membrane module.

In this study, 6FDA-DAT polyimide is chosen for the separation of CO_2 from the biogas feed due to its high CO_2/CH_4 selectivity (Wang et al., 2006). According to the high-temperature instability of membrane, the operating temperature of 298 K is assumed for these membrane modules. The values of parameters used in the calculation for the membrane module are summarized in Table 4.10.

Table 4.10 Membrane thickness and permeability of each gas component

Polyimide membrane (Wang et al., 2006)	
Membrane Thickness (μm)	0.1
Permeability (barrer)	
CH_4	0.69
CO_2	39.59
1 barrer = $(10^{-10} \text{ cm}^3 \text{ (STP) cm})/(\text{cm}^2 \text{ s cmHg})$	

The model of CO₂ separation by membrane is verified. The feed conditions and the parameters used in the model are summarized in Table 4.11. Again, our results show good agreement with those reported in the literature (Corti et al., 2004) as illustrated in Figure 4.9.

Table 4.11 Summary of feed characteristics and parameters used in the model verification of membrane separation.

<i>Parameters</i>	<i>Values</i>
Fuel mass flow rate (kg/s)	5.89
Fuel compositions (Mole fraction):	
CH ₄	0.068
H ₂	0.6714
CO	0.0068
CO ₂	0.1627
N ₂	-
H ₂ O	0.0911
Membrane parameters:	
Material used	PDMS
Membrane thickness (μm)	1.3
Operating pressure (bar):	
Permeate side	1
Retentate side	10
Permeability (barrer) at 298 K:	
CH ₄	940
CO	400
CO ₂	3200
H ₂	500
H ₂ O	10

$$1 \text{ barrer} = (10^{-10} \text{ cm}^3 \text{ (STP) cm}) / (\text{cm}^2 \text{ s cmHg}).$$

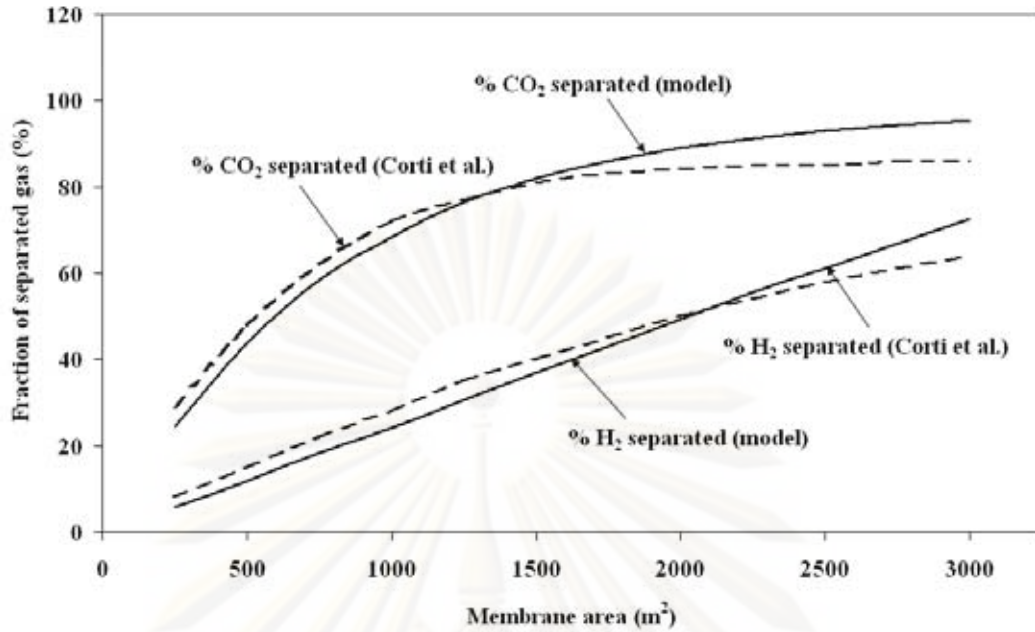


Figure 4.9 Verification of the membrane separation model.

4.6 CaO-CO₂ acceptor system

As described in Figure 4.10, CO₂-rich gas is fed simultaneously with circulating CaO at the bottom of the carbonator in which CaO solid is fluidized and reacts with CO₂ in gas phase (Eq (4.75)). Gas-solid mixture is discharged at the top of the bed and separated in the cyclone. Lean-CO₂ gas is fed out of CaO-CO₂ acceptor system and reacted-CaO is heated and then fed into the calciner bed. The calcination reaction which is the reverse of the carbonation reaction (Eq. (4.75)) takes place in the calcinations bed to regenerate CaO. Make-up CaO is also fed to the system in order to keep the capture efficiency to be reasonably high.



The CO₂ capture efficiency is determined as the system performance indicator and defined as:

$$E_{carb} = \frac{\text{CO}_2 \text{ reacting with CaO in the bed}}{\text{CO}_2 \text{ entering the bed in the CO}_2 \text{ - rich gas}} \quad (4.76)$$

It depends on the CaO-circulating flow (F_R), CaO-make up flow (F_0) and CaO inventory (W_S) in the carbonation bed (Grasa et al., 2008). In this study, F_R/F_{CO_2} and W_S are kept to be constant at 10 and 50 kg, respectively. The calculation focuses on the estimation of F_0 to achieve the determined capture efficiency. In the calculation, plug flow of gas through perfectly mixed CaO bed is assumed. The average maximum carbonation conversion (X_{ave}) is firstly calculated employing Eqs. (4.77)-(4.79).

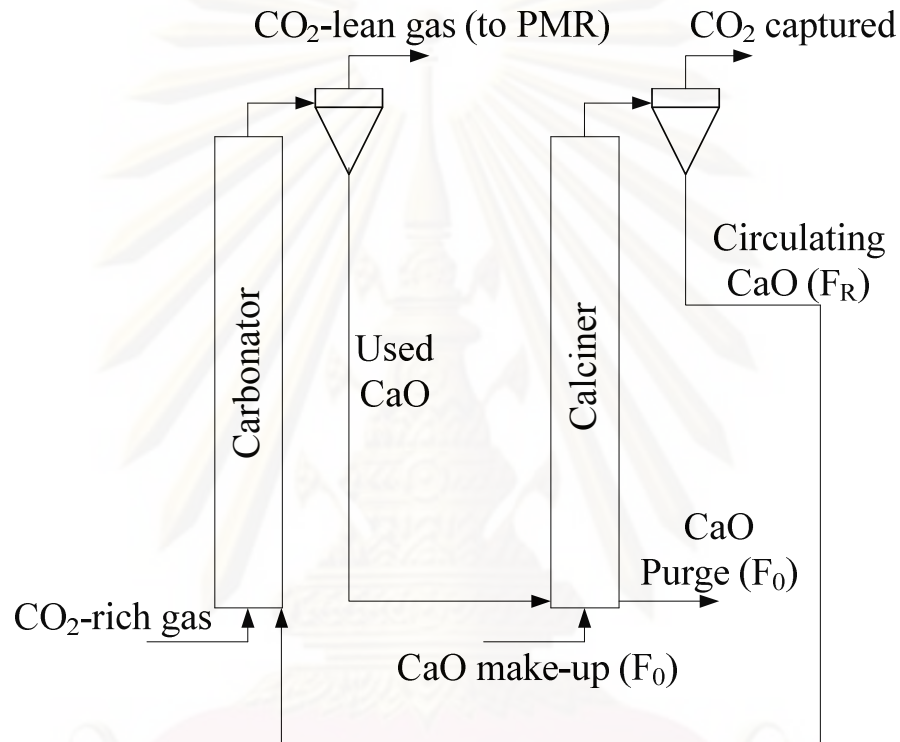


Figure 4.10 The scheme showing the basic working of the CaO-CO₂ acceptor.

$$X_N = \frac{1}{\frac{1}{(1-X_r)} + Nk} + X_r \quad (4.77)$$

$$r_N = \frac{F_0 F_R^{N-1}}{(F_0 + F_R)^N} \quad (4.78)$$

$$X_{ave} = \sum_{N=1}^{\infty} r_N X_N \quad (4.79)$$

The values of k and X_r are 0.52 and 0.075, respectively (Abanades, 2002). The capture efficiency can be calculated employing Eqs. (4.80)-(4.82) (Grasa et al., 2008).

$$E_{carb} = \frac{F_R}{F_{CO_2}} X_{ave} \frac{f_a}{\ln\left(\frac{1}{1-f_a}\right)} \quad (4.80)$$

$$\frac{F_{CO_2} \cdot M_{CaO}}{W_S \cdot k_S \cdot S_{ave} \cdot \rho_{M,g} \cdot f_a} \left[\frac{-f_0}{f_0 f_e - f_0} E_{carb} + \frac{f_0(f_0 - 1)}{(f_0 f_e - f_0)^2} \ln\left(\frac{(f_0 - f_e) + (f_0 f_e - f_0) E_{carb}}{(f_0 - f_e)}\right) \right] = 1 \quad (4.81)$$

$$S_{ave} = \frac{V_{M,CaCO_3} X_{ave}}{M_{CaO} e_{max}} \rho_{CaO} \quad (4.82)$$

Mole fraction of CO₂ at equilibrium condition (f_e) is calculated using Eq. (4.83) (Lee et al., 2006). With Eqs. (4.80) and (4.81), two unknown variables, i.e. f_a and E_{carb} , can be estimated. The CO₂-rich gas velocity is always controlled to be higher than gas terminal velocity (v_t). Gas terminal velocity and pressure drop along the carbonation fluidized bed can be calculated employing Eq. (4.84) and Eq. (4.85), respectively (Walas, 1988). Model parameters employed in the calculation of CaO-CO₂ acceptor are summarized in Table 4.12.

$$f_e = \frac{4.137 \times 10^7 e^{\frac{20474}{T}}}{P} \quad (4.83)$$

$$v_t = \frac{0.153 \times g^{0.71} \times d_p^{1.14} \times (\rho_{CaO} - \rho_f)^{0.71}}{\rho_f^{0.29} \times \mu^{0.43}} \quad (4.84)$$

$$\frac{\Delta P}{L_b} = \rho_{CaO}(1-\varepsilon)g + \rho_f \varepsilon g + \frac{2f_f \rho_f \varepsilon u_f^2}{D} + \frac{2f_p \rho_{CaO}(1-\varepsilon)u_p^2}{D} \quad (4.85)$$

Table 4.12 Value of model parameters used in the calculation of CaO-CO₂ acceptor.

<i>Parameters</i>	<i>Value</i>
CaO-CO₂ acceptor (carbonator) (Alvarez and Abanades, 2005; Grasa et al., 2008)	
T	973 K
M_{CaO}	56 g/mol
d_p	0.3 mm
ρ_{CaO}	3313.6 kg/m ³
$V_{M,CaCO_3}$	36.9 cm ³ /mol
e_{max}	50 nm
k_S	4 x 10 ⁻¹⁰ m ⁴ /(mol.s)
ε	0.6

4.7 Boundary of carbon formation

4.7.1 Direct-internal reforming SOFC (DIR-SOFC)

In the calculation of the boundary of carbon formation, the equilibrium composition of gas mixture in the anode channel of SOFC is initially computed. For DIR-SOFC, it can be categorized into two types based on the electrolytes; i.e., the oxygen ion-conducting electrolyte (SOFC-O²⁻) and the proton-conducting electrolyte (SOFC-H⁺). The sets of equation employed in the calculation of equilibrium composition for SOFC-O²⁻ are given in Section 4.1.2.1. For SOFC-H⁺, its mass balance equations are almost identical to that of SOFC-O²⁻. However, the change is required for the mass balance of steam component as shown in the following equation:

$$n_{H_2O,f+1}^a = n_{H_2O,f}^a - x_{steam,f}^a - x_{WGS,f}^a \quad (4.86)$$

The thermodynamic equilibrium composition can be determined by solving a system of nonlinear equations relating the moles of each component to the equilibrium constants of the reactions whose values are given in Figure 4.11.

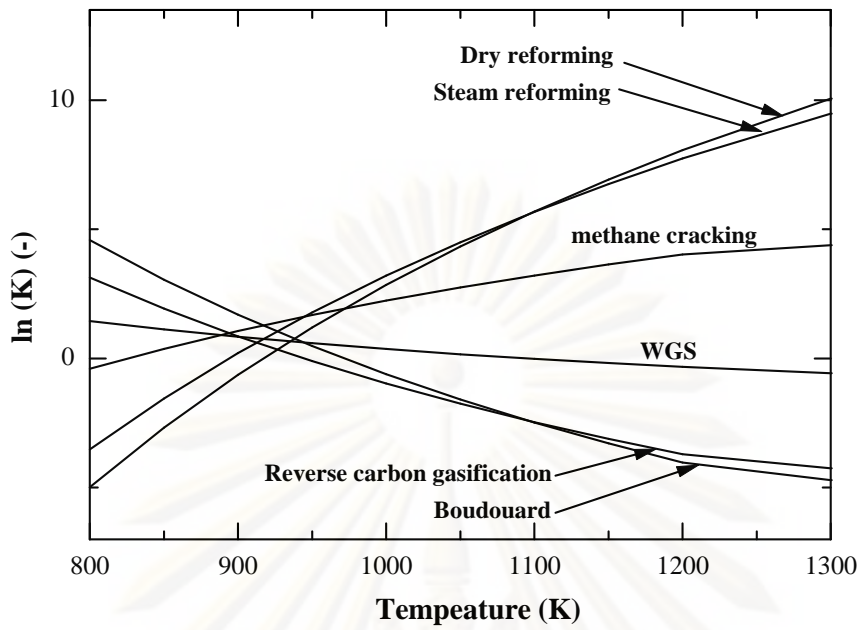
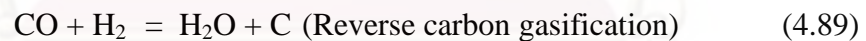
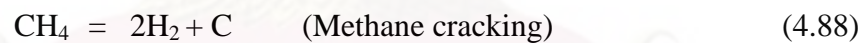


Figure 4.11 Values of equilibrium constants.

The following reactions are the most probable carbon formation reactions in the system (Pietrogrande et al., 1993).



It should be noted that due to the endothermic nature of the reforming of methane (Eq. 4.32) and the mildly exothermic nature of the WGS reaction (Eq. 4.33), the amount of CO becomes significant at high operating temperature. All reactions are employed to examine the thermodynamic possibility of carbon formation by calculating the values of their carbon activities (α_c) as defined in Eqs. (4.90)-(4.92).

$$\alpha_{c,Bou} = \frac{K_{Bou} p_{\text{CO}}^2}{p_{\text{CO}_2}} \quad (4.90)$$

$$\alpha_{c,MC} = \frac{K_{MC} p_{\text{CH}_4}}{p_{\text{H}_2}^2} \quad (4.91)$$

$$\alpha_{c,RCG} = \frac{K_{RCG} P_{CO} P_{H_2}}{P_{H_2O}} \quad (4.92)$$

where K_{Bou} , K_{MC} and K_{RCG} represent the equilibrium constants of the reactions (4.87), (4.88) and (4.89), respectively, and p_i the partial pressure of component i . When $\alpha_c > 1$, the system is not in equilibrium and carbon formation is observed. The system is at equilibrium when $\alpha_c = 1$. It is noted that the carbon activity is only the indicator for the presence of carbon in the system. It does not give the information regarding the amount of carbon formed. Finally, when $\alpha_c < 1$, carbon formation is thermodynamically impossible.

To find the range of SOFC operation which does not suffer from the carbon formation, the operating temperature and the extent of the electrochemical reaction of hydrogen are specified. Then the initial values of the CO_2/CH_4 , or H_2O/CH_4 , or air/CH_4 ratios are varied and the corresponding values of α_c are calculated. The carbon formation boundary is defined as the values of these ratios whose value of $(1 - \alpha_c)$ is approaching zero. This value represents the minimum quantity of the reforming agent (CO_2 , or H_2O , or O_2) at which carbon formation in the equilibrium mixture is thermodynamically impossible.

It should be noted that although recent investigators have estimated the carbon concentration in the reforming reactions by the method of Gibbs energy minimization (Grace et al., 2001), the principle of equilibrated gas to predict the carbon formation in this study is still meaningful since the calculations are carried to find the carbon formation boundary where the carbon just begins to form. In addition, other factors such as mass and heat transfer or rate of reactions may also affect the prediction of the carbon formation boundary. Local compositions which allow the local carbon formation may exist, although the carbon formation is unfavorable according to the calculations based on equilibrium bulk compositions. Moreover, other forms of carbonaceous compounds such as C_nH_m may be formed and result in comparable damages.

4.7.2 Conventional fuel processor

The calculation of the boundary of carbon formation of the conventional fuel processor is almost similar to that of the anode channel of DIR-SOFC. Eqs. (4.23)-

(4.29) and (4.34)-(4.36) can be used in the calculation of equilibrium composition of the conventional fuel processor; however, the extent of electrochemical is equal to zero. The probable carbon formation reactions and the equations employed in the estimation of carbon activities in case of the conventional fuel processor are identical to those in case of DIR-SOFC (Eqs. (4.87)-(4.92)).

4.8. Economic consideration

For the economic analysis, the change in the value of money with time is neglected (Interest rate and inflation rate are assumed to be zero.). In the following consideration, the electricity output is set to be identical for all scenarios and the required biogas (methane) fuel feed rate in each scenario is computed. Therefore, only the capital costs of SOFC stack, supplementary equipments; i.e., palladium membrane reactor, high-pressure compressor, vacuum pump, CO₂ separator and CaO-CO₂ acceptor, and fuel cost were taken into account. The economic indicator considered in this study is net cost saving which could be calculated, viz;

$$\text{Net cost saving} = \text{Saving in capital cost of SOFC stack} - \text{Additional cost of supplementary equipments} + \text{Saving in fuel cost} \quad (4.93),$$

where saving in capital cost of SOFC stack is the difference between stack cost of conventional SOFC system and stack cost of interested SOFC configuration. Also, the saving in fuel cost is equal to the fuel cost of conventional SOFC system minus the fuel cost of interested SOFC configuration. Positive net cost saving indicates that the interested SOFC configuration is economically superior to the conventional SOFC system. The costing models and parameters used in the economic analysis are listed in Table 4.13.

Moreover, the benefit obtained from CO₂ capture is evaluated in term of “cost of CO₂ capture”. The cost of CO₂ capture stands for the additional cost (relative to CON-SOFC) used in CO₂ capture per unit of CO₂ capture and is defined as;

$$\text{Cost of CO}_2 \text{ capture} (\$/\text{ton}) = - \frac{\text{Net cost saving} (\$)}{\text{Rate of CO}_2 \text{ capture} (\frac{\text{ton}}{a}) \times \text{Plant life time} (\text{year})} \quad (4.94)$$

Table 4.13 Costing models and parameters used in the economic analysis (Walas, 1988; Amelio et al., 2007; Palazzi et al., 2007; Vivanpatarakij et al., 2008; Wong et al., 2009).

Costing model	
Cell cost (\$)	$C_{\text{cell}} = A_{\text{single cell}} \times 0.1442^*$
Number of cells	$N_{\text{cell}} = A_{\text{total}} / A_{\text{single cell}}$
Number of stacks	$N_{\text{stack}} = N_{\text{cell}} / 100$
Fuel cell stacks cost (\$)	$C_{\text{stack}} = 2.7 \times (C_{\text{cell}} \times N_{\text{cell}} + 2 \times N_{\text{stack}} \times A_{\text{single cell}} \times 0.46425)$
Palladium membrane cost (\$/kg)	6,700
Project life time (year)	5
CaO sorbent (\$/ton)	60
Plant operating hour (h/a)	8,600
Compressor (\$)	$C_{\text{compressor}} = 1.49 \times HP^{0.71} \times 10^3$
Vacuum pump (\$)	$C_{\text{vacuum pump}} = 2.59 \times X^{1.03} \times 10^5$
	where: $0.01 < X < 0.52$ (lbs/h)/(suction Torr)

*A single cell area is fixed at 200 cm^2

CHAPTER V

DETERMINATION OF BOUNDARY OF CARBON FORMATION FOR DRY REFORMING OF METHANE IN SOLID OXIDE FUEL CELL

In this chapter, boundary of carbon formation for the dry reforming of methane in direct internal reforming solid oxide fuel cells (DIR-SOFCs) with different types of electrolyte (i.e., an oxygen ion-conducting electrolyte (SOFC-O²⁻) and a proton-conducting electrolyte (SOFC-H⁺)) was determined by employing the detailed thermodynamic analysis. The benefits of the presences of H₂O, CO₂ and air in the SOFC anode chamber on suppression of carbon formation were also investigated.

5.1 Introduction

Recent developments on SOFCs seem to move towards to two main issues; intermediate temperature operation and use of other fuels instead of hydrogen. The uses of various alternative fuels; i.e., natural gas, bio-ethanol, coal, biomass, biogas, methanol, gasoline and other oil derivatives, in SOFCs have been investigated (Maggio et al., 1998; Brown, 2001; Douvartzides et al., 2003). As SOFCs are operated at such a high temperature, these fuels can be internally reformed at the anode side of SOFCs producing a H₂-CO rich gas, which is eventually used to generate the electrical energy and heat. This operation is called a direct internal reforming (DIR-SOFCs). Regarding the global environmental problems and current fossil fuel crisis, the development of SOFCs fed by renewable fuels attracts more attention as an alternative method for power generation in the near future. Among renewable sources, biogas is a promising candidate, since it is produced readily from the fermentation of biomasses and agricultural wastes. Typically, biogas consists mainly of methane and carbon dioxide. Due to the rich CO₂ for biogas, carbon dioxide (or dry) reforming reaction would be one of the most suitable processes to convert

biogas to hydrogen or synthesis gas (CO and H₂) for later utilization in SOFCs or other processes.

However, in order to operate SOFCs on the direct feed of alternative fuels (i.e. biogas) rather than hydrogen, several major problems remain to be solved. One of them is the problem of carbon deposition on the anode, causing loss of active site and cell performance as well as poor durability. The growth of carbon filaments attached to anode crystallites can generate massive forces within the electrode structure leading to its rapid breakdown (Clarke et al., 1997). A number of efforts have been carried out to alleviate this problem. One approach is to search for appropriate anode formulations and operating conditions. A number of additives were added to the anode to lower the rate of carbon formation. For example, the addition of molybdenum and cerium metal oxides to Ni-based anode was reported to reduce carbon deposition, and in some cases, to increase fuel conversion (Finnerty and Ormerod, 2000; Park et al., 2000). The addition of alkali such as potassium can accelerate the reaction of carbon with steam and also neutralize the acidity of the catalyst support, hence reducing carbon deposition (Finnerty et al., 1998).

Another conventional approach to avoid carbon deposition is the addition of extra oxidant to the feed. According to the dry reforming of methane, it was suggested that the use of excess carbon dioxide in the dry reforming reaction could avoid carbon formation (Ruckenstein and Hu, 1995). Experimental studies on the dry reforming using an excess of carbon dioxide with carbon dioxide to methane (CO₂/CH₄) ratios of 3/1 and 5/1 over nickel catalyst supported on alumina were carried out. It was reported that the rate of disintegration is smaller for the case with higher ratio. Selection of a suitable CO₂/CH₄ ratio is therefore an important issue (Ruckenstein and Hu, 1995). Carbon formation can occur when the SOFCs are operated at low CO₂/CH₄ ratio. However, use of high CO₂/CH₄ ratio is unattractive as it lowers electrical efficiency of the SOFCs by the dilution of fuel, yield of hydrogen production, and the system efficiency. Consequently, it is necessary to find the CO₂/CH₄ ratio at the boundary of carbon formation whose value represents the minimum ratio required to operate the SOFCs at carbon-free condition.

In this chapter, a detailed thermodynamic analysis is carried out to predict the boundary of carbon formation for DIR-SOFCs fueled by mixtures of methane and carbon dioxide. The effects of electrolyte type (i.e. oxygen ion-conducting and proton-conducting electrolytes), operating temperature, and extent of electrochemical

reaction on the required CO_2/CH_4 ratio are investigated. Thermodynamic calculations have taken place to predict the required $\text{H}_2\text{O}/\text{fuel}$ ratio for SOFCs fed by methane (Sangtongkitcharoen et al., 2005) and methanol (Assabumrungrat et al., 2005). It was found that the SOFCs with an oxygen-conducting electrolyte (SOFC- O^{2-}) require less $\text{H}_2\text{O}/\text{fuel}$ ratio than that with a hydrogen-conducting electrolyte (SOFC- H^+) because extra water generated from the electrochemical reaction is available for use in the anode chamber. In this present work, alternative methods to alleviate the carbon formation by adding water or air to the system are also considered as it is practical to add these components along with methane and carbon dioxide in the feed to reduce the degree of carbon deposition.

5.2 Results and discussion

Influences of inlet CO_2/CH_4 ratio on equilibrium compositions of the dry reforming reaction in a conventional reactor at isothermal condition ($T = 900 \text{ K}$) are shown in Figure 5.1. It was found that the amounts of carbon monoxide and hydrogen increase with increasing mole of carbon dioxide in the feed, and that some hydrogen is converted to water particularly at high CO_2/CH_4 ratio due to the reverse water gas shift reaction (RWGS) and methanation reaction (reverse steam reforming of methane). However, at higher operating temperature, the contribution of the methanation reaction is much less pronounced due to the high value of the equilibrium constant of the steam reforming of methane as shown in Figure 4.11. It should be noted that some methane still exists even with high CO_2/CH_4 ratio at moderate temperature of 900 K.

For SOFC- O^{2-} operation, hydrogen is electrochemically consumed and water is generated in the anode chamber. It is shown in Figure 5.2a that negligible amount of methane is observed because the consumption of hydrogen moves the dry reforming of methane forwardly and, in addition, the steam reforming of methane promotes the methane consumption. When the extent of carbon dioxide in the feed is increased, lower amount of hydrogen and higher amount of water are observed according to the RWGS reaction. For SOFC- H^+ operation, hydrogen is also electrochemically consumed; however, the electrochemical water appears in the cathode chamber and plays no role in the anode reactions unlike in the SOFC- O^{2-} . It should be noted that the SOFC- H^+ behaves quite similar to a membrane reactor in

which the forward reaction is enhanced by removing some products (e.g. hydrogen) from the reaction zone. From Figure 5.2b, it was observed that the amounts of hydrogen and water involved in the SOFC- H^+ are much less than those in the SOFC- O^{2-} . Moreover, when higher amount of carbon dioxide is added in the feed, more hydrogen is converted to water and slight increase of carbon monoxide is observed.

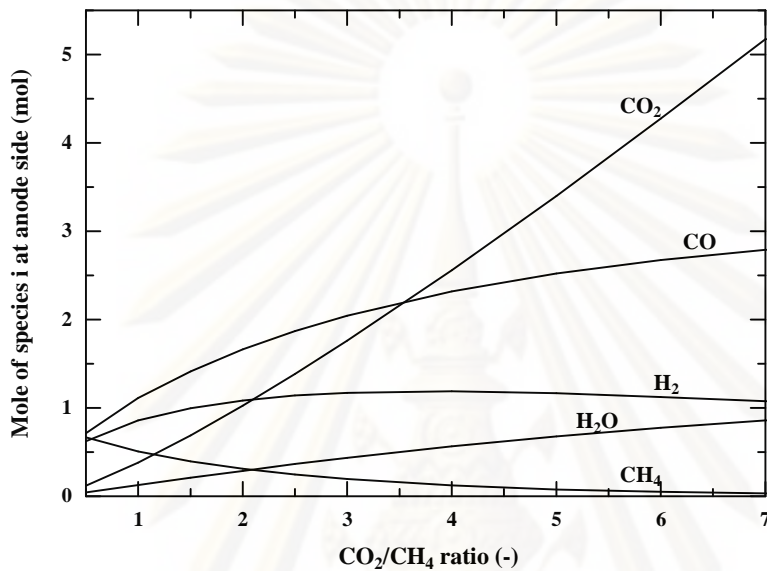
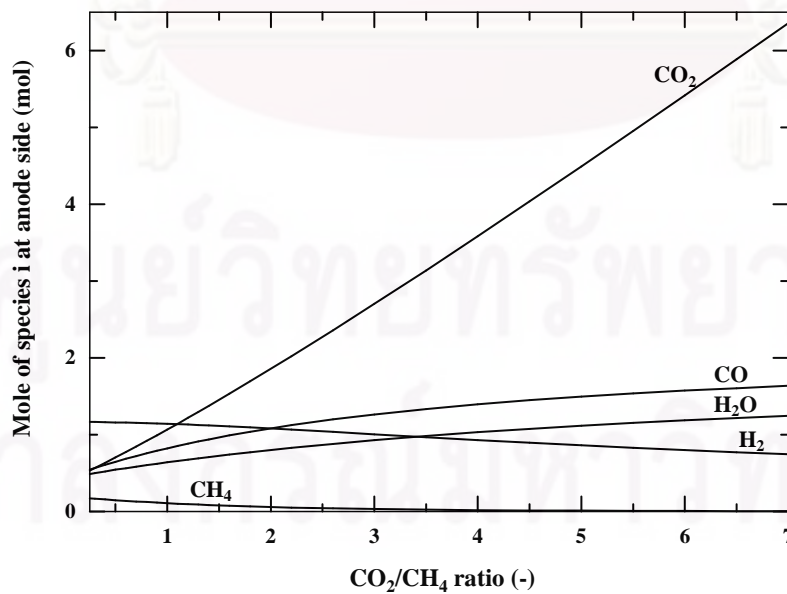
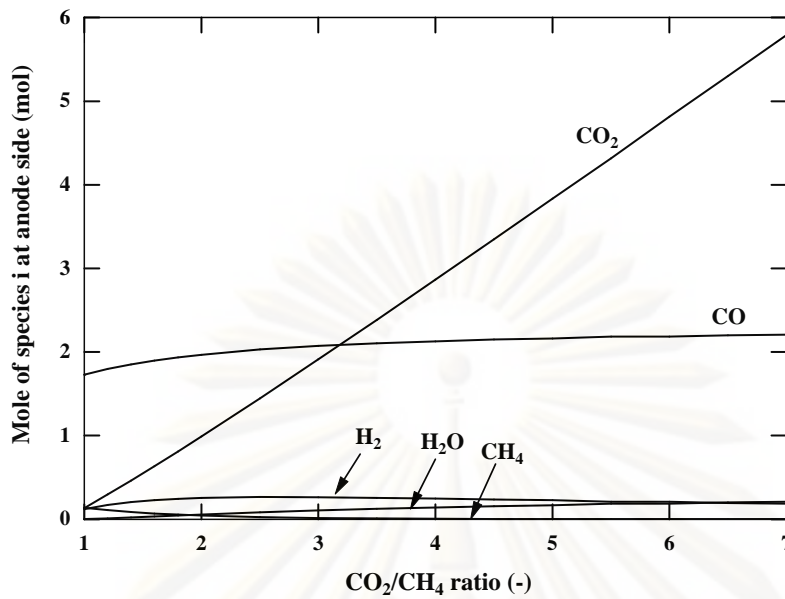


Figure 5.1 Effect of inlet CO_2/CH_4 ratio on mole of each component in a conventional reformer ($n_{CH_4, in}^a = 1$ mol, $P = 101.3$ kPa and $T = 900$ K).



(a)



(b)

Figure 5.2 Effect of inlet CO₂/CH₄ ratio on mole of each component mole: a) SOFC-O²⁻, and b) SOFC-H⁺ ($n_{CH_4,in}^a = 1$ mol, $e = 1.6$ mol, $P = 101.3$ kPa and $T = 900$ K).

The effect of inlet CO₂/CH₄ ratio on the carbon activity for the conventional reformer is shown in Figure 5.3. The carbon activity decreases dramatically with increasing CO₂/CH₄ ratio and operating temperature, implying that the opportunity of carbon formation can be rapidly decreased by adding CO₂ in the system or operating the system at high temperature. Increasing the amount of CO₂ in the feed promotes the consumption of methane and generation of water which reduce the possibility of carbon formation. Because the Boudard (Eq. (4.87)) and reverse carbon gasification (Eq. (4.89)) reactions are exothermic, the carbon activity significantly reduces at high operating temperature. Although the carbon formation from the methane cracking (Eq. (4.88)) should be more significant at high temperature, the much higher values of the equilibrium constants of the dry and steam reforming reactions compared to that of the methane cracking make it become less likely at high operating temperature (see Figure 4.11). It should be noted that the carbon activity calculated from Eqs. (4.90), (4.91) and (4.92) yield the same value, which is in good agreement with previous literatures (Nagata et al., 2001; Sangtongkitcharoen et al., 2005).

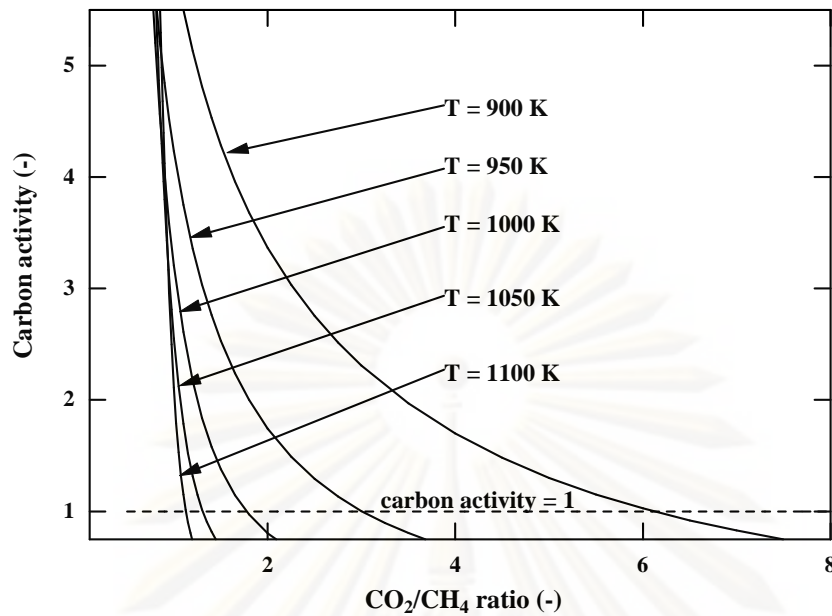


Figure 5.3 Effect of inlet CO_2/CH_4 ratio on carbon activity (conventional reactor, $n_{\text{CH}_4, \text{in}}^a = 1$ mol, and $P = 101.3$ kPa).

Figure 5.4 shows the required CO_2/CH_4 ratio at the boundary of carbon formation for the SOFC- O^{2-} at different temperature and extent of electrochemical reaction of hydrogen (e). Lower CO_2/CH_4 is required for the SOFC- O^{2-} compared to that of the conventional reformer due to the presence of electrochemical water in the anode chamber. The difference is particularly pronounced at higher extent of electrochemical reaction. For the SOFC- H^+ , at moderate operating temperature ($T = 800\text{-}1000$ K) when the extent of electrochemical reaction (e) is increased, the lower CO_2/CH_4 ratio is sufficient to alleviate the carbon formation as shown in Figure 5.5a. However, the opposite trend is observed at higher operating temperature ($T > 1000$ K) as shown in Figure 5.5b. The trend at lower operating temperature is quite unusual as it has been reported earlier for the systems of the steam reforming methane (Sangtongkitcharoen et al., 2005) of and methanol (Assabumrungrat et al., 2005) that higher $\text{H}_2\text{O}/\text{fuel}$ ratio is required at higher extent of electrochemical reaction because hydrogen is consumed and no benefit of electrochemical water is realized in the anode gas mixture in the SOFC- H^+ . In addition, it was a general concern for using a membrane reactor for dehydrogenation reactions that the carbon formation problem

should be more severe due to the removal of hydrogen from the reaction system. Therefore, it is likely that for the SOFC-H⁺, higher carbon dioxide should be needed when the extent of electrochemical reaction is higher in the dry reforming system.

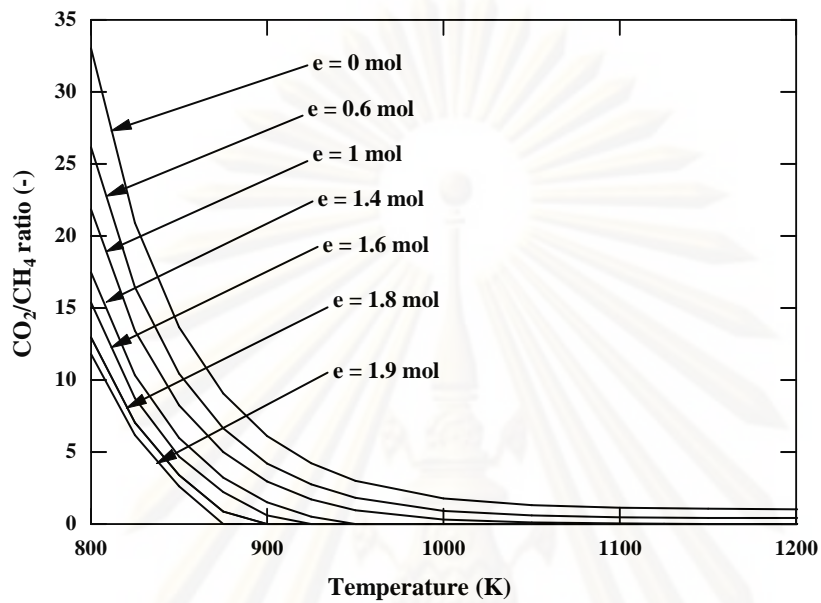
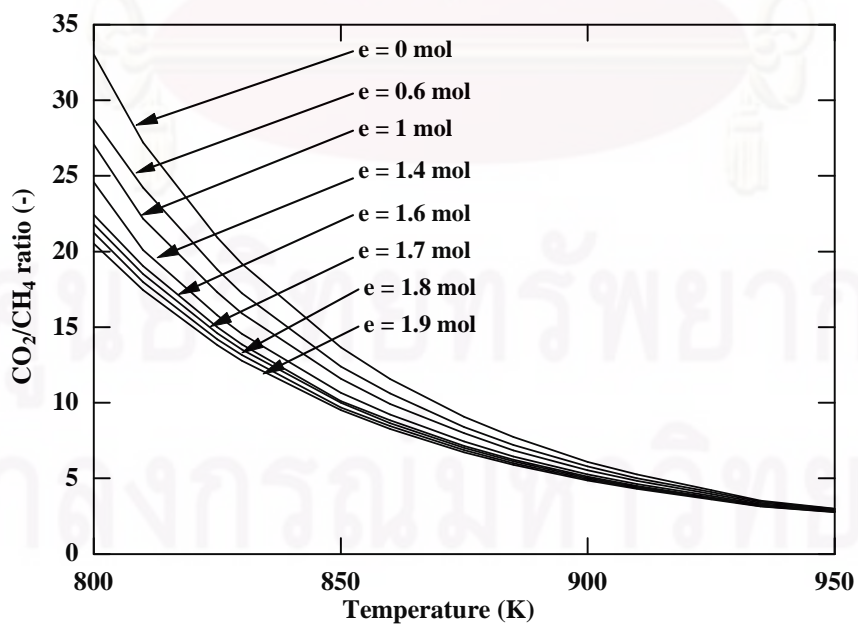
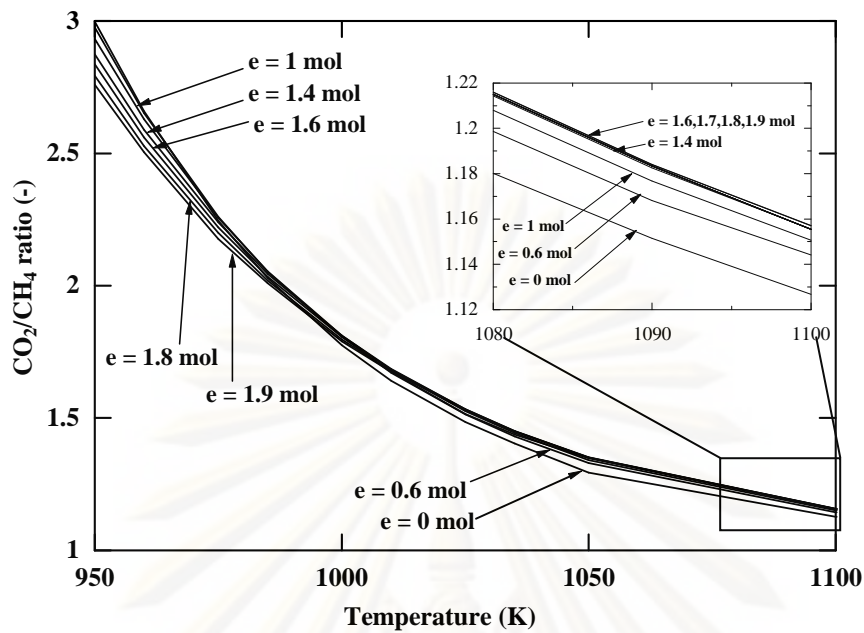


Figure 5.4 Influence of the extent of electrochemical reaction of H₂ on the requirement of inlet CO₂/CH₄ ratio at different operating temperature (SOFC-O²⁻, $n_{CH_4, in}^a = 1$ mol and $P = 101.3$ kPa).



(a)



(b)

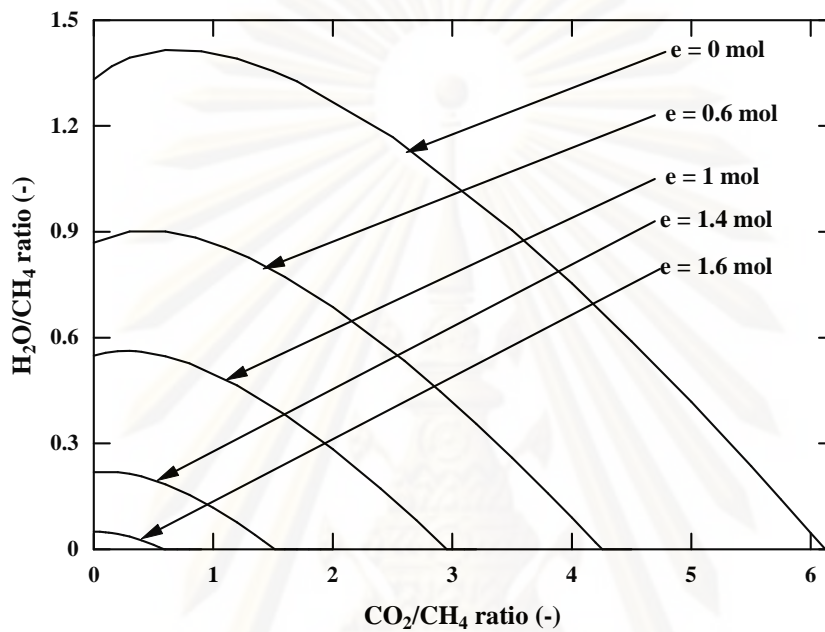
Figure 5.5 Influence of the extent of electrochemical reaction of H_2 on the requirement of inlet CO_2/CH_4 ratio at different operating temperature: a) $T = 800-950$ K, and b) $950-1100$ K (SOFC- H^+ , $n_{CH_4, in}^a = 1$ mol and $P = 101.3$ kPa).

To explain the reasons for the unusual behavior of the dry reforming of methane in the SOFC- H^+ at moderate temperatures (800-1000 K), the moles of each species at different CO_2/CH_4 ratios at $T = 900$ K for the conventional reactor (Figure 5.1) and the SOFC- H^+ (Figure 5.2b) are compared. Note that because the carbon activity of all possible carbon formation reactions provide the same value when the gas mixtures are at their equilibrium conditions, for simplicity the carbon activity based on the Boudard reaction (Eq. (4.87)) is considered as an example for understanding the behavior of the system when carbon dioxide is added to the system. From the figures, when hydrogen is electrochemically removed from the anode gas mixture, the dry reforming of methane moves forwardly, resulting in low content of CH_4 in the gas mixture. It is observed that the mole of CO in the gas mixture for the SOFC- H^+ is less dependent on the CO_2/CH_4 ratio than that for the conventional reactor because the RWGS plays less significant role when smaller amount of hydrogen is present in the system. Consequently, the value of the carbon activity ($K_1 p_{CO}^2 / p_{CO_2}$) for the SOFC- H^+ decreases with the increase of the CO_2/CH_4 ratio more

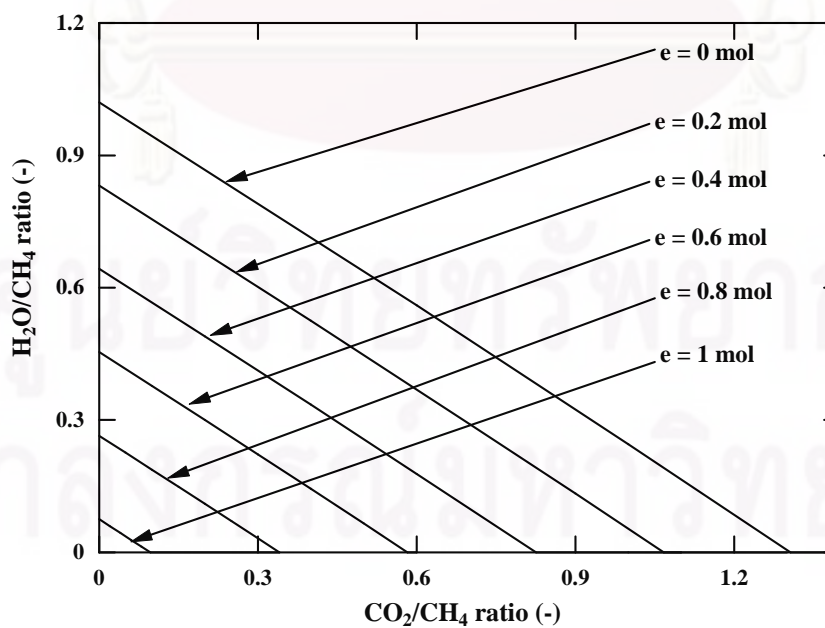
rapidly than that for the conventional reactor and, therefore, reaches the boundary of carbon formation ($\alpha_c = 1$) at lower value of CO_2/CH_4 ratio.

In real operation, it is unlikely to add carbon dioxide to the system to suppress the carbon formation. Other components such as water and air are more practical choices. The calculations were carried out to find the required $\text{H}_2\text{O}/\text{CH}_4$ or air/CH_4 ratio for different inlet CO_2/CH_4 ratio, extent of electrochemical reaction and operating temperature. This information is important for selecting a suitable feed composition which is safe from the carbon formation problem. Figures 5.6 and 5.7 show the $\text{H}_2\text{O}/\text{CH}_4$ ratio at the boundary of carbon formation for different CO_2/CH_4 ratio in the feed for SOFC- O^{2-} and SOFC- H^+ , respectively. It was found that for the SOFC- O^{2-} the required $\text{H}_2\text{O}/\text{CH}_4$ ratio decreases with the increases of inlet CO_2/CH_4 ratio, extent of electrochemical reaction and operating temperature. The operation at high extent of electrochemical reaction and high temperature significantly reduces the risk from carbon formation. For the SOFC- H^+ , the required $\text{H}_2\text{O}/\text{CH}_4$ ratio also decreases with the increases of inlet CO_2/CH_4 ratio and operating temperature. Higher $\text{H}_2\text{O}/\text{CH}_4$ ratio is required at higher extent of electrochemical reaction. However, the reverse trend is observed when the system is operated at moderate operating temperature ($T = 900 \text{ K}$) with high inlet CO_2/CH_4 ratio (approximately higher than 1.5) which is in good agreement with the previous case in which only carbon dioxide was used as the carbon suppresser. When comparing between the required $\text{H}_2\text{O}/\text{CH}_4$ ratio of the case with no carbon dioxide present in the inlet feed (CO_2/CH_4 ratio = 0) and the required CO_2/CH_4 of the case without the addition of water for both SOFC- O^{2-} and SOFC- H^+ , it is clear that water shows more pronounced influence on inhibiting the carbon formation than carbon dioxide particularly at low operating temperature. The results also reveal that for the SOFC- H^+ the extent of electrochemical reaction has no significant effect on the required $\text{H}_2\text{O}/\text{CH}_4$ ratio at high temperature. It should be noted that when comparing between the dry reforming and the steam reforming of methane with addition of carbon dioxide and water, respectively, as the components for inhibiting the carbon formation, the addition of water always provides beneficial effect to the system as water reacts with methane to reduce the extent of methane and it also reacts with carbon monoxide to reduce the extent of carbon monoxide, forming hydrogen and carbon dioxide. The presence of high amounts of carbon dioxide, hydrogen and water is important for preventing the

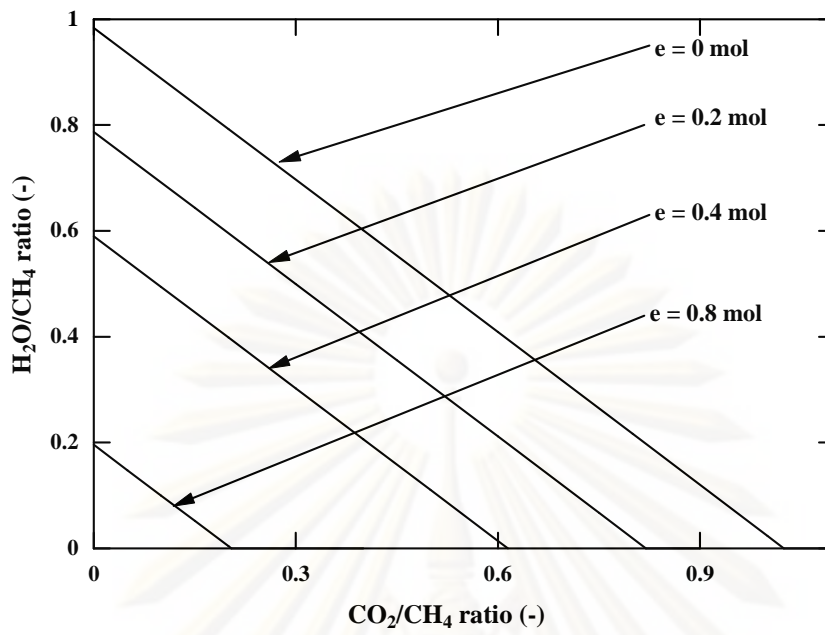
carbon formation in the system. For the case with addition of carbon dioxide, although extra carbon dioxide promotes the consumption of methane from the dry reforming reaction, carbon dioxide unlike water does not help reduce the extent of carbon monoxide in the system. In addition, more carbon monoxide can be generated by the RWGS reaction.



(a)

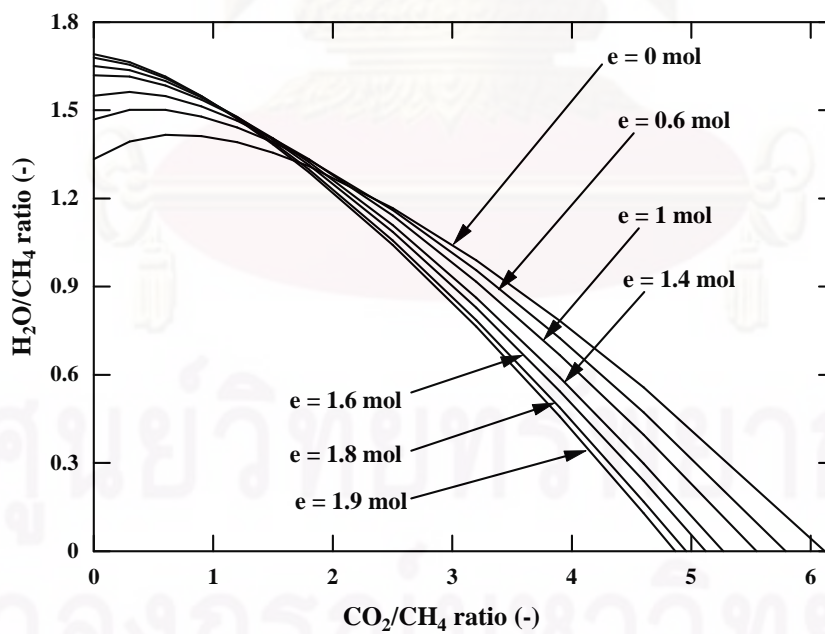


(b)

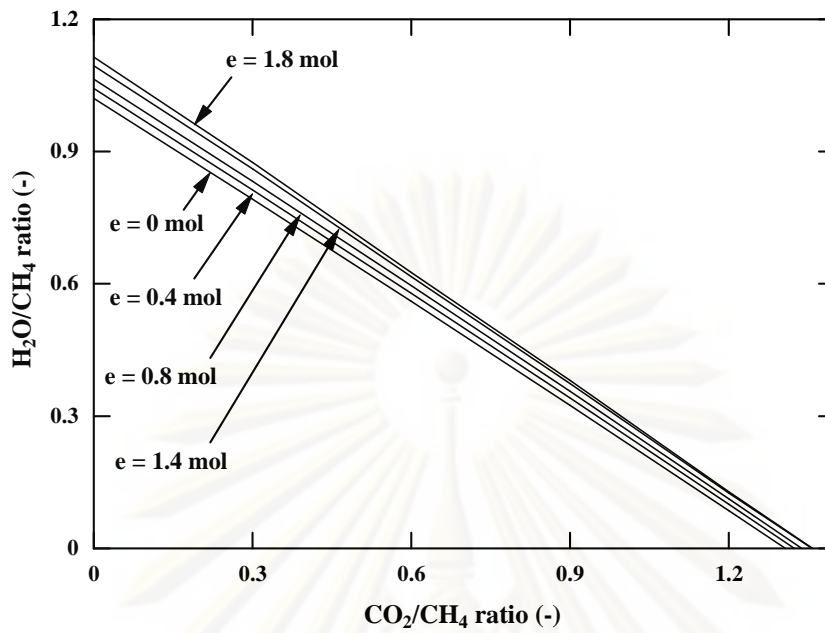


(c)

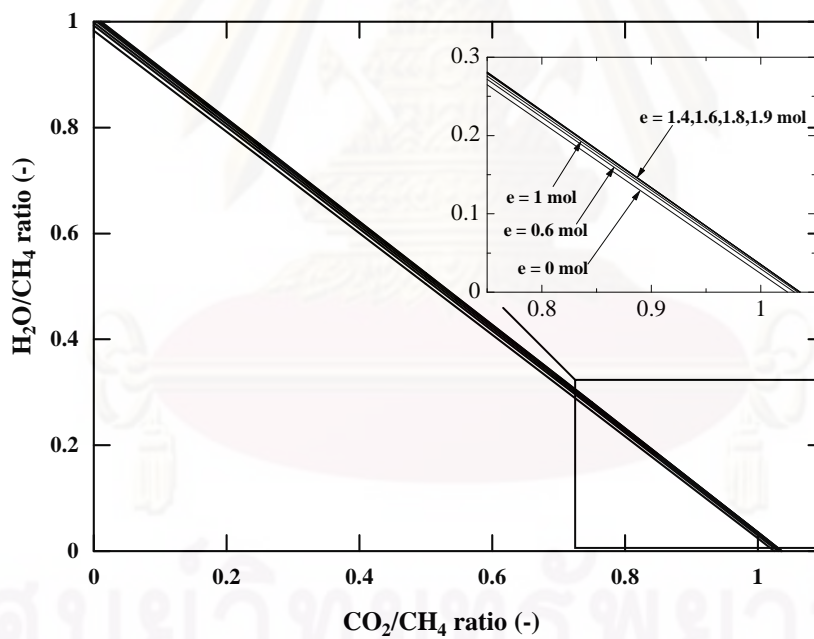
Figure 5.6 Required inlet $\text{H}_2\text{O}/\text{CH}_4$ ratio at different inlet CO_2/CH_4 ratio: a) $T = 900$ K, b) $T = 1050$ K and c) $T = 1200$ K (SOFC- O^{2-} , $n_{\text{CH}_4, \text{in}}^a = 1$ mol and $P = 101.3$ kPa).



(a)



(b)

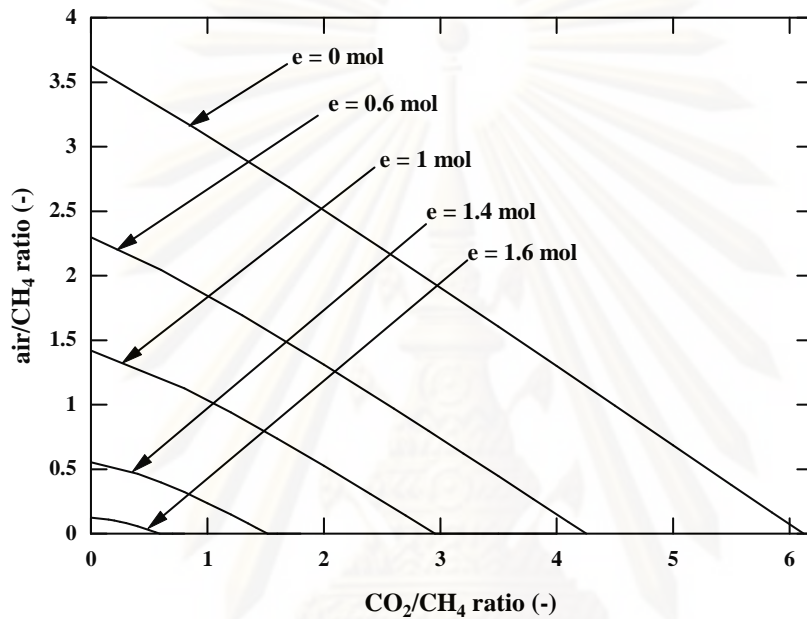


(c)

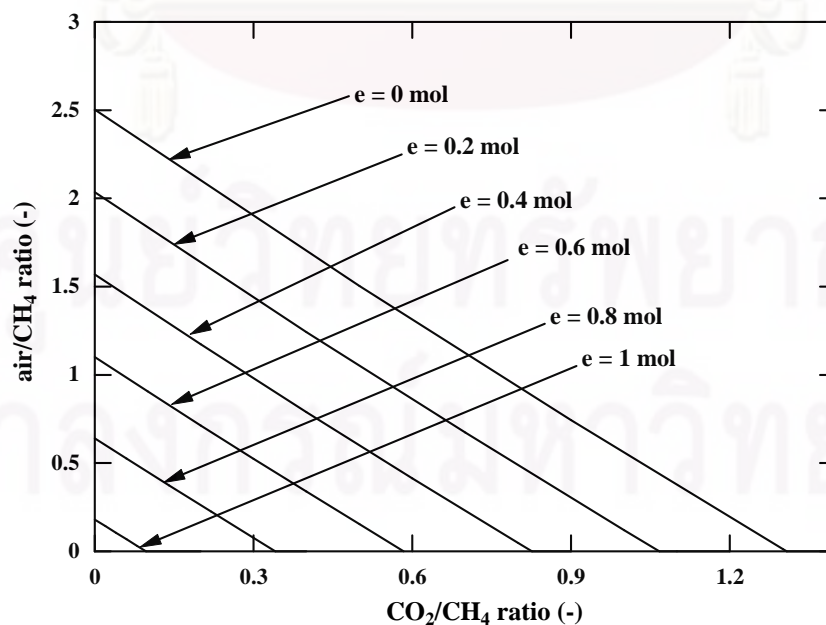
Figure 5.7 Required inlet $\text{H}_2\text{O}/\text{CH}_4$ ratio at different inlet CO_2/CH_4 ratio: a) $T = 900$ K, b) $T = 1050$ K and c) $T = 1200$ K (SOFC- H^+ , $n_{\text{CH}_4, \text{in}}^a = 1$ mol and $P = 101.3$ kPa).

When air is used as an alternative oxidant for preventing the carbon formation, oxygen in air can react with methane, carbon monoxide or hydrogen whose products are beneficial for preventing the carbon formation. Figures 5.8 and 5.9 show the

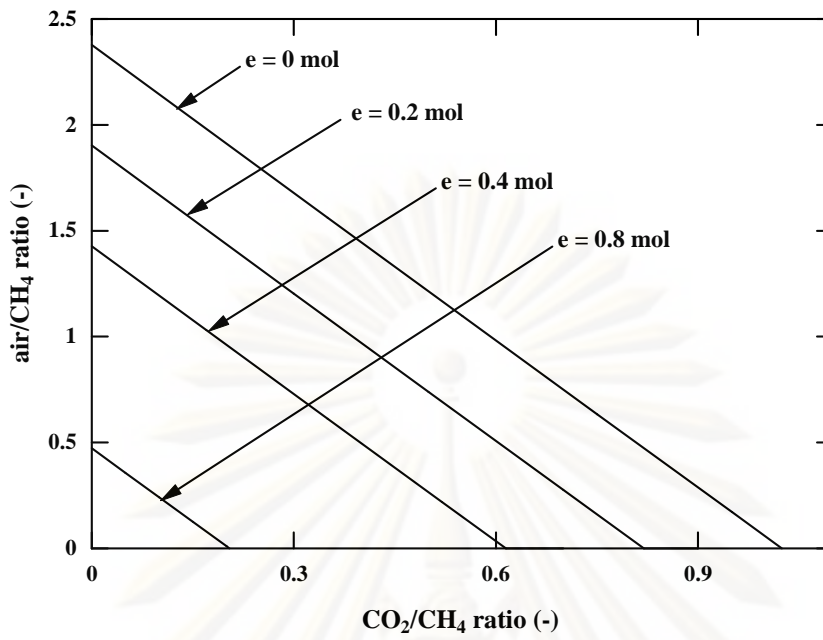
required air/CH₄ ratios for the SOFC-O²⁻ and SOFC-H⁺, respectively. It was found that the similar trend as that of the addition of water is observed for both cases. It should be noted, regarding the advantage of air addition, that although the presence of nitrogen dilutes the partial pressure of hydrogen in the anode gas mixture which results in lower fuel cell performance, the exothermic heat from the oxidation reactions is useful for the endothermic dry reforming reaction in the system.



(a)

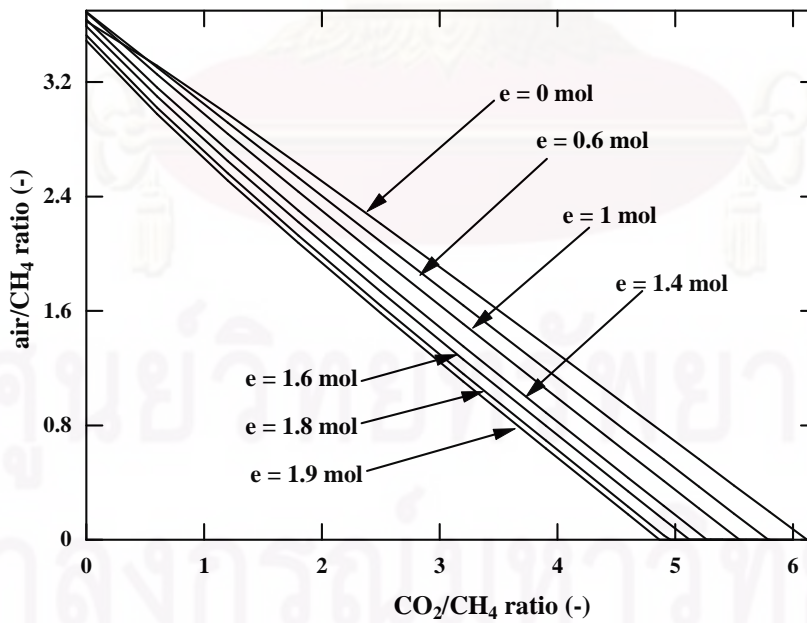


(b)

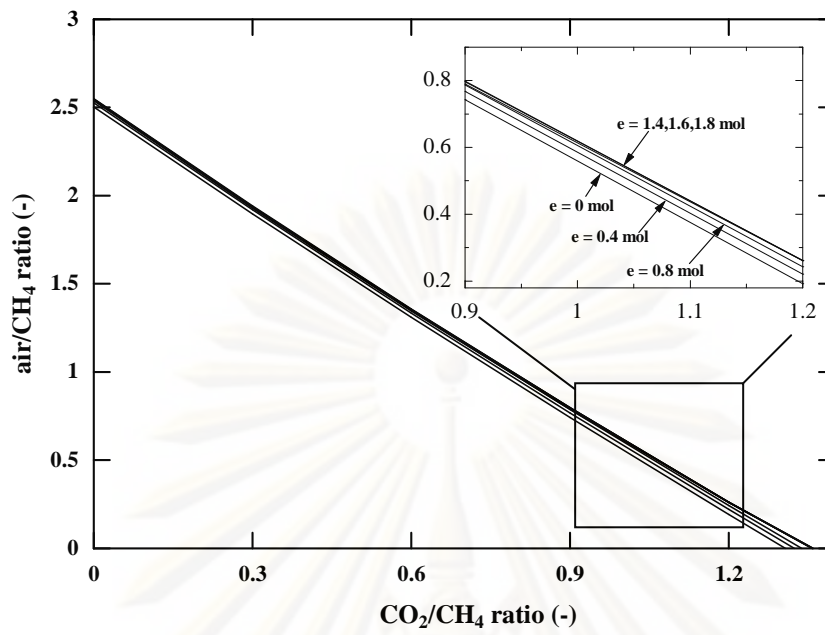


(c)

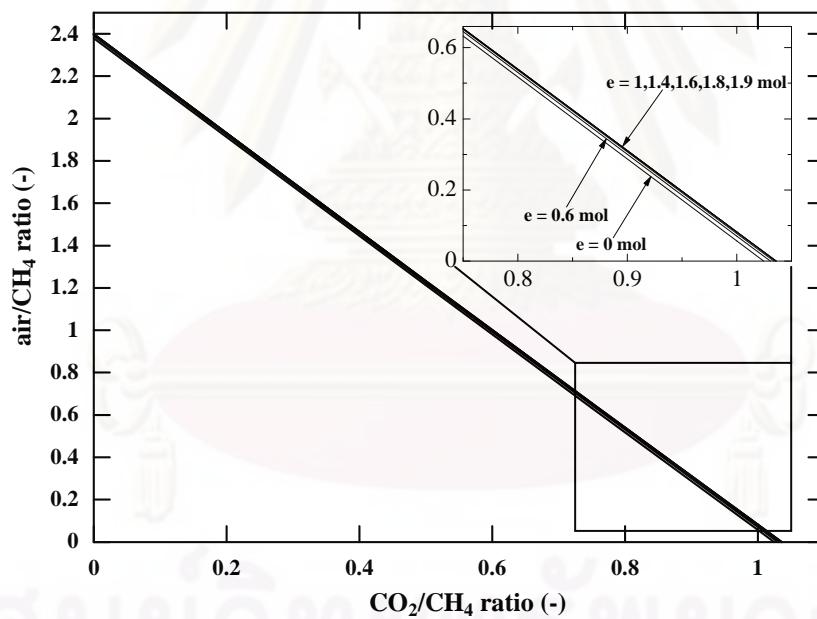
Figure 5.8 Required inlet air/CH₄ ratio at different inlet CO₂/CH₄ ratio: a) $T = 900$ K, b) $T = 1050$ K and c) $T = 1200$ K (SOFC-O²⁻, $n_{CH_4,in}^a = 1$ mol and $P = 101.3$ kPa).



(a)



(b)



(c)

Figure 5.9 Required inlet air/CH₄ ratio at different inlet CO₂/CH₄ ratio: a) $T = 900$ K, b) $T = 1050$ K and c) $T = 1200$ K (SOFC-H⁺, $n_{CH_4, in}^a = 1$ mol and $P = 101.3$ kPa).

5.3. Conclusions

Thermodynamic analysis was employed to predict the boundary of carbon formation for DIR-SOFCs. It was found that the required CO_2/CH_4 ratio to prevent the carbon formation is determined by operating temperature, electrolyte type and extent of electrochemical reaction. Operation at high temperature dramatically reduces the required inlet CO_2/CH_4 ratio. The benefit of the presence of electrochemical H_2O in the anode chamber on suppression of carbon formation is realized in the SOFC- O^{2-} which results in lower requirement of CO_2/CH_4 ratio. For the SOFC- H^+ , due to the disappearance of H_2 without gaining the benefit of the electrochemical H_2O in the anode chamber, higher CO_2/CH_4 ratio is necessary. However, at moderate temperature ($T = 800\text{-}1000\text{ K}$) the unusual opposite trend was observed. The additions of water and air in a feed with a certain inlet CO_2/CH_4 ratio were considered as alternative strategies for suppressing the carbon formation. Water is a more effective choice than CO_2 particularly at low temperature. Although air is less attractive than water, the benefit of the exothermic heat from the reactions with oxygen may make the system become interesting.

It should be noted that although the thermodynamic calculations can be used to predict the boundary of carbon formation, the deactivation of anode is not solely the result from the deposition of carbon. Deposition of other forms of carbonaceous compounds such as polymeric coke (C_nH_m) may result in comparable damage. Therefore, the results obtained in this study should be considered only as crude guideline for selecting suitable operating conditions of SOFCs and other related reactors.

ศูนย์วิจัยทรัพยากร

จุฬาลงกรณ์มหาวิทยาลัย

CHAPTER VI

SELECTION OF APPROPRIATE FUEL PROCESSOR FOR BIOGAS-FUELLED SOFC SYSTEM

In this chapter, the performance of desulfurized biogas-fuelled SOFC systems utilizing different reforming agents (steam, air and combined air/steam) was investigated via thermodynamic analysis to determine the most suitable feedstock. The boundary of carbon formation was initially calculated to specify the minimum amount of each reforming agent necessary to avoid carbon formation. The effect of the reforming agent type, the quantity of reforming agent and the feed quality on the performance of biogas-fuelled SOFC systems were also examined. The electrical efficiency and power density were computed as performance indicator.

6.1 Introduction

Generally, an SOFC system can be divided into three main parts: 1) a fuel processor to reform the raw fuel into hydrogen gas, 2) SOFC stacks which subsequently generate electricity and useful heat from the reformed gas and 3) an afterburner where the residual fuel is combusted in order to supply heat to the preheaters and the fuel processor. Within the fuel processor, four main chemical reactions, namely; steam reforming, dry reforming, partial oxidation and autothermal reforming are possible (Ferreira-Aparicio et al., 2005). Dry reforming is perhaps the most interesting option for the SOFC system fed by biogas since the major components of the biogas are carbon dioxide and methane. However, it gives less hydrogen yields compared with steam reforming reaction. For steam and dry reforming, an external heat source is required to supply the endothermic fuel processor and to preheat the reforming agent (steam and CO_2) and this reduces the overall efficiency of the fuel processor. This problem can be overcome by applying an exothermic partial oxidation reaction which utilizes air as the reforming agent. However, it is accompanied by a lower hydrogen yield. Moreover, the hydrogen partial pressure of the gas product obtained from the partial oxidation is low due to the dilution effect of nitrogen present in air. In order to circumvent this drawback, the

partial oxidation can operate simultaneously with steam reforming to improve hydrogen yield in a route referred to as autothermal reforming. If methane is the fuel, autothermal reforming leads to a higher efficiency (93.9 %) - defined as the lower heating value (LHV) of hydrogen generated divided by the LHV of the methane fuel - than that of the steam reforming (91.3 %) even though the latter gives a higher hydrogen yield. This is because higher heating power is required to generate steam in the case of the steam reforming. In addition, steam reforming is more prone to carbon formation compared to the partial oxidation and autothermal reforming (Ahmed and Krumpelt, 2001).

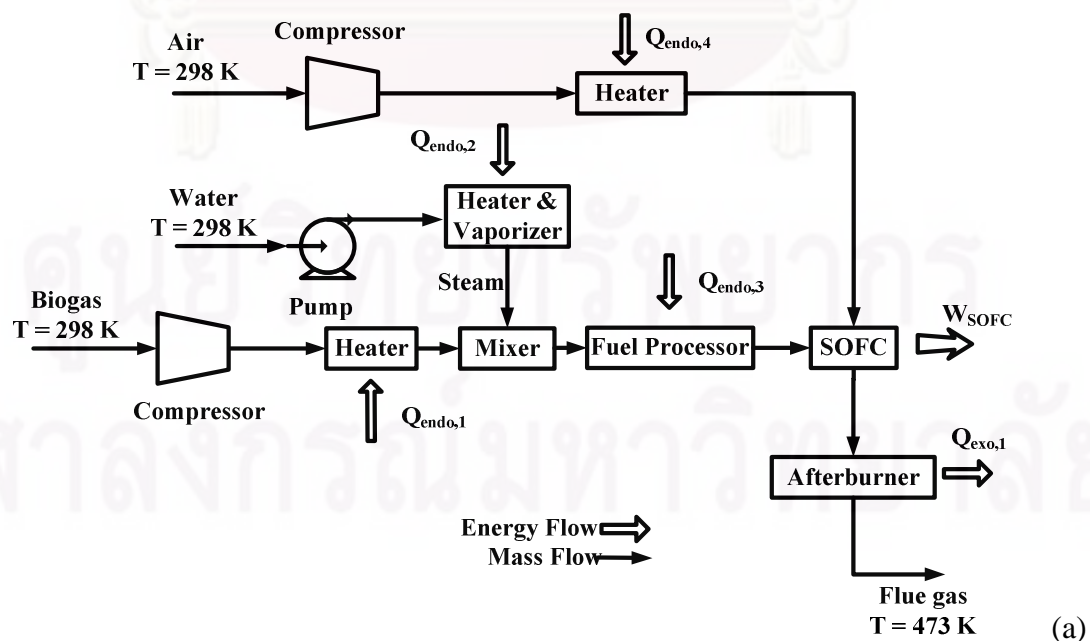
When biogas is considered as a feedstock for the fuel processor, dry reforming may become a co-reaction due to the large amount of CO_2 present in biogas. However, the quantity of carbon dioxide available is not sufficient to convert all methane in biogas into hydrogen. Air and steam are the common reforming agents to combine with CO_2 in the fuel processor. The combination of the dry reforming with partial oxidation helps reduce the reformer size and softens the operating conditions. Furthermore, the desired H_2/CO ratio can be achieved by tuning the composition of the reforming agent (Vernon et al., 1992; O'Connor and Ross, 1998; Rostrup-Nielsen, 2002). Combined steam and dry reforming gives a higher $\text{H}_2:\text{CO}$ ratio compared to sole dry reforming, however, large amount of heat must be supplied to the fuel processor (Froment, 2000; Rostrup-Nielsen et al., 2002).

Although the advantages and disadvantages of the use of each reforming agent in the fuel processor have been widely reported (Froment, 2000; Rostrup-Nielsen et al., 2002), the determination of a suitable reforming agent when the fuel processor is integrated with an SOFC system is still a matter for further investigation. The performance analysis of integrated biogas-fed SOFC systems should provide better insights into proper selection guidelines and hence, the rationale for this study. Thermodynamic analysis was performed to compare the relevant performance indices (overall electrical efficiency and the power density) of the SOFC systems with different reforming agents.

6.2 SOFC system configurations

Three biogas-fuelled SOFC systems are considered in this chapter, i.e. SOFC using steam as the reforming agent (steam-fed SOFC), SOFC using air as the reforming agent (air-fed SOFC) and SOFC using both air and steam as the reforming

agents (co-fed SOFC). The plant configuration for the steam-fed SOFC is illustrated in Figure 6.1a. Several unit operations are included in this configuration consisting of a fuel processor, SOFC stack, an afterburner, a mixer, a vaporizer and preheaters. Steam is generated via the vaporizer, preheated and then mixed with biogas. The mixture gas is then fed into the fuel processor. In the fuel processor, the steam reforming, dry reforming and WGS take place to produce H₂-rich gas and the total heat consumed in these reactions is supplied from heat generated in the afterburner. The H₂-rich gas produced in the fuel processor is fed into the SOFC stack where the electrical energy is generated. The heat generated in the SOFC stack due to the irreversibility is utilized for air and H₂-rich gas preheating. The residue fuel gas released from the SOFC stack is burned up in the afterburner in order to supply heat to the vaporizer and the fuel processor. A high temperature flue gas which mainly contains carbon dioxide and steam released from the afterburner is used in preheating biogas, steam and oxidizing agent (air) before being discharged to the environment at low temperature. For the calculation, the flue gas temperature released from the system is kept at 473 K. To achieve a desired temperature of the SOFC stack, an oxidizing agent (air) temperature is tuned up employing the energy balance in the SOFC stack. The energy self-sufficient point is also found out in this study. A trial-and-error is performed by tuning the fuel utilization until the total energy generated in the system is equal to the total energy consumption ($\sum Q_{endo} - \sum Q_{exo} = 0$).



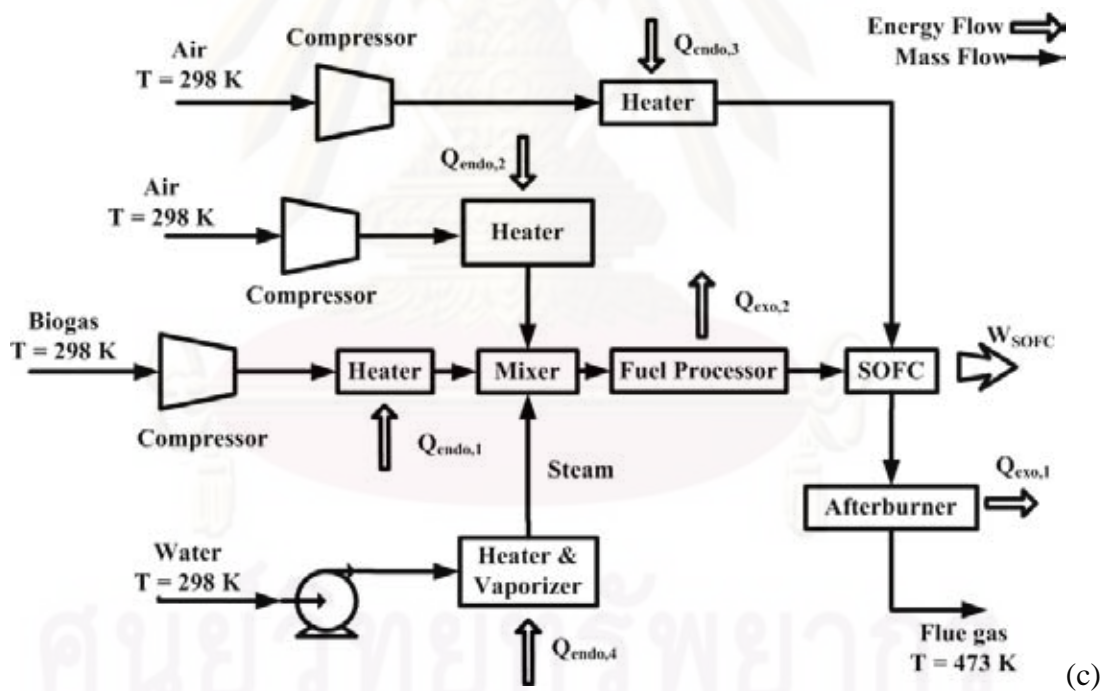
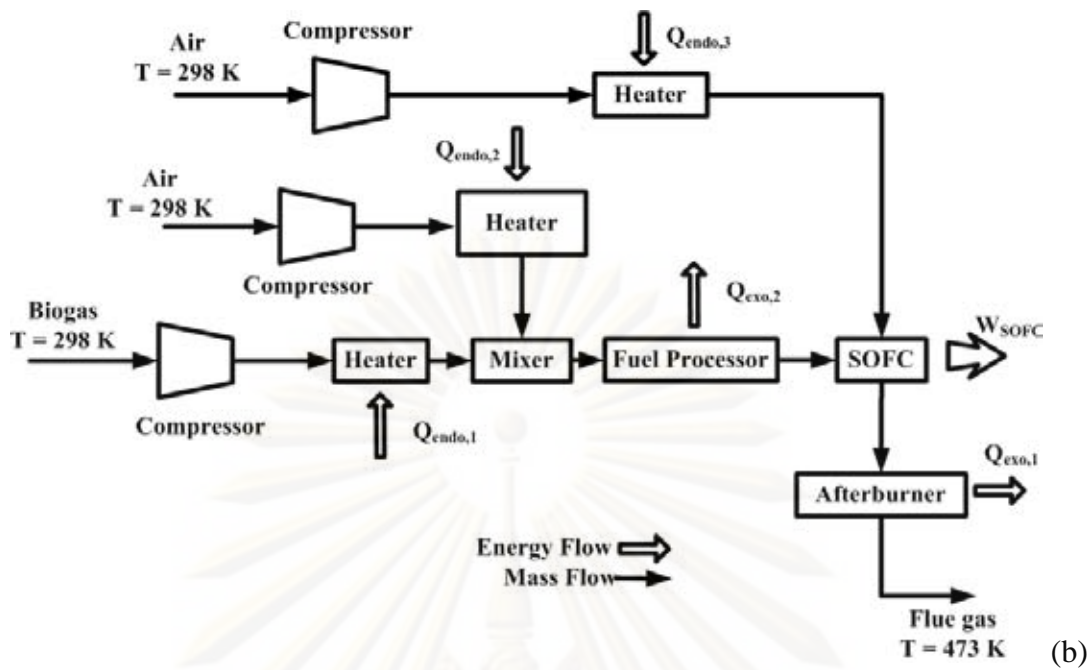


Figure 6.1 The plant configurations for a) the steam-fed SOFC, b) the air-fed SOFC and c) the co-fed SOFC.

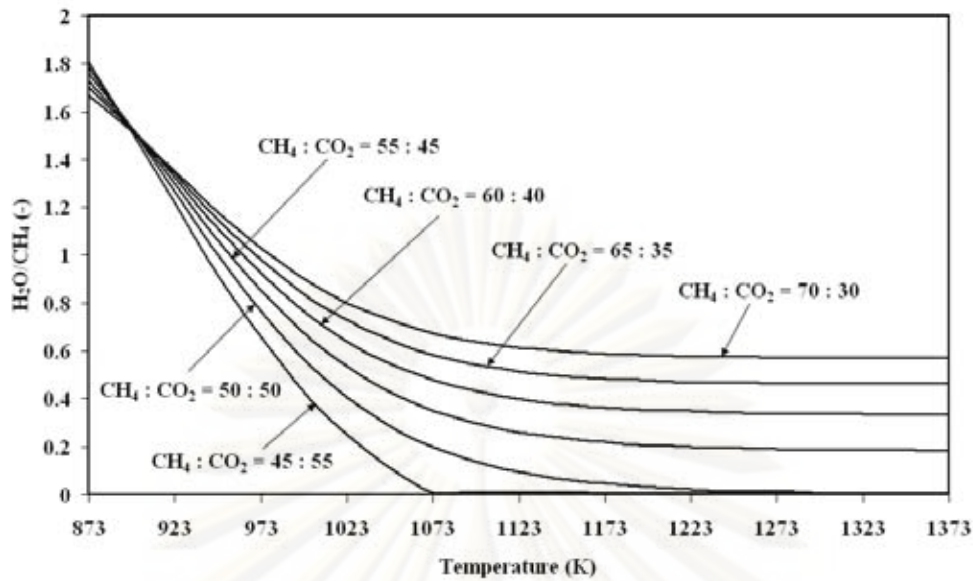
For the air-fed SOFC, its plant configuration and calculation procedure are almost similar to that of the steam-fed SOFC as illustrated in Figure 6.1b. However, it is difficult for the former one to achieve the energy self-sufficient operation. Its heat

demand is extremely lower than that of the steam-fed SOFC since the partial oxidation which takes place in its fuel processor is exothermic. Therefore, almost all hydrogen in the anode gas can be utilized in the SOFC stack for the air-fed SOFC and the power density also reduces following to the increase in the fuel utilization. To achieve a reasonable power density, the hydrogen mole fraction of the SOFC anode output stream is controlled to be higher than 1.5 mol%. In this case, the heat residue from the afterburner is fed into the steam turbine to generate more electricity. The electrical efficiency of steam turbine is assumed to be 30%.

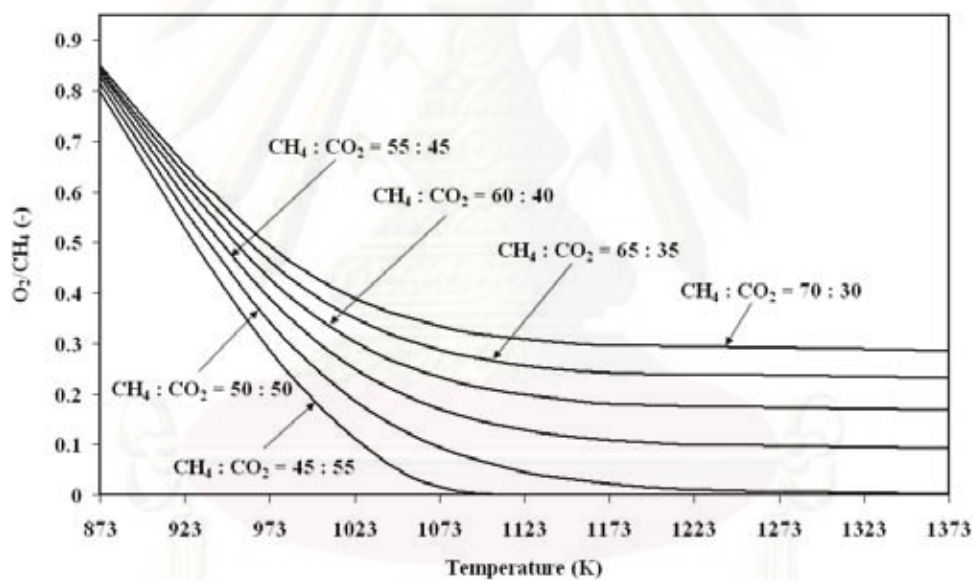
According to the plant configuration of the co-fed SOFC, most of the configurations and calculation procedures are identical to that of the air-fed SOFC as illustrated in Figure 6.1c; nevertheless, more heat is generated in the afterburner than the former in order to generate steam. It should be noted that, in all cases, the quantities of air fed as the oxidant into the SOFC cathode are 5 times of theoretical air required to combust the biogas fuel. The excessive amount of air is required in order to avoid the overheating of the stack which would cause cell damages. Operating temperature of each fuel processor and SOFC stack is kept to be 973 K and 1073 K, respectively.

6.3 Results and discussion

The boundaries of carbon formation indicating the minimum amount of a reforming agent required to avoid the carbon formation for the biogas steam reforming and partial oxidation are illustrated in Figures 6.2a and 6.2b, respectively. It is obvious that less reforming agent (steam or air) is required in order to inhibit the carbon formation when the reforming temperature increases. In fact, the moles of reforming agent per methane required decreased almost hyperbolically with temperature attaining nearly constant value beyond about 1173 K. Biogas with a higher content of methane is more prone to carbon formation than that with a lower amount of methane. These trends are corresponding well with the previous literatures (Edwards and Maitra, 1995; Assabumrungrat et al., 2006).



(a)



(b)

Figure 6.2 Boundary of carbon formation for the biogas-fed fuel processors with different reforming agents; a) steam and b) air.

The effect of fuel utilization and steam contents on the energy self-sufficient point and power density of the steam-fed SOFC were firstly investigated as shown in Figure 6.3. With low steam contents, high fuel utilization is required to achieve energy self-sufficient point since heat loads in steam heater and fuel processor are low. The operation at high fuel utilization of steam-fed SOFC offers low power

density due to the lack of H_2 at the outlet of SOFC stack. For the energy self-sufficient mode ($\Delta Q = 0$), the operation at high steam contents is desired for the steam-fed SOFC to achieve utmost power density. This can be explained by the fact that the presence of large amount of steam in SOFC anode feed can reduce the activation loss in SOFC as described in Eq. (4.6). However, the operation at high steam contents causes higher heat contents in the flue gas and the electrical efficiency of steam-fed SOFC is thus inhibited as illustrated in Figure 6.4. Hence, intermediate value of steam content is desired for steam-fed SOFC for offering reasonable power density and electrical efficiency.

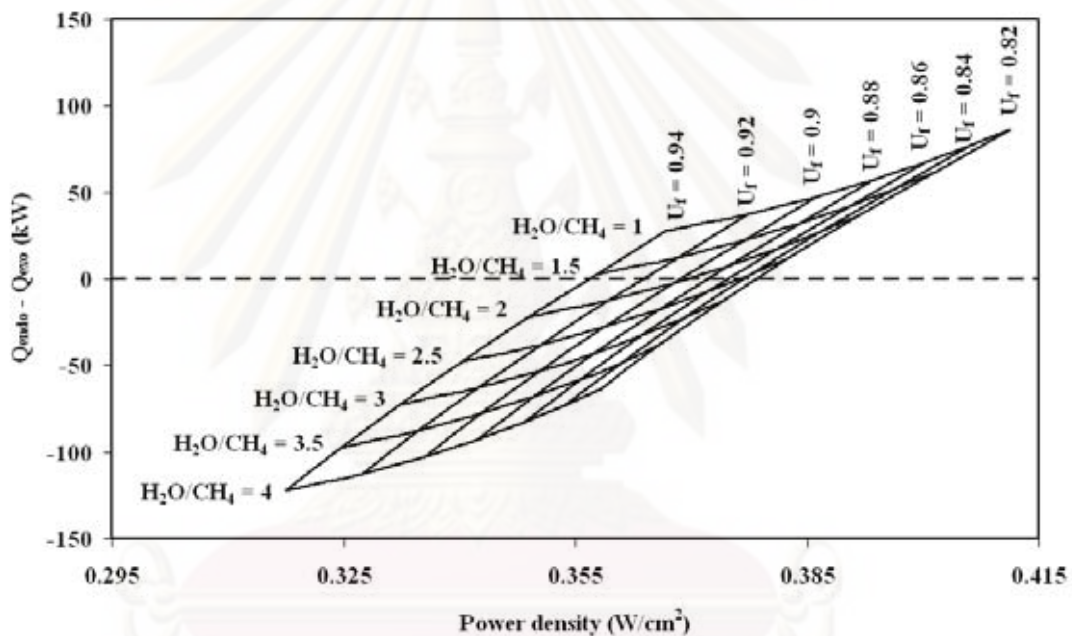


Figure 6.3 The effect of fuel utilization and steam contents on the power density and energy self-sufficient point of steam-fed SOFC. ($V = 0.64$ V and $CH_4:CO_2 = 60:40$)

The composition of biogas ($CH_4:CO_2$) varies with its source; therefore, the effect of biogas composition on SOFC performance should be also investigated. As shown in Figure 6.5, high fuel utilization is required for SOFC fuelled by biogas with low CH_4 contents in energy self-sufficient operation, and the power density of steam-fed SOFC increases as CH_4 contents in biogas increase. As the methane content in the biogas increases, the reformed gas contains hydrogen at a higher concentration and, therefore, a higher power density is achieved. Moreover, the smaller content of CO_2 in

the biogas reduces the energy loss by the exhaust gas of the system. Consequently, the electrical efficiency is improved as observed in Figure 6.4.

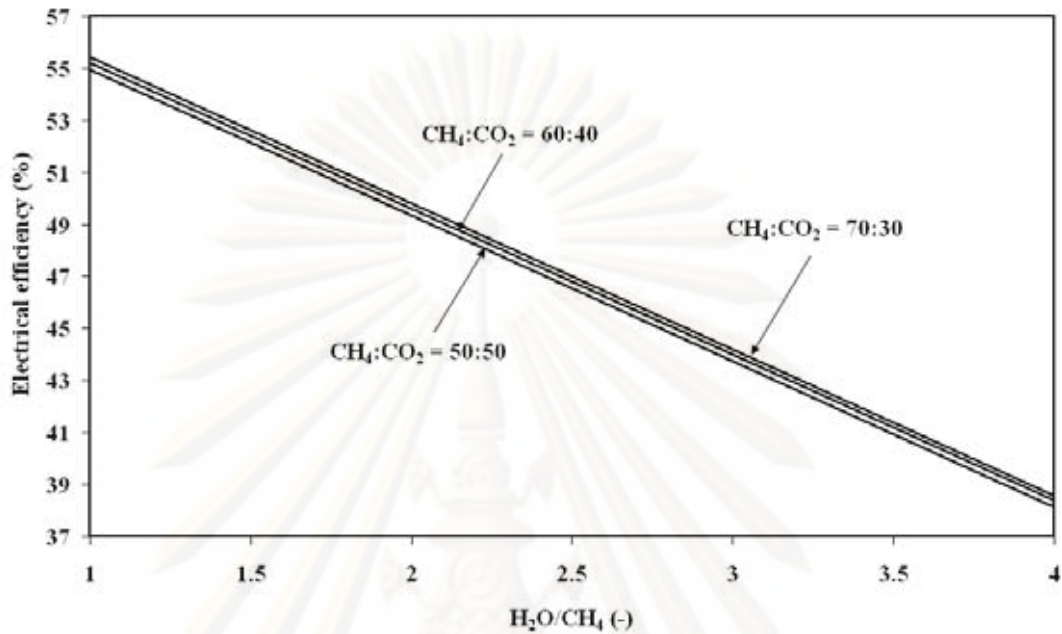


Figure 6.4 The effect of steam contents on electrical efficiency of steam-fed SOFC.

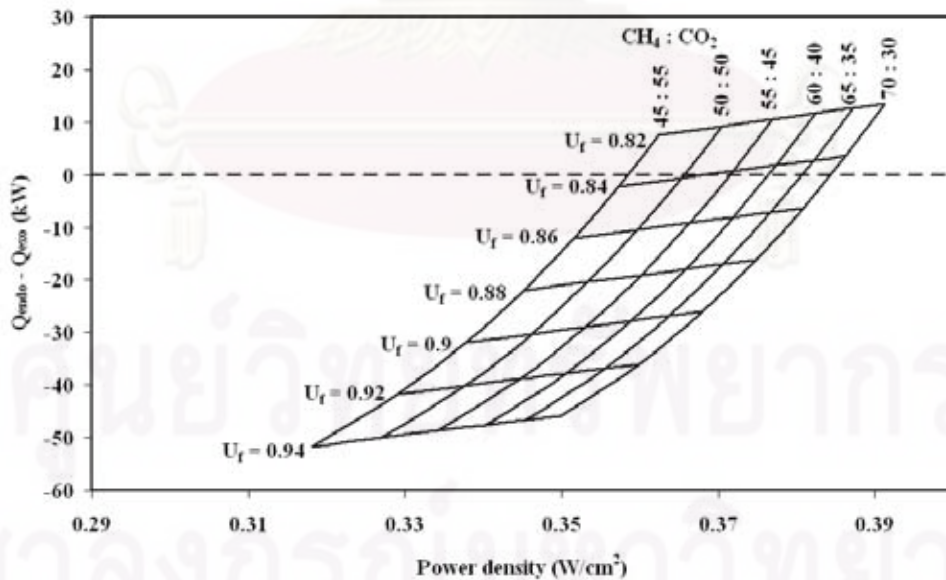


Figure 6.5 The effect of fuel utilization and CH₄:CO₂ ratios in biogas on the power density and energy self-sufficient point of steam-fed SOFC. ($V = 0.64$ V and $H_2O/CH_4 = 2.5$)

As discussed above, the energy self-sufficient operation at each operating condition can be achieved as the fuel utilization is well selected. Figure 6.6 shows the performance of steam-fed SOFC operating at energy self-sufficient point at different operating voltage and steam contents. The optimum operating voltage which offers utmost power density is found at each H_2O/CH_4 . As the operating voltage is lower than the optimum value, the power density increases as operating voltage decreases due to the increase in H_2 consumption in SOFC stack (fuel utilization). However, this benefit is not observed for the operation at excessively low operating voltage. The superior power density is found for SOFC operating at higher steam contents. Operating at H_2O/CH_4 of 4, the power density of steam-fed SOFC can reach 0.446 W/cm^2 as its optimum operating voltage is 0.52 volt. This value of power density is far higher than that of SOFC operating at H_2O/CH_4 of 2.5 which its optimum operating voltage and power density are 0.58 volt and 0.398 W/cm^2 , respectively. However, the electrical efficiency drops from 46.81 % to 38.39 % as H_2O/CH_4 increases from 2 to 4 as described in Figure 6.4.

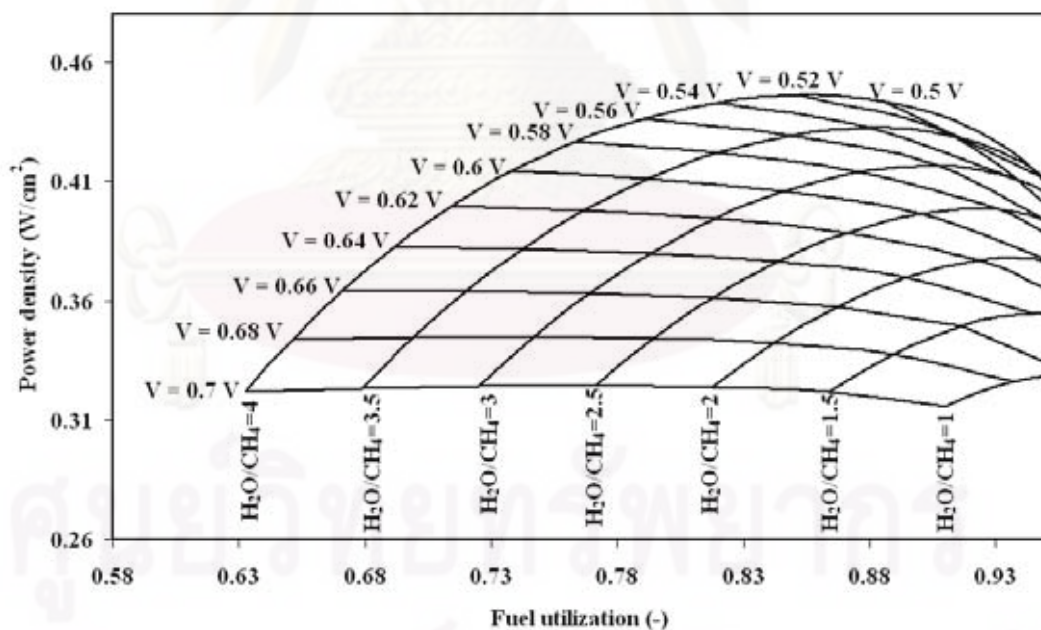
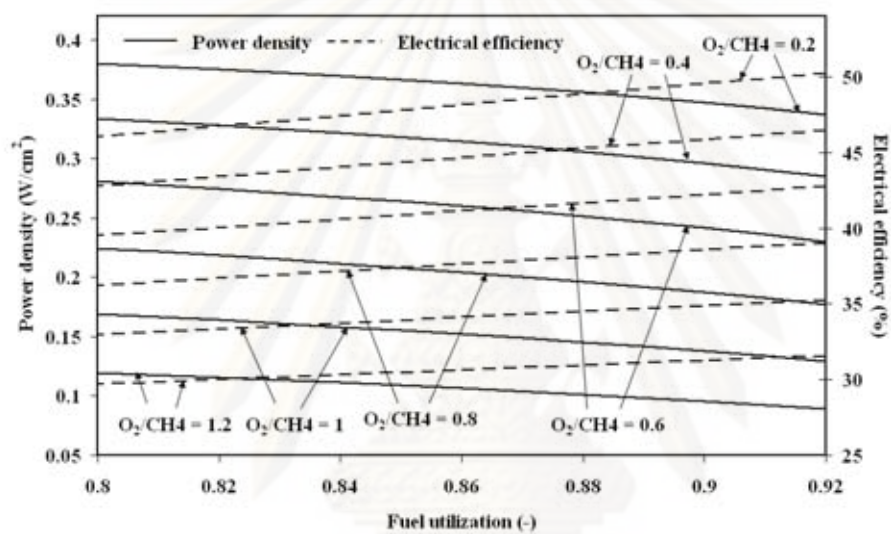


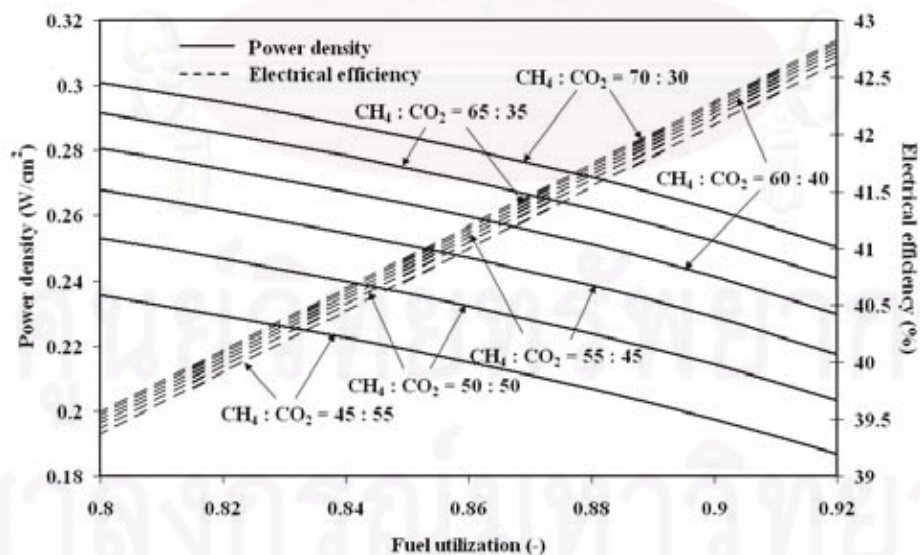
Figure 6.6 The effect of operating voltage and steam contents on the power density of steam-fed SOFC operating at energy self-sufficient point. ($CH_4:CO_2 = 60:40$)

Unlike the steam-fed SOFC, heating energy is not required for the steam generator and the fuel processor for air-fed SOFC. Moreover, heating energy can be

generated in the fuel processor. This is due to the exothermicity of the partial oxidation reaction which takes place in the fuel processor. Hence, air-fed SOFC can operate at high fuel utilization. However, hydrogen fuel cannot be used entirely in the SOFC stack, as some fuel must remain in the SOFC outlet stream in order to maintain a high power density for the SOFC. Figure 6.7 shows that the power density of air-fed SOFC decreases as the fuel utilization increases. This implies that the power density of air-fed SOFC can be improved as hydrogen fuel content remaining in the SOFC outlet stream increases.



(a)



(b)

Figure 6.7 The effect of the fuel utilization on the power density and electrical efficiency at different (a) O₂/CH₄ (CH₄:CO₂ = 60:40) and (b) CH₄:CO₂ ratios in biogas (O₂/CH₄ = 0.6). ($V = 0.64$ V)

The effect of variation in the $O_2:CH_4$ ratio was also investigated. As shown in Figure 6.7a, the power density of air-fed SOFC decreases as air content increases. The decrease in power density is mainly due to the significant increase in inert nitrogen in the inlet stream (anode). Like in case of the power density, the electrical efficiency dwindles as O_2/CH_4 increases. The decrease in the electrical efficiency may be ascribed to the excessive air fed to the reformer, occasioning higher energy loss from the increased amount of exhaust gas. Similar to the case of the steam-fed SOFC, both plant efficiency and power density improve as the quantity of methane in biogas increases as illustrated in Figure 6.7b. Although low $O_2:CH_4$ ratio can improve both power density and electrical efficiency of air-fed SOFC, the issue of carbon formation should be also carefully considered. As described in Figure 6.2b, $O_2:CH_4$ should be higher than 0.5 which is boundary of carbon formation for the operation at 973 K.

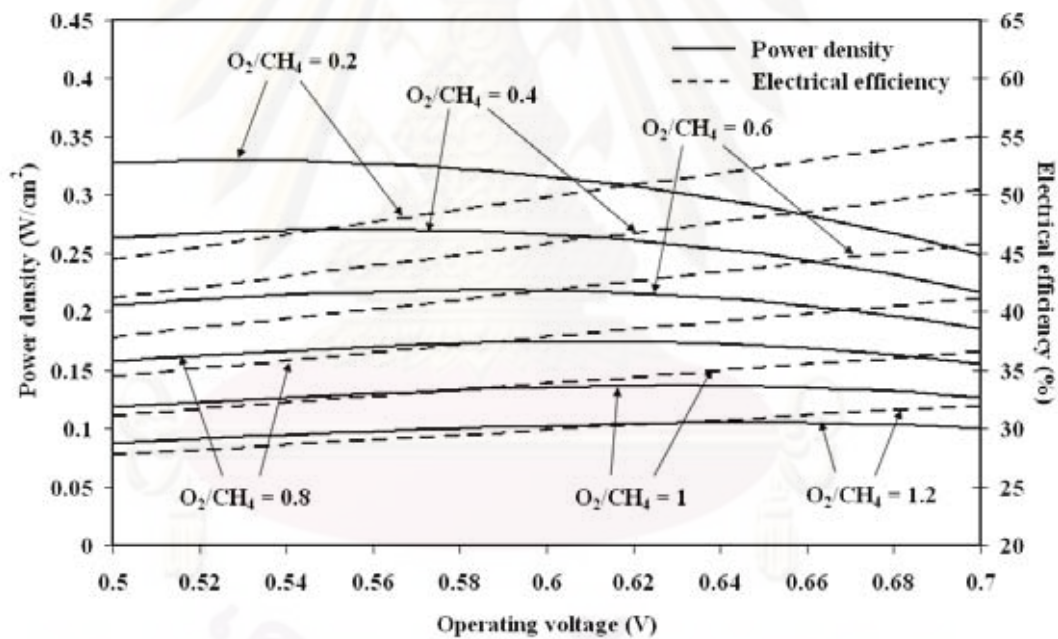


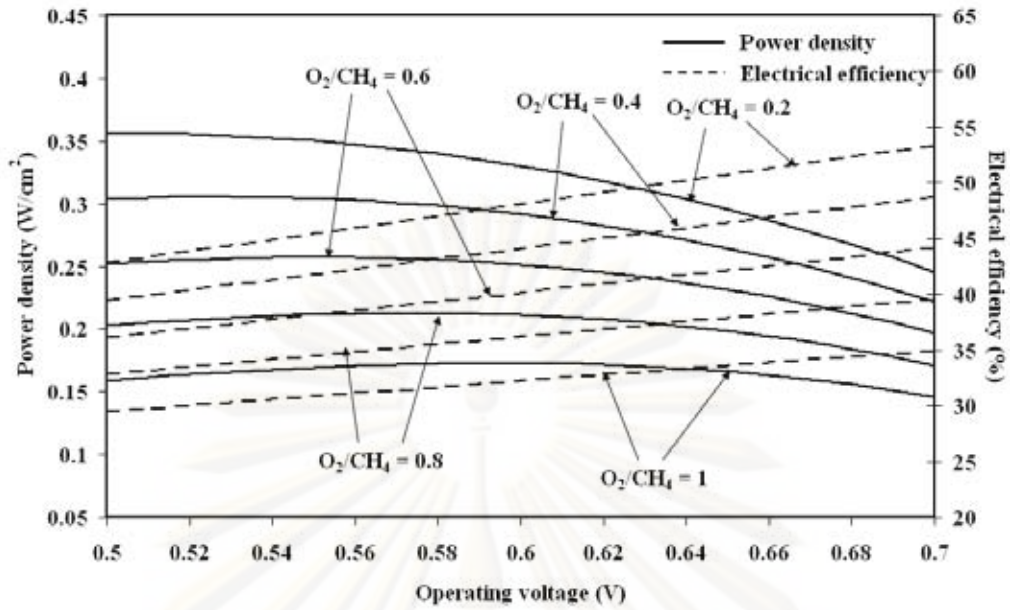
Figure 6.8 Electrical efficiency and power density of air-fed SOFC at different operating voltage and air contents. ($CH_4:CO_2 = 60:40$)

Figure 6.8 shows the effect of the variation of the operating voltage and O_2/CH_4 on the system performance of air-fed SOFC. Unlike the steam-fed SOFC, air-fed SOFC cannot offer energy self-sufficient operation. Hence, for the calculation of air-fed SOFC, the fuel utilization is tuned up until the hydrogen mole fraction of the SOFC anode output stream is controlled to be higher than 1.5 mol% to achieve

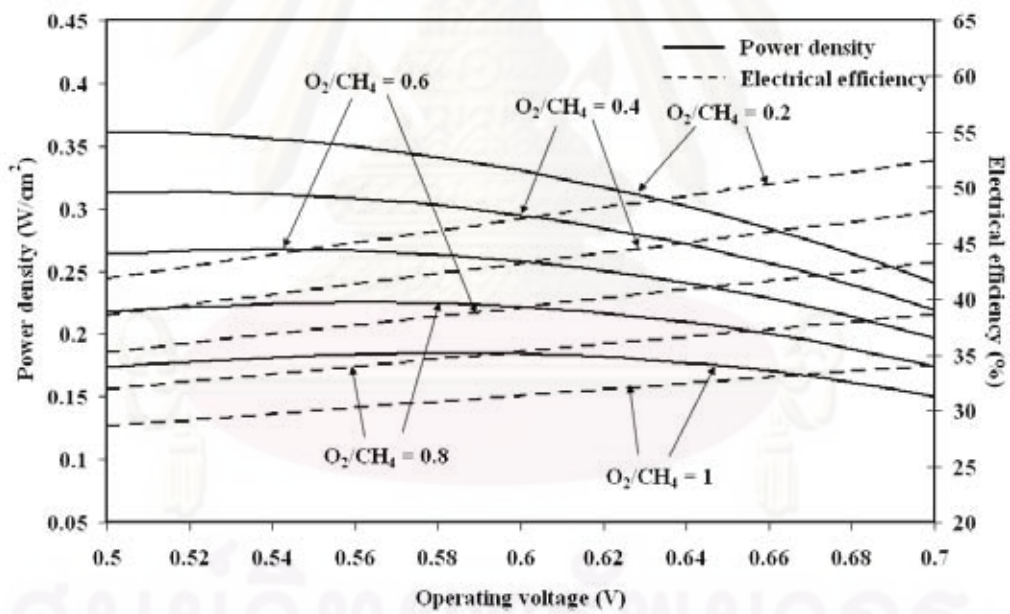
reasonable power density and electrical efficiency. Similar to the case of steam-fed SOFC, the optimum operating voltage which offers utmost power density is also found in air-fed SOFC. As shown in Figure 6.8, the operation at high air contents is not desirable for air-fed SOFC. For the operation at $O_2:CH_4$ ratio of 0.6 which is the condition that is not prone to carbon formation, air-fed SOFC fuelled by biogas with $CH_4:CO_2$ ratio of 60:40 offers the power density and electrical efficiency of 0.218 W/cm^2 and 41.44 %, respectively for the optimum operating voltage of 0.59 volt.

Compared with the case of the steam-fed SOFC, the power density is much lower. This is due to the fact that the partial oxidation reaction (Eq. (4.53)) can produce only two moles of hydrogen per mole of methane compared with three moles of hydrogen per mole of methane in the case of the steam reforming reaction (Eq. (4.32)). In addition, the high proportion of nitrogen present in air also reduces the hydrogen concentration in the reformed gas. Consequently, the hydrogen partial pressure of the product gas derived from the partial oxidation is lower than that derived from the steam reforming, leading to a lower SOFC power density.

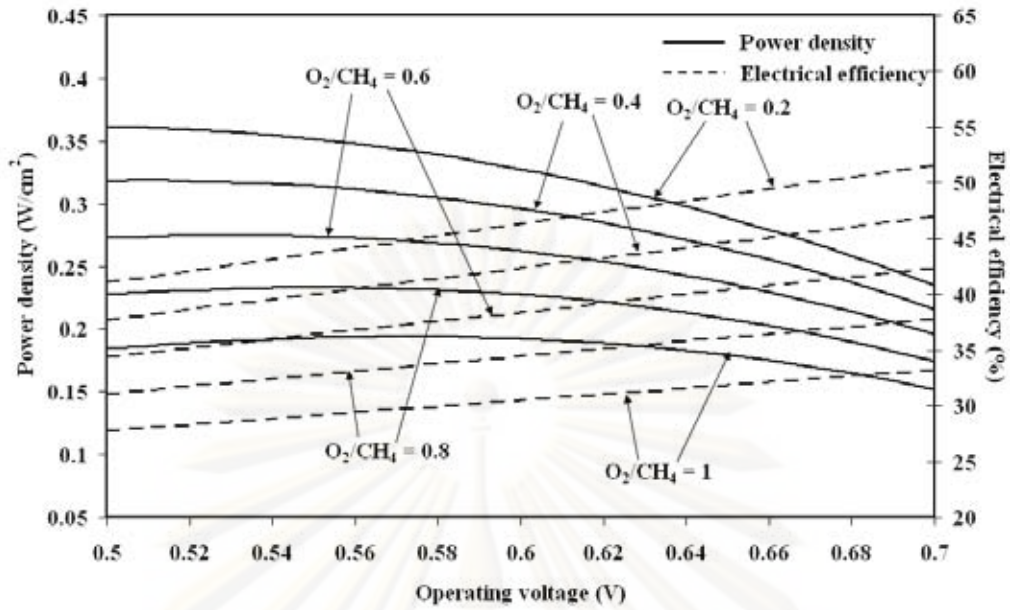
As a third option, the co-fed SOFC was also investigated. Unlike the steam-fed SOFC, there is no energy supplied to the fuel processor due to the participation of exothermic partial oxidation reaction; however, some heating energy produced in the afterburner must be supplied to the vaporizer to generate steam. Furthermore, the residue heat from the co-fed SOFC system is supplied to the steam turbine to generate more electricity like in the case of the air-fed SOFC. The plant electrical efficiency and the power density at different $O_2:CH_4$ and $H_2O:CH_4$ ratios are illustrated in Figure 6.9. In this study, the biogas composition ($CH_4:CO_2$) is kept at 60:40. Like the case of steam-fed SOFC, the electrical efficiency of the co-fed SOFC decreases, and the power density of co-fed SOFC increases with the increase in the steam content. However, the change in these performance indicators of co-fed SOFC is extremely smaller compared with that found in steam-fed SOFC. Similar to the air-fed SOFC, the power density and electrical efficiency of co-fed SOFC decrease as the $O_2:CH_4$ ratio increases due to the presence of large amount of nitrogen in air. The electrical efficiency of co-fed SOFC is improved as the operating voltage increases. The optimum operating voltage which offers ultimate power density is also found like in case of the other SOFC systems.



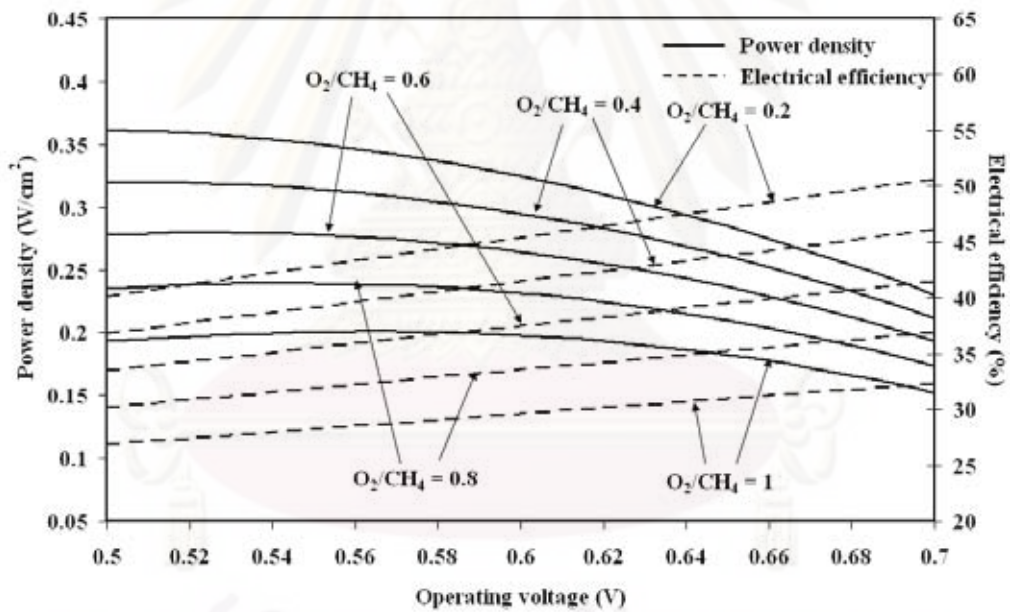
(a)



(b)



(c)



(d)

Figure 6.9 Electrical efficiency and power density of co-fed SOFC operating at $\text{H}_2\text{O}:\text{CH}_4$ ratios of (a) 1, (b) 1.5, (c) 2 and (d) 2.5 at different operating voltage and air contents. ($\text{CH}_4:\text{CO}_2 = 60:40$)

In order to select a suitable reforming agent, the performance of the SOFC systems with different reforming agents is compared as shown in Figure 6.10. It is obvious that steam is the most attractive reforming agent for the biogas-fed SOFC

regarding the power density. The power density and electrical efficiency of air-fed SOFC are much lower due to the high content of nitrogen in air. By adding air to the steam-fed SOFC, the electrical efficiency can be slightly improved but the power density extremely reduced. Because the stack is among the most expensive part of the SOFC system, it is likely that the use of steam as the reforming agent is the most suitable for the biogas-fed SOFC although the electrical efficiency is slightly lower than the use of combined steam and air.

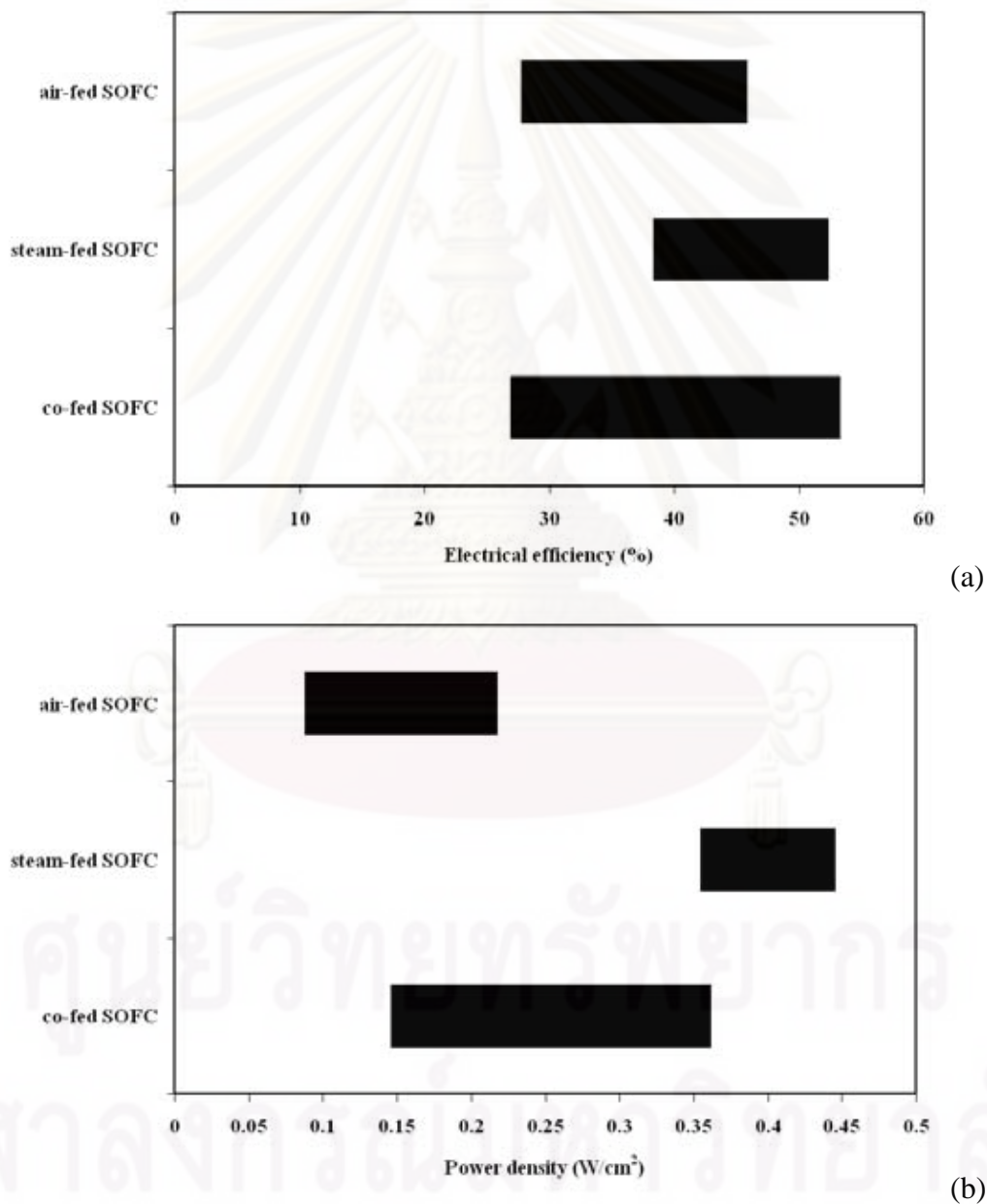


Figure 6.10 SOFC performance: a) overall electrical efficiency and b) power density (CH₄:CO₂ = 60:40).

6.4 Conclusions

Performance of the desulfurized biogas-fed SOFC systems with different reforming agents (steam, air and combined steam/air) was determined in order to find a suitable reforming agent. The boundary of carbon formation was firstly calculated to specify a minimum amount of each reforming agent necessary to avoid carbon formation. For the steam-fed SOFC, when the amount of steam increases, the power density always increases. Inversely, the electrical efficiency decreases with steam contents. For the air-fed SOFC, both power density and electrical efficiency always decrease with the increased amount of air due to the dilution effect of nitrogen in air. However, the intermediate air content is desired for air-fed SOFC to alleviate the carbon formation. Steam is considered to be the most suitable reforming agent in this study as the steam-fed SOFC offers much higher power density and electrical efficiency than the air-fed SOFC. When steam is added in the air-fed SOFC as in the case of the co-fed SOFC, both electrical efficiency and power density can be improved; however, its power density cannot reach the power density of steam-fed SOFC.

CHAPTER VII

PERFORMANCE OF BIOGAS-FED SOLID OXIDE FUEL CELL SYSTEMS INTEGRATED WITH CO₂ CAPTURE TECHNOLOGY

The objective of this chapter is to examine the performance and potential benefit of desulfurized biogas-fuelled SOFC system cooperating with CO₂ capture technology. Two configurations of biogas-fed SOFC, i.e., SOFC system cooperating with CO₂-selective membrane (M-SOFC) and SOFC system cooperating with CaO-CO₂ acceptor (A-SOFC) were investigated. The conventional SOFC system (CON-SOFC) is employed as a base case. Similar to chapter 6, the electrical efficiency and power density are considered as the performance indicators. The composition of biogas considered in this study is kept at 60 percent of methane and 40 percent of carbon dioxide. All mathematical models used in calculation were written in Visual basic.

7.1 Introduction

As mentioned earlier, the presence of CO₂ in the feedstock could cause the falling down in SOFC cell potential. However, the removal of CO₂ from feedstock requires the complicated technology and consumes a lot of energy. The removal of CO₂ from biogas is widely investigated. Several technologies are proposed; i.e., absorption, adsorption and membrane technology. Membrane technology has been widely tested and presently applicable in the capture of CO₂ in natural gas (Granite and O'Brien, 2005). Compared with CO₂ absorption technology which is conventionally used, membrane technology offers the advantages of operational flexibility in handling feed streams with variable flow rates and compositions. Polymeric membrane is one of the interesting choices due to its low capital investment costs compared with other types of membrane (Alexander Stern, 1994). Moreover, the process equipment for the polymeric membrane operation is also simple and easy to handle. Selection of polymeric membrane for gas separation is

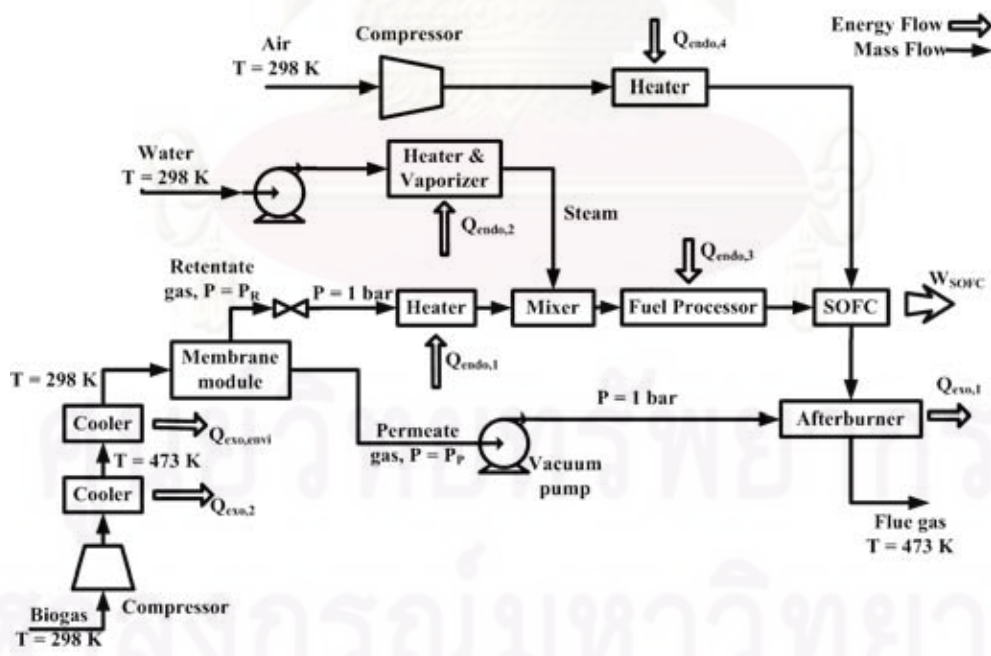
based on two parameters; permeability and permselectivity. Polyimide membrane is the more attractive gas separator because it offers higher permselectivity and permeability compared to membranes derived from other polymers (Shekhawat et al., 2003). The use of capillary module with polyimide membrane for the CH₄ enrichment in biogas mixtures (CH₄, CO₂ and H₂S) was also investigated and the results showed that CH₄ concentration in biogas increases from 55-85% up to 91-94.4% (Harasimowicz et al., 2007). The drawback of the polyimide membrane is that it cannot operate at high temperature. Adsorption is also interesting CO₂-capture technology. A favorite adsorbent used in CO₂ capture is Calcium oxide (CaO). With this technology, CO₂ in the gas mixture reacts with CaO particle (Eq. (4.75)), and CaCO₃ is produced. The major drawback of this technology is that the regeneration of the adsorbent is required. In the mature process, CO₂-rich gas is fed simultaneously with CaO into the low-temperature adsorption column (Grasa et al., 2008). Lean-CO₂ gas is released from this column in the top section. CaO-CaCO₃ particle derived from the bottom section of the low-temperature column is then fed into high-temperature column to convert all CaCO₃ into CaO which can be reused in CO₂ capture. Even if CaO can be regenerated, the make-up CaO is necessary to this cycle due to the sintering of CaO at high operating temperature (773-1073 K) after several CO₂ capture cycle (Abanades, 2002).

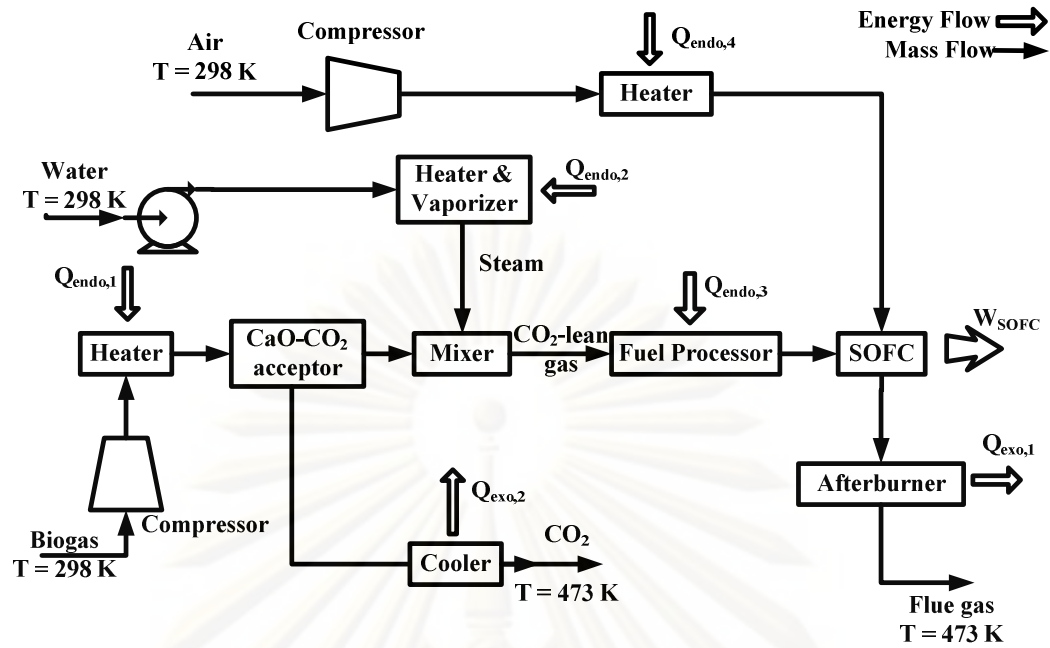
In this chapter, an integration of a biogas-fuelled SOFC system and CO₂-capture technology was investigated. The improvement in the SOFC power density following to the installation of CO₂ separator was considered. Two configurations are applied in this study: 1) the SOFC cooperating with CO₂-selective membrane (M-SOFC) and 2) the SOFC cooperating with the CaO-CO₂ acceptor (A-SOFC). Thermodynamic analysis was performed to evaluate the performance indicators (overall electrical efficiency and power density) of these configurations and to compare them with those of the SOFC system without CO₂ separator installation (CON-SOFC). Lastly, an economic analysis was employed to identify whether the CO₂ separators should be installed into the SOFC system.

7.2 SOFC system configurations

Two desulfurized biogas-fed SOFC systems cooperating with CO₂ capture unit are proposed in this study, i.e. the SOFC system with CO₂-selective membrane (M-SOFC) and the SOFC system with the CaO-CO₂ acceptor (A-SOFC). It should be

noted that steam is chosen as the reforming agent in the subsequent study according to the result in chapter 6. Moreover, the steam to methane ratio in the fuel processor feed is set to be 2.5 for the studies the following chapters to alleviate the carbon formation in the system. Their configurations are almost identical to that of the conventional SOFC system (CON-SOFC) which is illustrated in Figure 6.1a. However, for the M-SOFC (Figure 7.1a), biogas is compressed, cooled down and then fed into the polyimide membrane module where CO_2 is captured. To increase the CO_2 separation performance, vacuum pump is included in the system in order to increase the partial pressure difference of retentate and permeate section of membrane module. The retentate gas is depressed, preheated and then fed into the fuel processor whereas the permeate gas is fed into the afterburner to produce more heat. For the A-SOFC (Figure 7.1b), biogas is compressed and fed into the CaO-CO_2 acceptor in which CO_2 is separated without the loss of methane. CO_2 -lean gas is mixed with steam and then fed into the fuel processor. Similar to the plant configuration of CON-SOFC, the flue gas temperature released from the system is kept at 473 K. Like the calculation in chapter 6, the energy self-sufficient operating ($\Delta Q = 0$) is also examined in this chapter.





(b)

Figure 7.1 The plant configurations for (a) the M-SOFC and (b) the A-SOFC.

7.3 Results and discussion

Prior to the SOFC system investigation, the performance of membrane modules for CO_2 separation was examined. The feed gas composition for the polyimide membrane is based on a raw biogas. The % CO_2 removal and % CH_4 loss at different operating pressure at permeate section (P_P) and retentate section (P_R) is summarized in Figure 7.2. It is obvious that the increases in P_P and P_R can raise the extent of CO_2 removal. At P_P of 30 bar and P_R of 0.1 bar, polyimide membrane can remove 95% of CO_2 in the feed gases. However, some CH_4 (5.85%) also permeate together with CO_2 through polyimide into the permeate side. It should be noted that, in this study, the permeate gas which contains fuel gas (CH_4) is fed into the afterburner to produce more heat to supply the system as illustrated in Figure 7.1a. Even if the polyimide membrane module which operates at high P_R and low P_P can separate more CO_2 , the electricity consumptions in compressor and vacuum pump of M-SOFC which operates at these conditions are extremely high as shown in Figure 7.3.

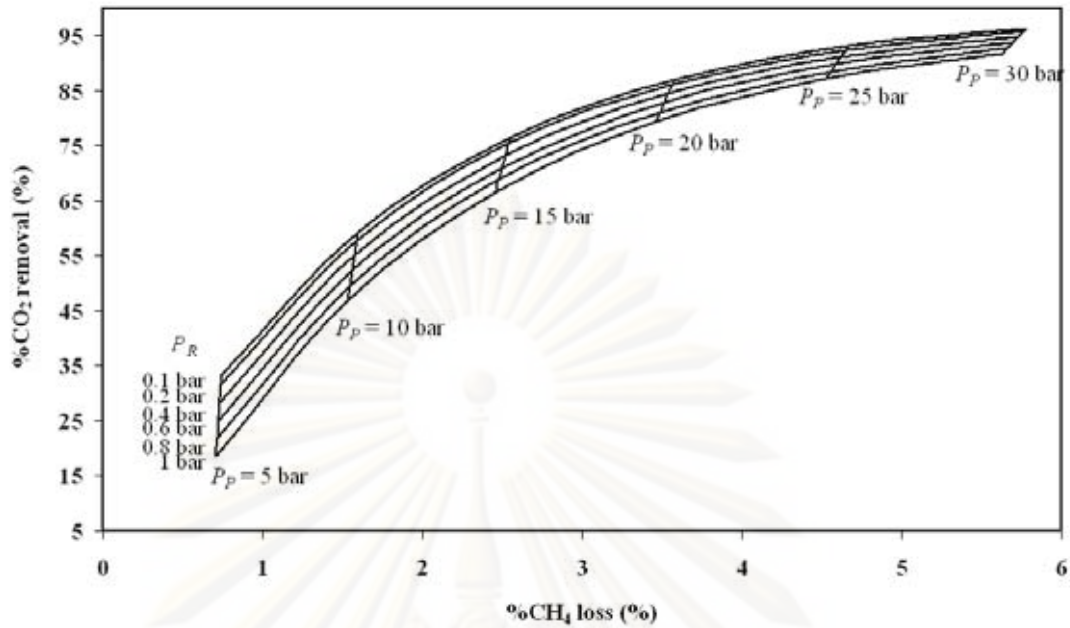


Figure 7.2 The %CO₂ removal and %CH₄ loss at different operating pressure at permeate section (P_p) and retentate section (P_R).

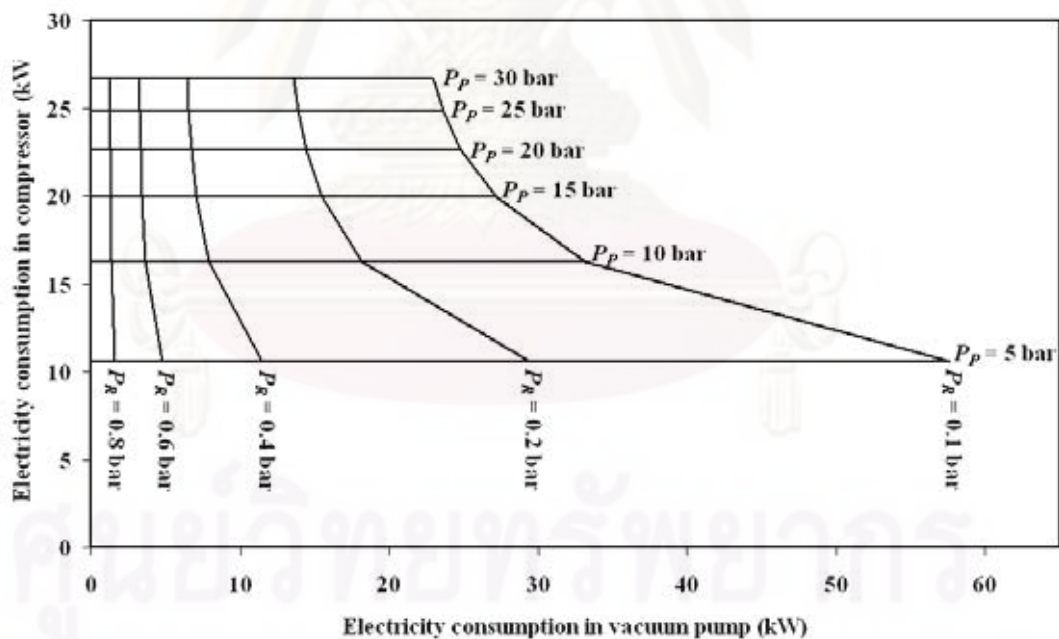
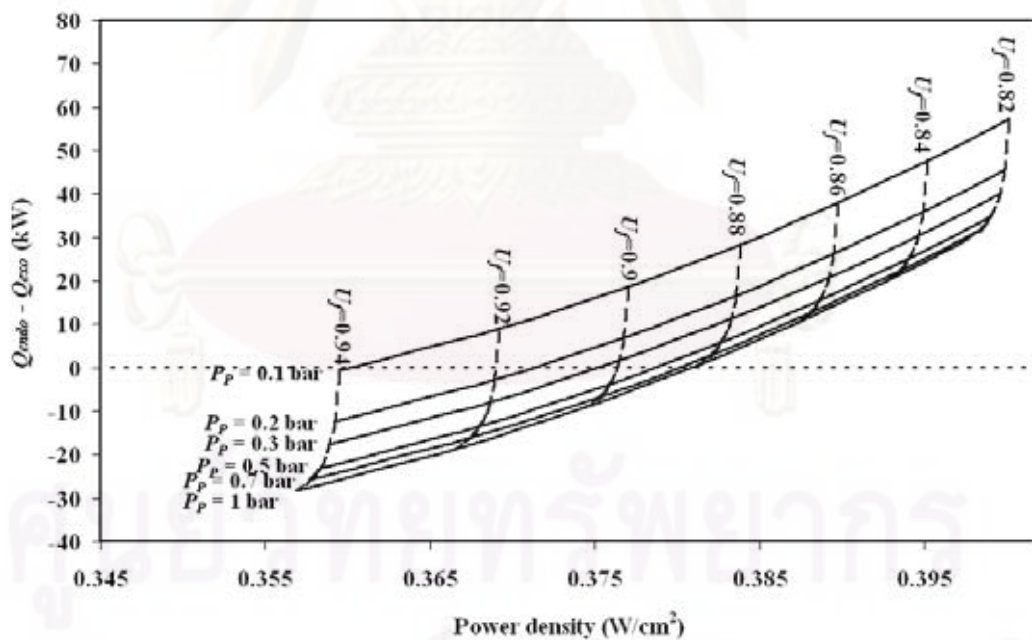


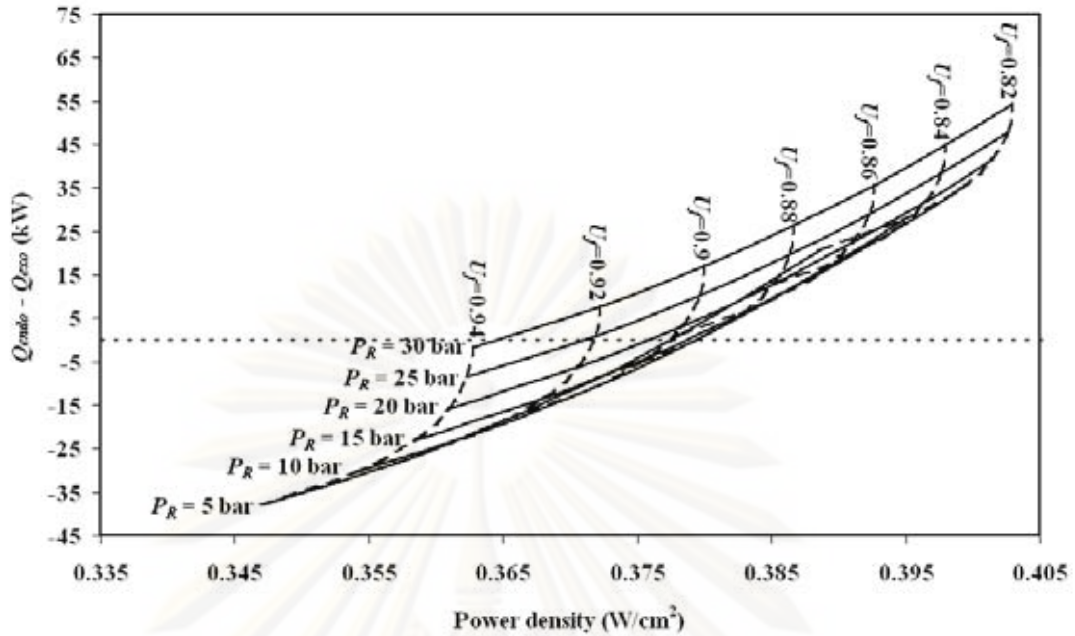
Figure 7.3 The electricity consumption in compressor and vacuum pump at different P_p and P_R .

Following this preliminary run, the performance of the M-SOFC system is then investigated. Figures 7.4 show the effect of the operating pressure of membrane

module and fuel utilization on the energy self-sustainable point and the power density of M-SOFC. Figure 7.4a focuses on the effect of P_p . The fuel utilization of 0.94 is required for SOFC operating at P_p of 0.1 bar to achieve the energy self-sustainable operation, as the fuel utilization of 0.88 is enough for the operation at P_p of 1 bar which is the condition that the vacuum pump does not work. This is due to the reason that the heat generation in the compression process of the vacuum pump is high as the M-SOFC system operates at low P_p , and more hydrogen fuel can be used in SOFC stack. Moreover, more electricity is consumed in vacuum pump for SOFC operating at low P_p . However, the operating at high fuel utilization is not desired for SOFC since it offers low power density at this condition. As shown in Figure 7.4a, for the operation at the operating voltage of 0.64 volt and P_R of 20 bar, M-SOFC operating at P_p of 0.1 bar offers the power density of 0.36 W/cm² which is lower compared with 0.38 W/cm² in case of M-SOFC operating at P_p of 1 bar. This is similar to the conclusion in chapter 6 which informs that some hydrogen fuel should remain in the exit gas of SOFC anode.



(a)

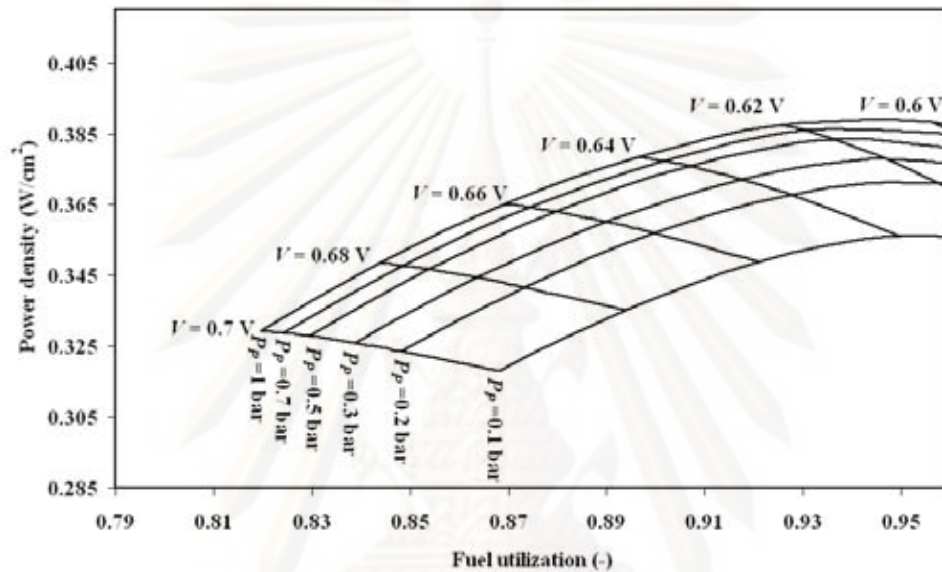


(b)

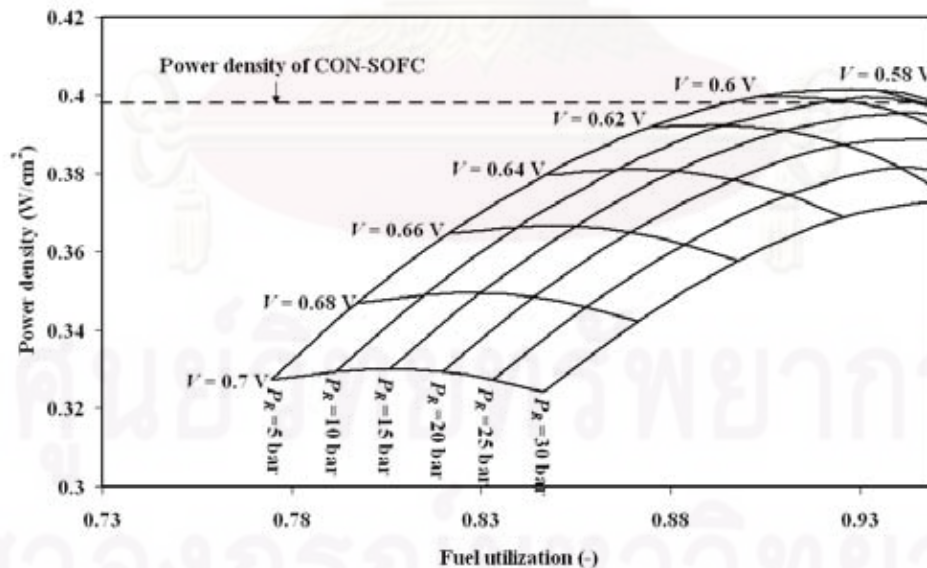
Figure 7.4 The effect of a) P_P ($P_R = 20$ bar) and b) P_R ($P_P = 0.5$ bar) on the energy self-sustainable point and the power density of M-SOFC. ($V = 0.64$ volt)

For the study of the variation of P_R , as illustrated in Figure 7.4b, the energy self-sufficient operation is available for SOFC operating at high P_R as it operates at high fuel utilization. With high P_R , high electricity is required to produce so as to compensate the electricity consumption in high-pressure compressor. Again, even if the operation at low P_R offers lower CO_2 removal compared with the operation at high P_R , it offers higher power density since it can operate at lower fuel utilization. The effect of the operating voltage on the performance of M-SOFC operating at energy self-sufficient point was also investigated. As shown in Figure 7.5a, the power density of M-SOFC is always utmost as P_P is 1 bar. It can be concluded that the optimum P_P is at the atmospheric pressure and the vacuum pump is thus not required for M-SOFC system. Figure 7.5b shows the power density at different P_R and operating voltage of M-SOFC operating at energy self-sufficient point and P_P of 1 bar. The optimum operating voltage is always found at each operating condition. At high operating voltage, the intermediate P_R is preferred; however, low P_R become favored as the operating voltage is lower than 0.6 volt. With good operating condition selections, the power density of M-SOFC can become higher than that of CON-SOFC (dashed line) as illustrated in Figure 7.5b. For the operation at P_P and P_R of 1 and 5 bar,

respectively, M-SOFC can offer the power density of 0.401 W/cm^2 at the optimum operating voltage of 0.58 V , whereas the maximum power density CON-SOFC can achieve is 0.398 W/cm^2 . However, the maximum electrical efficiency of M-SOFC is 45.47% which is lower compared with that of CON-SOFC (46.81%). This is caused from heat loss to the environment from the biogas cooling prior to be fed to membrane module in M-SOFC system.



(a)



(b)

Figure 7.5 The effect of the operating voltage on the power density at different a) P_P ($P_R = 20 \text{ bar}$) and b) P_R ($P_P = 1 \text{ bar}$) in case that M-SOFC operates at energy self-sufficient point.

The cooperation of the SOFC with CaO-CO₂ acceptor (A-SOFC) was also investigated. The details used in the performance evaluation for CaO-CO₂ acceptor are given in chapter 4. CaO-CO₂ acceptor is employed in removing CO₂ from biogas prior to be fed to the fuel processor. With this technology, CO₂ can be removed from biogas without CH₄ loss. It can operate at low operating pressure; hence, there is no electricity consumption in this technology. However, some make-up adsorbents are required to maintain the adsorption efficiency at the reasonable value. As illustrated in Figure 7.6, with the CaO circulation rate: CO₂ feed rate ($F_R:F_{CO_2}$) of 10 and the CaO inventory of 50 kg, make-up CaO is not required as CO₂ removal rate is lower than 0.48 mol/s. Exceeding this value, CaO make-up rate increases as CO₂ removal rate increases. To remove CO₂ at the rate of 0.63 mol/s, CaO make-up rate of 0.0311 mol/s is required. It should be noted that the maximum CO₂ removal rate the CaO-CO₂ acceptor can offer is 0.63 mol/s. This limitation is caused from the equilibrium of the carbonation reaction.

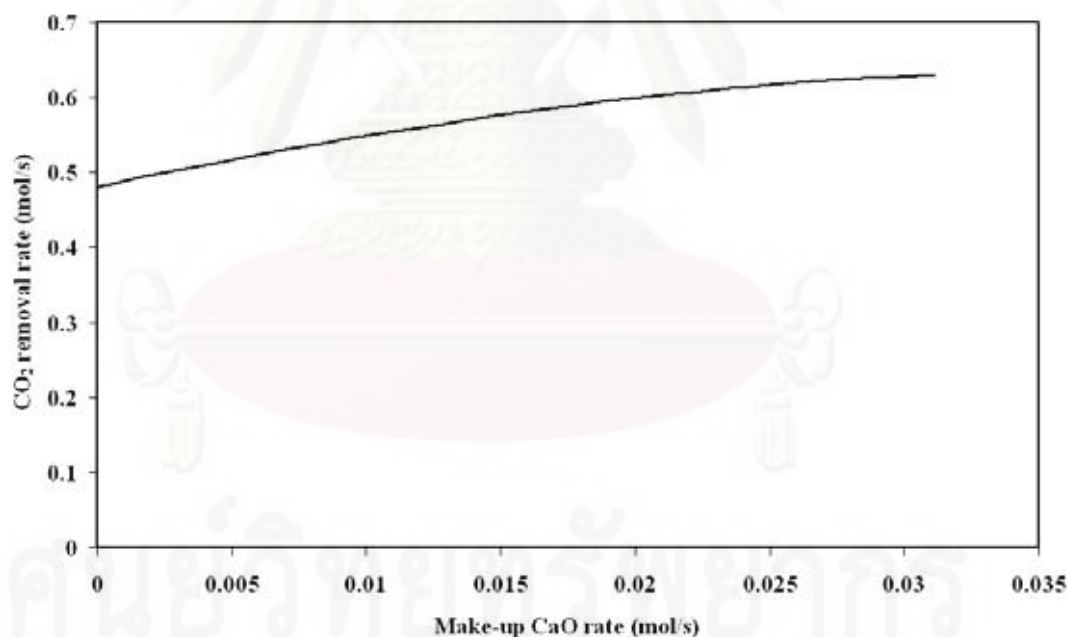


Figure 7.6 The correlation between make-up CaO rate and CO₂ removal rate for CaO-CO₂ acceptor technology. ($F_R/F_{CO_2} = 10$ and $W_S = 50$ kg)

The energy self-sufficient point of A-SOFC is also investigated as shown in Figure 7.7. Since there is no major electricity consumption in A-SOFC system, the fuel utilization that offers the energy self-sufficient operation is always at 0.845 for

the operation at the voltage of 0.64 volt. The power density at the energy self-sufficient condition increases as CO₂ removal rate increases due to the increase in H₂ and steam partial pressure and the decrease in CO₂ partial pressure of the feed gas of SOFC anode. Like the other configurations, the optimum voltage is also found for A-SOFC. As shown in Figure 7.8, the optimum operation of A-SOFC is found at the CO₂ removal rate of 0.6 mol/s with the optimum operating voltage of 0.58 volt. The power density achieved at this condition is 0.425 W/cm² which is far higher than 0.398 W/cm² in case of CON-SOFC. Unlike M-SOFC, the electrical efficiency of A-SOFC is 46.81 % which is equal to that of CON-SOFC.

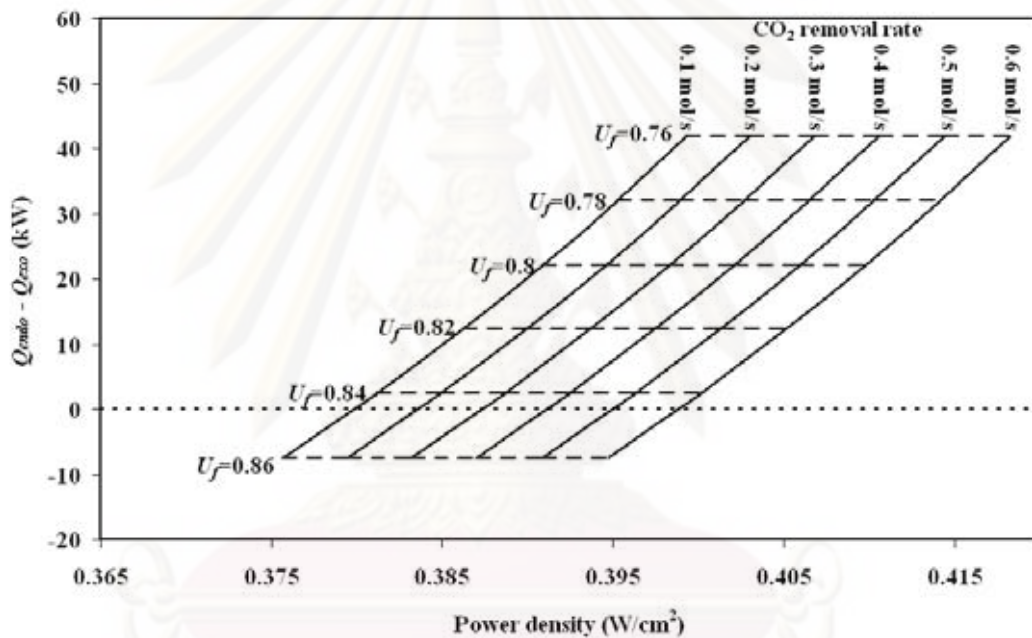


Figure 7.7 The effect of the CO₂ removal rate and fuel utilization on the energy self-sustainable point and the power density of A-SOFC. ($V = 0.64$ volt)

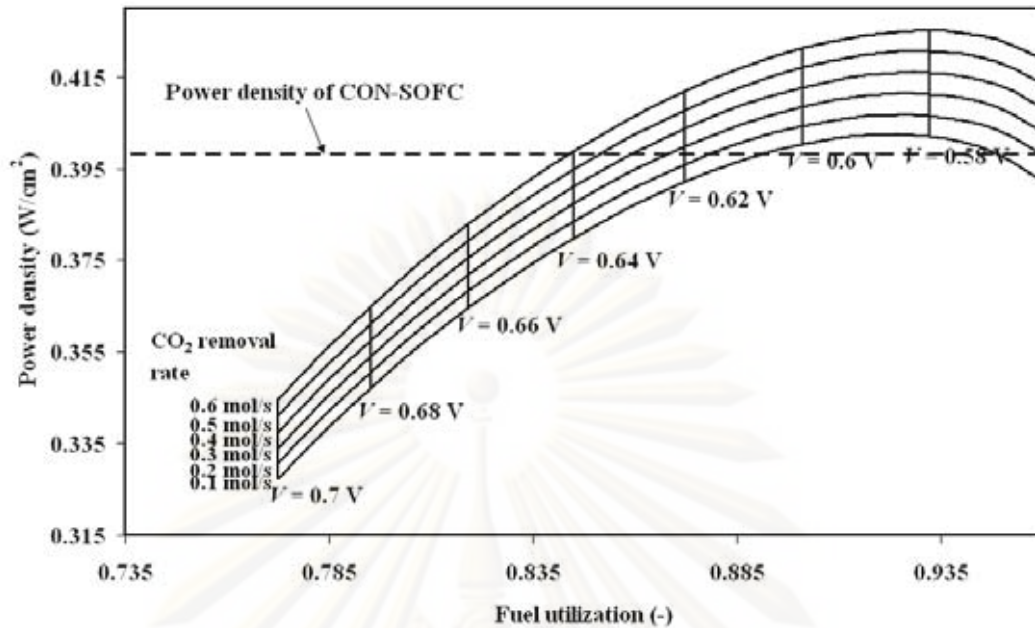


Figure 7.8 The effect of the operating voltage on the power density at different CO_2 removal rate in case that A-SOFC operates at energy self-sufficient point.

In summary, the operation of the M-SOFC offers lower electrical efficiency compared with that of the CON-SOFC. Moreover, although the power density the M-SOFC system can achieve is higher than that of the CON-SOFC as summarized in Table 7.1, the SOFC stack size of the former is quite larger since more electricity is required to produce in SOFC stack to supply the high-pressure compressor. These clearly indicate that the M-SOFC is not a good choice for the SOFC system. For the A-SOFC, it can offer higher power density compared with the CON-SOFC, and its electrical efficiency is equal to that of the CON-SOFC. Furthermore, its SOFC stack size is fairly smaller than that of CON-SOFC. Although the stack size of A-SOFC system is smaller compared with CON-SOFC, the additional cost of make-up CaO should be also taken into consideration. Therefore, only technical analysis is not adequate to identify which operation mode can provide utmost potential benefit for the SOFC system between CON-SOFC system and A-SOFC system.

Table 7.1 The summary of electrical efficiency, power density and stack size of each SOFC system. ($Q_E = 416.8$ kW)

SOFC systems	Electrical efficiency (%)	Power density (W/cm ²)	SOFC area (m ²)
CON-SOFC	46.81	0.398	104.62
A-SOFC			
0.1 mol/s CO ₂ capture	46.81	0.402	103.83
0.2 mol/s CO ₂ capture	46.81	0.407	102.64
0.3 mol/s CO ₂ capture	46.81	0.411	101.49
0.4 mol/s CO ₂ capture	46.81	0.416	100.36
0.5 mol/s CO ₂ capture	46.81	0.42	99.26
0.6 mol/s CO ₂ capture	46.81	0.425	98.18
M-SOFC			
$P_R = 5$ bar, $P_P = 1$ bar	45.47	0.401	106.64
$P_R = 10$ bar, $P_P = 1$ bar	45.47	0.399	108.73

To judge the potential benefit of A-SOFC system, the economic analysis is employed for the investigation. This analysis considers only the cost difference between the base case and the interested case. The CON-SOFC is considered as the base case in this study. There are three costs considered in this study: SOFC stack cost, compressor cost and make-up CaO cost. Other costs of the interested case are assumed to be similar to those of base case. All details employed in the economic consideration are given in chapter 4.

As shown in Figure 7.9, the A-SOFC system is more feasible to operate compared with CON-SOFC system since its net cost saving is a positive values. In the economic point of view, the optimum CO₂ removal rate can be found at about 0.5 mol/s. Below this optimum value, the increase in CO₂ removal rate can improve the profitability of the A-SOFC system due to the decrease in SOFC stack size. However, as CO₂ removal rate is higher than the optimum value, large amount of make-up CaO is required and the additional cost thus increases. With the CO₂ removal rate of 0.5 mol/s, the net cost saving of A-SOFC is \$19,612.91 based on the electricity production of 416.8 kW. Nevertheless, the disadvantage of this configuration is that It therefore seems that the A-SOFC can be the interesting operating mode for the

electricity production with SOFC both in technical and economical point of view, where M-SOFC configuration is not suitable for SOFC system.

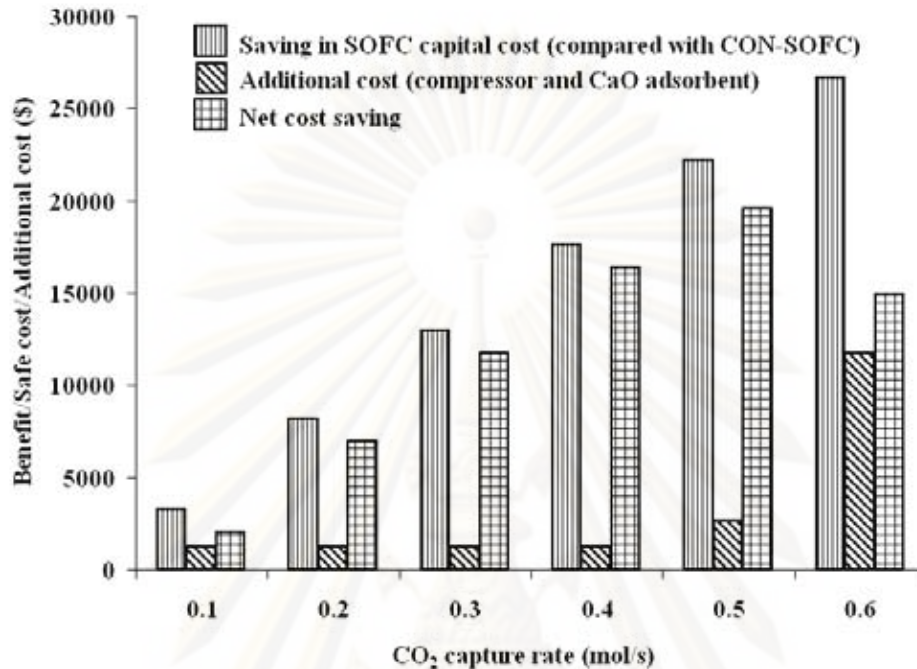


Figure 7.9 Saving in SOFC stack cost, additional cost, net cost saving, benefit of carbon credit and total benefit of A-SOFC at different CO₂ removal rate.

7.4 Conclusions

Performance of desulfurized biogas-fed SOFC system was analyzed to investigate the benefit of CO₂ capture technology installation. The two configurations, namely; M-SOFC (SOFC cooperating with CO₂-selective membrane) and A-SOFC (SOFC cooperating with CaO-CO₂ acceptor) were examined in terms of both engineering and economic models. The conventional SOFC system (CON-SOFC) is considered as a base case. It was observed that the power density is improved as CO₂-selective membrane is included in CON-SOFC; however, the decrease in SOFC stack size is not obtained. Moreover, its electrical efficiency is lower than that of CON-SOFC. It may therefore be concluded that the M-SOFC is not a good alternative for the SOFC system. It was also found that the installation of vacuum pump to the M-SOFC in order to increase CO₂ removal rate cannot improve its performance. The improvement in power density and the decrease in SOFC stack size are found as the CaO-CO₂ acceptor is installed to the CON-SOFC system. This indicates that A-SOFC

is interesting option for SOFC system in the technical point of view. Even if the stack size of A-SOFC is smaller compared with that of CON-SOFC, the additional cost of make-up CaO should be taken into consideration. Economic assessment was then employed to evaluate the feasibility study of A-SOFC operation. The results showed that the A-SOFC is superior to the CON-SOFC.



ศูนย์วิจัยทรัพยากร
จุฬาลงกรณ์มหาวิทยาลัย

CHAPTER VIII

INTEGRATION OF SOLID OXIDE FUEL CELL AND PALLADIUM MEMBRANE REACTOR: TECHNICAL AND ECONOMIC ANALYSIS

This chapter presents a technical and economic analysis of a solid oxide fuel cell system equipped with a palladium membrane reactor (PMR-SOFC) with the aim of determining the benefits of such an integrated unit over the conventional reformer module (CON-SOFC). Two types of fuels, i.e., methane and desulfurized biogas, are considered. The ratio of $\text{CO}_2:\text{CH}_4$ presenting in biogas is 40:60. The numerical algorithms to the models used in this study were written in Visual Basic.

8.1 Introduction

As described earlier, the performance of SOFC depends on the quality of feedstock. CO_2 , CO and CH_4 are not desired to be found in SOFC feedstock. The presence of CH_4 in fuel feed causes the carbon blocking in SOFC anode (Baron et al., 2004). CO_2 presenting in fuel inhibits the SOFC performance due to the effect of RWGS reaction (Suwanwarangkul et al., 2006). CO also inhibits the electrochemical reaction by increasing the activation and concentration overpotentials (Eguchi et al., 2002). By the reasons above, pure- H_2 is found to be ideal fuel for SOFC. However, it cannot be derived from the natural resources. The palladium membrane reactor is the interesting choice for transforming the conventional fuel into pure- H_2 . Due to high H_2 -permeability and H_2 -selectivity of palladium membrane, this technology can offer pure- H_2 with high productivity. Moreover, the conversion of methane is improved relative to the conventional fuel processor even at high operating pressure. Nevertheless, employing this technology, large amount of electrical energies are consumed in the palladium membrane reactor system and the availability of SOFC system cooperating with this technology should be thus carefully considered.

(Vivanpatarakij et al., 2009). Moreover, the increase in the capital cost due to the cost of palladium membrane is also taken into account (Sangtongkitcharoen et al., 2008).

In this chapter, a comprehensive analysis of two SOFC systems (one coupled to a membrane reactor and the other fitted with a conventional reformer) was carried out. Evaluation of the system performance was based on energetically self-sustaining operation. The effects of type of feed gas (methane and desulfurized biogas) and operating pressures in the permeate side on the system performance were investigated. Finally, the economic analysis was carried out to determine 'best' operating conditions for the SOFC system coupled to the membrane reactor when fed by different fuels.

8.2 SOFC system configurations

The SOFC system equipped with a palladium membrane reactor (PMR-SOFC) is considered in this study. The plant configuration of PMR-SOFC (cf. Figure 8.1) is almost identical to that of the conventional SOFC system (Figure 6.1a); however, the conventional fuel processor is replaced by PMR. The mixture of methane (biogas) and steam is compressed and then fed into the retentate side of membrane reactor. The set of chemical reactions (Eqs. (4.32), (4.33), and (4.60)) takes place in the retentate side and H_2 generated permeates through the palladium membrane to the permeate side. The permeate gas (H_2 -pure) is compressed to atmospheric pressure and then fed into the SOFC stack to generate the electricity, while high-pressure retentate gas is fed into the afterburner. The pressure drop in PMR is neglected and the hydrogen recovery (ζ) was fixed at 95% as it is a suitable value for the SOFC system that can be operated at an energy self-sustained condition. If the hydrogen recovery is lower than this value, large amount of H_2 and CO is released from the PMR at the retentate side and fed to the afterburner. This causes the generation of over-demand heat in the burner. As a result, the energy self-sufficient operation is difficult to be achieved under the operation at low hydrogen recovery (< 0.95). With too high hydrogen recovery, high retentate pressure and thus high additional cost of compressor is required.

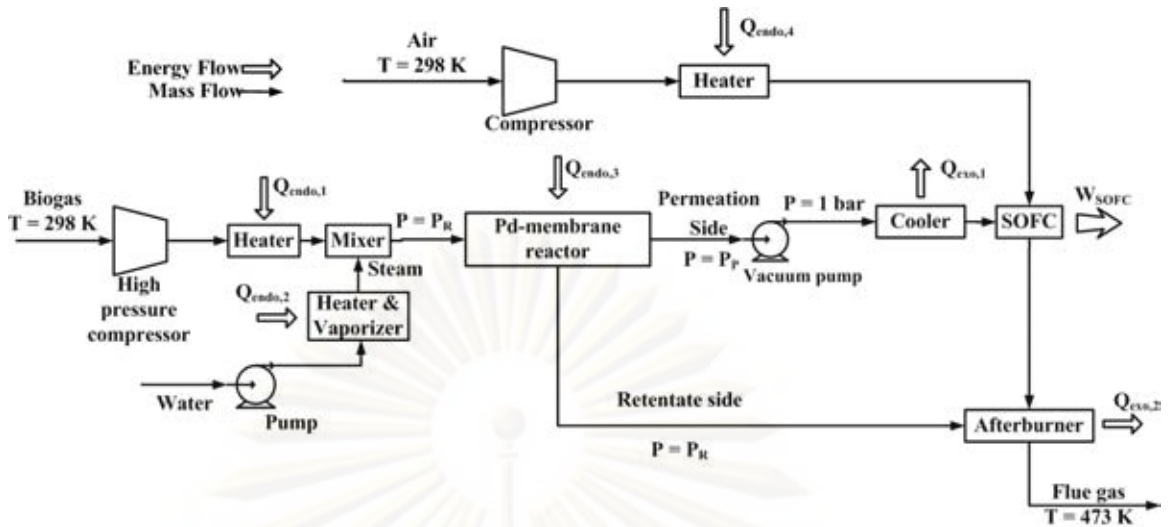


Figure 8.1 The plant configuration of the PMR-SOFC.

8.3 Results and discussion

Based on the result in chapter 6, the CON-SOFC system can stand alone without requirement of external heat sources (the energy self-sustained operation, $Q_{NET} \geq 0$) when it operates at suitable operating conditions. It is noted that Q_{NET} is the difference between heat generated and heat demanded within the SOFC system. Figure 8.2 shows that at different operating voltage, Q_{NET} can become zero when the appropriate fuel utilization (U_f) is chosen. At a higher operating voltage where the cell efficiency is high, the SOFC needs to be operated at lower fuel utilization so that the residual fuel can provide sufficient heat to the overall SOFC system after burning. It should be noted that a very low operating voltage is not recommended for practical operation due to the possible large in-stack temperature gradient arising from the difficulty in heat removal from the SOFC stack. In addition, the condition with $Q_{NET} = 0$ may not be possible. Two types of feed, i.e. pure methane and biogas were considered in this study. Generally, the composition of biogas varies depending on its source. It mainly contains methane (40-65%) and CO_2 (30-40%). In this work, the value of $CH_4:CO_2$ in biogas was set at 60:40. It should be noted that biogas usually contains a small amount of H_2S which can cause poisoning to catalysts and Pd membrane. In this study, it was assumed that H_2S is removed from biogas by a desulfurization process.

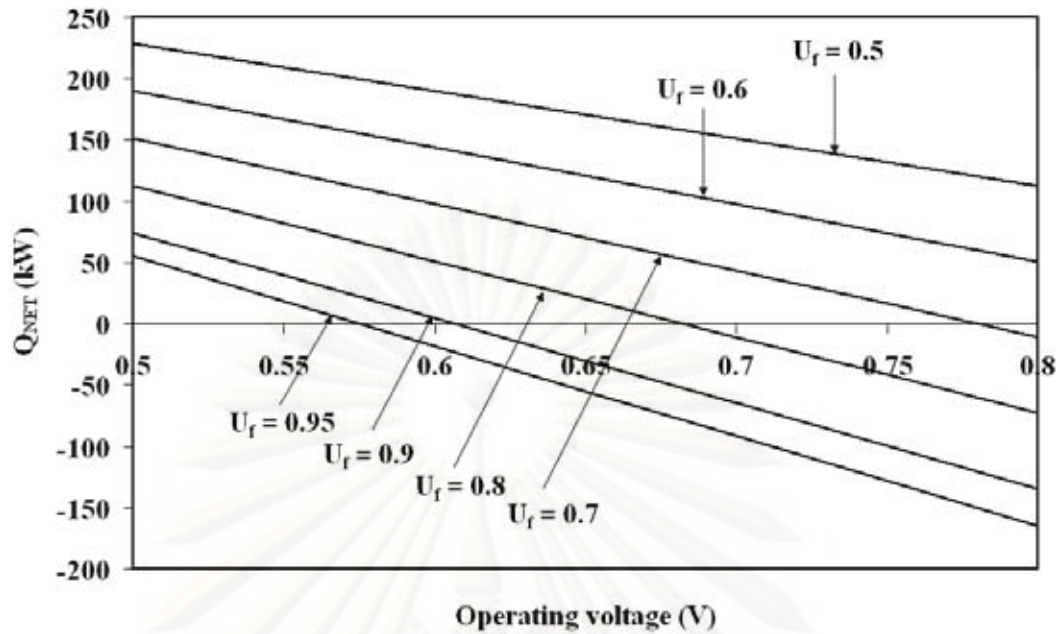


Figure 8.2 Q_{NET} at different operating voltage and fuel utilization for methane-fuelled CON-SOFC.

Figure 8.3 shows the effects of operating voltage on the power density and the fuel utilization of the CON-SOFC fed by methane and biogas for the case of $Q_{NET} = 0$. For both types of feed, it is clear that at a higher operating voltage, the SOFC system needs to operate at a lower value of fuel utilization. There exists an optimum operating voltage which offers the maximum power density for each type of feed. The maximum power density and the corresponding voltage are 0.423 W/cm^2 and 0.585 V , and 0.399 W/cm^2 and 0.585 V for the methane and biogas feeds, respectively. The lower methane concentration in biogas results in the lower achievable power density.

It should be noted that for the case of $Q_{NET} = 0$, the decrease in operating voltage can initially improve the power density of the SOFC; however, the resulting higher fuel utilization for achieving the energetically self-sustaining condition results in the poorer cell performance particularly near the exit of the SOFC stack where concentration of fuel is low, and, consequently the power density later decreases at much lower operating voltages.

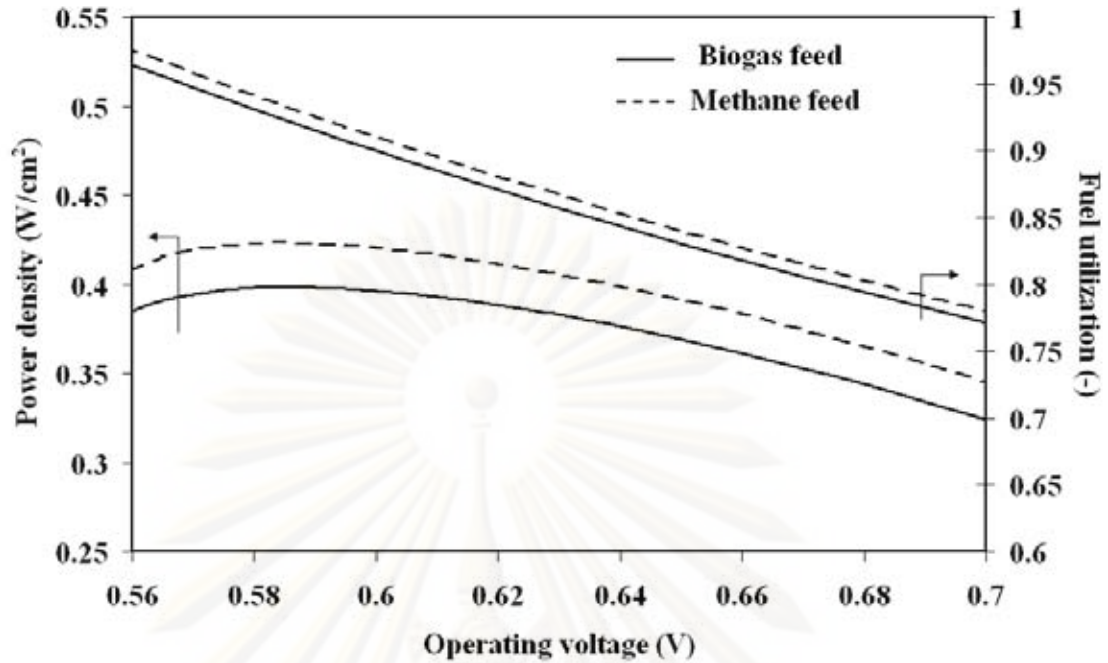
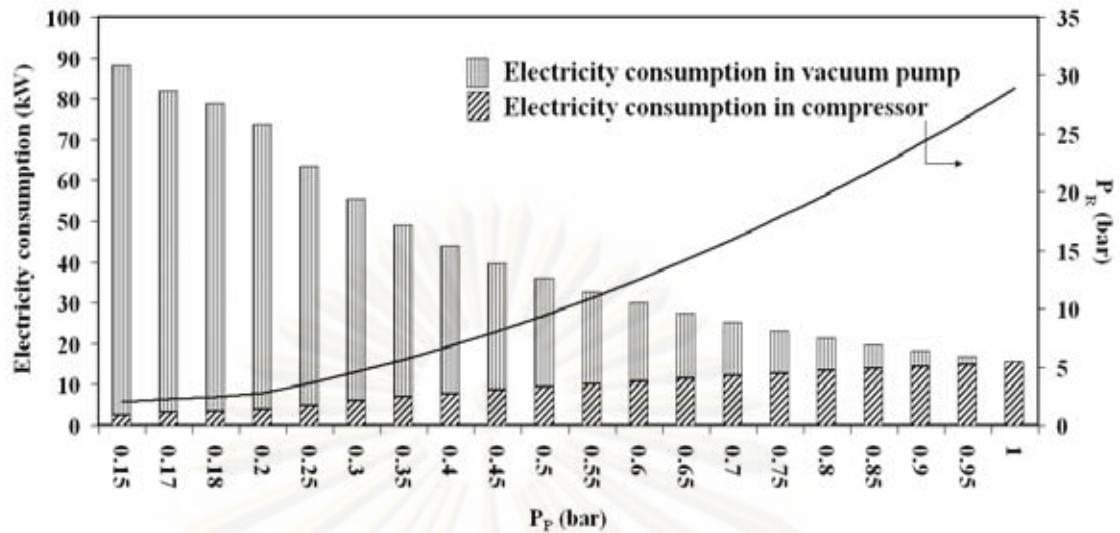
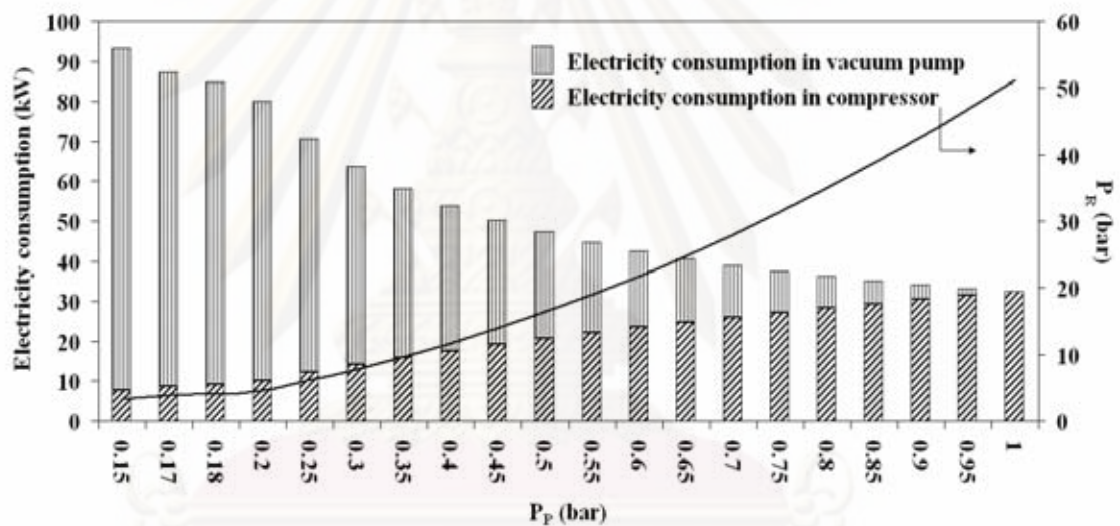


Figure 8.3 Power density and fuel utilization at different operating voltage in case that $Q_{NET} = 0$.

For PMR-SOFC, a part of electrical energy produced in SOFC stack is supplied to a high-pressure compressor (HPC) and a vacuum pump. The electrical power consumption in these equipments varies with the operating pressures of the HPC (retentate pressure, P_R) and vacuum pump (permeation pressure, P_P). The sum of the electrical power consumed in the HPC and the vacuum pump to obtain the hydrogen recovery of 0.95 is illustrated in Figures 8.4a and 8.4b for pure methane and biogas feeds, respectively. The electrical consumption decreases as P_P increases and the minimum electricity load can be found when P_P equals to 1 bar (vacuum pump does not operate). The results also indicate that the electrical power consumption in the PMR for the pure methane feed is lower than that for the biogas feed which contains 40% CO_2 . It should be noted that even if an operation at the permeation pressure of 1 bar can offer the minimum electricity load, P_R is extremely high and the structure of PMR may be damaged. Therefore, the limitation of PMR structure should also be carefully considered.



(a)



(b)

Figure 8.4 Electrical power consumed in HPC and vacuum pump at different retentate pressure (P_R) and permeate pressure (P_P) in case that $\zeta = 0.95$ for (a) methane feed and (b) biogas feed.

The change in P_P also affects the heat management in the PMR-SOFC system. Operation at a lower P_P causes higher heat generation during vacuum pump compression. Some heat removal may be required to reduce the temperature of gas discharged from the vacuum pump prior to being fed into SOFC anode. Therefore, for the operation at low P_P , the SOFC system requires an operation at a higher fuel

utilization to achieve energetically self-sustained operation, resulting in a lower power density. As illustrated in Figure 8.5, operation of the PMR-SOFC fed by pure methane at P_P of 0.1 bar cannot be self-sustained, whilst U_f should be set to be 0.965 for the operation at P_P of 0.2 bar. Hence, operation at high P_P is preferable since the condition with $Q_{NET} = 0$ can be achieved and the corresponding power density is higher.

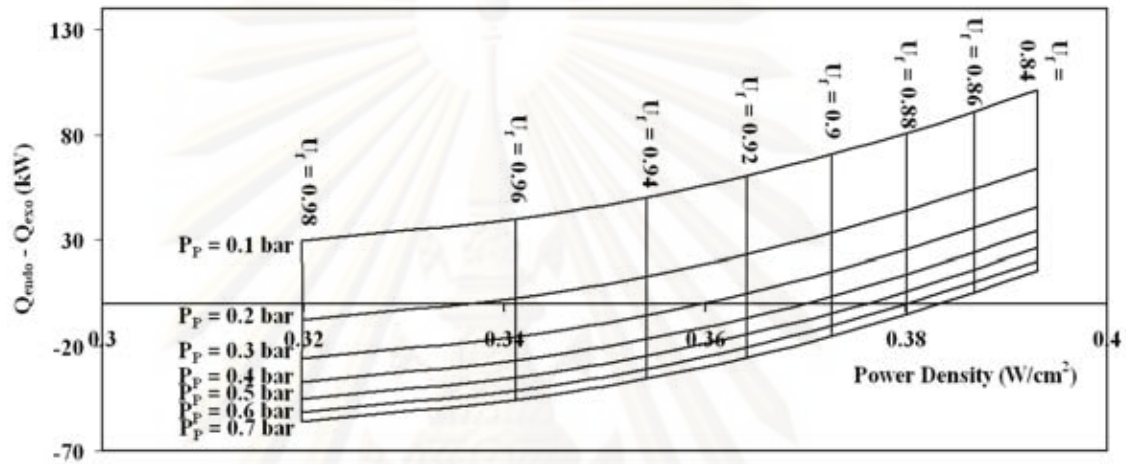
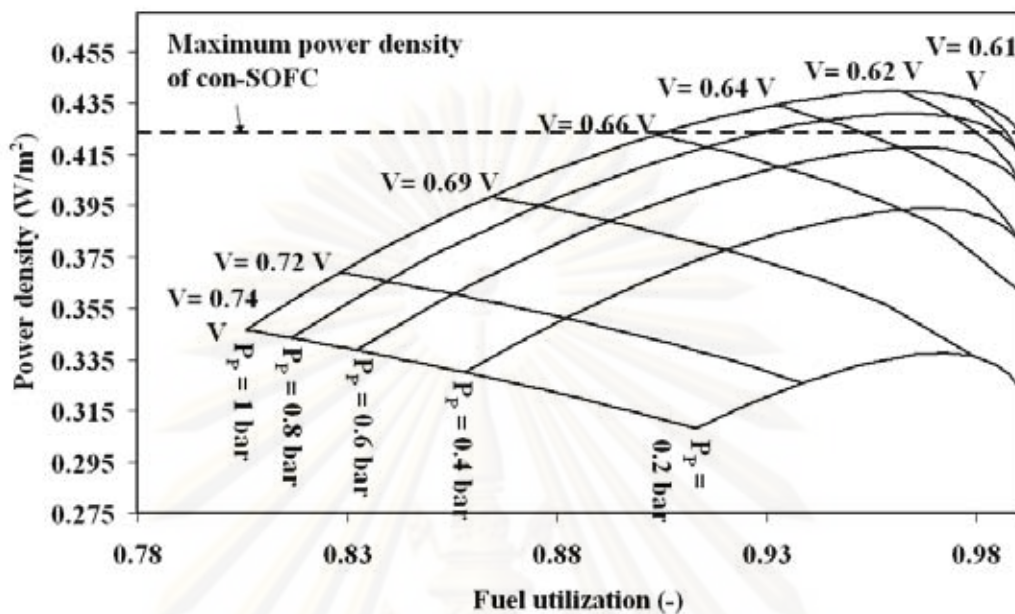


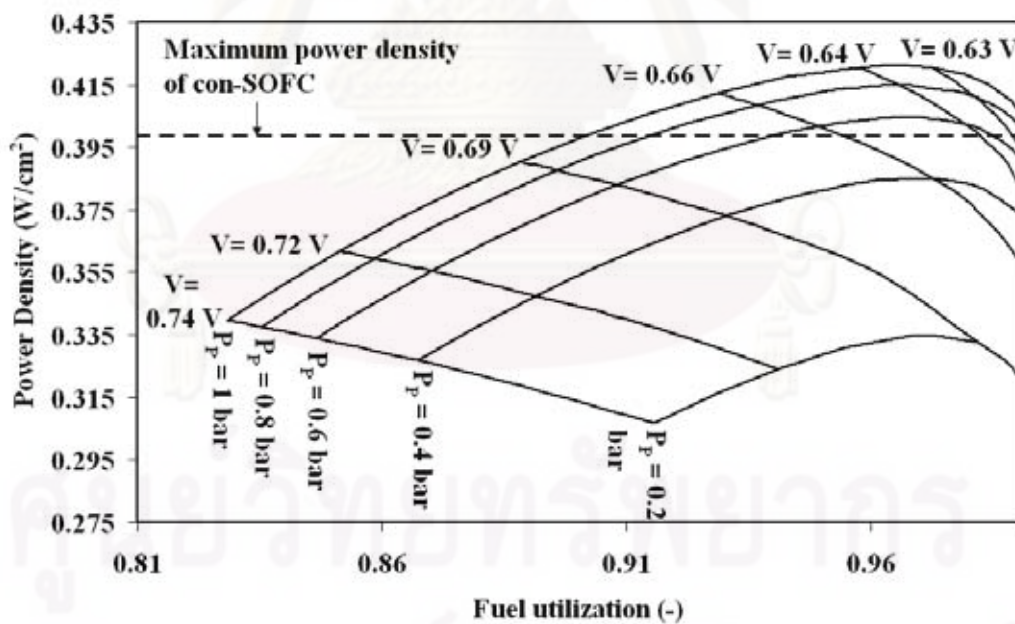
Figure 8.5 Q_{NET} and power density at different permeate pressure and fuel utilization (U_f) for PMR-SOFC in the case of methane feed.

The performance of PMR-SOFC and CON-SOFC under energetically self-sustained operation ($Q_{NET} = 0$) are compared as seen in Figure 8.6. It is clear that the PMR-SOFC can offer higher power density compared with the CON-SOFC when the operating voltage and P_P are judiciously chosen. Figures 8.6a and 8.6b show that the power density of the PMR-SOFC fueled by methane and biogas is improved as P_P increases. Maximum power density may be achieved when P_P is 1 bar. An optimum operating voltage that provides a maximum power density is observed. The effect of variation in P_P on the power density and the SOFC area at the optimum operating voltage is summarized in Figures 8.7a and 8.7b, respectively. The power density of the PMR-SOFC fed by pure methane and biogas is higher than that of the CON-SOFC when P_P is higher than 0.67 and 0.52 bar, respectively, and the benefit gained from the reduction in SOFC stack area of the PMR-SOFC over the CON-SOFC can be found when P_P is higher than 0.98 bar for methane feed. Nevertheless, the reduction

in SOFC stack area over the CON-SOFC is not achieved for PMR-SOFC fuelled by biogas.

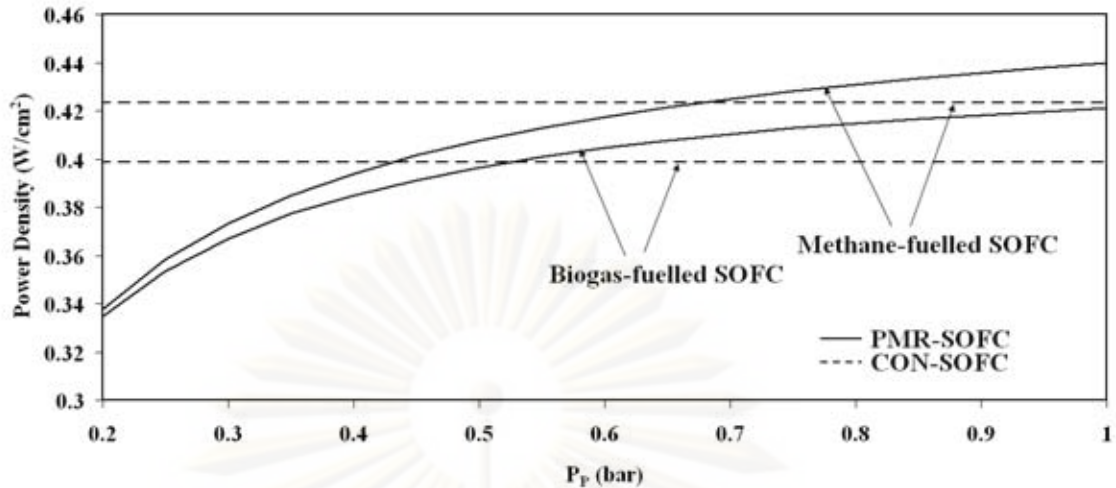


(a)

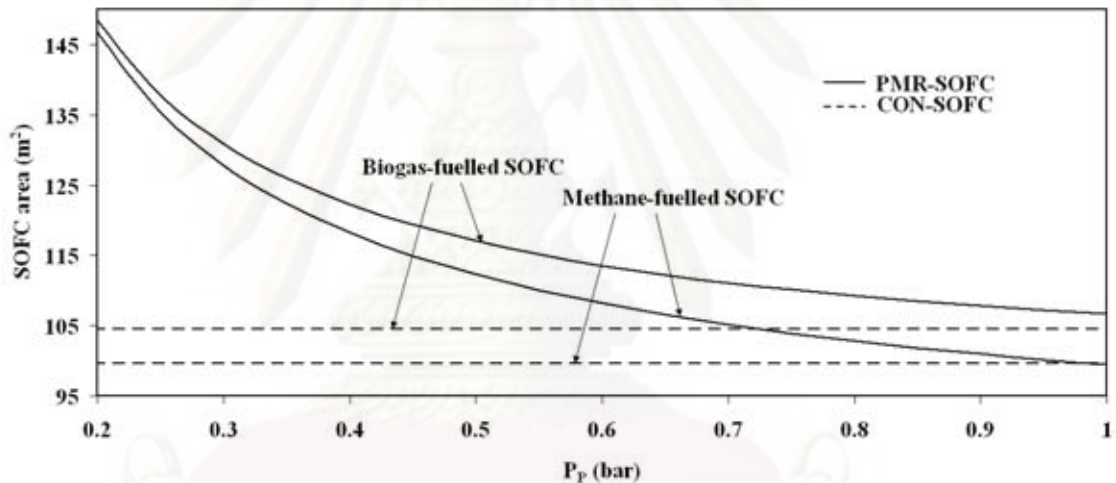


(b)

Figure 8.6 Power density and fuel utilization at different permeate pressure and operating voltage in case that $Q_{NET} = 0$ for (a) methane-fuelled PMR-SOFC and (b) biogas-fuelled PMR-SOFC.



(a)



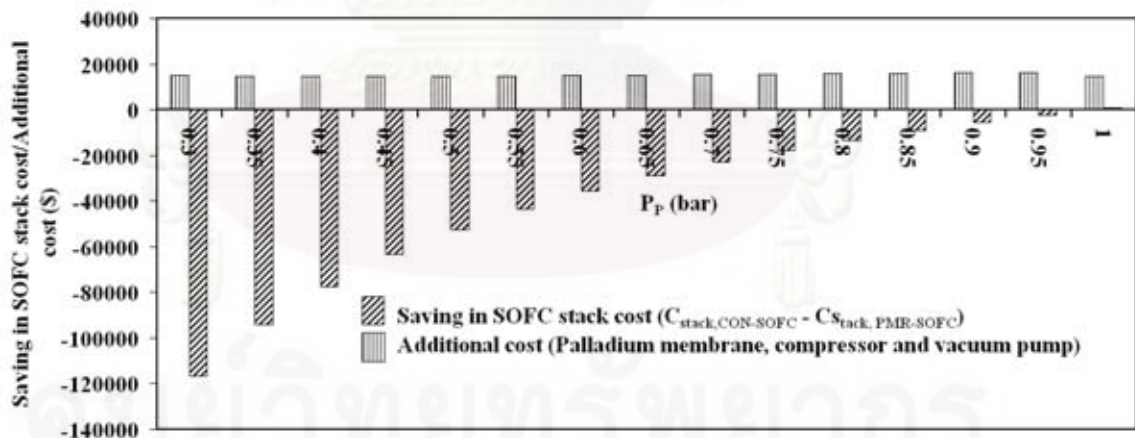
(b)

Figure 8.7 The effect of change in permeate pressure on (a) power density and (b) SOFC area at optimum operating voltage in case that $Q_{NET} = 0$.

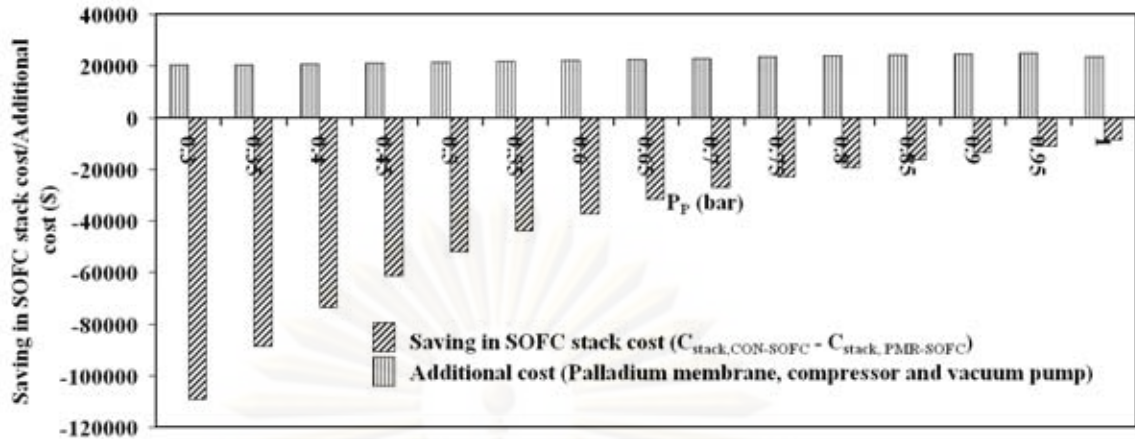
Even if the use of PMR in the SOFC system can reduce the SOFC stack size in case of methane feed, the additional capital costs from the supporting units, i.e., PMR, HPC, and vacuum pump, need to be taken into account. Therefore, an economic analysis is employed to examine the potential benefit of the use of PMR in the SOFC system for both methane and biogas feeds. In the following analysis, the methane feed rate was kept at 1 mol/s for all scenarios to achieve negligible fuel feed cost. Furthermore, since the SOFC system under the energetically self-sustained operation was considered, additional energy or electricity from the outside of the system is not

necessary. Therefore, only the capital costs of SOFC stack, PMR, HPC, and vacuum pump were taken into account. It should be noted that when the PMR is operated at high pressure, it may cause an additional cost on reinforcing the palladium membrane structure; however, this cost is not taken into account for the economic analysis in this study. The parameters and the expressions used in the capital cost estimation for these equipment items are summarized in Chapter 4. Net cost saving was calculated as an economic index.

Figures 8.8a and 8.8b indicate that the replacement of a conventional reformer with a membrane reactor in the SOFC system is not advantageous in economic point of view as the saving stack cost is always lower than the additional capital costs of PMR, HPC and vacuum pump. The saving stack cost increases as permeate pressure increases due to the improvement of the power density. The saving stack cost is always negative for PMR-SOFC fuelled by biogas since SOFC stack area reduction over the CON-SOFC is not achieved. The additional cost of PMR-SOFC system in case of biogas feed is always higher than that in case of methane feed since higher retentate pressure and thus higher compressor load are required for the former one.



(a)



(b)

Figure 8.8 Saving in SOFC stack cost/additional cost at different permeate pressure (optimum operating voltage and $Q_{NET} = 0$) for a) methane-fuelled PMR-SOFC and b) biogas-fuelled PMR-SOFC.

All technical and economic analyses of four scenarios are summarized in Table 8.1. The optimum condition is chosen for each scenario. With the use of PMR in the SOFC system (PMR-SOFC), the power density improvement of 3.9% and 5.69% can be observed, compared with the CON-SOFC, for methane and biogas feeds, respectively. Although the replacement of CON-SOFC by PMR-SOFC can improve the power density, higher electrical power is generated in SOFC stack for the latter one to supply the demand of electricity in HPC. This is the reason why the SOFC stack area reduction over CON-SOFC is not achieved for PMR-SOFC fed by biogas feed and the required SOFC stack area of PMR-SOFC fed by methane is only decreased by 0.17%. From this economic consideration, it seems that both methane-fuelled PMR-SOFC and biogas-fuelled PMR-SOFC offer negative net cost saving (-\$13,883.20 and -\$32,071.51). The operation at high retentate pressure of both methane-fuelled PMR-SOFC (28.94 bar) and biogas-fuelled PMR-SOFC (51.27 bar) extremely affects their HPC cost and electricity load in HPC. The HPC cost of \$12,886.86 and \$21,712.86 is paid for the methane and biogas feeds, respectively, whereas the electrical power of 15.53 kW and 32.46 kW is consumed in HPC for the methane and biogas feeds, respectively. These results imply that the improvement in the permeability of palladium membrane can reduce retentate pressure, the electricity load and thus the profitability of PMR-SOFC. Finally, it may be concluded that the

PMR-SOFC fed by either methane or biogas is attractive for its technical benefits, however, the economic benefit is not found in these operations.

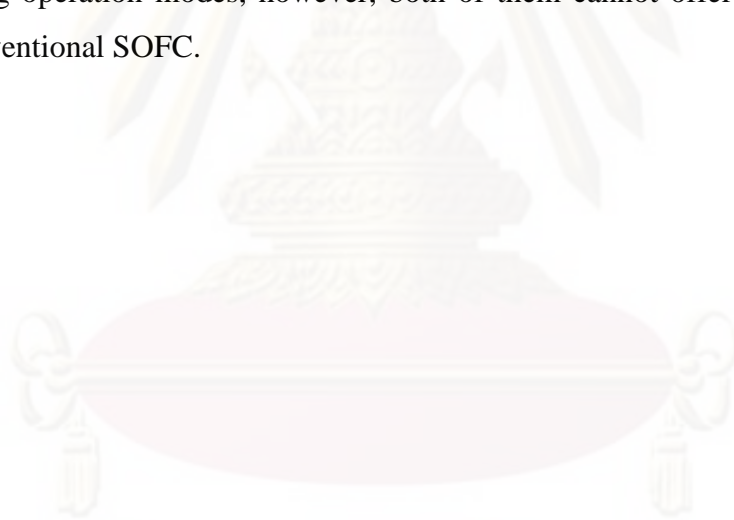
Table 8.1 The technical and economical comparison of four scenarios.

	Methane-fuelled		Biogas-fuelled	
	CON-SOFC	PMR-SOFC	CON-SOFC	PMR-SOFC
Feed rate (mol/s)	1	1	1.667	1.667
% methane in feed	100	100	60	60
Retentate pressure (bar)	-	28.94	-	51.27
Permeate pressure (bar)	-	1	-	1
Operating voltage (V)	0.585	0.62	0.585	0.635
Power density (W/cm ²)	0.4233	0.4398	0.3986	0.4213
% improvement in power density	-	3.90	-	5.69
Electricity produced in SOFC (kW)	421.68	437.34	416.79	449.30
Net electricity produced (kW)	421.68	421.68	416.79	416.79
Electricity consumed in compressor (kW)	-	15.53	-	32.46
SOFC active area (m ²)	99.62	99.45	104.57	106.66
% improvement in SOFC area	-	0.17	-	-2.00
Palladium membrane area (m ²)	-	4.71	-	4.71
Capital cost of SOFC (\$)	412,814.40	412,114.22	433,358.34	442,000.46
Capital cost of Pd membrane (\$)	-	1,716.52	-	1,716.52
Capital cost of compressor (\$)	-	12,866.86	-	21,712.86
Saving cost on SOFC (\$)	-	700.18	-	-8,642.13
Net cost saving (\$)	-	-13,883.20	-	-32,071.51

8.4 Conclusions

The performance improvement of SOFC system by replacing a conventional reformer (CON-SOFC) by a palladium membrane reactor (PMR-SOFC) is investigated. Methane and desulfurized biogas are used as feed streams for SOFC

system. The energetically self-sustained operation ($Q_{NET} = 0$) for each mode may be obtained by tuning up the fuel utilization (U_f). The decrease in operating voltage can improve the power density; however, when it is too low, a high U_f is required to achieve the condition for $Q_{NET} = 0$ and no power density improvement is obtained. For the PMR-SOFC, the change in permeate pressure (P_P) also affects the SOFC power density and energy self-sufficiency point. Increase in P_P can improve the power density due to the decrease in U_f which offers zero Q_{NET} . It is found that the values of power density of the PMR-SOFC are 3.9% and 5.69% higher than those of the CON-SOFC for methane feed and biogas feed, respectively. The use of PMR in the methane-fuelled SOFC can reduce the SOFC area by 0.17%, however, SOFC stack area reduction over CON-SOFC is not achieved for biogas feed. For economic study, it was found that both methane-fuelled PMR-SOFC and biogas-fuelled PMR-SOFC always offer the negative net cost saving. It may be concluded from this study that both of the methane-fuelled and biogas-fuelled PMR-SOFCs are technically interesting operation modes, however, both of them cannot offer economic benefits over conventional SOFC.



ศูนย์วิจัยทรัพยากร

จุฬาลงกรณ์มหาวิทยาลัย

Chapter IX

TECHNICAL AND ECONOMIC STUDIES OF THE INTEGRATED SYSTEM OF SOLID OXIDE FUEL CELL, CaO-CO₂ ACCEPTOR AND PALLADIUM MEMBRANE REACTOR

This chapter presents the study on the integrated system of solid oxide fuel cell (SOFC), palladium membrane reactor (PMR) and sorption enhancement (SE) by CaO-CO₂ acceptor. Desulfurized biogas is considered as the feedstock and the CH₄:CO₂ ratio of 60:40 is assumed as the composition of biogas. Again, all mathematic models used in this simulation are written in Visual Basic.

9.1 Introduction

According to the conclusions in Chapter 8, the SOFC system equipped the palladium membrane reactor (PMR-SOFC) could not offer benefit over the conventional SOFC system (CON-SOFC) due to high electricity consumption at the compressor. To achieve the hydrogen recovery of 0.95, retentate pressure of 51 bar is required. To minimize the electricity load in the compressor of PMR-SOFC, the idea of CO₂ removal from biogas prior to be fed to PMR is proposed in this chapter. With this idea, the concentration of H₂ at the retentate section of PMR is increased and therefore more H₂ can permeate to the permeate section. As shown in Chapter 8, the use of methane instead of biogas as feedstock of PMR-SOFC can decrease the retentate pressure from 51 bar to 29 bar and the electricity load therefore decreases. The CaO-CO₂ acceptor is proposed as the CO₂ separator in Chapter 7. Using this technology, large amount of CaO particles is supplied to the system as make-up adsorbent and the operating cost thus increases. From this reason, the use of CaO-CO₂ acceptor in PMR-SOFC system should be carefully considered in both technical and economic points of view.

In this study, the performance of biogas-fuelled SOFC systems with different configurations is investigated. Four systems are considered, i.e. SOFC with conventional reformer (CON-SOFC), SOFC with palladium membrane reactor (PMR-SOFC), SOFC with palladium membrane reactor and sorption enhancement (SE) by CaO-CO₂ acceptor (SE-PMR-SOFC) and SOFC with palladium membrane reactor, CaO-CO₂ acceptor and retentate gas recycle (SER-PMR-SOFC). Both technical and economic analyses were carried out in order to determine an appropriate configuration for the biogas-fuelled SOFC system. Again, to obtain actual SOFC efficiency, the energy-sufficient point ($Q_{NET}=0$) (Jamsak et al., 2007) is also employed.

9.2 SOFC system configurations

The use of CaO-CO₂ acceptor in an SOFC system integrated with PMR (SE-PMR-SOFC and SER-PMR-SOFC) is investigated in this study. To evaluate the feasibility of this configuration, the performance of the SOFC working with conventional fuel processor (CON-SOFC) and also that working with PMR (PMR-SOFC) is computed as base cases. The plant configuration for the CON-SOFC is illustrated in Figure 6.1a. Considering PMR-SOFC, SE-PMR-SOFC and SER-PMR-SOFC (Figure 9.1), their plant configurations are almost identical to that of CON-SOFC. However, for these systems, the conventional fuel processor is replaced by different fuel processing systems. Prior to be fed to fuel processing system, biogas is initially compressed to achieve an operating pressure of the retentate section. Pure-H₂ obtained from each fuel processing system is preheated and fed to the SOFC where the electrochemical reaction takes place, while the high-pressure retentate gas is fed into the afterburner.

For the fuel processing system in PMR-SOFC (Figure 9.2a), the mixture of compressed biogas and steam is fed directly to the retentate section of PMR. Pure-H₂ is obtained in the permeate section of PMR. Considering the fuel processing system in SE-PMR-SOFC (Figure 9.2b), compressed biogas is initially fed to a CaO-CO₂ acceptor where CO₂ presenting in biogas is removed. The CO₂-removed gas is subsequently cooled down, mixed with compressed steam and fed to PMR. In case of the fuel processing system in SER-PMR-SOFC (Figure 9.1c), some retentate gas is recycled, mixed with biogas, and subsequently fed to CaO-CO₂ acceptor. In CaO-CO₂ acceptor, CO₂ is captured until reaching the equilibrium value. Prior to be fed to PMR, the CO₂-removed gas is cool down and mixed with compressed steam.

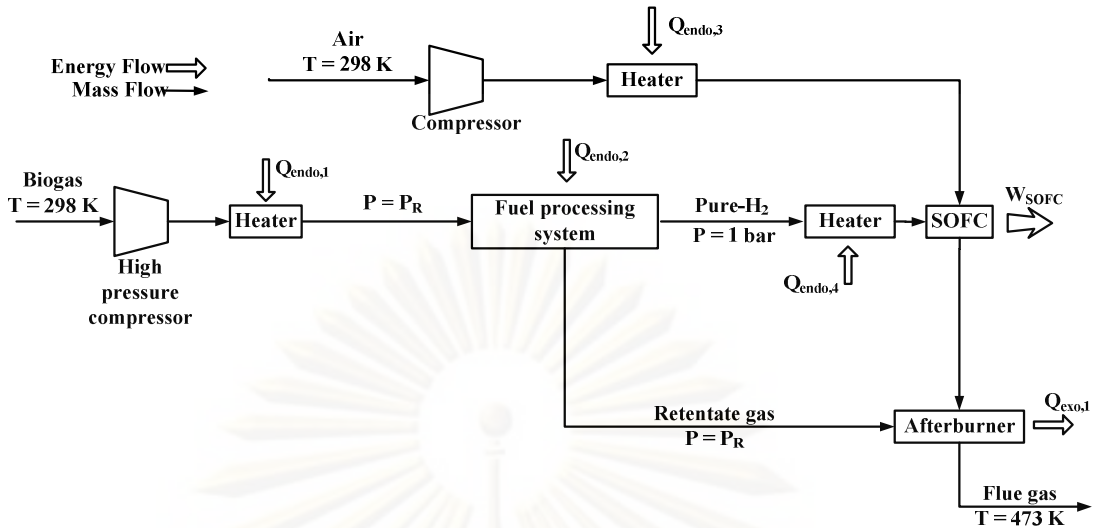
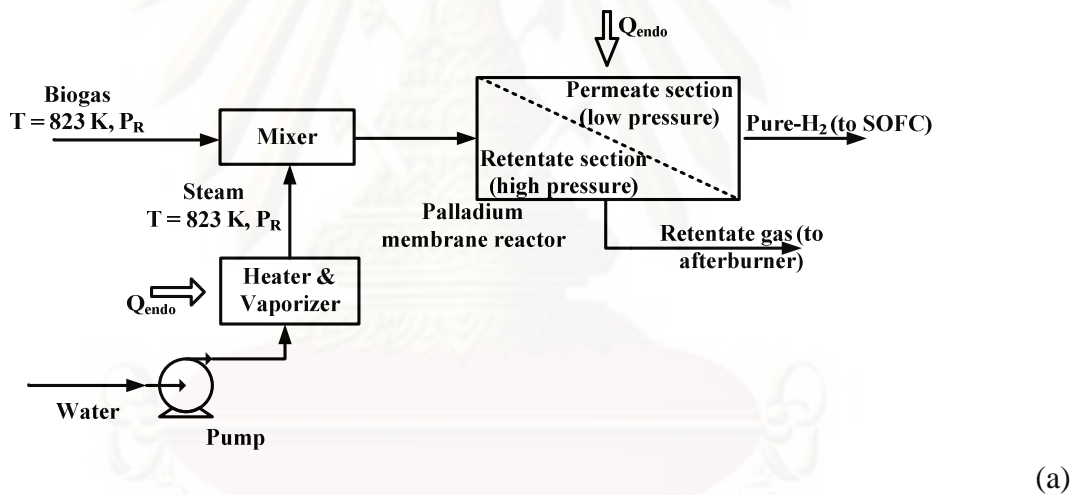
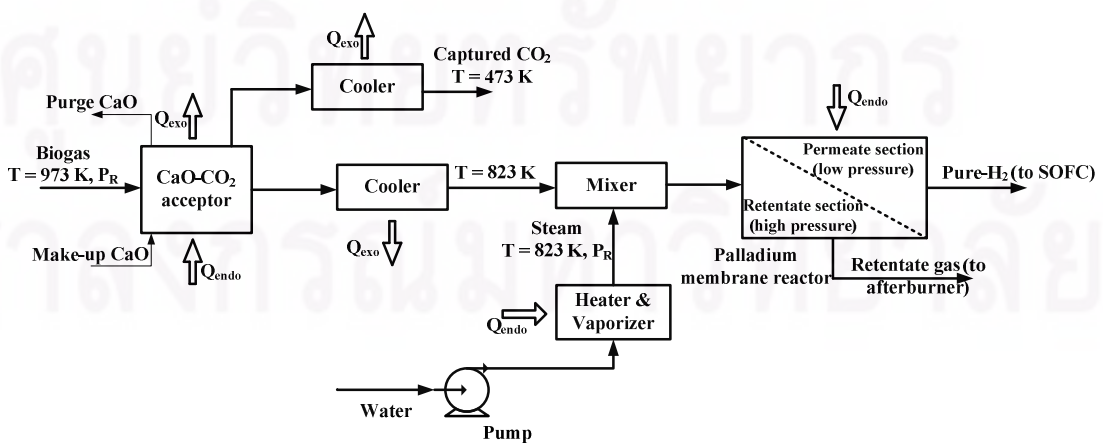


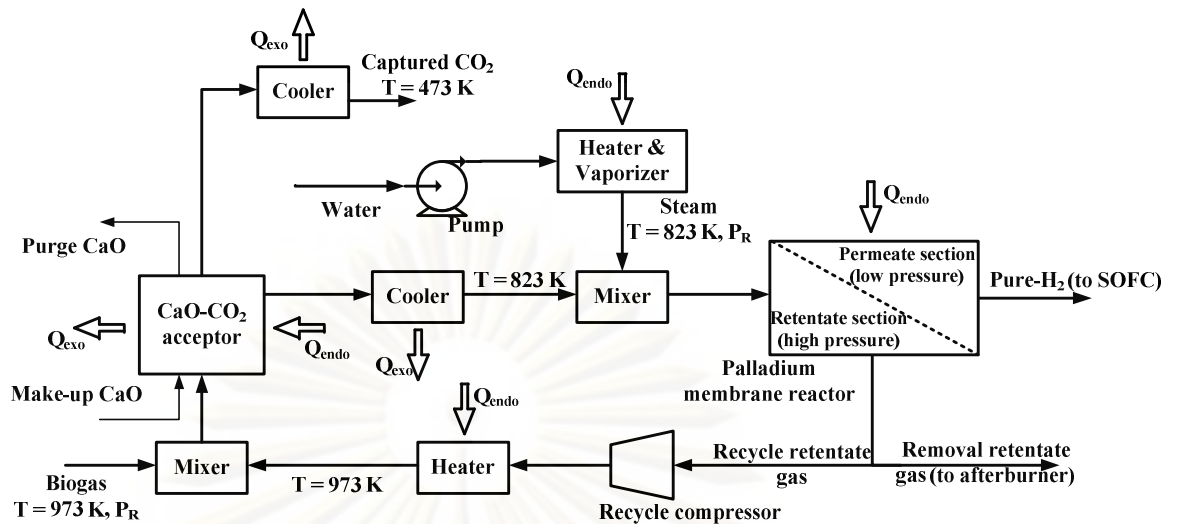
Figure 9.1 The plant configuration of the PMR-SOFC, SE-PMR-SOFC and SER-PMR-SOFC.



(a)



(b)



(c)

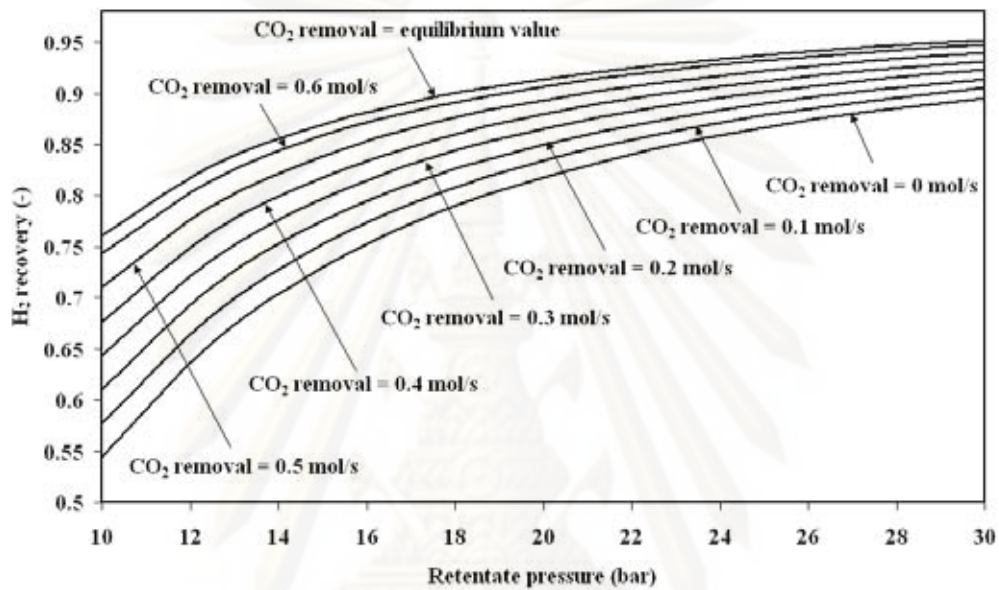
Figure 9.2 Fuel processing systems of a) PMR-SOFC, b) SE-PMR-SOFC and c) SER-PMR-SOFC.

Similar to the studies in previous chapters, the operation called “energy self-sustainable operation” (Jamsak et al., 2007) is considered in this chapter. With this operation, SOFC system can stand alone without external heat source supplement ($Q_{NET} = 0$) (Q_{NET} is the difference between heat demand and heat generated in SOFC system.). To achieve self-sustainable operation, fuel utilization is tuned up until Q_{NET} becomes zero. Like the previous chapters, the following assumptions are determined in this chapter; a) isothermal operation of SOFC stack and b) constant operating voltage along SOFC stack.

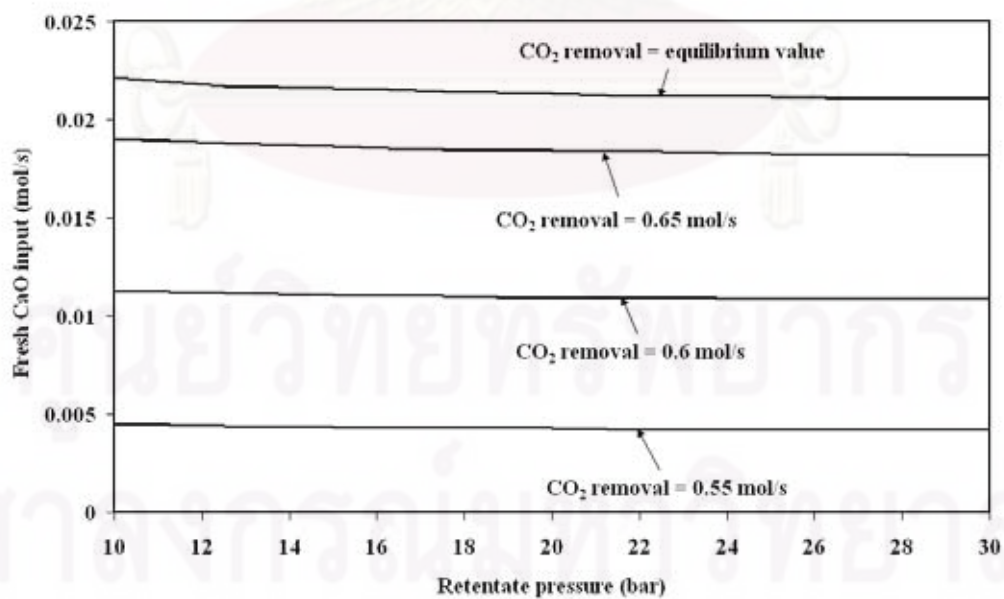
9.3 Results and discussion

The effects of the extent of CO_2 captured and the retentate pressure on H_2 recovery of PMR are firstly investigated as illustrated in Figure 9.3a. As shown in the case of the SE-PMR-SOFC system, the improvement of H_2 recovery can be found as CO_2 content in PMR feed decreases due to the shift of the equilibrium of WGS reaction. The increase in retentate pressure can also improve H_2 recovery. It should be noted that the retentate pressure in the range of 10-30 bar is investigated in this study. As described in the previous chapter, the operation of PMR-SOFC at excessively high retentate pressure (>40 bar) is not economically feasible; nevertheless, with low retentate pressure, H_2 recovery may not be adequately high. With the retentate

pressure of 30 bar, PMR without CO₂ removal offers H₂ recovery of 0.896 which is significantly lower than that obtained from PMR with CO₂ removal rate at equilibrium value which is equal to 0.952. Even if the removal of CO₂ can improve the H₂ recovery of PMR, large amount of fresh CaO sorbent is required to achieve high extent of CO₂ removal. As described in Figure 9.3b, fresh CaO supplying rate of 0.021 mol/s (36.5 ton/a) is required to achieve CO₂ removal rate at equilibrium value.



(a)

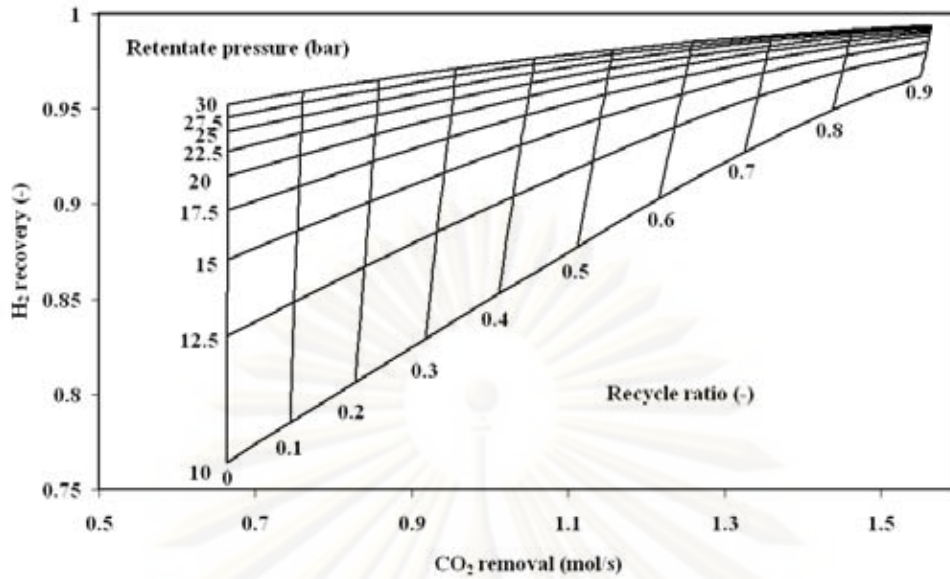


(b)

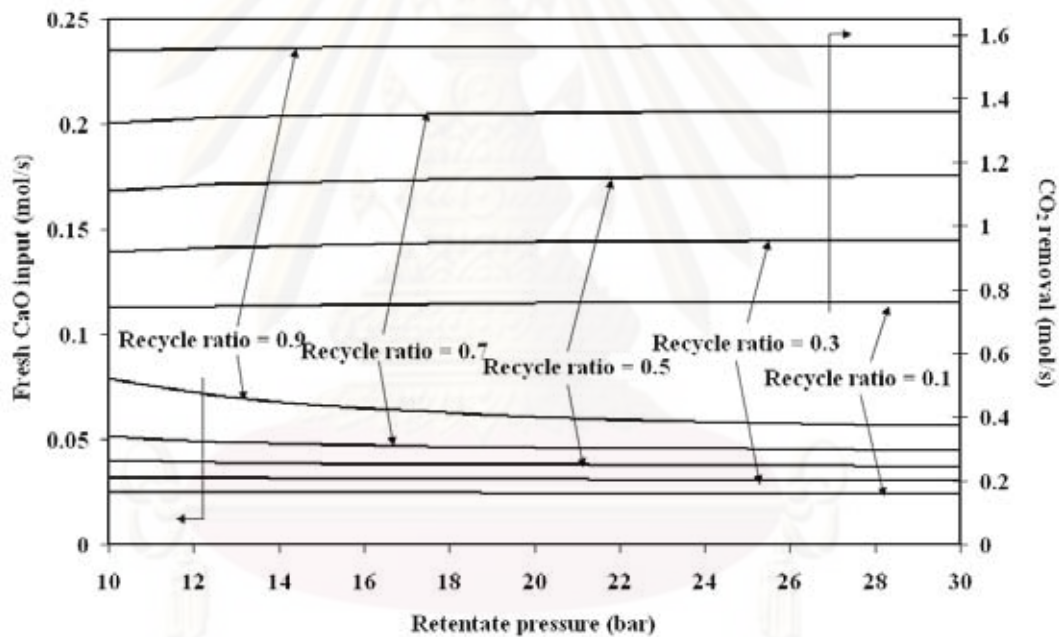
Figure 9.3 The effect of the extent of CO₂ removal and retentate pressure on a) H₂ recovery and b) fresh CaO feed rate in case of SE-PMR-SOFC system.

With the SE-PMR-SOFC configuration, CO₂ removal rate is limited at 0.667 mol/s (the amount of CO₂ present in biogas feed rate of 1.667 mol/s) and large amounts of CO₂ and CO generated in PMR cannot be captured. Moreover, methane conversion and H₂ recovery in PMR are inhibited by the presence of CO₂ and CO in the retentate gas. To solve these problems, the SER-PMR-SOFC configuration is proposed. With this configuration, some retentate gas is recycled and mixed with biogas prior to be fed to the CaO-CO₂ acceptor where CO₂ is captured until reaching equilibrium.

The influences of the recycle ratio and retentate pressure on H₂ recovery and CO₂ removal rate are illustrated in Figure 9.4a. The increase in recycle ratio can significantly improve both H₂ recovery and CO₂ removal rate especially at low retentate pressure. At the retentate pressure of 10 bar and the recycle ratio of 0.9, H₂ recovery of 0.967 and CO₂ removal rate of 1.55 mol/s can be achieved. These values are extremely higher compared with those of the case with no recycle (H₂ recovery = 0.761, CO₂ removal rate = 0.664 mol/s). Furthermore, H₂ recovery can reach 0.994 as the retentate pressure and recycle ratio are 30 bar and 0.9, respectively. At high recycle ratio, the increase in retentate pressure does not significantly improve H₂ recovery and, therefore, the operation at high retentate pressure (>17.5 bar) may not be superior due to the waste of high-pressure compressor load. Although the increase in recycle ratio can improve both H₂ recovery and also CO₂ removal rate, the supplying rate of fresh CaO of SER-PMR-SOFC raises as well. As shown in Figure 9.4b, for the operation at the recycle ratio of 0.9, fresh CaO supplying rate is 3 times higher than that of the operation with no recycle of the retentate gas. Moreover, the increase in recycle ratio may cause high velocity of retentate gas and also the generation of pressure drop in PMR which is not considered in this study.



(a)



(b)

Figure 9.4 The effect of the recycle ratio and retentate pressure on a) H_2 recovery, CO_2 removal rate and b) fresh CaO feed rate, CO_2 removal rate in case of SER-PMR-SOFC system.

The effect of fuel utilization and CO_2 removal rate on the power density and energy self-sufficient point for the SE-PMR-SOFC system is illustrated in Figure 9.5. With high CO_2 removal rate, high fuel utilization is required for the SE-PMR-SOFC to reach energy self-sufficient point. Under energy self-sufficient operation, the

increase in CO₂ removal rate improves the SOFC power density due to the increase in H₂ recovery. However, the improvement of power density with CO₂ removal rate becomes less pronounced at high CO₂ removal rate. Figure 9.6 shows the energy self-sufficient operation of SE-PMR-SOFC with equilibrium CO₂ removal rate at each operating voltage and retentate pressure. At each retentate pressure, there exists an optimum operating voltage. A higher fuel utilization is required as operating voltage decreases to achieve energy self-sustainable operation. The decrease in operating voltage can improve the power density, however, at excessively low operating voltage a fuel utilization close to 1 is required to achieve energy self-sustainable operation. The reduction in power density is found when decreasing an operating voltage due to low value of H₂ concentration near the exit of SOFC stack. The power density is improved as the retentate pressure increases owing to the improvement in H₂ recovery. With good operating condition selection, SE-PMR-SOFC can offer higher power density compared with PMR-SOFC and CON-SOFC. The operation of SE-PMR-SOFC with equilibrium CO₂ capture and operating voltage and retentate pressure of 0.626 V and 30 bar, respectively, offers the power density of 0.431 W/cm², as the power densities of PMR-SOFC (retentate pressure = 51.24 bar) and CON-SOFC are 0.421 and 0.398 W/cm², respectively.

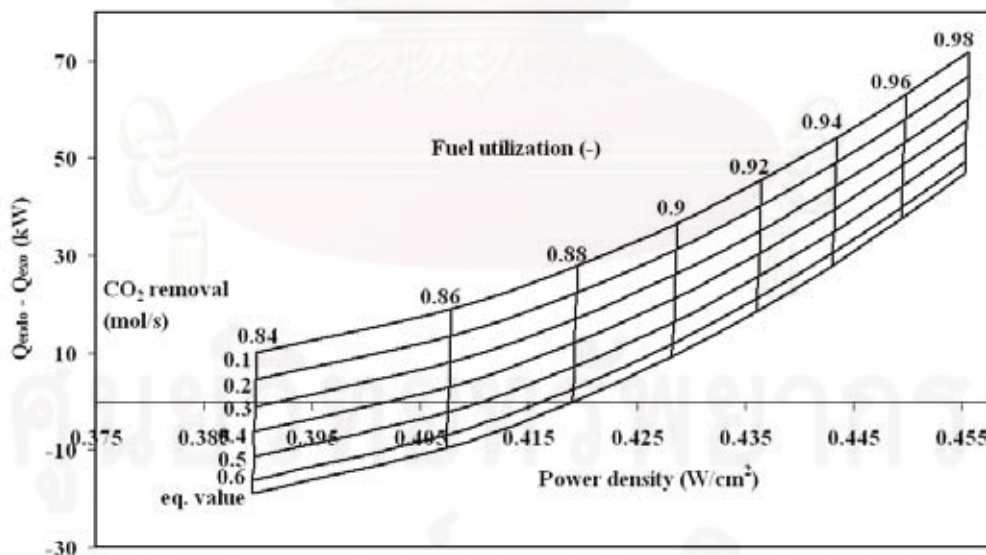


Figure 9.5 The effect of fuel utilization and CO₂ removal rate on the power density and energy self-sufficient point for SE-PMR-SOFC system (retentate pressure = 25 bar, $V = 0.65$ V).

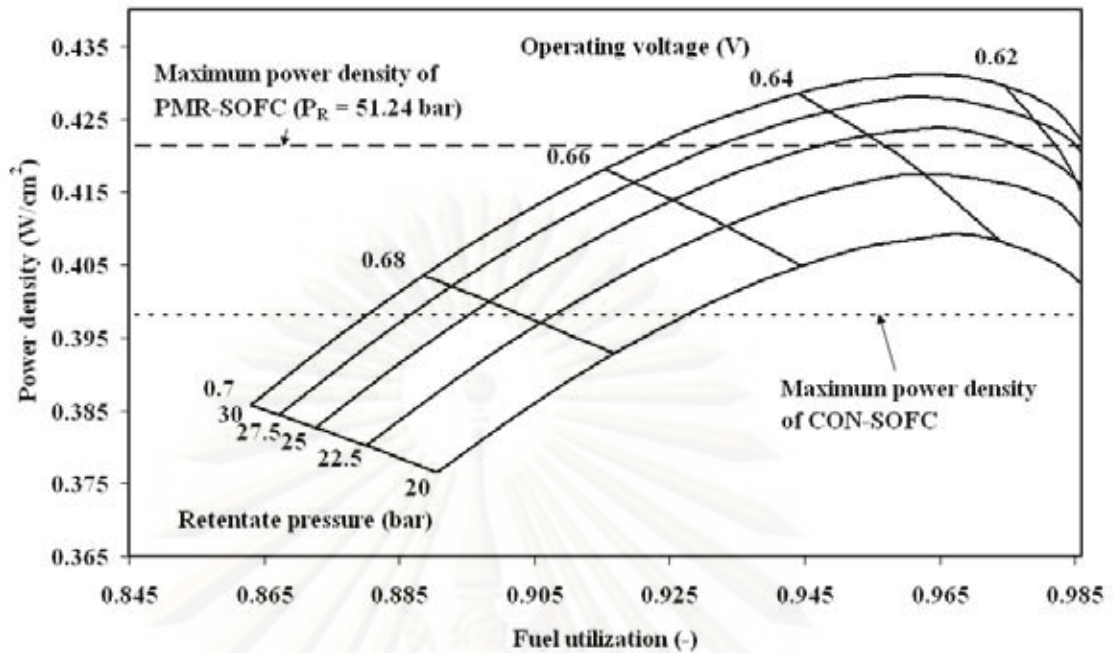


Figure 9.6 The power density of SE-PMR-SOFC system with equilibrium CO₂ removal rate operating at energy self-sufficient point at each operating voltage and retentate pressure.

Considering the SER-PMR-SOFC configuration, the effects of recycle ratio and fuel utilization on the power density and energy self-sustainable operation are illustrated in Figure 9.7. High fuel utilization is required to achieve energy self-sustainable operation for SER-PMR-SOFC operating at high recycle ratio. When operating at energy self-sustainable point, the increase in recycle rate can improve the power density. These operating characteristics are similar to those of the SE-PMR-SOFC since the operation at high recycle ratio offers high CO₂ removal rate. The study on the effects of permeate pressure and operating pressure on the power density for the SER-PMR-SOFC operated at a recycle ratio of 0.5 are depicted in Figure 9.8a. Similar to the SE-PMR-SOFC, the increase in the retentate pressure can improve the power density due to the increase in H₂ recovery. Also, the optimum operating voltage is found. As shown in Figure 9.8a, with the recycle ratio of 0.5, the optimum operating voltage is at around 0.61-0.62 V and the maximum power density of which the SER-PMR-SOFC can offer is about 0.45 W/cm². As illustrated in Figure 9.8b, operating voltage of PMR-SOFC operating at recycle ratio of 0.5 cannot be lower than 0.6 V which is the condition that the fuel utilization is close to 1. The results in

Figures 9.8a and 9.8b also imply that the intermediate fuel utilization (around 0.94-0.96) is preferred for the operation of SOFC system. For the operation at a recycle ratio of 0.9, the optimum operating voltage is observed at around 0.6-0.61 V. Moreover, the optimum retentate pressure is also found at around 15 bar as illustrated in Figure 9.9a. Even if the increase in the retentate pressure can improve H_2 recovery and also SOFC power density, the dwindle in power density caused from the increase in electricity consumption at the high-pressure compressor may overshadow this benefit especially at high recycle ratio in which H_2 recovery is not improved significantly with the increase in the retentate pressure as described in Figure 9.4a. Like in case of the operation at a recycle ratio of 0.5, the intermediate fuel utilization (around 0.94-0.96) is also preferred in the SER-PMR-SOFC system with the recycle ratio of 0.9 as shown in Figure 9.9b. With the recycle ratio of 0.9, the power density that the SER-PMR-SOFC system can achieve is 0.462 W/cm^2 which is extremely higher than that of PMR-SOFC (0.421 W/cm^2) and CON-SOFC (0.398 W/cm^2).

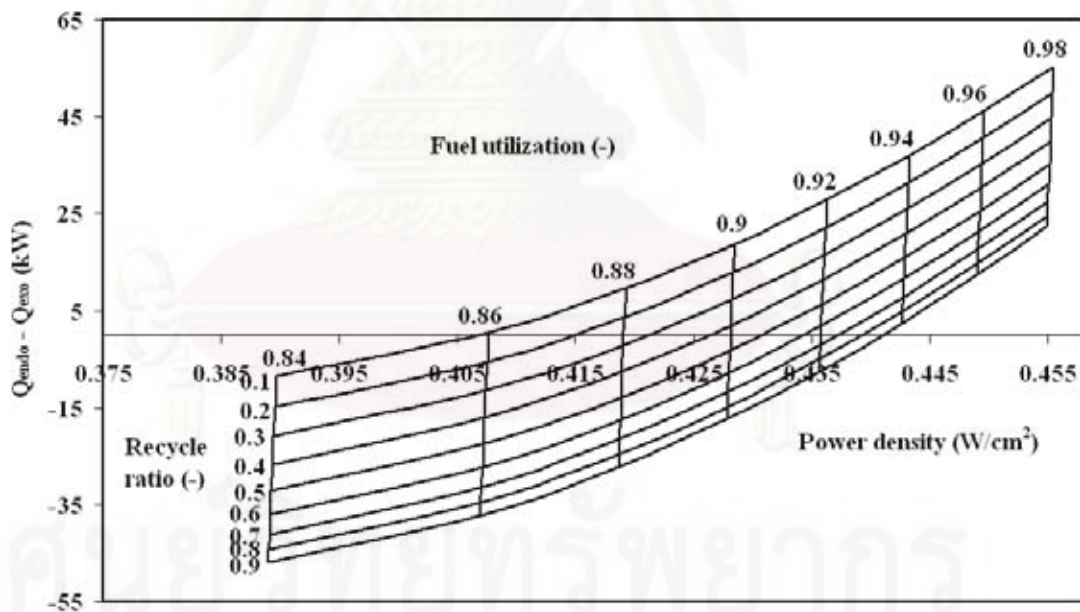
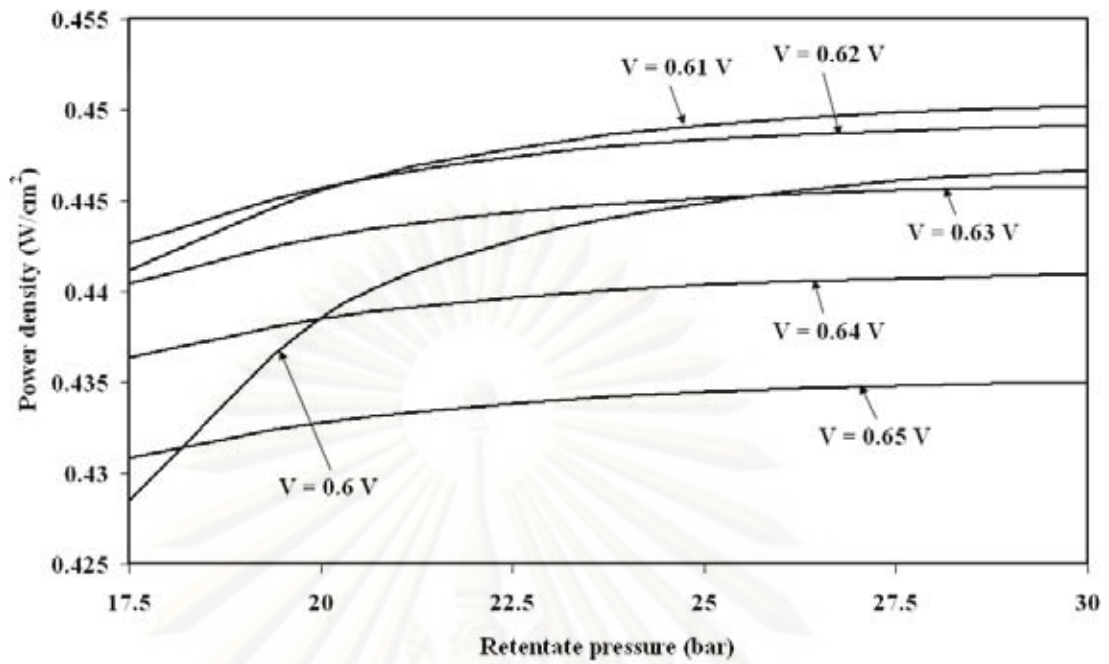
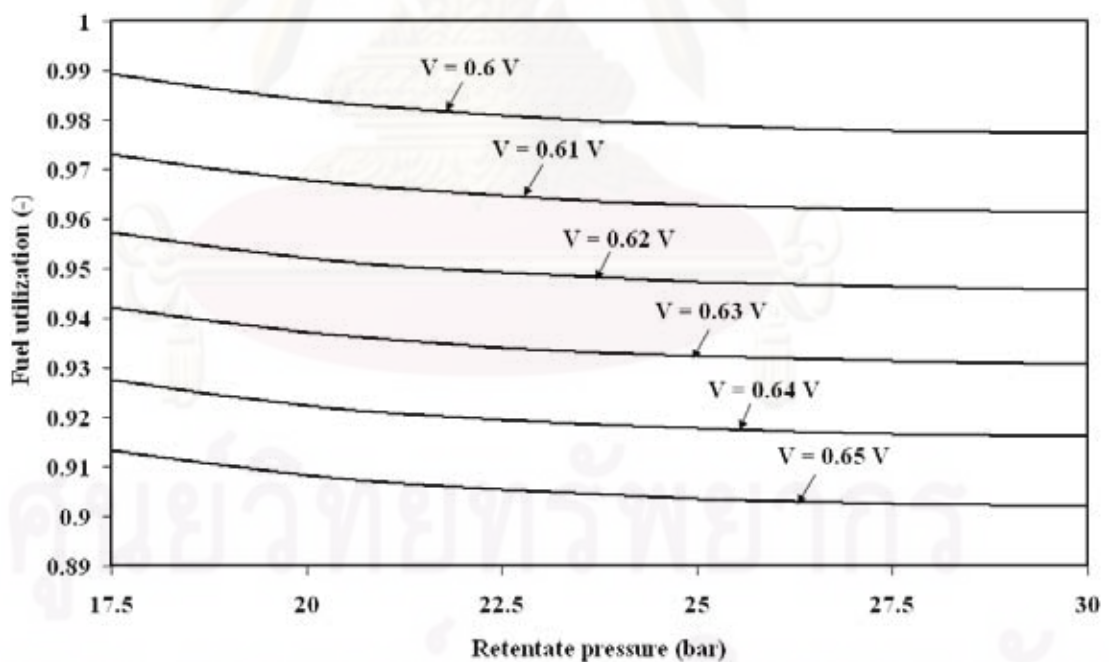


Figure 9.7 The effect of fuel utilization and recycle ratio on the power density and energy self-sufficient point for SER-PMR-SOFC system (retentate pressure = 17.5 bar, $V = 0.65 \text{ V}$).

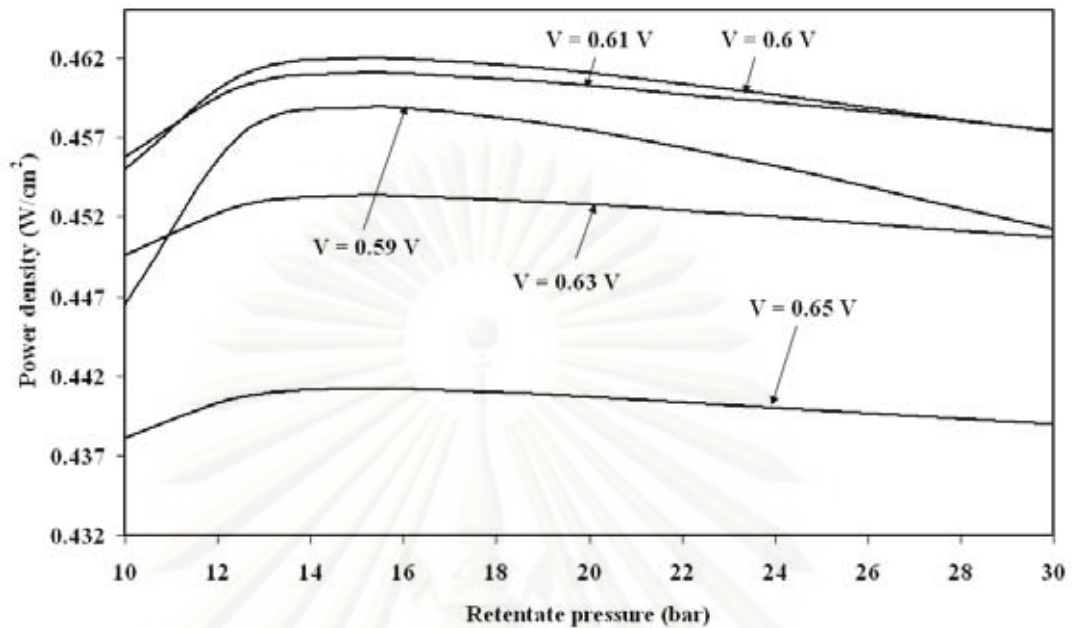


(a)

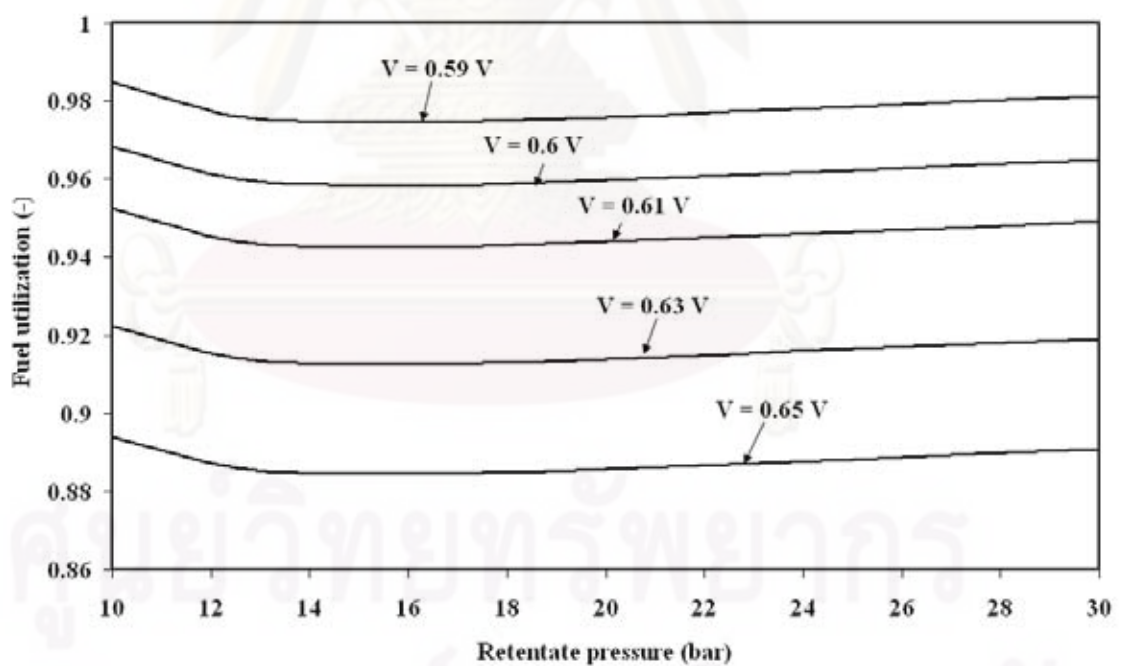


(b)

Figure 9.8 The effect of permeate pressure and operating pressure on a) the power density and b) fuel utilization for SER-PMR-SOFC system operating at energy self-sufficient point and recycle ratio of 0.5.



(a)



(b)

Figure 9.9 The effect of permeate pressure and operating pressure on a) the power density and b) fuel utilization for SER-PMR-SOFC system operating at energy self-sufficient point and recycle ratio of 0.9.

As illustrated in Figure 9.10 demonstrating the maximum power density of the SER-PMR-SOFC that can be achieved, SOFC stack size and the fresh CaO supplying rate at each recycle ratio, the stack size of SER-PMR-SOFC is always smaller than that of PMR-SOFC and CON-SOFC for every recycle ratio. The increase in recycle ratio can improve the power density; however, the amount of fresh CaO used in CaO-CO₂ acceptor also increases. It can be concluded that the operation of both SE-PMR-SOFC and SER-PMR-SOFC systems can significantly improve the power density and also reduce the size of the SOFC stack, nevertheless, large amount of fresh CaO sorbents should also be taken into account.

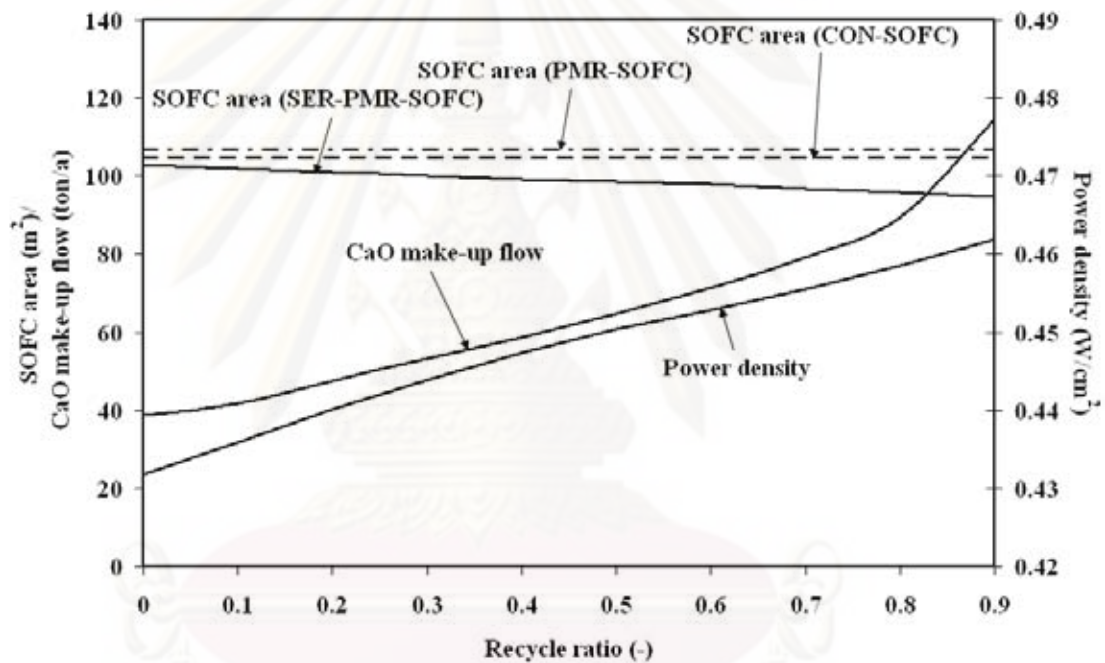


Figure 9.10 The maximum power density SER-PMR-SOFC can achieve, SOFC stack size and the fresh CaO supplying rate at each recycle ratio in case that $Q_{NET} = 0$.

To study the potential benefit of PMR-SOFC, SE-PMR-SOFC and SER-PMR-SOFC systems, the economic analysis is employed. CON-SOFC is considered as a base case. The influence of the recycle ratio on the potential benefit of SER-PMR-SOFC is also examined. In this analysis, the biogas feed rate was kept at 1.667 mol s^{-1} for all scenarios, therefore fuel feed cost is neglected. Furthermore, since the SOFC system considered is under the energy self-sustained operation, additional heat or electricity from the outside of the system is not necessary. Therefore, only the capital

costs of SOFC stack, PMR and high-pressure compressor (HPC), and the operating cost of fresh CaO sorbent are taken into account. Net cost saving is determined as economical index and can be calculated employing Eq. (4.93). The cost of fresh CaO sorbent is computed from the total cost of fresh CaO used in the life time. All parameters used in capital cost estimation and economic study are summarized in Table 4.13. The additional benefit obtained from CO₂ capture is also considered in this study. Two indicators; i.e. % total CO₂ capture and cost of CO₂ capture are defined. For % total CO₂ capture, it can be calculated using the following expression;

$$\% \text{ total } CO_2 \text{ capture} = \frac{\text{Rate of } CO_2 \text{ capture} \left(\frac{\text{ton}}{a} \right)}{\text{Total } CO_2 \text{ in flue gas in case of CON - SOFC} \left(\frac{\text{ton}}{a} \right)} \times 100 \quad (9.1)$$

where cost of CO₂ capture can be computed using Eq. (4.94). % Total CO₂ capture represents the CO₂ capture efficiency of SER-PMR-SOFC configuration, whereas cost of CO₂ capture stands for the additional cost (relative to CON-SOFC) used in CO₂ capture per unit of CO₂ capture.

As illustrated in Figure 9.11, PMR-SOFC configuration is not an attractive SOFC system due to high retentate pressure and also electricity consumption in HPC. The use of SE-PMR-SOFC configuration in SOFC system (equilibrium CO₂ capture) is more beneficial compared with PMR-SOFC since it can offer high H₂ recovery with low retentate pressure. However, the negative net cost saving of the former indicates that its potential benefit does not reach that of CON-SOFC. For SER-PMR-SOFC, maximum net cost saving is observed at the recycle ratio of 0.8. The operation at the recycle ratio of 0.9 is not favored even if high power density is achieved since its CaO cost is extremely higher compared to low recycle ratio as illustrated in Figure 9.11. Although the net cost saving of SER-PMR-SOFC is superior to SE-PMR-SOFC, it is a negative value, indicating that both SE-PMR-SOFC and SER-PMR-SOFC are not the good configuration for SOFC system. The additional study on the benefit of CO₂ capture takes place as shown in Figure 9.12. The operation at high recycle ratio is preferred if high total CO₂ capture efficiency is required. Moreover, cost of CO₂ capture is reduced as the recycle ratio increases. Considering SER-PMR-SOFC

operating at the recycle ratio of 0.9, its cost of CO₂ capture is \$20.4/ton CO₂ capture at % total CO₂ capture of 93. With the identical % total CO₂ capture, this cost of CO₂ capture is far lower than \$228/ton CO₂ capture reported in the literature (Vivanpatarakij et al., 2008) reporting the cost of CO₂ capture from the flue gas of methane fuelled CON-SOFC system.

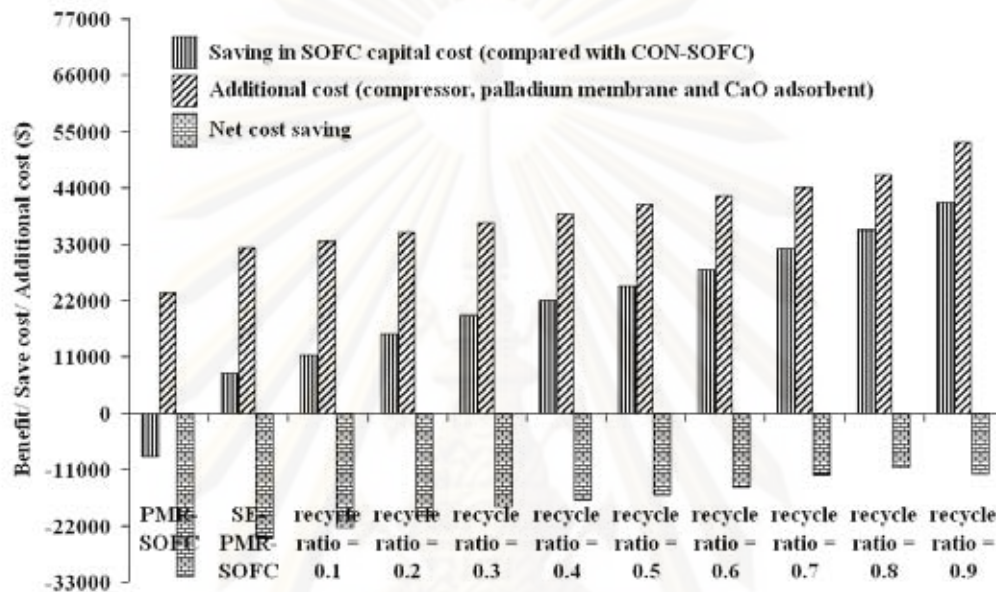


Figure 9.11 Saving in SOFC stack cost, additional cost and net cost saving of PMR-SOFC, SE-PMR-SOFC with equilibrium CO₂ capture and SER-PMR-SOFC operating at different recycle ratios.

The results of the technical and economical studies for all SOFC configurations are summarized in Table 9.1. On the basis of similar biogas feed rate of 1.667 mol/s with net electricity production of 416.79 kW, the improvement in power densities relative to CON-SOFC are 8.21 and 15.11% for SE-PMR-SOFC and SER-PMR-SOFC with recycle ratio of 0.8, respectively. Also, the decreases in SOFC stack size of SE-PMR-SOFC and SER-PMR-SOFC with recycle ratio of 0.8 compared with CON-SOFC are about 1.55 and 8.27%, respectively. Even if SE-PMR-SOFC and SER-PMR-SOFC can offer higher performance compared with CON-SOFC, the operations of SOFC with these configurations are not feasible in economic point of view since their net cost saving are negative (-\$25,068.78 for SE-PMR-SOFC and -\$10,631.73 for SER-PMR-SOFC). However, these two configurations acquire

the additional benefit caused from CO₂ capture. Their CO₂ capture costs are extremely low (\$137.27 for SE-PMR-SOFC and \$23.79 for SER-PMR-SOFC) especially for SER-PMR-SOFC configuration with high recycle ratio.

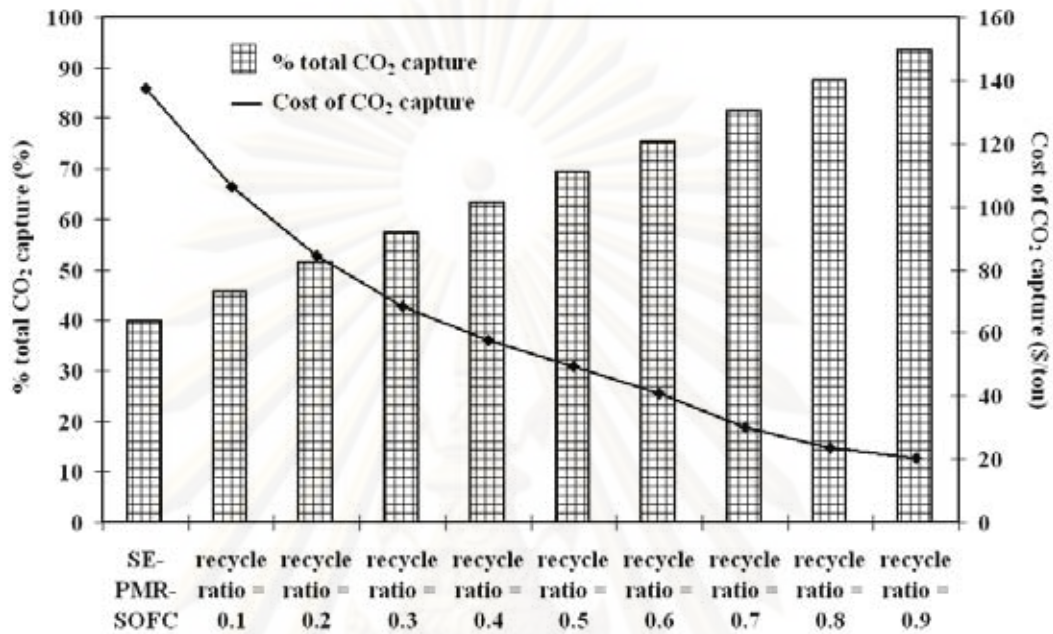


Figure 9.12 %Total CO₂ capture and cost of CO₂ capture of SE-PMR-SOFC with equilibrium CO₂ capture and SER-PMR-SOFC operating at different recycle ratio.

Table 9.1 The technical and economical comparison among different configurations of SOFC system.

	CON-SOFC	PMR-SOFC	SE-PMR-SOFC (equilibrium CO ₂ capture)	SER-PMR-SOFC	
				Recycle ratio =0.5	recycle ratio =0.8
Feed rate (mol/sec)	1.667	1.667	1.667	1.667	1.667
Retentate pressure (bar)	-	51.24	30	30	20
H ₂ recovery (-)	-	0.95	0.959	0.981	0.986
The amount of CO ₂ capture (ton/a)	-	-	903.38	1575.13	1987.26
Fresh CaO feed rate (ton/a)	-	-	36.5	64.7	89.4
Power density (W/cm ²)	0.3984	0.4213	0.4311	0.4503	0.4586
% improvement in power density	-	5.75	8.21	13.03	15.11
Electricity produced in SOFC (kW)	416.79	449.30	444.04	444.11	440.12
Net electricity produced (kW)	416.79	416.79	416.79	416.79	416.79
Electricity consumed in compressor (kW)	-	32.46	27.25	27.32	23.33
SOFC active area (m ²)	104.62	106.66	103	98.62	95.97
% improvement in SOFC area	-	-1.95	1.55	5.74	8.27
Palladium membrane area (m ²)	-	4.71	4.71	4.71	4.71
Capital cost of SOFC (\$)	433,559.29	442,000.46	426,842.12	408,698.58	397,703.18
Capital cost of Pd membrane (\$)	-	1,716.37	1,716.37	1,716.37	1,716.37
Capital cost of compressor (\$)	-	21,712.84	19,112.23	19,698.13	17,959.49
Cost of fresh CaO sorbent in life time (\$)	-	-	10,957.36	19,413.52	26,811.97
Saving cost on SOFC (\$)	-	-8,441.17	6,717.18	24,860.72	35,856.11
Net cost saving (\$)	-	-31,870.37	-25,068.78	-15,967.30	-10,631.73
% total CO ₂ capture (%)	-	-	39.79	69.38	87.53
Cost of CO ₂ capture (\$/ton CO ₂ capture)	-	-	137.27	49.35	23.79

9.4 Conclusions

The concept of the cooperation of SOFC system, palladium membrane reactor (PMR) and CaO-CO₂ acceptor is proposed in this study. With this concept, CaO-CO₂ acceptor is placed to capture CO₂ in biogas prior to be fed to PMR in which pure-H₂ generated. Three configurations of SOFC system; i.e., PMR-SOFC, SE-PMR-SOFC and SER-PMR-SOFC are considered. CON-SOFC is determined as a base case in the analysis. The concept of energy self-sustainable operation ($Q_{NET}=0$) is also employed to evaluate the real performance of SOFC system. The technical analysis reveals that low value of retentate pressure (<30 bar) is enough to achieve high H₂ recovery (>0.95) as CaO-CO₂ acceptor is included in SOFC system. The increase in CO₂ removal rate of SE-PMR-SOFC can improve the power density of SOFC; however, the supply of fresh CaO sorbent is required. The recycle of retentate gas in case of SER-PMR-SOFC can improve CO₂ capture rate, H₂ recovery and also SOFC power density; however, the increase in fresh CaO supplying rate should also be taken into account. Compared with CON-SOFC, the stack size of SE-PMR-SOFC and SER-PMR-SOFC with the recycle ratio of 0.8 is reduced for 1.55 and 8.27%, respectively. However, this benefit is not found in PMR-SOFC configuration. The economic study was also carried out to evaluate the potential benefit of each configuration of SOFC system. It is found that PMR-SOFC, SE-PMR-SOFC and SER-PMR-SOFC are not attractive configurations in the economic point of view due to their negative net cost saving relative to CON-SOFC. Nevertheless, SE-PMR-SOFC and SER-PMR-SOFC can offer high %total CO₂ capture and low cost of CO₂ capture. For SER-PMR-SOFC with the recycle ratio of 0.8, its cost of CO₂ capture is \$23.79/ton CO₂ capture which is far lower compared to \$228/ton CO₂ capture reported in the literature which studied the cost of CO₂ removal from the flue gas of CON-SOFC system fed by methane.

CHAPTER X

OPERATION VIABILITY AND PERFORMANCE OF SOLID OXIDE FUEL CELL FUELLED BY DIFFERENT FEEDS

The performances of solid oxide fuel cells (SOFC) fed by different types of feed, i.e. biogas, biogas-reformed feed, methane-reformed feed and pure hydrogen, are simulated in this chapter. Maximum temperature gradient and maximum cell temperature are regarded as indicators for operation viability investigation whereas power density and electrical efficiency are considered as performance indicators.

10.1 Introduction

Several configurations were proposed in the previous chapters in order to improve the performance of SOFC system. In each configuration, the conventional fuel processor was improved so as to diminish CH_4 , CO and CO_2 contents in SOFC feed since the presence of these gases can cause the performance drop in SOFC stack. According to the results in the previous chapters, pure- H_2 seems to be high-performance feedstock for SOFC as the power density is considered as performance indicator. Nevertheless, not only electricity that is produced in SOFC stack, but heat is also generated due to the irreversibility of the electrochemical reaction. Excess heat generation can cause the damage of the structure of SOFC stack. Although the use of pure H_2 as SOFC feed can offer high power density, its rapid electrochemical reaction may cause high temperature gradient in solid part of SOFC. Therefore the selection of suitable feedstock for SOFC is also an interesting issue in thermal consideration. Moreover, operating conditions; e.g. operating voltage, oxidizing agent contents, rate of fuel supply, etc., should be carefully tuned up to minimize the heat generation in the SOFC stack. In this consideration, the temperature gradient is regarded as the indicator to judge the operation viability of SOFC stack. The maximum allowable

temperature gradient of YSZ which is widely used as SOFC electrolyte is around 10 K cm^{-1} (Lim et al., 2005).

In this chapter, the performance and thermal behavior of SOFC depend on the type of feedstock and operating conditions. In this study, the performance of SOFC is analyzed employing 1-D analysis. The effect of operating voltage, inlet fuel flow rate and inlet air flow rate (% excess air) on maximum temperature gradient and maximum temperature of solid part in the SOFC stack and the power density are investigated for four types of SOFC feedstock, i.e. biogas, biogas-reformed feed, methane-reformed feed and pure- H_2 . To consider the viability of the operation of SOFC, maximum acceptable temperature gradient and maximum acceptable cell temperature are set to 10 K cm^{-1} and 1273 K , respectively.

10.2 Type of feed in consideration

Four feed types, i.e. biogas, reformed-biogas, reformed-methane and pure- H_2 , are considered in this study. Their compositions are determined by the following hypotheses;

Biogas: In this study, the quantity of methane and carbon-dioxide in biogas is assumed to be 60 and 40%, respectively (biogas feed rate = $F_{CH_4,eq}/0.6$). Steam is fed together with biogas into the SOFC cell. The amount of steam is 2.5 times of methane in biogas.

Biogas-reformed feed: Biogas (biogas feed rate = $F_{CH_4,eq}/0.6$) and steam is fed into reformer prior to be fed to SOFC cell. The quantity of steam fed is equal to that in case of biogas feed. Two chemical reactions, i.e. steam reforming (Eq. (4.32)) and WGS (Eq. (4.33)), take place in the reformer. Thermodynamic equilibrium is assumed for the calculation of reformer.

Methane-reformed feed: The calculation of SOFC feed composition for methane-reformed feed is identical to that for biogas-reformed feed; however, the reformer feed is changed from biogas to methane (methane feed rate = $F_{CH_4,eq}$).

Pure- H_2 : H_2 is fed directly into SOFC cell. Its feed rate is equal to 4 times of $F_{CH_4,eq}$. (H_2 feed rate = $4 \times F_{CH_4,eq}$)

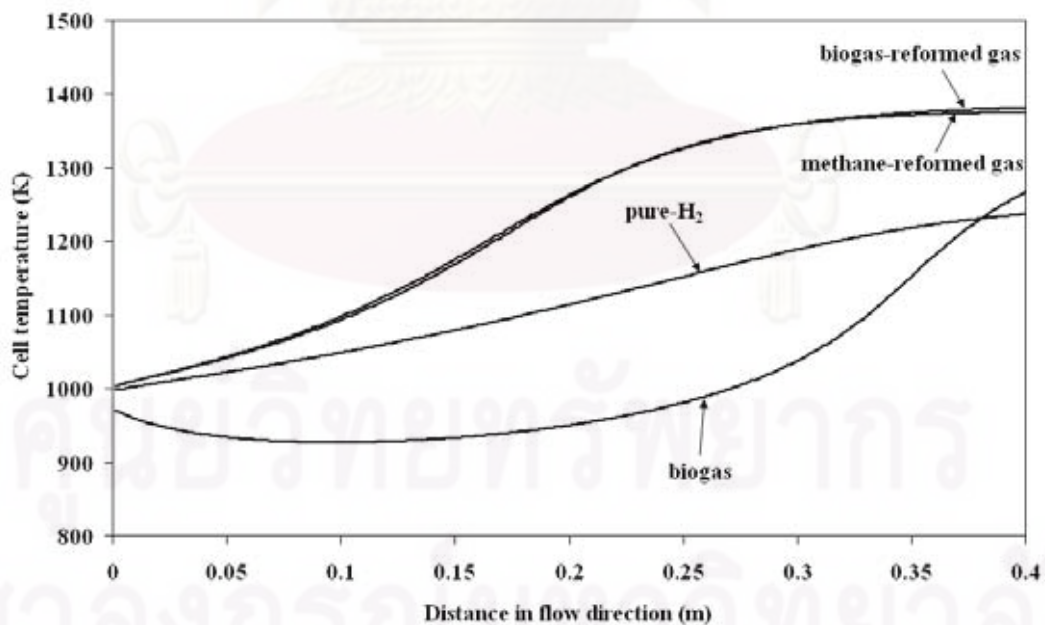
10.3 Results and discussion

Temperature profiles of the solid part in SOFC fed by different feeds are first investigated. A base case is determined as given in Table 10.1. The operating voltage for each case is tuned up to achieve $U_f = 80\%$ at constant percent excess air and $F_{CH_4,eq}$. As described in Table 10.1, SOFC fed by pure-H₂ offers higher power density than the other feed types since it operates at higher operating voltage. Moreover, the maximum temperature gradient and maximum cell temperature of the pure-H₂ feed are much lower than those of the other feed types.

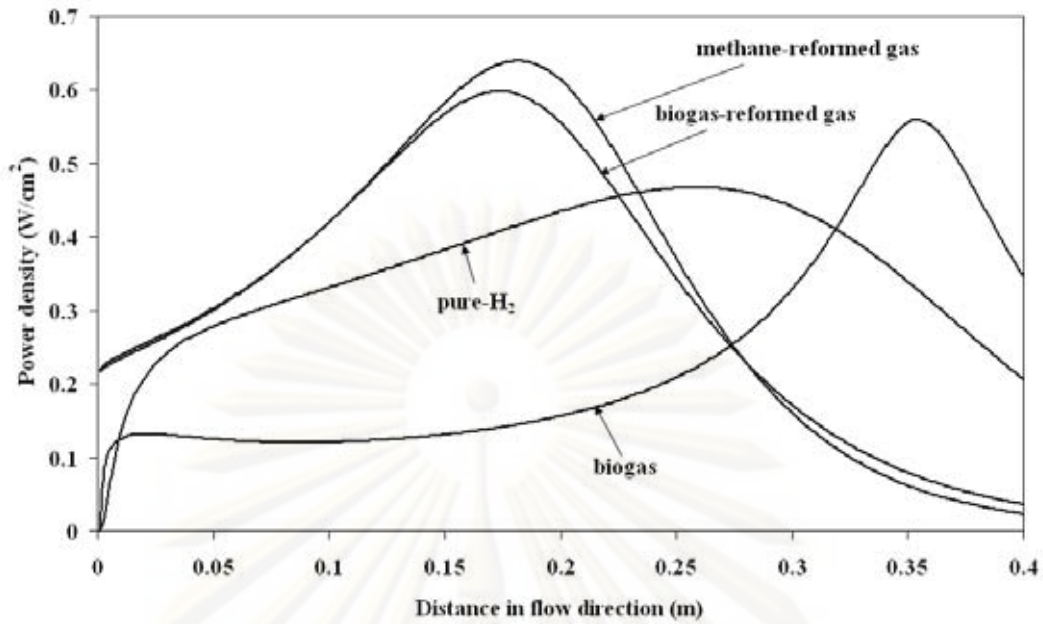
As illustrated in Figure 10.1a, excluding SOFC fed by biogas, temperature of the solid part of SOFC increases along the flow direction due to the release of heat generated from irreversibility of the electrochemical reaction. The increase in temperature of the solid part of SOFC with the cell distance is more severe for the biogas-reformed feed and the methane-reformed feed compared with that of the pure-H₂ feed. It is obvious that the operation at high operating voltage can reduce irreversibility loss and also temperature gradient of solid part in the SOFC cell. For the SOFC fed by biogas, the decrease in cell temperature with cell distance is found at the inlet of the cell. This is due to the effect of the endothermic steam reforming reaction. Considering power density profile, power density increases with cell distance as shown in Figure 10.2b. The increase in cell temperature along the cell distance causes the reduction of ohmic loss and consequently the power density increases. The increase in power density inside the SOFC cell fed by biogas-reformed feed and methane-reformed feed is more severe than in the case of pure-H₂ feed which is conformed to the increase of temperature with distance in Figure 10.1a. However, near the gas outlet of the SOFC cell, the decrease in power density with cell distance is observed even if the increase in cell temperature with cell distance is observed. This implies that the effect of the depletion of H₂ concentration with cell distance dominates the effect of the increase in cell temperature near the gas outlet of SOFC. Similar to the change in cell temperature in the flow direction, the decrease in power density of SOFC fed by biogas with cell distance is observed at the gas inlet of the SOFC cell.

Table 10.1 Base case in consideration for different feed ($U_f = 0.8$).

Type of feed	Biogas	Biogas- reformed feed	Methane- reformed feed	Pure-H ₂
$F_{CH_4,eq}$ (mol/s)	0.0003	0.0003	0.0003	0.0003
%excess air (%)	400	400	400	400
Operating voltage (V)	0.511	0.695	0.714	0.769
Power density (Wcm ⁻¹)	0.234	0.322	0.33	0.357
Current density (A cm ⁻¹)	0.457	0.463	0.463	0.464
Electrical efficiency (%)	38.86	42.74	44.51	49.14
U_f (-)	0.8	0.8	0.8	0.8
Electricity produced (W)	93.53	128.67	132.12	142.61
Maximum temperature gradient (K cm ⁻¹)	28.75	18.08	18.65	7.68
Maximum cell temperature (K)	1267.5	1381.5	1375.7	1236.6



(a)

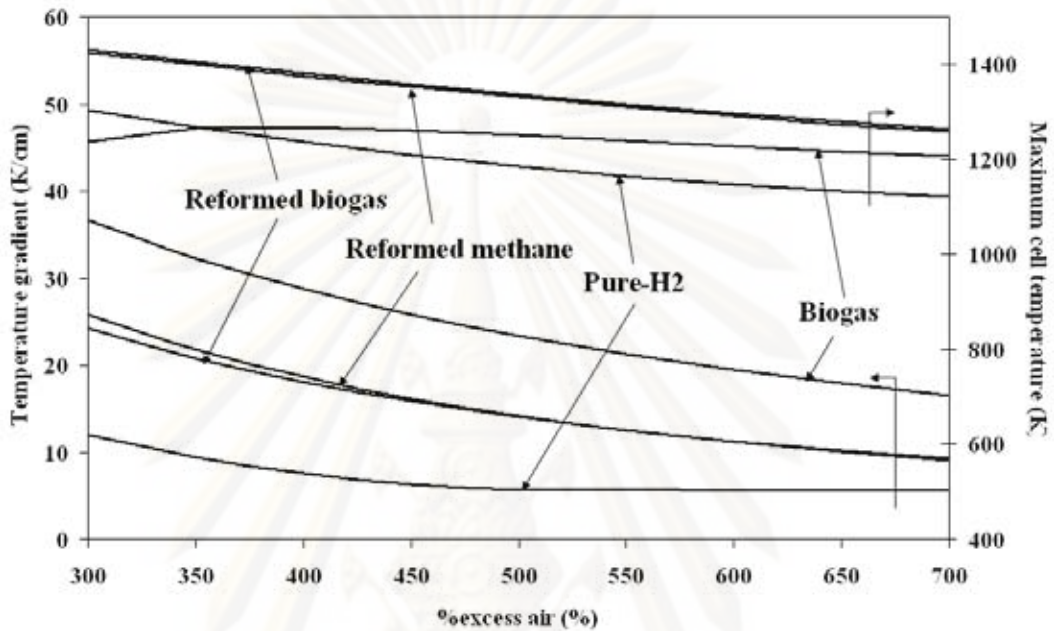


(b)

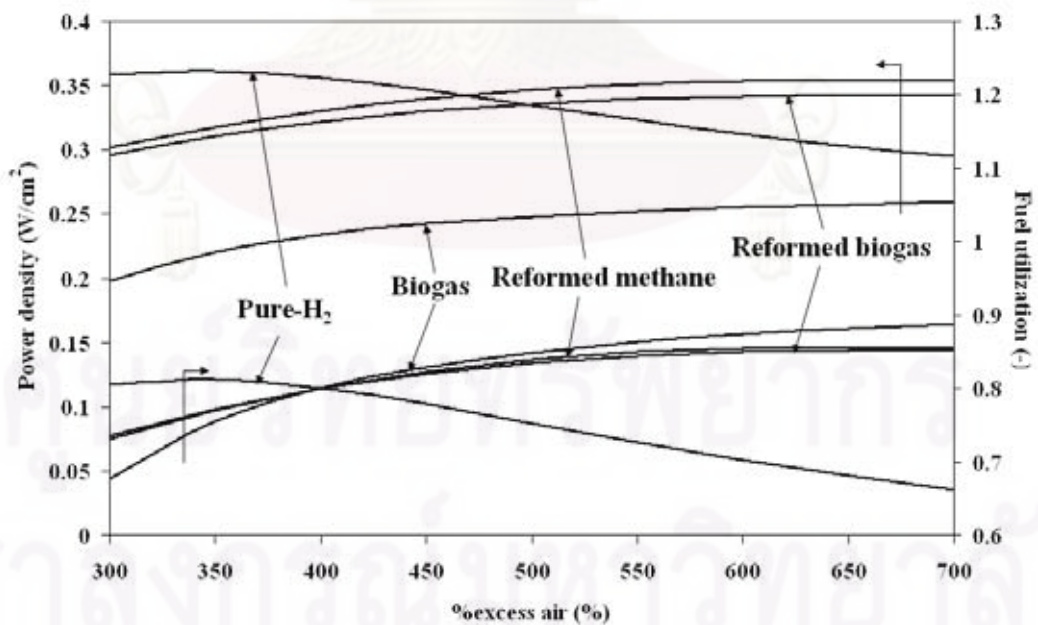
Figure 10.1 The variation of a) cell temperature and b) power density with cell distance in SOFC cell fed by different types of feed. ($F_{CH_4,eq} = 3 \times 10^{-4} \text{ mol s}^{-1}$, Percent excess air = 400%, $U_f = 0.8$)

The effect of the change in percent excess air on the maximum temperature gradient and maximum cell temperature of the solid part of SOFC fed by different types of feed is investigated as illustrated in Figure 10.2a. As percent excess air increases, maximum temperature gradient and maximum temperature of the solid part in SOFC cell decrease, implying that SOFC is more feasible to operate at high percent excess air. However, using large amount of oxidizing agent (air), massive air compressor is required and much of electricity generated in SOFC must be supplied to it. Hence, the appropriate percent excess air value should be carefully selected. Even if the operation with high percent excess air can improve the operation viability (lower temperature gradient) of SOFC, the power density and fuel utilization are inhibited for SOFC fed by pure- H_2 as shown in Figure 10.2b. This is due to the decrease in cell temperature which results in the increase in ohmic loss as percent excess air increases. Inversely, the power density and fuel utilization obtained from biogas-reformed feed, methane-reformed feed and biogas increases with the increase in percent excess air. This is due to the effect of the increase in electromotive force as the cell temperature decreases could defeat the effect of the increase in ohmic loss.

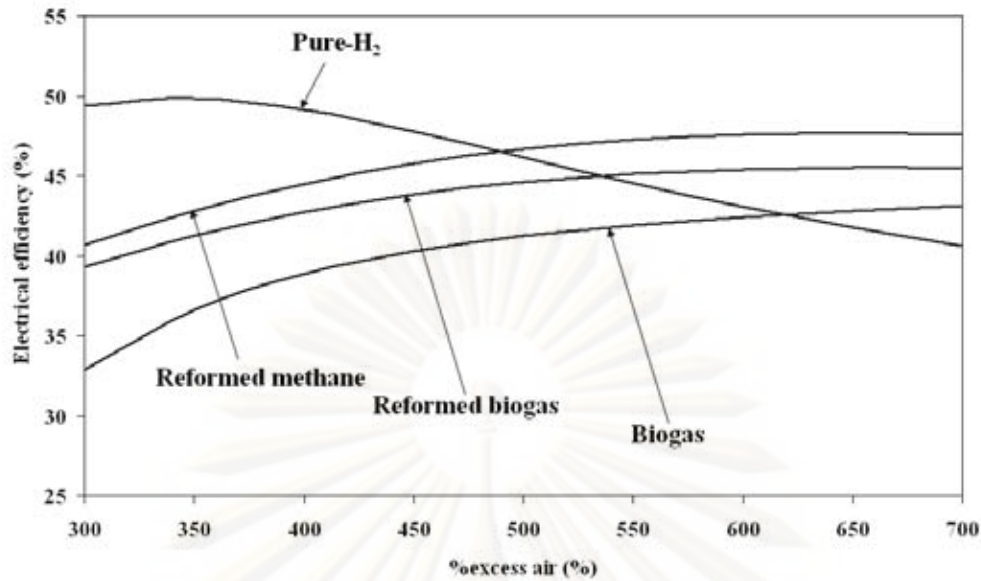
The influence of %excess air on the electrical efficiency of SOFC stack is also studied as illustrated in Figure 10.2c. Similar to power density and fuel utilization, optimum electrical efficiency is found at low % excess air for SOFC fed by pure-H₂ and the electrical efficiency increases with %excess air for SOFC fed by the other feeds.



(a)



(b)

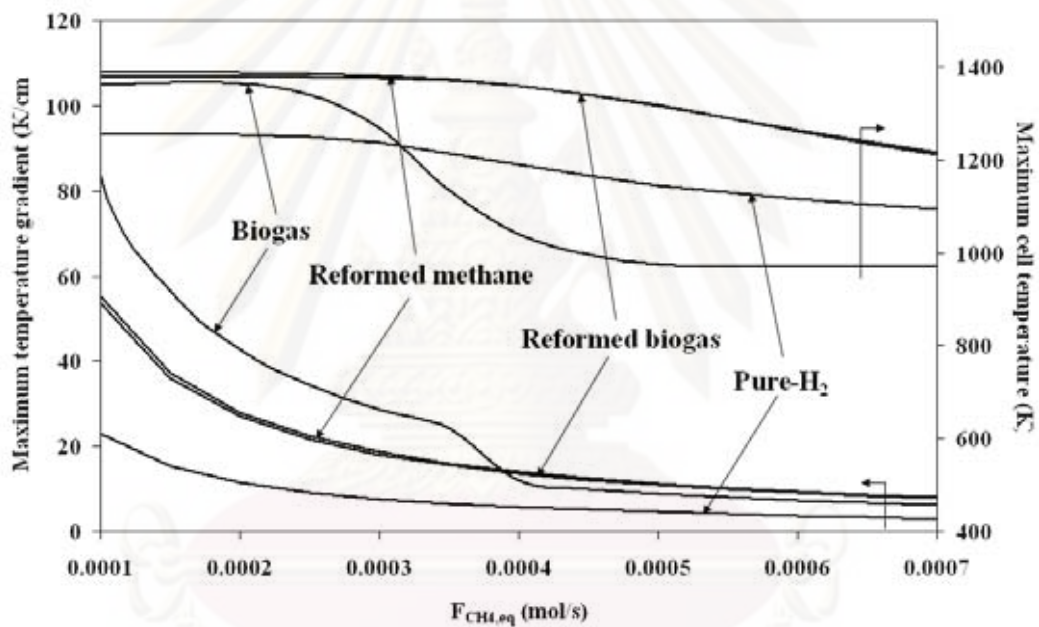


(c)

Figure 10.2 The effect of the change in percent excess air on a) the maximum temperature gradient, maximum cell temperature, b) power density, fuel utilization and c) electrical efficiency for SOFC fed by different types of feed. ($F_{CH_4,eq}$ and operating voltage are equal to base case values.)

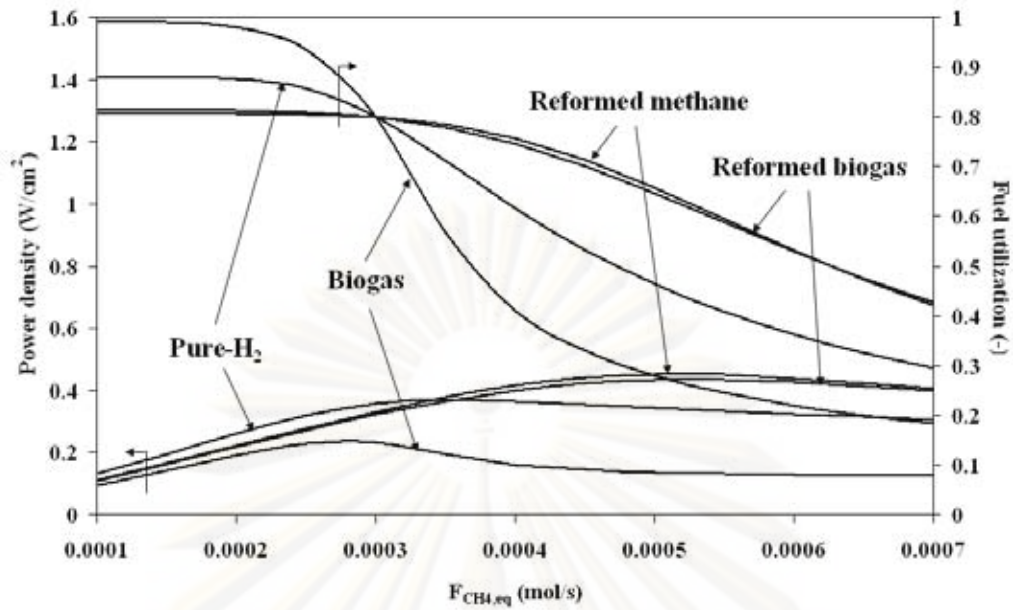
Figure 10.3a shows effect of the change in $F_{CH_4,eq}$ on maximum temperature gradient and maximum cell temperature of the solid part in SOFC fed by different types of feed. The increase in $F_{CH_4,eq}$ can decrease both maximum temperature gradient and maximum temperature in SOFC cell. This is due to the fact that fuel utilization and also the irreversibility are very high for SOFC with low feed rate and they decrease as $F_{CH_4,eq}$ increases as illustrated in Figure 10.3b. However, for SOFC fed by biogas, severe decrease in fuel utilization, maximum temperature gradient and maximum cell temperature with the increase in $F_{CH_4,eq}$ can be found at around 3×10^{-4} - 4×10^{-4} mol s⁻¹. It can be explained by the fact that CH₄ in biogas cannot be entirely reformed when $F_{CH_4,eq}$ is higher than 3×10^{-4} mol/s. The optimum power density can be obtained when $F_{CH_4,eq}$ is well tuned up. When the feed rate is low, the increase in feed rate can improve the power density because the fuel utilization does not significantly decrease with the feed velocity. However, for SOFC with high feed rate, the fuel utilization significantly drops as the feed velocity increases while the power

density does not significantly decrease with the increase of feed rate. These results imply that $F_{CH_4,eq}$ should be carefully considered to achieve a suitable value. With low $F_{CH_4,eq}$, the solid part in SOFC cell may be damaged due to extremely high temperature. However, with excessively high $F_{CH_4,eq}$, fuel utilization and power density of SOFC may be inhibited. The study on the effect of the change in feed flow rate on the electrical efficiency (Figure 10.3c) also indicates that the intermediate fuel flow rate is preferred. Optimum electrical efficiency is found and does not change with feed velocity at low to intermediate fuel feed rates, however, when operating at high fuel velocities, it decreases as the fuel feed rate increases.

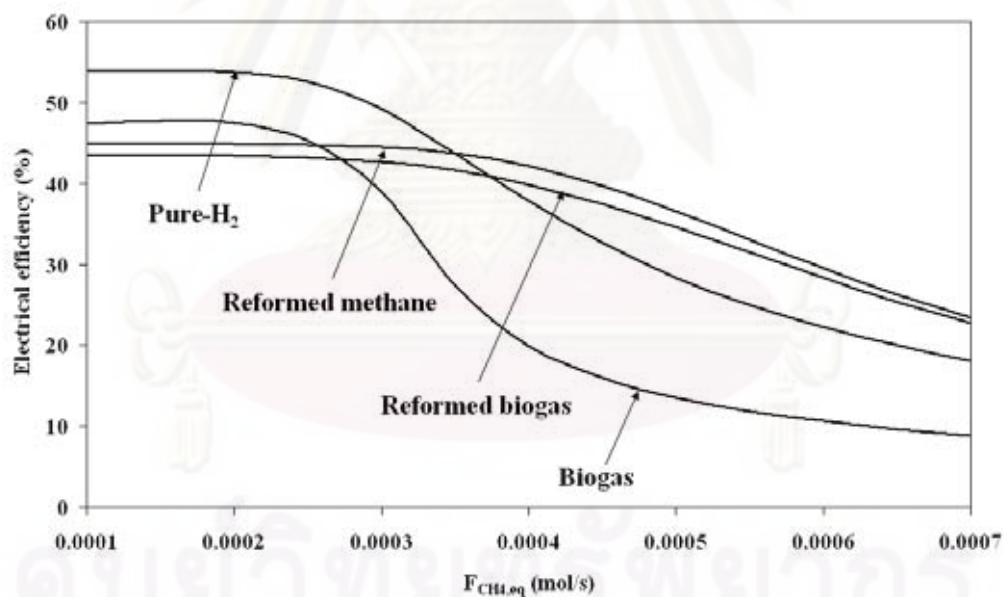


(a)

ศูนย์วิทยทรัพยากร
จุฬาลงกรณ์มหาวิทยาลัย



(b)

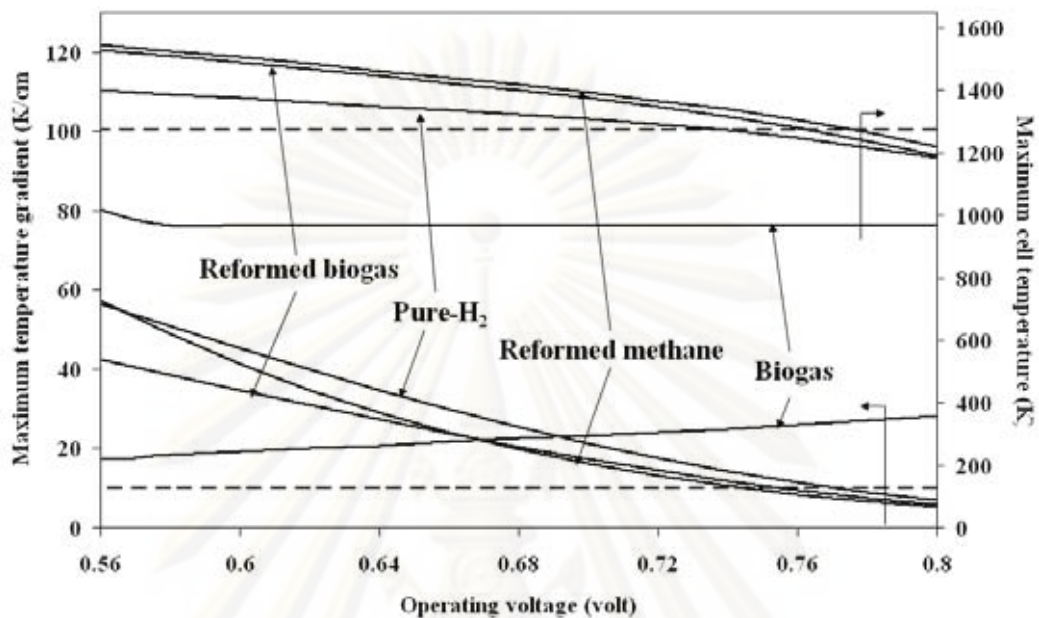


(c)

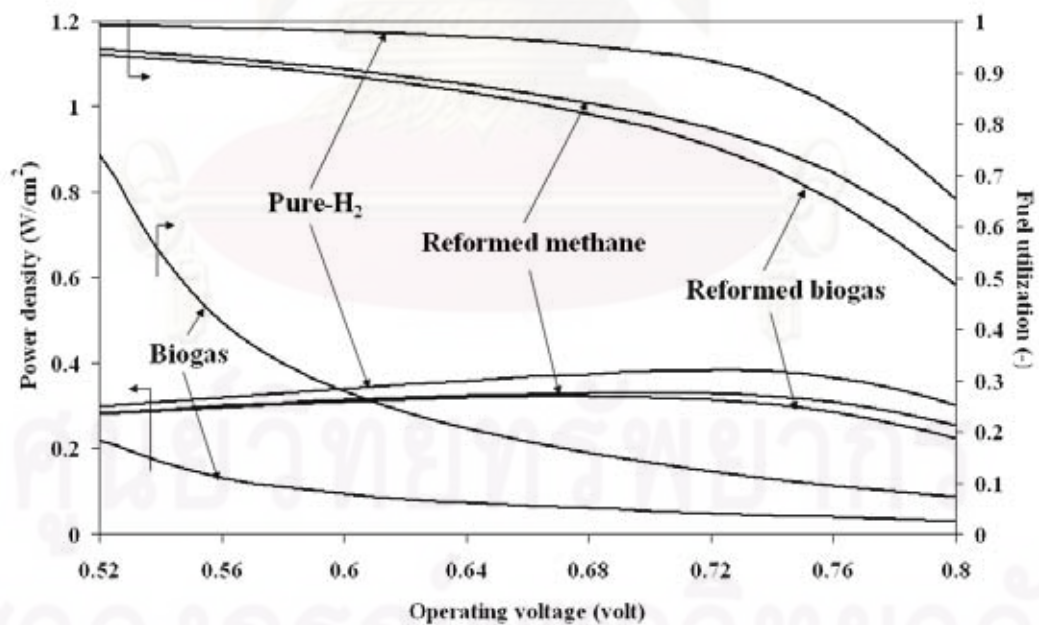
Figure 10.3 The effect of the change in $F_{CH_4,eq}$ on a) the maximum temperature gradient, maximum cell temperature, b) power density, fuel utilization and c) electrical efficiency for SOFC fed by different types of feed. (percent excess air and operating voltage are equal to base case values.)

To compare the performance of SOFC fed by different feed, the effects of the operating voltage on the maximum temperature gradient, maximum cell temperature, power density and fuel utilization were investigated as shown in Figures 10.4 and 10.5 for $F_{CH_4,eq}$ of 3×10^{-4} and 5×10^{-4} mol/s, respectively. The percent excess air is kept to be constant at the base case of 400% excess. The dash lines in Figures 10.4a and 10.5a represent the maximum acceptable temperature gradient (MATG), 10 K/cm, and maximum acceptable cell temperature (MACT), 1273 K. As shown in Figures 10.4a and 10.5a, excluding SOFC fed by biogas, the increase in operating voltage can improve the operation viability of SOFC. As the operating voltage increases, heat generation caused from the irreversibility is reduced and the cell temperature drops. Inversely, for SOFC fed by biogas, the operation at low operating voltage is preferred since large amount of heating energy generated from the irreversibility can be used in endothermic methane steam reforming and the decreasing rate of cell temperature in the flow direction is reduced. The results in Figures 10.4a and 10.5a also imply that it is difficult to operate SOFC fed by biogas at percent excess air is lower than 400% since the maximum temperature gradient and maximum cell temperature would increase. Moreover, as illustrated in Figures 10.4b, 10.4c, 10.5b and 10.5c, the fuel utilization, power density and electrical efficiency of SOFC fed by biogas are significantly lower than those of SOFC fed by the other feeds. Therefore, it can be concluded that direct biogas feed is not a recommended feedstock for SOFC. The operation at high operating voltage is desired to minimize the temperature and temperature gradient of solid part in SOFC. However, the fuel utilization obtained at this condition is not satisfied, as shown in Figures 10.4b and 10.5b, the fuel utilization decreases as the operating voltage increases. When operating at the same operating voltage, SOFC fed by pure-H₂ offers higher fuel utilization compared with SOFC fed by the other feed types. This implies that H₂ concentration is the important factor which affects the rate of electrochemical reaction. The optimum operating voltage which offers maximum power density can be observed as illustrated in Figures 10.4b and 10.5b. When the operating voltage is lower than the optimum value, the increase in operating voltage can improve the power density since fuel utilization does not significantly decrease. The pronounced decrease in fuel utilization with the increase in operating voltage can be found as the operating voltage is higher than the optimum value; hence, power density also decreases. The change in electrical efficiency with

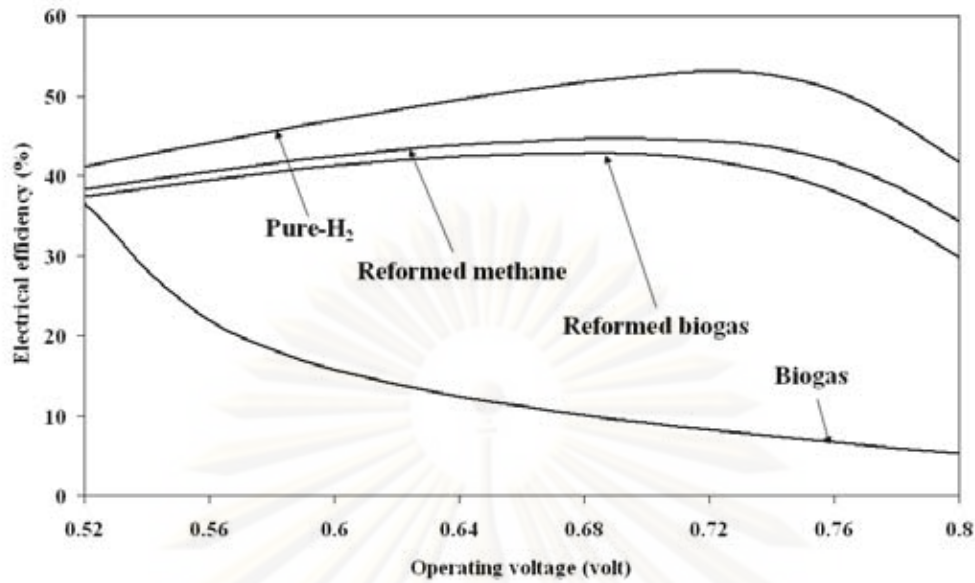
the operating voltage is in the same tendency as the change in power density as shown in Figures 10.4c and 10.5c.



(a)

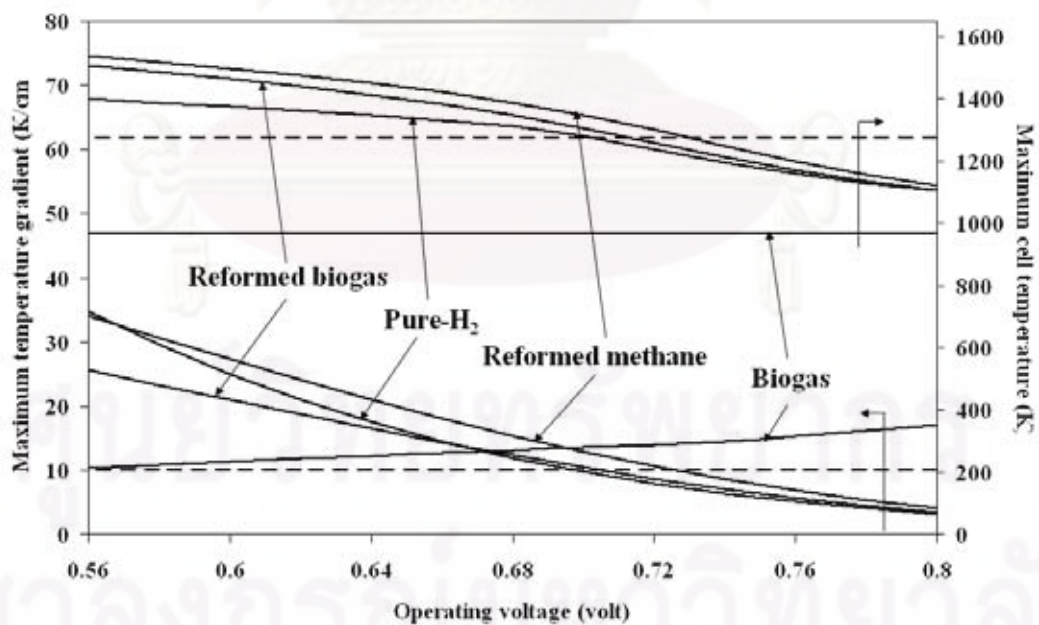


(b)

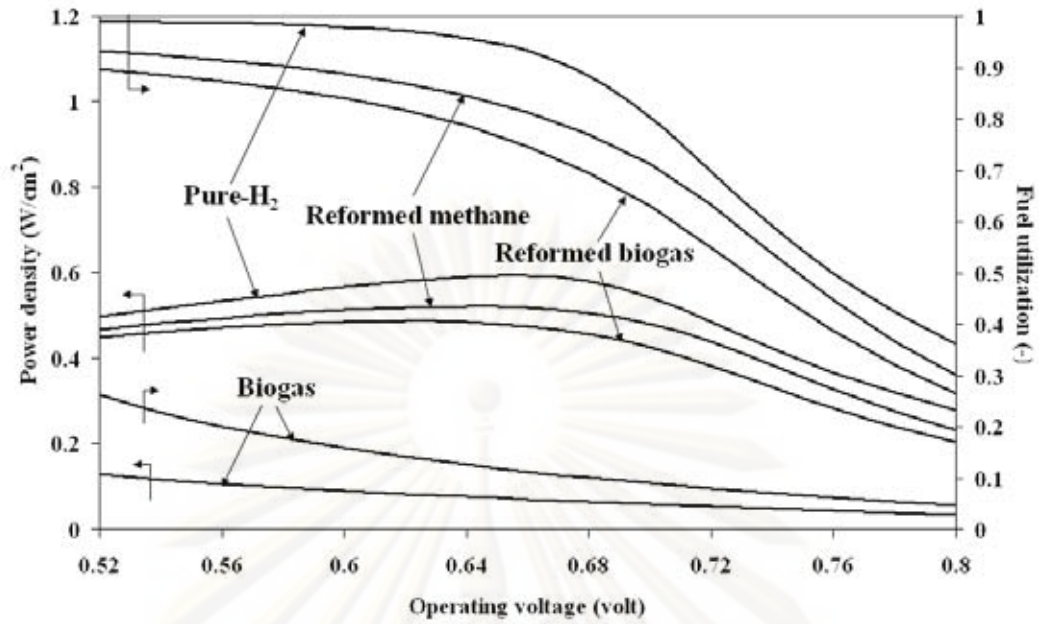


(c)

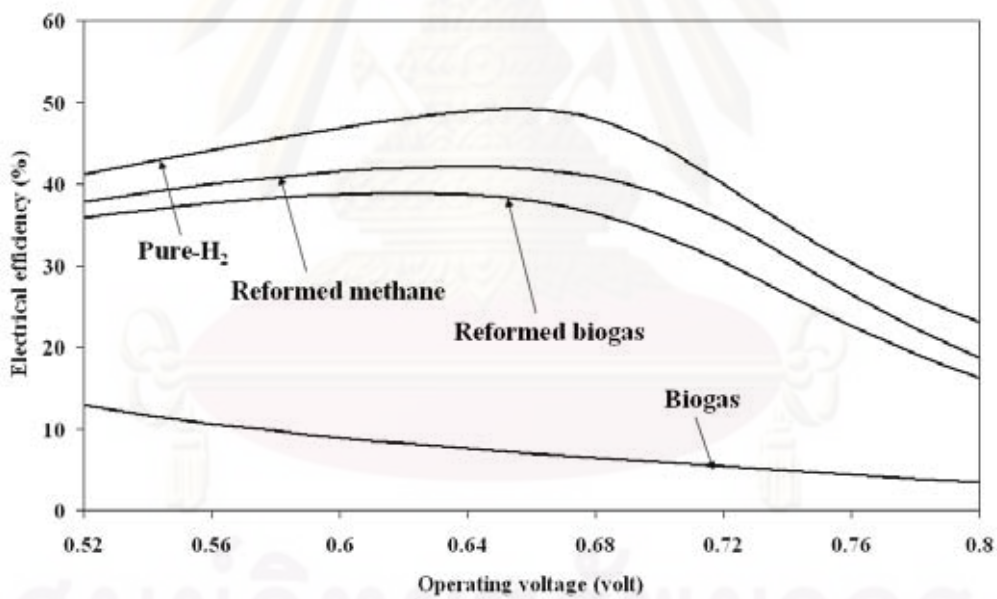
Figure 10.4 The effect of the change in operating voltage on a) the maximum temperature gradient, maximum cell temperature, b) power density, fuel utilization and c) electrical efficiency for SOFC fed by different types of feed in case that $F_{CH_4,eq}$ is equal to $3 \times 10^{-4} \text{ mol s}^{-1}$. (percent excess air is equal to base case values.)



(a)



(b)



(c)

Figure 10.5 The effect of the change in operating voltage on a) the maximum temperature gradient, maximum cell temperature, b) power density, fuel utilization and c) electrical efficiency for SOFC fed by different types of feed in case that $F_{CH_4,eq}$ is equal to $5 \times 10^{-4} \text{ mol s}^{-1}$. (Percent excess air is equal to base case values.)

Tables 10.2 and 10.3 summarize the optimum operating condition of SOFC fuelled by each feed type for $F_{CH_4,eq} = 3 \times 10^{-4}$ and 5×10^{-4} mol s⁻¹, respectively. These results imply that, with the same cell dimension, percent excess air and $F_{CH_4,eq}$, SOFC fed by pure-H₂ feed offers higher power density than SOFC fed by the other fuel types. For $F_{CH_4,eq}$ of 3×10^{-4} and 5×10^{-4} mol s⁻¹, power density of SOFC fuelled by pure-H₂ is 0.379 and 0.532 W cm⁻², respectively. Also, the values of electrical efficiency of 52.20 and 43.97% are achieved for SOFC fed by pure-H₂ with $F_{CH_4,eq}$ of 3×10^{-4} and 5×10^{-4} mol s⁻¹, respectively. Methane-reformed feed is fairly better than biogas-reformed feed due to its higher hydrogen concentration. With percent excess air of 400%, biogas-fed SOFC is not viable to operate when $F_{CH_4,eq}$ is equal to 3×10^{-4} mol s⁻¹. On the other hand, at 5×10^{-4} mol s⁻¹ of $F_{CH_4,eq}$ the SOFC fed by biogas offers extremely lower power density (0.167 W cm⁻²) compared with the other feeds.

Table 10.2 Summary of SOFC fed by different feed operating at the optimum operating condition in case that $F_{CH_4,eq}$ and %excess air are equal to 3×10^{-4} mol/s and 400%, respectively.

Type of feed	Biogas	Biogas-reformed feed	Methane-reformed feed	Pure-H ₂
$F_{CH_4,eq}$ (mol/s)	0.0003	0.0003	0.0003	0.0003
%excess air (%)	400	400	400	400
Operating voltage (V)	n.a.	0.764	0.778	0.746
Power density (Wcm ⁻¹)	n.a.	0.282	0.29	0.379
Current density (A cm ⁻¹)	n.a.	0.369	0.373	0.508
Electrical efficiency (%)	n.a.	37.48	39.13	52.20
U_f (-)	n.a.	0.638	0.645	0.877
Electricity produced (W)	n.a.	112.82	116.14	151.48
Maximum temperature gradient (K cm ⁻¹)	n.a.	9.09	9.21	9.95
Maximum cell temperature (K)	n.a.	1272.06	1271.71	1267.26

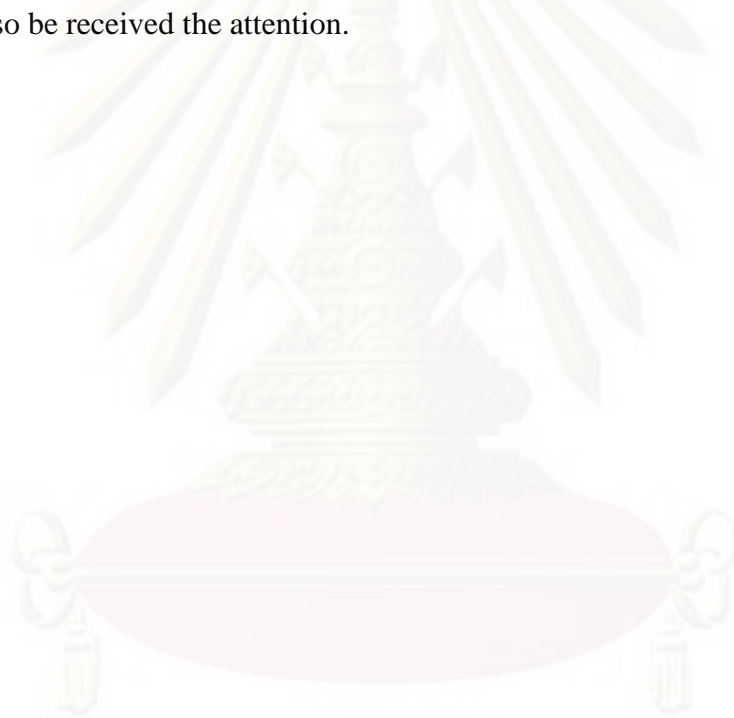
Table 10.3 Summary of SOFC fed by different feed operating at the optimum operating condition in case that $F_{CH_4,eq}$ and Percent excess air are equal to 5×10^{-4} mol s^{-1} and 400%, respectively.

Type of feed	Biogas-		Methane-	Pure-H ₂
	Biogas	reformed feed	reformed feed	
$F_{CH_4,eq}$ (mol/s)	0.0005	0.0005	0.0005	0.0005
%excess air (%)	400	400	400	400
Operating voltage (V)	0.48	0.715	0.732	0.704
Power density (Wcm ⁻¹)	0.167	0.393	0.407	0.532
Current density (A cm ⁻¹)	0.349	0.55	0.556	0.755
Electrical efficiency (%)	16.69	31.35	32.91	43.97
U_f (-)	0.366	0.57	0.577	0.783
Electricity produced (W)	66.97	157.27	162.79	212.69
Maximum temperature gradient (K cm ⁻¹)	9.74	9.09	9.35	9.38
Maximum cell temperature (K)	1030.88	1271.67	1271.80	1272.52

10.4 Conclusions

Mathematical model of SOFC has been developed for investigating operation viability and performance of SOFC fed by different feeds. Four types of fuel feed, i.e. biogas, biogas-reformed feed, methane-reformed feed and pure-H₂, are considered in this study. In operation viability investigation, maximum temperature gradient and maximum cell temperature are employed as the indicators. Additionally, power density and electrical efficiency are considered as performance indicators. The effect of the change in operating conditions, i.e. percent excess air, fuel feed rate and operating voltage, are also investigated. The increase in percent excess air can improve the operation viability of SOFC; however, with surplus percent excess air, its power density is inhibited. Also, the operation of SOFC is viable at high fuel feed rate. Nevertheless, excess high fuel feed rate is not favored since the SOFC cell could be saturated with current, resulting in the dropping of the fuel utilization. Excluding SOFC fed by biogas, SOFC becomes operation viable as it operates at high operating

voltage. Inversely, for biogas-fuelled SOFC, the operation at low operating voltage is preferred in thermal management point of view. The optimum operating voltage which offers utmost power density can be observed. Conclusively, the value of percent excess air, fuel feed rate and operating voltage should be carefully adjusted to obtain best possible power density and reasonable temperature and temperature gradient. SOFC fed by pure-H₂ offers highest power density compared with that fed by the other feeds. Biogas-fed SOFC can become operation viable as it operates at high percent excess air; nevertheless, its power density is extremely lower than SOFC fuelled by the other feeds. Methane-reformed feed offers higher SOFC power density compared with biogas-reformed feed since its H₂ concentration is higher. Although pure-H₂ is an attractive fuel for SOFC, the transformation process of fossil fuel to H₂ should also be received the attention.



ศูนย์วิจัยทรัพยากร
จุฬาลงกรณ์มหาวิทยาลัย

CHAPTER XI

CONCLUSIONS AND RECOMMENDATION

11.1 Conclusions

In this research, the computer simulation was employed for analyzing the performance of desulfurized biogas-fuelled SOFC system. The study was divided into four major sections; i.e. the investigation of carbon formation in SOFC system, the selection of suitable reforming agent for SOFC system, the technical and economic analyses of different configurations of SOFC system, and the study on the operation viability of SOFC stack fed by different feedstocks. The following conclusion can be drawn from the studies.

11.1.1 The investigation of carbon formation in SOFC system

In this section, the carbon formation in SOFC system was investigated using the indicator named “carbon activity, α_c ”. If α_c is more than 1, the SOFC system is prone to carbon formation. Considering biogas as feedstock, CO₂ presenting in biogas can be used as the reforming agent. The carbon formation can easily take place when biogas with low CO₂ content is solely fed into SOFC system. The addition of steam and/or air as the additional reforming agent is required to diminish the prone to carbon formation. The carbon formation can also be alleviated as the SOFC stack and fuel processor operates at high temperature. SOFC operating with oxygen ion-conducting electrolyte seems to be more applicable compared to SOFC operating with proton-conducting electrolyte since steam generated in the anode chamber of the former can help diminish the prone to carbon formation.

11.1.2 The selection of suitable reforming agent for SOFC system

In this section, the conventional SOFC systems fed by three different reforming agents; i.e. steam, air, and combined steam and air, were investigated. Heat management of SOFC system was also analyzed in this section. It is found that the SOFC system can operate solely without the supply external heat source ($Q_{NET} = 0$) if the fuel utilization is well tuned up. This operation is named “energy self-sustainable operation”. From the reason above, the performance of SOFC system operating at

energy self-sustainable operating should be the actual performance. Employing the performance investigation, steam was suggested to be the most suitable reforming agent for biogas-fuelled SOFC system. SOFC system fed by steam could offer superior power density to that fed by air, where their electrical efficiencies were almost identical. The performance of SOFC fed by both steam and air was also investigated. With this operation, the electrical efficiency was fairly improved relative to SOFC fed by steam; however, the power density was extremely inhibited.

11.1.3 The technical and economic analyses of different configurations of SOFC system

In this section, three major configurations of SOFC system were proposed in this study; i.e., SOFC equipped with palladium membrane reactor, SOFC equipped with CO₂ separator and SOFC equipped with both palladium membrane reactor and CO₂ separator. For SOFC cooperating with palladium membrane reactor (PMR-SOFC), the conventional fuel processor is replaced by the palladium membrane reactor (PMR). Pure-H₂ is produced in the PMR as feedstock of SOFC anode. The performance investigation indicated that PMR-SOFC could offer superior power density to CON-SOFC; however, it was not a good choice from an economic viewpoint because of the requirement of a large high-pressure compressor for feeding gas to the membrane reactor. SOFC system cooperating with CO₂ separator could be categorized into two configurations based on type of CO₂ separator; i.e., SOFC system cooperating with CO₂-selective membrane (M-SOFC) and SOFC system cooperating with CaO-CO₂ acceptor (A-SOFC). In these configurations, CO₂ was removed from biogas prior to be fed to the fuel processor. According to the performance examination, M-SOFC was not the interesting alternative due to the loss of CH₄ to the permeation section of CO₂-selective membrane. CaO-CO₂ acceptor was regarded as the attractive CO₂ separator since it can separate CO₂ from biogas without CH₄ loss. With this advantage, A-SOFC could offer high power density compared to CON-SOFC; nevertheless, the additional cost due to the make-up CaO should be also taken into account. The economic study showed that A-SOFC was the beneficial configuration for the SOFC operation since it offered the positive net cost saving. Nevertheless, considering the amount of CO₂ capture as indicator, A-SOFC was not the supreme configuration since only CO₂ present in biogas was captured.

The third option for SOFC system was SOFC equipped with both palladium membrane reactor and CO₂ separator (SE-PMR-SOFC). With this configuration, CO₂ present in biogas was separated in CaO-CO₂ acceptor and pure-CH₄ was fed into PMR. Pure-H₂ generated in PMR was subsequently fed into SOFC anode. The advantage of this configuration was that the compressor load was reduced relative to PMR-SOFC. Moreover, higher hydrogen productivity over PMR-SOFC system could be achieved. The technical study showed that the power density of A-PMR-SOFC was extremely higher compared with CON-SOFC and PMR-SOFC. However, SE-PMR-SOFC was not the good choice in economic point of view due to its high compressor load and high CaO cost. The recycle of the retentate gas was proposed for SE-PMR-SOFC to improve its performance. This new configuration could be called as “SER-PMR-SOFC”. Hydrogen productivity achieved in this configuration was superior to the other configurations. Moreover, SER-PMR-SOFC configuration could offer utmost power density relative to the others. The performance of SER-PMR-SOFC increased with the recycle ratio. However, the economic study indicated that RA-PMR-SOFC was not the beneficial alternative for SOFC operation. Another advantage of SER-PMR-SOFC was that almost all CO₂ produced in the system were captured in the CaO-CO₂ acceptor. It could be concluded that A-SOFC was the suitable configuration according to the technical and economic study. SER-PMR-SOFC was the environmental-friendly configuration since it could offer high CO₂ capture efficiency.

11.1.4 The study on the operation viability of SOFC stack fed by different feedstocks

Operation viability and performance of solid oxide fuel cell fuelled by different feeds was finally examined employing one-dimensional analysis (1-D analysis). Four types of feedstock; i.e., biogas, biogas-reformed feed, methane-reformed feed and pure hydrogen were considered. Maximum temperature gradient and maximum cell temperature were regarded as indicators for operation viability investigation whereas power density and electrical efficiency were considered as performance indicators. The results of 1-D analysis indicated that the change in operating parameters, i.e. excess air, fuel feed rate and operating voltage, could affect the performance and operation viability of SOFC. Hence, these operating parameters should be carefully selected. Pure hydrogen feed offers the highest performance for

SOFC among the other feeds. Extremely high excess air is required for SOFC fed by biogas to become operation viable. Moreover, its power density is much lower than those of SOFCs fed by the other feeds. Methane-reformed feed offers higher power density than biogas-reformed feed since H_2 concentration of the former one is higher. Nevertheless, the performance of SOFC stacks fuelled by methane-reformed or biogas-reformed feeds did not reach that of SOFC stack fuelled by pure- H_2 .

11.2 Recommendation for future works

- a) Even if the heat management was investigated in this study and energy self-sustainable operation was achieved, the quality of heat was not considered. The quality of heat means the temperature of heat source. Heating energy cannot transfer from lower temperature source to higher temperature sources. Hence, heat exchange network should further take place to obtain the real process flow diagram of SOFC system.
- b) Though the operating conditions of SOFC stack were well tuned up to alleviate the damage of stack structure, the decrease in electricity load named “part-load operation” which always happen in the real operation can cause the increase in temperature gradient in stack. As the operation of SOFC stack is switched from “full-load” to “part-load”, the operating voltage is reduced and the irreversibility therefore increases. To solve this problem, the further study should focus on the control of the temperature gradient to be reasonable value by real-time tuning the operating conditions; e.g. flow rate of oxidizing agent, fuel/oxidizing agent inlet temperature, etc.
- c) Further economic analysis should take place by including cost of heat exchangers.

REFERENCES

English

- Abanades, J.C., The maximum capture efficiency of CO₂ using a carbonation/calcination cycle of CaO/CaCO₃. Chem. Eng. J. 90 (2002): 303-306.
- Achenbach, E., Three-dimensional and time dependent simulation of a planar solid oxide fuel cell stack. J. Power Sources 49 (1994): 333-348.
- Achenbach, E. & Riensche, E., Methane/steam reforming kinetics for solid oxide fuel cells. J. Power Sources 52 (1994): 283-288.
- Aguiar, P., Adjiman, C.S. & Brandon, N.P., Anode-supported intermediate temperature direct internal reforming solid oxide fuel cell. I: model-based steady-state performance. J. Power Sources 138 (2004): 120-136.
- Aguiar, P., Chadwick, D. & Kershenbaum, L., Modelling of an indirect internal reforming solid oxide fuel cell. Chem. Eng. Sci. 57 (2002): 1665-1677.
- Aguiar, P., Chadwick, D. & Kershenbaum, L., Effect of methane slippage on an indirect internal reforming solid oxide fuel cell. Chem. Eng. Sci. 59 (2004): 87-97.
- Ahmed, S. & Krumpelt, M., Hydrogen from hydrocarbon fuels for fuel cells. Int. J. Hydrogen Energy 26 (2001): 291-301.
- Alexander Stern, S., Polymers for gas separations: the next decade. Journal of Membrane Science 94(1) (1994): 1-65.
- Alvarez, D. & Abanades, J.C., Determination of the critical product layer thickness in the reaction of CaO with CO₂. Ind. Eng. Chem. Res. 44 (2005): 5608-5615.
- Amelio, M., Morrone, P., Gallucci, F. & Basile, A., Integrated gasification gas combined cycle plant with membrane reactors: Technological and economical analysis. Energy Convers. Manage. 48(10) (2007): 2680-2693.
- Assabumrungrat, S., Laosiripojana, N., Pavarajarn, V., Sangtongkitcharoen, W., Tangjitmatee, A. & Praserttham, P., Thermodynamic Analysis of Carbon Formation in a Solid Oxide Fuel Cell with a Direct Internal Reformer Fuelled by Methanol. J. Power Sources 139 (2005): 55-60.
- Assabumrungrat, S., Laosiripojana, N. & Piroonlerkgul, P., Determination of the boundary of carbon formation for dry reforming of methane in a solid oxide fuel cell. J. Power Sources 159(2) (2006): 1274-1282.

- Balasubramanian, B., Lopez Ortiz, A., Kaytakoglu, S. & Harrison, D.P., Hydrogen from methane in a single-step process. Chem. Eng. Sci. 54 (1999): 3543-3552.
- Baron, S., Brandon, N., Atkinson, A., Steele, B. & Rudkin, R., The impact of wood-derived gasification gases on Ni-CGO anodes in intermediate temperature solid oxide fuel cells. J. Power Sources 126 (2004): 58-66.
- Basile, A., Paturzo, L. & Gallucci, F., Co-current and counter-current modes for water gas shift membrane reactor. Catal. Today 82(1-4) (2003): 275-281.
- Bharadwaj, S.S. & Schmidt, L.D., Synthesis gas formation by catalytic oxidation of methane in fluidized bed reactors. J. Catal. 146 (1994): 11-21.
- Blom, R., Dahl, I.M., Slagtem, A., Sortland, B., Spjelkavik, A. & Tangstad, E., Carbon dioxide reforming of methane over lanthanum-modified catalysts in a fluidized-bed reactor. Catal. Today 21 (1994): 535-543.
- Bouarab, R., Akdim, O., Auroux, A., Cherifi, O. & Mirodatos, C., Effect of MgO additive on catalytic properties of Co/SiO₂ in the dry reforming of methane. Appl. Catal. A:Gen 264 (2004): 161-168.
- Bove, R., Lunghi, P. & Sammes, N., SOFC Mathematic Model for system simulation. Part one: from a micro-detailed to a macro-black-box model. Int. J. Hydrogen Energy 30(2) (2005): 181-187.
- Bove, R. & Ubertini, S., Modeling solid oxide fuel cell operation: Approaches, techniques and results. J. Power Sources 159 (2006): 543-559.
- Bracht, M., Alderliesten, P.T., Kloster, R., Pruschek, R., Haupt, G., Xue, E., Ross, J., Koukou, M. & Papayanakos, N., Water gas shift membrane reactor CO₂ Control in IGCC systems: techno-economic feasibility study. Paper presented at ICCDR-3 Boston 1996
- Bradford, M.C.J. & Vannice, M.A., Catalytic reforming of methane with carbon dioxide over nickel catalysts II. Reaction kinetics. Appl. Catal. A: Gen 142 (1996): 97-122.
- Brown, L.F., A comparative study of fuel cells for on-board hydrogen production for fuel cell-powered automobiles. Int. J. Hydrogen Energy 26 (2001): 381-397.
- Chan, S.H., Khor, K.A. & Xia, Z.T., A complete polarization model of a solid oxide fuel cell and its sensitivity to the change of cell component thickness. J. Power Sources 93(1-2) (2001): 130-140.
- Chan, S.H. & Xia, Z.T., Polarization effects in electrolyte electrode-supported solid oxide fuel cells. J. Appl. Electrochem. 32 (2002): 339-347.

- Chen, Z., Po, F., Grace, J.R., Lim, C.J., Elnashaie, S., Mahecha-Botero, A., Rakib, M., Shirasaki, Y. & Yasuda, I., Sorbent-enhanced/membrane-assisted steam-methane reforming. Chem. Eng. Sci. 63 (2008): 170-182.
- Clarke, S.H., Dicks, A.L., Pointon, K., Smith, T.A. & A., S., Catalytic aspects of the steam reforming of hydrocarbons in internal reforming fuel cells. Catal. Today 38 (1997): 411-423.
- Condorelli, P., Smelser, S.C., Mc Cleary, G.J., G.S., B. & Stuart, R.J., Engineering and Economic Evaluation of CO₂ Removal from Fossil-Fuel-Fired Power Plants Volume 2: Coal Gasification Combined-Cycle Power Plants. EPRI IE-7365 2 1991
- Corti, A., Fiaschi, D. & Lombardi, L., Carbon dioxide removal in power generation using membrane technology. Energy 29(12-15) (2004): 2025-2043.
- Costamagna, P., Magistri, L. & Massardo, A.F., Design and part-load performance of a hybrid system based on a solid oxide fuel cell reactor and a micro gas turbine. J. Power Sources 96(2) (2001): 352-368.
- Costamagna, P., Selimovic, A., Borghi, M.D. & Agnew, G., Electrochemical model of the integrated planar solid oxide fuel cell (IP-SOFC). Chem. Eng. J. 102 (2004): 61-69.
- Cui, Y., Zhang, H., Xu, H. & Li, W., Kinetic study of the catalytic reforming of CH₄ with CO₂ to syngas over Ni/ α -Al₂O₃ catalyst: The effect of temperature on the reforming mechanism. Appl. Catal. A: Gen (318) (2006): 79-88.
- Dayton, D.C., Fuel cell integration-a study of the impacts of gas quality and impurities. 2001
- Dias, J.A.C. & Assaf, J.M., The advantages of air addition on the methane steam reforming over Ni/ γ -Al₂O₃. J. Power Sources 137 (2004): 264-268.
- Dicks, A.L., Hydrogen generation from natural gas for the fuel cell systems of tomorrow. J. Power Sources 61 (1996): 113-124.
- Ding, Y. & Alpay, E., Adsorption-enhanced steam-methane reforming. Chem. Eng. Sci. 55 (2000): 3929-3940.
- Docter, A. & Lamm, A., Gasoline fuel cell systems. J. Power Sources 84 (1999): 194-200.
- Douvartzides, S.L., Coutelieri, F.A., Demin, K. & Tsiakaras, P.E., Fuel options for Solid Oxide Fuel Cells: A Thermodynamic Analysis. AIChE J. 49 (2003): 248-257.

- Dvorak, K., van Nusselrooy, P.F.M.T., Vasalos, I.A., Berger, R.J., Olsbye, U., Verykios, X.E.R., M.P., Hildebrandt, U. & Hageman, R., Catalytic partial oxidation of methane to synthesis gas. Report of EU Contract JOF3-CT95-0026 1998
- Edwards, J.H. & Maitra, A.M., The chemistry of methane reforming with carbon dioxide and its current and potential applications. Fuel Proc. Tech. 42 (1995): 269-289.
- Effendi, A., Hellgardt, K., Zhang, Z.G. & Yoshida, T., Optimising H₂ production from model biogas via combined steam reforming and CO shift reactions. Fuel 84(7-8) (2005): 869-874.
- Eguchi, K., Kojo, H., Takeguchi, T., Kikuchi, R. & Sasaki, K., Fuel flexibility in power generation by solid oxide fuel cells. Solid State Ionics 152-153 (2002): 411-416.
- Ferguson, J.R., Fiard, J.M. & Herbin, R., Three-dimensional numerical simulation for various geometries of solid oxide fuel cells. J. Power Sources 58(2) (1996): 109-122.
- Fernandes, F.A.N. & Soares Jr, A.B., Methane steam reforming modeling in a palladium membrane reactor. Fuel 85 (2006): 569-573.
- Ferreira-Aparicio, P., Benito, M.J. & Sanz, J.L., New trends in reforming technologies: from hydrogen industrial plants to multifuel microreformers. Catal. Rev. 47 (2005): 491-588.
- Finnerty, C.M., Coe, N.J., Cunningham, R.H. & Ormerod, R.M., Carbon formation on and deactivation of nickel-based/zirconia anodes in solid oxide fuel cells running on methane. Catal. Today 46 (1998): 137-145.
- Finnerty, C.M. & Ormerod, R.M., Internal reforming over nickel/zirconia anodes in SOFCS operating on methane: influence of anode formulation, pre-treatment and operating conditions. J. Power Sources 86 (2000): 390-394.
- Fleig, J., SOLID OXIDE FUEL CELL CATHODES: Polarization Mechanisms and Modeling of the Electrochemical Performance. Annu. Rev. Mater. Res. 33 (2003): 361-382.
- Froment, G.F., Production of synthesis gas by steam- and CO₂-reforming of natural gas. J. Mol. Catal. A: Chem. 163 (2000): 147-156.

- Gallucci, F., Paturzo, L. & Basile, A., A simulation study of the steam reforming of methane in a dense tubular membrane reactor. Int. J. Hydrogen Energy 29(6) (2004): 611-617.
- Gottlicher, G. & Pruschek, E., Comparison of CO₂ removal systems for fossil-fuelled power plant processes. Energy Convers. Mgmt. 38 (1997): 173-178.
- Goula, G., Kiouisis, V., Nalbandian, L. & Yentekakis, I.V., Catalytic and electrocatalytic behavior of Ni-based cermet anodes under internal dry reforming of CH₄+CO₂ mixtures in SOFCs. Solid State Ionics 177(19-25) (2006): 2119-2123.
- Grace, J.R., Li, X. & Lim, C.J., Equilibrium modelling of catalytic steam reforming of methane in membrane reactors with oxygen addition. Catal. Today 64 (2001): 141-149.
- Granite, E.J. & O'Brien, T., Review of novel methods for carbon dioxide separation from flue and fuel gases. Fuel Proc. Tech. 86 (2005): 1423-1434.
- Grasa, G.S., Abanades, J.C., Alonso, M. & Gonzalez, B., Reactivity of highly cycled particles of CaO in a carbonation/calcination loop. Chem. Eng. J. 137 (2008): 561-567.
- Harasimowicz, M., Orluk, P., Zakrzewska-Trznadel, G. & Chmielewski, A.G., Application of polyimide membranes for biogas purification and enrichment. Journal of Hazardous Materials 144(3) (2007): 698-702.
- Hernández-Pacheco, E., Mann, M.D., Hutton, P.N., Singh, D. & Martin, K.E., A cell-level model for a solid oxide fuel cell operated with syngas from a gasification process. Int. J. Hydrogen Energy 30 (2005): 1221-1233.
- Hickman, D.A. & Schmidt, L.D., The role of boundary layer mass transfer in partial oxidation selectivity. J. Catal. 138 (1992): 300-308.
- Huften, J.R., Mayorga, S. & S., S., Sorption-enhanced reaction process for hydrogen production. AIChE J. 45 (1999): 248-256.
- Iordanidis, A.A., Kechagiopoulos, P.N., Voutetakis, S.S., Lemonidou, A.A. & Vasalos, I.A., Autothermal sorption-enhanced steam reforming of bio-oil/biogas mixture and energy generation by fuel cells: Concept analysis and process simulation. Int. J. Hydrogen Energy 31 (2006): 1058-1065.
- Jamsak, W., Assabumrungrat, S., Douglas, P.L., Croiset, E., Laosiripojana, N., Suwanwarangkul, R. & Charojrochkul, S., Performance of ethanol-fuelled

- solid oxide fuel cells: Proton and oxygen ion conductors. Chem. Eng. J. 133 (2007): 187-194.
- Jamsak, W., Assabumrungrat, S., Douglas, P.L., Croiset, E., Laosiripojana, N., Suwanwarangkul, R. & Charojrochkul, S., Thermodynamic assessment of solid oxide fuel cell system integrated with bioethanol purification unit. J. Power Sources 174(1) (2007): 191-198.
- Jenne, M., Dörk, T. & Schuler, A., in: U. Bossel (Ed.), Proceedings of the Fifth European Solid Oxide Fuel Cell Forum, Lucerne, Switzerland. European Forum Secretariat CH 5442-Oberrohrdorf 2002
- Jiang, S.P. & Badwal, S.P.S., Hydrogen oxidation at the nickel and platinum electrodes on yttria-tetragonal zirconia electrolyte. J. Electrochem Soc 144(11) (1997): 3777-3784.
- Jiang, S.P. & Badwal, S.P.S., An electrode kinetics study of H₂ oxidation on Ni/Y₂O₃-ZrO₂ cermet electrode of the solid oxide fuel cell. Solid State Ionics 123(1-4) (1999): 209-224.
- Joensen, F. & Rostrup-Nielsen, J.R., Conversion of hydrocarbons and alcohols for fuel cells. J. Power Sources 105 (2002): 195-201.
- Kaneko, T., Brouwer, J. & Samuelsen, G.S., Power and temperature control of fluctuating biomass gas fueled solid oxide fuel cell and micro gas turbine hybrid system. J. Power Sources 160(1) (2006): 316-325.
- Khaleel, M.A., Lin, Z., Singh, P., Surdoval, W. & Collin, D., A finite element analysis modeling tool for solid oxide fuel cell development: coupled electrochemistry, thermal and flow analysis in MARC(R). J. Power Sources 130 (2004): 136-148.
- Laosiripojana, N., Sutthisripok, W. & Assabumrungrat, S., Synthesis gas production from dry reforming of methane over CeO₂ doped Ni/Al₂O₃: Influence of the doping ceria on the resistance toward carbon formation. Chem. Eng. J. 112 (2005): 13-22.
- Larminie, J. & Dicks, A., Fuel cell systems explained. West Sussex, England: Wiley. 2003
- Layi Fagbenle, R., Oguaka, A.B.C. & Olakoyejo, O.T., A thermodynamic analysis of a biogas-fired integrated gasification steam injected gas turbine (BIG/STIG) plant. Appl. Therm. Eng. 27 (2005): 2220-2225.

- Lee, D.K., An apparent kinetic model for the carbonation of calcium oxide by carbon dioxide. Chem. Eng. J. 100 (2004): 71-77.
- Lee, D.K., Baek, I.H. & Yoon, W.L., A simulation study for the hybrid reaction of methane steam reforming and in situ CO₂ removal in a moving bed reactor of a catalyst admixed with a CaO-based CO₂ acceptor for H₂ production. Int. J. Hydrogen Energy 31 (2006): 649-657.
- Lee, J., Lee, E., Joo, O. & Jung, K., Stabilization of Ni/Al₂O₃ catalyst by Cu addition for CO₂ reforming of methane. Appl. Catal. A: Gen 269 (2004): 1-6.
- Lim, L.T., Chadwick, D. & Kershenbaum, L., Achieving autothermal operation in internally reformed solid oxide fuel cells: Simulation studies. Ind. Eng. Chem. Res. 44 (2005): 9609-9618.
- Lu, G.Q., Diniz da Costa, J.C., Duke, M., Giessler, S., Socolow, R., Williams, R.H. & Kreutz, T., Inorganic membranes for hydrogen production and purification: A critical review and perspective. J. Colloid Interface Sci. 314(2) (2007): 589-603.
- Lunghi, P. & Ubertini, U., Solid oxide fuel cells and regenerated gas turbines hybrid systems: a feasible solution for future ultra high efficiency power plants. in: Proceedings of the Seventh International Symposium on Solid Oxide Fuel Cells (SOFC-VII) 2001
- Maggio, G., Freni, S. & Cavallaro, S., Light alcohols/methane fuelled molten carbonate fuel cells: a comparative study. J. Power Sources 74 (1998): 17-23.
- Martinez, R., Romero, E., Guimon, C. & Bilbao, R., CO₂ reforming of methane over coprecipitated Ni–Al catalysts modified with lanthanum. Appl. Catal. A: Gen 274 (2004): 139-149.
- Massman, W.J., A review of the molecular diffusivities of H₂O, CO₂, CH₄, CO, O₃, SO₂, NH₃, N₂O, NO, and NO₂ in air, O₂ and N₂ near STP. Atmos. Environ. 32(6) (1998): 1111-1127.
- Merkel, T.C., Gupta, R.P., Turk, B.S. & Freeman, B.D., Mixed-gas permeation of syngas components in poly(dimethylsiloxane) and poly(1-trimethylsilyl-1-propyne) at elevated temperatures. Journal of Membrane Science 191(1-2) (2001): 85-94.
- Nagaoka, K., Takanabe, K. & Aika, K., Modification of Co/TiO₂ for dry reforming of methane at 2 MPa by Pt, Ru or Ni. Appl. Catal. A: Gen 268 (2004): 151-158.

- Nagata, S., Momma, A., Kato, T. & Kasuga, Y., Numerical analysis of output characteristics of tubular SOFC with internal reformer. J. Power Sources 101 (2001): 60-71.
- Ni, M., Leung, M.K.H. & Leung, D.Y.C., Parametric study of solid oxide fuel cell performance. Energy Convers. Manage. 48 (2007): 1525-1535.
- O'Connor, A.M. & Ross, J.R.H., The effect of O₂ addition on the carbon dioxide reforming of methane over Pt/ZrO₂ catalysts. Catal. Today 46 (1998): 203-210.
- Palazzi, F., Autissier, N., Marechal, F.M.A. & Favrat, D., A methodology for thermo-economic modeling and optimization of solid oxide fuel cell systems. Appl. Therm. Eng. 27(16) (2007): 2703-2712.
- Park, S., Gorte, R.J. & Vohs, J.M., Applications of heterogeneous catalysis in the direct oxidation of hydrocarbons in a solid-oxide fuel cell Appl. Catal. A: Gen 200 (2000): 55-61.
- Patel, K.S. & Sunol, A.K., Modeling and simulation of methane steam reforming in a thermally coupled membrane reactor. Int. J. Hydrogen Energy 32(13) (2007): 2344-2358.
- Petruzzi, L., Cocchi, S. & Fineschi, F., A global thermo-electrochemical model for SOFC systems design and engineering. J. Power Sources 118(1-2) (2003): 96-107.
- Pietrogrande, P., Bezzeccheri, M., Blomen, L.J.M.J. & Mugerwa, M.N., Fuel Cell Systems, Plenum Press, New York. 1993
- Rayment, C. & Sherwin, S. (2003). Introduction to Fuel Cell Technology. Department of Aerospace and Mechanical Engineering, University of Notre Dame, USA.
- Rostrup-Nielsen, J.R., Syngas in perspective. Catal. Today 71 (2002): 243-247.
- Rostrup-Nielsen, J.R., Sehedsted, J. & Norskov, J.K., Hydrogen and synthesis gas by steam- and CO₂ reforming. Adv. Catal. 47 (2002): 65-139.
- Ruckenstein, E. & Hu, Y.H., Carbon dioxide reforming of methane over nickel/alkaline earth metal oxide catalysts. Appl. Catal. A: Gen 133 (1995): 149-161.
- Sangtongkitcharoen, W., Assabumrungrat, S., Pavarajarn, V., Laosiripojana, N. & Praserttham, P., Comparison of Carbon Formation Boundary for Different Types of Solid Oxide Fuel Cells with Methane Feed. J. Power Sources 142 (2005): 75-80.

- Sangtongkitcharoen, W., Vivanpatarakij, S., Laosiripojana, N., Arpornwichanop, A. & Assabumrungrat, S., Performance analysis of methanol-fueled solid oxide fuel cell system incorporated with palladium membrane reactor. Chem. Eng. J. 138 (2008): 436-441.
- Shekhawat, D., Luebke, D.R. & Pennline, H., A review of carbon dioxide selective membranes; U.S. Department of Energy Topical Report, DOE/NETL-2003/1200. 2003
- Shu, J., Grandjean, B.P.A. & Kaliaguine, S., Asymmetric Pd-Ag/stainless steel catalytic membranes for methane steam reforming. Catal. Today 25(3-4) (1995): 327-332.
- Smelser, S.C., Stock, R.M., Mc Cleary, G.J., Booras, G.S. & R.J., S., Engineering and Economic Evaluation of CO Removal from Fossil-Fuel-Fired Power Plants. Volume 1: Pulverized Coal-Fired Power Plants. EPRI IE-7365 1 1991
- Sorrentino, M., Pianese, C. & Guezennec, Y.G., A hierarchical modeling approach to the simulation and control of planar solid oxide fuel cells. J. Power Sources 180 (2008): 380-392.
- Staniforth, J. & Kendall, K., Biogas powering a small tubular solid oxide fuel cell. J. Power Sources 71 (1998): 275-277.
- Suwanwarangkul, E., Croiset, E., Fowler, M.W., Douglas, P.L., Entchev, E. & Douglas, M.A., Performance comparison of Fick's, dusty-gas and Stefan-Maxwell models to predict the concentration overpotential of a SOFC anode. J. Power Sources 122 (2003): 9-18.
- Suwanwarangkul, R., Croiset, E., Entchev, E., Charojrochkul, S., Pritzker, M.D., Fowler, M.W., Douglas, P.L., Chewathanakup, S. & Mahaudom, H., Experimental and modeling study of solid oxide fuel cell operating with syngas fuel. J. Power Sources 161 (2006): 308-322.
- Swaan, H.M., Kroll, V.C.H., Martin, G.A. & Mirodatos, C., Deactivation of supported nickel catalysts during the reforming of methane by carbon dioxide. Catal. Today 21 (1994): 571-578.
- Takeguchi, T., Kani, Y., Yano, T., Kikuchi, R. & Eguchi, K., Study on steam reforming of CH₄ and C₂ hydrocarbons and carbon deposition on Ni/YSZ cermets. J. Power Sources 112 (2002): 588-595.

- Tao, G., Armstrong, T. & Virkar, A., Intermediate temperature solid oxide fuel cell (IT-SOFC) research and development activities at MSRI. In: Nineteenth annual ACERC&ICES conference. Utah 2005
- Torniainen, P.M., Chu, X. & Schmidt, L.D., Comparison of monolith-supported metals for the direct oxidation of methane to syngas. J. Catal. 146 (1994): 1-10.
- Van herle, J., Maréchal, F., Leuenberger, S., Membrez, Y., Bucheli, O. & Favrat, D., Process flow model of solid oxide fuel cell system supplied with sewage biogas. J. Power Sources 131 (2004): 127-141.
- Van Herle, J., Membrez, Y. & Bucheli, O., Biogas as a fuel source for SOFC co-generators. J. Power Sources 127 (2004): 300-312.
- Vernon, P.D.F., Green, M.L.H., Cheetham, A.K. & Ashcroft, A.T., Partial oxidation of methane to synthesis gas, and carbon dioxide as an oxidising agent for methane conversion. Catal. Today 13 (1992): 417-426.
- Vivanpatarakij, S., Laosiripojana, N., Arpornwichanop, A. & Assabumrungrat, S., Performance improvement of solid oxide fuel cell system using palladium membrane reactor with different operation modes. Chem. Eng. J. 146(1) (2009): 112-119.
- Vivanpatarakij, S., Laosiripojana, N., Kiatkittipong, W., Arpornwichanop, A., Soottitantawat, A. & Assabumrungrat, S., Simulation of solid oxide fuel cell systems integrated with sequential CaO–CO₂ capture unit. Chem. Eng. J. 147 (2008): 336-341.
- Walas, S.M. (1988). Chemical process equipment selection and design, Butterworth, Inc.
- Wang, Z., Zhou, J., Wang, Q., Fan, J. & Cen, K., Thermodynamic equilibrium analysis of hydrogen production by coal based on Coal/CaO/H₂O gasification system. Int. J. Hydrogen Energy 31 (2006): 945-952.
- Wong, B.T., Show, K.Y., Lee, D.J. & Lai, J.Y., Carbon balance of anaerobic granulation process: Carbon credit. Bioresour. Technol. 100 (2009): 1734–1739.
- Xiao, T., Suhartanto, T., York, A.P.E., Sloan, J. & Green, M.L.H., Effect of molybdenum additives on the performance of supported nickel catalysts for methane dry reforming. Appl. Catal. A: Gen 253 (2003): 225-235.

- Xu, J. & Froment, G.F., Methane steam reforming, methanation and water-gas shift: I. Intrinsic kinetics. *AIChE J.* 35(1) (1989): 88-96.
- Yakabe, H., Hishinuma, M., Uratani, M., Matsuzaki, Y. & Yasuda, I., Evaluation and modeling of performance of anode-supported solid oxide fuel cell. *J. Power Sources* 86(1-2) (2000): 423-431.
- Zhao, F. & Virkar, A.V., Dependence of polarization in anode-supported solid oxide fuel cells on various cell parameters. *J. Power Sources* 141 (2005): 79-95.



ศูนย์วิจัยทรัพยากร
จุฬาลงกรณ์มหาวิทยาลัย



APPENDICES

ศูนย์วิทยทรัพยากร
จุฬาลงกรณ์มหาวิทยาลัย

APPENDIX A

THERMODYNAMIC DATA OF SELECTED COMPONENT

Table A1 Heat capacities of selected component (C_p)

Components	$C_p/R = a + bT + cT^2 + dT^{-2} + eT^3$ [J/mol]				
	a	$b \times 10^{-4}$	$c \times 10^{-6}$	$d \times 10^3$	e
Methane	1.702	90.800	-2.164	0.000	0.000
Carbon monoxide	3.376	5.570	0.000	-3.100	0.000
Carbon dioxide	5.457	10.500	0.000	-116.000	0.000
Water	3.470	14.500	0.000	12.100	0.000
Hydrogen	3.249	4.220	0.000	8.300	0.000
Nitrogen	3.280	5.930	0.000	4.000	0.000
Oxygen	3.639	5.060	0.000	-22.700	0.000

Table A2 Heat of formation (H_f^0) and entropy (S^0) of selected component at standard state (298 K, 1 atm)

Components	H_f^0 (kJ/mol)	S^0 (J/mol.K)
Methane	-74.52	186.27
Carbon monoxide	-110.53	197.70
Carbon dioxide	-393.51	213.80
Water	-241.82	188.80
Hydrogen	0.00	130.70
Nitrogen	0.00	191.60
Oxygen	0.00	205.20

ศูนย์วิทยทรัพยากร

จุฬาลงกรณ์มหาวิทยาลัย

APPENDIX B

DETERMINING GIBBS ENERGY AND EQUILIBRIUM CONSTANT

B1. Determining Gibbs energy (G) at any temperatures by equations below:

$$G = H - TS \quad (\text{B1})$$

$$dG = dH - d(TS) \quad (\text{B2})$$

Take integration to the equation above:

$$\int dG = \int dH - \int d(TS) \quad (\text{B3})$$

$$G_T - G_{STD} = \int_{298}^T dH - \int_{298}^T d(TS) \quad (\text{B4})$$

Where

$$H_f(T) = H_f^0 + \int_{298}^T C_p dT \quad (\text{B5})$$

$$S(T) = S^0 + \int_{298}^T \frac{C_p}{T} dT \quad (\text{B6})$$

B2. Determining the equilibrium constant (K)

$$G_T = RT \ln K \quad (\text{B7})$$

Rearrange the above equation;

$$K = \exp\left(-\frac{G_T}{RT}\right) \quad (\text{B8})$$

APPENDIX C

LIST OF PUBLICATIONS

International publications

- 1) S. Assabumrungrat, N. Laosiripojana, P. Piroonlerkgul, Determination of boundary of carbon formation for dry reforming of methane in a solid oxide fuel cell, J. Power Sources, 159, 1274-1282 (2006).
- 2) P. Piroonlerkgul, S. Assabumrungrat, N. Laosiripajana, A.A. Adesina, Selection of appropriate fuel processor for biogas-fuelled SOFC system, Chem. Eng. J., 140, 341-351 (2008).
- 3) P. Piroonlerkgul, N. Laosiripajana, A.A. Adesina, S. Assabumrungrat, Performance of biogas-fed solid oxide fuel cell systems integrated with membrane module for CO₂ removal, Chemical Engineering and Processing: Process Intensification, 48, 672-682 (2009).

ศูนย์วิทยทรัพยากร

จุฬาลงกรณ์มหาวิทยาลัย

VITAE

Mr. Pakorn Piroonlerkgul was born in May 1, 1983 in Bangkok, Thailand. He finished high school from Triam Udom Suksa School, Bangkok in 2001. He received his Bachelor's Degree in Chemical Engineering, from the Department of Chemical Engineering, Chulalongkorn University in 2005. Afterward, he continued studying Doctoral degree of Chemical Engineering, Chulalongkorn University since November 2005 and received Royal Golden Jubilee Scholarship from Thailand Research Fund. During his Doctoral degree, he collaborated with Professor Adesoji A. Adesina and did some parts of his research in School of Chemical Sciences and Engineering, University of New South Wales, Australia for eight months.



ศูนย์วิทยทรัพยากร
จุฬาลงกรณ์มหาวิทยาลัย